~~SECRET~~

CONFIDENTIAL

U. S. AIR FORCE-U. S. NAVY NATIONAL ADVISORY COMMITTEE FOR AERONAUTICS

RESEARCH - AIRPLANE - COMMITTEE REPORT ON CONFERENCE ON THE PROGRESS OF THE X - 15 PROJECT

A COMPILATION OF THE PAPERS PRESENTED

IAS Building
Los Angeles, California

July 28-30, 1958

~~SECRET~~

CONFIDENTIAL

U. S. AIR FORCE - U. S. NAVY

NATIONAL ADVISORY COMMITTEE FOR AERONAUTICS

RESEARCH-AIRPLANE-COMMITTEE REPORT ON CONFERENCE ON THE PROGRESS OF THE X-15 PROJECT* [U]

A Compilation of the Papers Presented

IAS Building
Los Angeles, California

July 28-30, 1958

*Title, Unclassified

TABLE OF CONTENTS

Page

INTRODUCTION vii

LIST OF CONFEREES ix

TECHNICAL PAPERS PRESENTED

July 28, 1958

SESSION CHAIRMAN: Walter C. Williams

DEVELOPMENT STATUS

1. X-15 Research Airplane Development Status . . . by L. P. Greene 1

STABILITY AND CONTROL

2. High-Speed Static Stability Characteristics of the X-15 Airplane . . . by Jim A. Penland and David E. Fetterman, Jr. 19

3. Effects of Rocket Jet on Stability and Control at High Mach Numbers . . . by David E. Fetterman, Jr. 31

4. The Measured and Estimated Rotary Stability Derivatives of the X-15 Airplane . . . by Bruce Tinling, True Surber, Phillips J. Tunnell, and Armando Lopez 43

5. Low-Speed Stability and Control and Spinning Characteristics of Dynamic Models of the X-15 Airplane . . . by Donald E. Hewes, James S. Bowman, Jr., and James L. Hassell, Jr. 57

6. Aerodynamic Characteristics of the X-15/B-52 Combination . . . by William J. Alford, Jr., and Robert T. Taylor 69

SIMULATOR TESTING

7. Flight and Analog Studies of Landing Techniques Pertinent to the X-15 Airplane . . . by Thomas W. Finch, Gene J. Matranga, Joseph A. Walker, and Neil A. Armstrong 83

8. X-15 Flight Simulation Studies . . . by George B. Merrick and C. H. Woodling 93

9. Centrifuge Simulation of the X-15 . . . by Carl Clark 107

PILOT CONSIDERATIONS

10. Pilot Protection for the X-15 Airplane . . . by Edwin G. Vail and Richard G. Willis 117

11. Development of X-15 Escape System . . . by J. F. Hegenwald . . 129

12. Aeromedical Support of the X-15 Program . . . by Burt Rowen 147

MISSION INSTRUMENTATION

13. Status of High-Range and Flow-Direction Sensor . . . by G. M. Truszynski and W. D. Mace 151

14. All-Attitude Flight-Data System for the X-15 Research Airplane . . . by M. L. Lipscomb and J. A. Dodgen 159

July 29, 1958

SESSION COCHAIRMEN: L. P. Greene and Hartley A. Soulé

THERMODYNAMICS

15. Wind-Tunnel Investigation of the Heat Transfer to the X-15 Airplane . . . by William V. Feller and Paige B. Burbank 171

16. Effects of Aerodynamic Heating on X-15 Temperatures . . . by Martin R. Kinsler 183

STRUCTURES

17. X-15 Structural Loads . . . by Gerald H. Johnson 197

18. X-15 Structure and Structural Development
. . . by C. L. Davis 213

19. Flutter, Noise, and Buffet Problems Related to the X-15
. . . by Harry L. Runyan and Harold R. Sweet 231

MATERIALS AND FABRICATION

20. X-15 Forming and Fabrication Methods . . . by I. J. Wilson . . 243

21. X-15 Material and Process Development
. . . by F. R. Kostoch 259

SUBSYSTEMS

22. The XLR99-RM-1 Engine for the X-15 Airplane
. . . by Robert W. Seaman 275

23. X-15 Propellant System Description . . . by J. W. Gibb 285

24. X-15 Hydraulic-System Development . . . by R. J. Culleton . . 293

25. X-15 Auxiliary Power Units and Reaction Controls
. . . by Bruce O. Wagner 303

26. Landing-Gear Design and Development Testing for the
X-15 Airplane . . . by L. L. Rhodes 313

27. X-15 Conditioning and Pressurization System
. . . by C. P. Bouman 321

RESEARCH OBJECTIVES

28. X-15 Research Objectives . . . by De E. Beeler 327

July 30, 1958

X-15 HARDWARE EXHIBIT, NORTH AMERICAN AVIATION PLANT

INTRODUCTION

This document is a compilation of the papers presented at the Conference on Progress of the X-15 Project held at the IAS Building, Los Angeles, California, July 28-30, 1958. This conference was held by the Research Airplane Committee of the U. S. Air Force, the U. S. Navy, and the National Advisory Committee for Aeronautics to report on the technical status of this research airplane. The papers were presented by members of the staffs of North American Aviation, Inc.; Reaction Motors Division, Thiokol Chemical Corp.; Naval Air Development Center; Wright Air Development Center; Air Force Flight Test Center; and National Advisory Committee for Aeronautics.

LIST OF CONFEREES

The following were registered at the Conference on the Progress of the X-15 Project, IAS Building, Los Angeles, Calif., July 28-30, 1958.

ABBOTT, Ira H.	NACA Headquarters
ABRAHAM, Lewis H.	NACA Subcommittee on Structures
AGNEW, George Edward	Ryan Aeronautical Company
ALEXANDER, John D.	Boeing Airplane Company
ALFORD, William J., Jr.	NACA - Langley Laboratory
ALLEN, Lee T.	Air Ballistic Missile Agency
AMES, Milton B., Jr.	NACA Headquarters
ANDERSON, Olof	United Aircraft Corporation
ANDERSON, Roger A.	NACA - Langley Laboratory
ANDREWS, Wilbur A.	North American Aviation, Incorporated
ANGLE, E. E.	Ramo-Wooldridge Corporation
ANTONATAS, P. P.	Wright Air Development Center
ANTONIDES, Joseph W.	Reaction Motors Div., Thiokol Chemical Corp.
ARMSTRONG, Col. J. L.	NACA Subcommittee on Rocket Engines
AULD, Charles Donald	Naval Ordnance Laboratory
AUSTIN, Lt. Comdr. Frank H., Jr.	Naval Air Test Center
BACHMANN, Lt. Col. Frederick Clemens	Air Technical Intelligence Center
BAILEY, Albert Robert	Lockheed Aircraft Corporation
BAKER, Thomas F.	NACA High-Speed Flight Station
BALL, J. Norman	Cornell Aeronautical Laboratory
BANNER, Richard D.	NACA High-Speed Flight Station
BARBER, Arthur	Air Force Cambridge Research Center
BARCUS, Ronald	Bendix Aviation Corporation
BARNES, W. H.	Wright Air Development Center
BATDORF, Samuel Burbridge	Institute for Defense Analyses
BAUM, C. Philemon	Bureau of Aeronautics
BEAUPRE, Merle A.	North American Aviation, Incorporated
BECK, Neils J.	Douglas Aircraft Company, Inc.
BEELER, De E.	NACA High-Speed Flight Station
BELL, E. B.	Wright Air Development Center
BELLINGER, Comdr. Duane Jacobs	Bureau of Aeronautics
BELLMAN, Donald R.	NACA High-Speed Flight Station
BELSHEIM, Robert Oscar	Naval Research Laboratory
BELSLEY, Steven E.	NACA - Ames Laboratory
BENNER, Roland L.	North American Aviation, Incorporated
BESTERVELT, Lt. Col. James	Air Research and Development Command

BEZBATCHENKO, John William	Goodyear Aircraft Corporation
BIRNBAUM, Arnold	Federal Telecommunication Laboratories
BLAIR, Morgan M.	NACA Subcommittee on Low-Speed Aerodynamics
BLAIS, Robert Alfred	Gilfillan Brothers, Incorporated
BLEAKNEY, William M.	Hughes Aircraft Company
BLISSELL, Walter Augustine, Jr.	Boeing Airplane Company
BOCK, Capt. Charles Cornelius, Jr.	Air Force Flight Test Center
BOSEE, Capt. Roland A.	Naval Air Material Center
BOUMAN, C. P.	North American Aviation, Incorporated
BRAASCH, Herman Lynn	Ryan Aeronautical Company
BRANAHL, Erwin Fred	McDonnell Aircraft Corporation
BRAUN, Max Thomas	Boeing Airplane Company
BRICKER, Ethelbert Irvin	Lockheed Aircraft Corporation
BRIGLIO, Anthony, Jr.	Jet Propulsion Laboratory - C.I.T.
BROWN, Charles G.	Douglas Aircraft Company, Inc.
BROWNE, Thomas P.	Douglas Aircraft Company, Inc.
BRUMBAUGH, Vernon W.	Applied Physics Laboratory - J.H.U.
BRUNOW, Charles Lloyd	Temco Aircraft Corporation
BURGGRAF, Odus Ray	Aerophysics Development
BURKE, James Donahue	Jet Propulsion Laboratory - C.I.T.
CALDWELL, Col. Robert	Air Research and Development Command
CAMPBELL, Gordon	North American Aviation, Incorporated
CARHART, Nathan A.	Douglas Aircraft Company, Inc.
CARLSON, John M.	Air Force Flight Test Center
CASEY, Daniel F.	Air Proving Ground Center
CASSELL, James Calder	Northrop Aircraft, Incorporated
CATTON, Col. Jack Joseph	Stategic Air Command
CHAMPINE, Robert A.	NACA - Langley Laboratory
CLARK, Dr. Carl	Naval Air Development Center
CLARK, Clayton C.	North American Aviation, Incorporated
CLARK, Dr. David Myron	David Clark Company
CLARK, Edward E.	The Martin Company
CLARK, John R.	NACA Subcommittee on High-Speed Aerodynamics
CLARKE, Capt. Roderick W.	Air Research and Development Command
CLAYBOURNE, John P.	Air Ballistic Missile Agency
CLEMENTSON, Col. Gerhardt Christopher	U. S. Air Force Academy
CLOUSING, Lawrence A.	NACA - Ames Laboratory
COATES, Rear Adm. L. D.	NACA Committee on Aircraft, Missile, and Spacecraft Aerodynamics
COCHRAN, D.	NACA Committee on Aircraft, Missile, and Spacecraft Propulsion
COHN, Benedict	Boeing Airplane Company
COLLIER, Maj. Robert Edward	U. S. Air Force Academy

COLLINS, Maj. H.	Wright Air Development Center
COLMAN, Lt. Lawrence P.	Aero-Medical Laboratory, Wright-Patterson AFB
CONLON, John W.	Reaction Motors Div., Thiokol Chemical Corp.
COOLEY, D. E.	Wright Air Development Center
COOPER, Norman Ralph	North American Aviation, Incorporated
COVINGTON, Carl Ashby	Office of Assistant Secretary of Defense for Research and Development
CRISSMAN, Ronald B.	Bell Aircraft Corporation
CRONE, Robert	North American Aviation, Incorporated
CROSSFIELD, A. Scott	North American Aviation, Incorporated
CROUCH, Jack Graham	Air Force Institute of Technology
CROWLEY, John W., Jr.	NACA Headquarters
CULLETON, R. J.	North American Aviation, Incorporated
CULVER, Irving Harold	Lockheed Aircraft Corporation
DANE, Col. Paul H.	U. S. Air Force Academy
DAUGHADAY, Hamilton	Cornell Aeronautical Laboratory
DAUM, Fred L.	NACA Subcommittee on Vibration and Flutter
DAVIDSON, Ralph B.	NACA Committee on Aircraft, Missile, and Spacecraft Construction
DAVIS, C. L.	North American Aviation, Incorporated
DAVIS, Robert Arthur	RAND Corporation
DeCALLIES, Lt. Comdr. Richard N.	Office of Naval Research
DENTEL, Keith Eugene	Bureau of Aeronautics
DETTWYLER, Hans Rudolph	Marquardt Aircraft Company
DEVLIN, Leo J.	Douglas Aircraft Company, Inc.
DEYARMOND, Albert Bonnell	General Electric Company
DICK, Lt. Col. Wagner Warner	U. S. Air Force Headquarters
DICKINSON, Monroe Miller, Jr.	International Business Machines Corp.
DIEHL, Capt. Walter S., USN (Ret.)	NACA Subcommittee on Aerodynamic Stability and Control
DIETZ, Comdr. Willard D.	Office of Chief of Naval Operations
DIXON, Howard Henry	Douglas Aircraft Company, Inc.
DODGEN, J. A.	NACA - Langley Laboratory
DONELY, Philip	NACA - Langley Laboratory
DOUGLASS, C. W.	Wright Air Development Center
DRAPER, Dr. C. Stark	NACA Committee on Aircraft, Missile, and Spacecraft Propulsion
DRELL, Harry	NACA Subcommittee on Internal Flow
DUKES, Wilfred H.	Bell Aircraft Corporation
DUNFORD, Ernest Frank	Chrysler Corporation
DUNHOLTER, Dr. H. F.	NACA Subcommittee on Rocket Engines
DURAND, Jack Alphonse	ARO, Inc.
DURHAM, Capt. Samuel C.	Air Force Flight Test Center

EBER, Gerhard Richard	Air Force Missile Development Center
EDDY, Edwyn A.	Republic Aviation Corporation
EIMER, Manfred	Jet Propulsion Laboratory - C.I.T.
ELDER, Donald L.	Douglas Aircraft Company, Inc.
EMMONS, Paul C.	Bell Aircraft Corporation
ENGEN, Comdr. Donald E.	U. S. Naval Air Test Center
EPSTEIN, Albert	NACA Subcommittee on Loads
ESTES, Capt. Hilliard D.	OCS, Ent AFB
EVANS, Albert J.	NACA Headquarters
EVANS, Howard A.	North American Aviation, Incorporated
EVANS, Joseph Ritchey, Jr.	Lockheed Aircraft Corporation
EVERETT, Maj. Phillip E.	Air Research and Development Command
FARRIOR, Col. William Owen	Air Technical Intelligence Center
FELLER, William V.	NACA - Langley Laboratory
FELTZ, Charles H.	North American Aviation, Incorporated
FERO, Lester K.	The Martin Company
FERRIS, Delacey F.	Reaction Motors Div., Thiokol Chemical Corp.
FETTERMAN, David E., Jr.	NACA - Langley Laboratory
FINCH, Thomas W.	NACA High-Speed Flight Station
FISCHEL, Jack	NACA High-Speed Flight Station
FISCHER, Comdr. Charles Fink	Naval Air Development Center
FISCHER, Richard Alfred	AiResearch Manufacturing Company
FLAGG, John Ernest	David Clark Company
FLEMING, Lt. Francis Lawrence, Jr.	Naval Air Missile Test Center
FLICKINGER, Gen. Don	Air Research and Development Command
FLINN, E.	Wright Air Development Center
FORREST, Casey L.	Bell Aircraft Corporation
FRANCIS, Thomas	North American Aviation, Incorporated
FRANKS, David Charles	Avco Manufacturing Corporation
FRICK, Charles William, Jr.	Convair
FURLONG, G. Chester	Arnold Engineering Development Center
GARDNER, Frederick H.	North American Aviation, Incorporated
GARNER, William Gerald	Army Rocket and Guided Missile Agency
GATEWOOD, Buford Echols	Air Force Institute of Technology
GAYNOR, Frank A.	NACA Subcommittee on Automatic Stabilization and Control
GEHRKENS, George Raymond	North American Aviation, Incorporated
GEISBERG, R.	Convair
GIBB, J. W.	North American Aviation, Incorporated
GILKESON, Capt. Fillmore B.	U. S. Naval Air Test Center
GOCKEL, Comdr. B. N.	USN Post Graduate School, Monterey
GOLDIN, Robert	NACA Subcommittee on Loads
GOLDMAN, C. C.	Wright Air Development Center
GRAY, E. Z.	NACA Subcommittee on Loads

GREEN, George Garner	Convair
GREENE, L. P.	NACA Subcommittee on High-Speed Aerodynamics
GRUFF, James J.	Bureau of Aeronautics
HABER, Bernard D.	North American Aviation, Incorporated
HAKES, Ralph Cary	Northrop Aircraft, Incorporated
HALE, Capt. Roy E., Jr.	NACA Subcommittee on Loads
HALSTED, George	Bell Aircraft Corporation
HAMILTON, William T.	NACA Subcommittee on Aerodynamic Stability and Control
HARDIN, William Ross	Bureau of Aeronautics
HARGIS, C. B.	Air Research and Development Command
HARRIS, Thomas A.	NACA - Langley Laboratory
HART, Capt. Joseph E.	USN Post Graduate School, Monterey
HARTMAN, Edwin P.	NACA - Western Coordination Office
HARVEY, Quinton C.	North American Aviation, Incorporated
HAWKINS, Wallace Kent	Tempco Aircraft Corporation
HEDDING, Rear Adm. Truman J.	Bureau of Aeronautics
HEDEMAN, Walter Rider	Texas Instrument Company
HEDGEPETH, John M.	NACA - Langley Laboratory
HEGENWALD, J. F.	North American Aviation, Incorporated
HELFMAN, Sidney	The Martin Company
HENDERSON, Maj. William J.	NACA Subcommittee on Rocket Engines
HEPPE, Ralph Richard	NACA Subcommittee on Low-Speed Aerodynamics
HERMACH, Charles A.	NACA - Ames Laboratory
HEWES, Donald E.	NACA - Langley Laboratory
HIGGINS, Harry Clark	Boeing Airplane Company
HIRT, Gerald Edwin	Talco Engineering Company
HOEY, Robert G.	Air Force Flight Test Center
HOGE, H. J.	NACA Subcommittee on Loads
HOLBACK, George E.	The Martin Company
HOLDEN, Capt. G. M., Jr.	Wright Air Development Center
HOLLENBERG, Harold O.	Bureau of Aeronautics
HOLM, Col. Florian A.	Air Research and Development Command
HOUSER, James Grover	The Martin Company
HOWARD, Ephraim Manasseh	Aerojet-General Corporation
HUBERT, Josef Johann	Grumman Aircraft Engineering Corp.
HUDSON, Verne Lyle	Boeing Airplane Company
HUGLIN, Col. H. P.	Wright Air Development Center
HUNTSBERGER, Ralph F.	NACA - Ames Laboratory
HYATT, Abraham	NACA Committee on Aircraft, Missile, and Spacecraft Aerodynamics
ILLER, Maj. W. J.	Wright Air Development Center
IRELAND, Col. Loren Elsworth	Headquarters, Air Command and Staff College

ISENBERG, Joel	Bell Aircraft Corporation
JACKSON, R. P.	NACA Subcommittee on High-Speed Aerodynamics
JENSEN, Raymond Walter	AiResearch Manufacturing Company
JEPPESEN, Norman Lutz	Goodyear Aircraft Corporation
JOFFS, Robert Edward	Naval Ordnance Laboratory
JOHNSON, Gerald H.	North American Aviation, Incorporated
JOHNSON, Henry Clay	NACA Subcommittee on Vibration and Flutter
JOHNSON, Orlando Theophilus	Ballistic Research Laboratories
JOHNSON, Theodore Lowell	Emerson Electric Manufacturing Co.
JOHNSTON, Edwin W.	North American Aviation, Incorporated
JONES, Lt. Col. Felix Henley	U. S. Atomic Energy Commission
JORDAN, Lynvel Ralph	Douglas Aircraft Company, Inc.
KAMM, Robert W.	Arnold Engineering Development Center
KAPLAN, Dr. Carl	Air Force Office of Scientific Research
KATKOV, Robert B.	NACA Subcommittee on Aerodynamic Stability and Control
KAUFMANN, Lt. Col. Frederick W.	Office of Deputy Chief of Staff, Development
KAVANAU, Dr. Lawrence L.	Aeronutronic Systems, Incorporated
KAYTEN, Gerald G.	The Martin Company
KIHLGREN, Theodore Ephraim	International Nickel Company, Inc.
KING, J.	Wright Air Development Center
KING, Robert L.	Air Force Flight Test Center
KINSLER, Martin R.	North American Aviation, Incorporated
KIRCHNER, Mark Edwin	Boeing Airplane Company
KIRKBRIDE, John Frederick	Boeing Airplane Company
KIRSCH, Lt. Col. George A.	Air Force Flight Test Center
KLEINKNECHT, Kenneth S.	NACA High-Speed Flight Station
KNAPP, W. A.	Wright Air Development Center
KOCH, Harry A.	Reaction Motors Div., Thiokol Chemical Corp.
KOCHEVAR, Raymond J.	North American Aviation, Incorporated
KOCMANEK, Karl L.	NACA Subcommittee on Automatic Stabilization and Control
KONDO, Noboru	Sperry Gyroscope Company
KORYCINSKI, Peter F.	NACA - Langley Laboratory
KOSTOCH, F. R.	North American Aviation, Incorporated
KUCZON, Daniel T.	Convair
LAPIN, Ellis Eliah	Douglas Aircraft Company, Inc.
LECAT, Robert Joseph	Fairchild Guided Missiles Div.

LEE, J. M.	NACA Subcommittee on Automatic Stabilization and Control
LEMKE, George Anthony	Convair
LILLARD, Lt. Col. James W.	Air Research and Development Command
LINDELL, Lt. Col. Keith Gordon	U. S. Air Force
LIPSCOMB, M. L.	Wright Air Development Center
LOFTIN, Laurence K., Jr.	NACA - Langley Laboratory
LOHMAN, Robert L.	The Martin Company
LOMBARD, Dr. Albert E., Jr.	NACA Subcommittee on High-Speed Aerodynamics
LORENZO, Michael	Deputy Chief of Staff, Development
LOVELACE, Dr. W. Randolph, II	Lovelace Foundation for Medical Education and Research
LOWREY, Richard Owen	Lockheed Aircraft Corporation
LU, Hoshen R.	Republic Aviation Corporation
LUNDQUIST, William G.	Reaction Motors Div., Thiokol Chemical Corp.
MacDONALD, Lt. Col. Gilmore C.	Air Proving Ground Center
MACE, W. D.	NACA - Langley Laboratory
MAGNUS, Richard J.	Aerophysics Development Corporation
MANGURIAN, George N.	NACA Subcommittee on Structures
MARSHALL, Edmond Valentine	Chance Vought Aircraft
MARSHALL, Capt. Frank G., Jr.	Office of Chief of Naval Operations
MARSTILLER, James K.	The Martin Company
MATRANGA, Gene J.	NACA High-Speed Flight Station
MAY, Ralph W., Jr.	NACA Headquarters
McBREARTY, Jerome F.	Lockheed Aircraft Corporation
McCORMICK, Jack Everett	Boeing Airplane Company
McCRACKEN, Donald William	McDonnell Aircraft Corporation
McDONALD, Dr. John C.	NACA Committee on Aircraft, Missile, and Spacecraft Construction
McDOUGAL, Robert Lewis	Lockheed Aircraft Corporation
McGOUGH, Col. Edward Alexander, III	Tactical Air Command, Langley AFB
McGUIRE, Lt. Col. Troy	Air Research and Development Command
McLELLAN, Charles H.	NACA - Langley Laboratory
McMANUS, Richard Leo	General Electric Company
McRAE, Forbes William, Jr.	Boeing Airplane Company
MEIRS, John	Gruman Aircraft Engineering Corp.
MENARD, Joseph A., Jr.	NACA High-Speed Flight Station
MERRICK, George B.	North American Aviation, Incorporated
MESSINGER, Bernard Lee	Lockheed Aircraft Corporation
MICKS, William R.	RAND Corporation
MILLER, Joseph Anthony	Minneapolis-Honeywell Regulator Co.

MOISE, John C.	Aerojet-General Corporation
MONTEITH, Oscar Burr	Boeing Airplane Company
MOORE, Lt. Comdr, Robert Edward	Bureau of Aeronautics
MORAN, Leland P.	North American Aviation, Incorporated
MORGAN, Ralph Pierpont	Aeronutronic Systems, Incorporated
MORTON, Comdr. Wilbur	Bureau of Ordnance
MOSES, Harry Clark	Westinghouse Electric Corporation
MOWRER, Donald William	Ballistic Research Laboratories
MOYERS, Col. Frank N.	Air Force Office of Scientific Research
MULHOLLAND, Donald R.	NACA - Western Coordination Office
MURRAY, Maj. Arthur	Air Research and Development Command
MURRIN, John E.	Convair
MUSE, Thomas Calvert	Office of Assistant Secretary of Defense for Research and Development
NADEL, Aaron B.	General Electric Company
NASHOLD, Capt. Robert Leslie	Tactical Air Command, Langley AFB
NAY, Col. Paul F.	Air Research and Development Command
NECKER, Don E.	North American Aviation, Incorporated
NEIHOUSE, Anshal I.	NACA - Langley Laboratory
NELSON, Lt. Comdr. Joseph Williams	Bureau of Aeronautics
NEWBY, Clinton T.	NACA Subcommittee on Loads
NEWMAN, Theodore	American Bosch Arma Corporation
NICHOLSON, F. T.	Naval Air Development Center
NITIKMAN, Arthur	Northrop Aircraft, Incorporated
O'BRIEN, Norman Ray	Convair
O'CONNOR, Lt. J. M.	Wright Air Development Center
O'DONNELL, Dr. William J.	NACA Subcommittee on Internal Flow
OLIVER, Robert Norris	Convair
O'MALLEY, James A., Jr.	NACA Subcommittee on Low-Speed Aerodynamics
ORBAN, Lt. Col. Henry J.	Air Research and Development Command
OSWALD, William Bailey	Douglas Aircraft Company, Inc.
PAGLIANETE, Francis J.	Bureau of Aeronautics
PANTON, Lt. Ronald L.	Air Research and Development Command
PASSMAN, Richard A.	General Electric Company
PAVELKA, Jerry	Republic Aviation Corporation
PEARSON, Charles W.	Naval Air Material Center
PEARSON, John B.	North American Aviation, Incorporated
PEIRCE, Chester	Air Research and Development Command
PENLAND, Jim A.	NACA - Langley Laboratory
PENN, Maj. William W., Jr.	Air Research and Development Command
PEPPING, Raymond Austin	McDonnell Aircraft Corporation
PERKINS, O. R.	Navy Liaison Office - Edwards AFB

PETERS, Edward Frank	McDonnell Aircraft Corporation
PETERSEN, Lt. Comdr. Forrest S.	U. S. Naval Air Test Center
PETERSEN, Frank W.	North American Aviation, Incorporated
PETERSON, Col. Clayton L.	Office of Assistant Secretary of Defense for Research and Engineering
PITMAN, Duncan L.	NACA Subcommittee on Automatic Stabilization and Control
POPE, Alan Yates	Sandia Corporation
POTTER, Comdr. Robert Rhys	Bureau of Aeronautics
PROPPER, Edouard Michael	Convair
RAFFERTY, Christopher A.	Bendix Aviation Corporation
RAU, John M., Jr.	G. M. Giannini Company, Incorporated
RAUTIO, R. W.	Wright Air Development Center
RAY, George D.	NACA Committee on Aircraft, Missile, and Spacecraft Construction
RAYNESFORD, Kirk C.	Air Research and Development Command
REICHERT, Rudi	Air Ballistic Missile Agency
REID, Robert Reeves	General Electric Company
RHODE, Richard V.	NACA Headquarters
RHODES, Edgar P.	Bell Aircraft Corporation
RHODES, L. L.	North American Aviation, Incorporated
RICHOLT, Robert Russel	Lockheed Aircraft Corporation
RINEHART, Richard Dewey	Bell Aircraft Corporation
RINGGENBERG, Lt. R. L.	Wright Air Development Center
RIORDAN, Hugh E.	Applied Physics Laboratory - J.H.U.
RITCHIE, Dr. Donald Jeanne	Melpar, Incorporated
ROBINSON, Comdr. G.	Navy Liaison Officer, Edwards AFB
ROBINSON, Raun	North American Aviation, Incorporated
ROBISCHON, E. W.	Institute of the Aeronautical Sciences
RODERICK, Richard	Convair
ROSCHE, Melvin G.	NACA Headquarters
ROTELLI, Ranieri L.	Boeing Airplane Company
ROWEN, Lt. Col. Burt	Air Force Flight Test Center
RUEHLOW, Stanley E.	Office of Chief of Naval Operations
RUNSTAD, Harold J.	Boeing Airplane Company
RUNYAN, Harry L.	NACA - Langley Laboratory
RUSHWORTH, Capt. Robert A.	Air Force Flight Test Center
RUSSELL, Lt. Col. Harold G.	Air Force Flight Test Center
RYAN, Edwin M.	Bureau of Aeronautics
RYAN, John H.	Douglas Aircraft Company, Inc.
RYKER, Norman J., Jr.	North American Aviation, Incorporated
RYLE, Dallas M.	Lockheed Aircraft Corporation
SALTER, Robert M., Jr.	Lockheed Aircraft Corporation
SANDERSON, Kenneth C.	NACA High-Speed Flight Station
SANDOZ, Paul L.	Boeing Airplane Company
SANTI, G. P.	Wright Air Development Center

SCHAMBERG, Richard	RAND Corporation
SCHAUB, Lt. Jerry E.	Air Research and Development Command
SCHLEICHER, Richard L.	North American Aviation, Incorporated
SCHNEIDER, William A.	Stavid Engineering, Incorporated
SCHNITT, Arthur	Bell Aircraft Corporation
SCHOENFELDT, Milt	North American Aviation, Incorporated
SCHOLES, Kenneth M.	North American Aviation, Incorporated
SCHRADER, James H.	NACA - Langley Laboratory
SCHWICHTENBERG, Albert Henry	Lovelace Foundation for Medical Education and Research
SEABERG, Ernest C.	Radio Corporation of America
SEACORD, Charles Lynn	Convair
SEAMAN, Robert W.	Reaction Motors Div., Thiokol Chemical Corp.
SECHLER, Prof. E. E.	NACA Subcommittee on Structures
SEIDMAN, Oscar	NACA Subcommittee on High-Speed Aerodynamics
SELL, Charles L.	North American Aviation, Incorporated
SERRILL, Douglas E.	Boeing Airplane Company
SHAW, Spencer L.	Douglas Aircraft Company, Inc.
SHEWMAKER, Bruce P.	Aerojet-General Corporation
SHORR, Melvin	NACA Subcommittee on Aerodynamic Stability and Control
SIBILA, Alfred Ignatius	Chance Vought Aircraft, Incorporated
SIMON, Dorothy Martin	Avco Manufacturing Corporation
SMELT, Ronald	NACA Subcommittee on High-Speed Aerodynamics
SMITH, Emerson	North American Aviation, Incorporated
SMITH, Robert B.	Douglas Aircraft Company, Inc.
SMITH, William M.	Bell Aircraft Corporation
SMULL, Dr. Thomas L. K.	NACA Headquarters
SORENSEN, Arne	NACA Subcommittee on Structures
SOULÉ, Hartley A.	NACA - Langley Laboratory
SPAULDING, E. H.	NACA Subcommittee on Structures
SPIELBERG, I. N.	Ramo-Wooldridge Corp.
SPRAKER, Wilbur A., Jr.	Battelle Memorial Institute
STAUFFER, W. A.	NACA Subcommittee on Loads
STERNFIELD, Leonard	NACA - Langley Laboratory
STEVENS, Victor I.	NACA - Ames Laboratory
STEVENS, William P.	Radioplane, Div. of Northrop Aircraft, Incorporated
STEVENSON, C. H.	NACA Subcommittee on Structures
STONE, Melvin	Douglas Aircraft Company, Inc.
STOOLMAN, Dr. Leo	NACA Subcommittee on Loads
STORMS, H. A., Jr.	NACA Committee on Aircraft, Missile, and Spacecraft Aerodynamics
SWOFFORD, Maj. Gen. R. P., Jr.	NACA Committee on Aircraft, Missile, and Spacecraft Aerodynamics

TABACK, Israel	NACA - Langley Laboratory
THALE, James S.	Cook Technological Center
THURMOND, James C.	Convair
TIMMONS, Kenneth P. H.	Link Aviation, Incorporated
TINLING, Bruce	NACA - Ames Laboratory
TRENHOLM, John B., Jr.	Air Research and Development Command
TRIPP, Comdr. Jack H.	Office of Chief of Naval Operations
TRUSZYNSKI, G. M.	NACA High-Speed Flight Station
TURNER, Marion J.	NACA Subcommittee on Vibration and Flutter
TYRA, Capt. Thomas D.	Bureau of Aeronautics
UNDERWOOD, William J.	NACA Liaison Officer, Wright-Patterson AFB
UTSCH, Albert	McDonnell Aircraft Corporation
VAIL, Dr. Edwin G.	Wright Air Development Center
VALADE, Charles N.	NACA - Langley Laboratory
VAN EVERY, Kermit E.	Douglas Aircraft Company, Inc.
VENSEL, Joseph R.	NACA High-Speed Flight Station
VOEGELI, Capt. Jack B.	Air Force Special Weapons Center
VOGEL, Alvin R.	Northrop Aircraft, Incorporated
VOGELEY, Arthur W.	NACA - Langley Laboratory
WAGNER, Bruce O.	North American Aviation, Incorporated
WALDO, Robert D.	Aerojet-General Corporation
WALKER, Joseph A.	NACA High-Speed Flight Station
WARNER, Donald D.	Northrop Aircraft, Incorporated
WEBB, Capt. Leland D.	Aircraft Industries Association
WEIL, Joseph	NACA High-Speed Flight Station
WEISMAN, Yale	NACA Subcommittee on Loads
WEISS, Capt. K. E.	Wright Air Development Center
WEISSBERG, Stanley K.	Kearfott Company, Incorporated
WEISSMAN, Clem C.	Office of Naval Research
WESESKY, John L.	Air Force Flight Test Center
WHITE, Alvin S.	North American Aviation, Incorporated
WHITE, Nathan P., Jr.	Sperry Gyroscope Company
WHITE, Capt. Robert M.	Air Force Flight Test Center
WHITLOCK, Dr. C. M.	Convair
WHITNEY, Clair G.	Boeing Airplane Company
WILLIAMS, Walter C.	NACA High-Speed Flight Station
WILLIS, Capt. Richard G.	Wright Air Development Center
WILSON, Herbert A., Jr.	NACA - Langley Laboratory
WILSON, I. J.	North American Aviation, Incorporated
WIMPRESS, John K.	Boeing Airplane Company
WOLFE, Lt. Comdr. John M.	Naval Ordnance Testing Station
WOOD, Clotaire	NACA Headquarters

WOOD, Paul I.	Aerojet-General Corporation
WOODLING, C. H.	NACA - Langley Laboratory
WORTH, W.	Wright Air Development Center
WYSZPOLSKI, Eugene F.	Bureau of Aeronautics

X-15 RESEARCH AIRPLANE DEVELOPMENT STATUS

By L. P. Greene

North American Aviation, Inc.

INTRODUCTION

In the summary paper of the October 1956 conference on the X-15 airplane, it was remarked that "one of the primary reasons for the (X-15) project is to stimulate research." The fact is that much research development has been stimulated, and the purpose of this conference is to present the most pertinent results of the effort which the NACA, NAA, and the military services have jointly put into the project. It would be extremely presumptuous, however, to attempt at this time to summarize the information to be presented in this conference, especially since the individual authors, themselves, have only enough time to "skim off the cream" of the effort which is being reported upon.

Therefore, the purpose of this paper is to try to bridge the gap between the October 1956 conference and the material to be presented in this conference, and to try to orient the various papers to represent a complete research system.

DISCUSSION

To begin with, the October 1956 conference pointed up certain problem areas concerning static and dynamic stability, flutter, aerodynamic heating, materials, structural design and operational usage. Static and dynamic stability about all axes left something to be desired; a relatively new method of analysis through dynamic simulation had been initiated with three-degree-of-freedom solutions and some mechanization to approximate five or six degrees of freedom, but not much assurance was given for the success of this program; flutter phenomena at Mach 3 and above were almost completely unknown and were also subject to the new influences of aerodynamic heating; aerodynamic heating, itself, was beset by inconclusive theories and very little applicable experimental data; some materials had been selected but processing was vague, and although the structural design had progressed well, not more than a handful of samples had been tested; ideas and concepts had been proposed for pilot utilization and survival but deep concern was evident regarding the final outcome.

Today, it can be positively said that through the efforts of all concerned, the development of the X-15 research system has been successfully completed.

Figure 1 represents an inflight view of the airplane as it is now being fabricated in preparation for its final role of flight research which is scheduled to begin in about seven months.

Figure 2 shows a three-view and design brief of the X-15 with its pertinent dimensions and performance. It is to be recalled that the specific design requirements for the airplane were as follows:

(1) To achieve 6,600 feet per second maximum velocity

(2) To be capable of flying to at least 250,000 feet

(3) To have representative areas of the primary structure experience temperatures of 1,200° F

(4) To have some portions of these representative structures achieve heating rates of 30 Btu per square foot per second

It was intended that designing the airplane to these requirements would provide a manned vehicle which would be capable of exploring the spaceflight problems.

The design values for the weight of the X-15 are launching weight of 31,275 pounds and burnout weight of 12,971 pounds, with a usable propellant weight of 18,304 pounds.

The design load factor for the airplane is 7.33 at weights, Mach numbers, and temperatures commensurate with the design missions.

A detailed review of the weight breakdown and the load criteria for the airplane is to be presented in another paper.

The final configuration of the airplane (configuration 3) shown here is compared with the configuration which was presented in the October 1956 conference (configuration 2) in figure 3. Throughout this conference, reference will be made to configuration 2 as the 1956 configuration and configuration 3 as the final one. The changes are summarized as follows:

(1) The side fairings were shortened to improve longitudinal stability.

(2) The horizontal tail was moved 5.4 inches rearward, although the original fuselage location of the hinge line was retained. This

modification moved the hinge line from the 37 percent to the 25 percent mean aerodynamic chord of the exposed horizontal tail. Although flutter requirements dictated the change, this, combined with a 3.6-inch forward wing movement and the side-fairing changes, provided adequate longitudinal stability near zero lift at the maximum Mach number. This low-stability region was referred to as one of the problem areas at the last conference

(3) The vertical tail area was increased to provide adequate directional stability with the speed brakes retracted and a 10° full wedge section was found to be optimum. The plan form was then made nearly symmetrical for dynamic-stability considerations in the exit phase of the mission, since thrust asymmetry considerations in the zero to moderate angle-of-attack range necessitated a reduction in roll due to yaw.

(4) Thrust asymmetry effects also indicated the need for a low value of roll-due-to-yaw control in the low angle-of-attack region. For this purpose, an all-movable directional control was incorporated on the outer span of both the upper and lower vertical tails. Incorporating the control in the lower vertical tail was equally necessary for providing directional control at high angles of attack at high speed because of the ineffectiveness of the upper surface at these conditions. This, in turn, dictated some added complexity in the damper system. In order to obtain adequate ground clearance for landing, the lower directional control panel is jettisoned upon extension of the main landing skids.

(5) In order to avoid compounding flutter problems, the speed brakes were reduced in size and relocated on the inboard or fixed parts of the vertical tails.

The principal wind-tunnel testing planned for the X-15 has been completed, and the aerodynamic characteristics have been obtained throughout the complete Mach number and angle-of-attack range. In general, all of the data presented in this conference are either strictly applicable to this configuration or are distinctly stated otherwise. Specific papers will be given on all aspects of the aerodynamic characteristics including a more complete examination of the items discussed in this paper.

The flutter analysis of the various components of the airplane now shows them to be flutter-free for all design flight regions with more than adequate margin. This statement can now be made in spite of the concern that existed in October 1956 about the flutter possibilities at supersonic speeds. The results of the extensive program conducted to investigate these phenomena are contained in a specific paper on this subject.

A major redirection of the program has been concerned with the carrier airplane for the X-15. In May 1957, the U.S. Air Force requested

North American Aviation, Inc. to study the feasibility of using a B-52 as the carrier for the X-15 airplane instead of the B-36. NACA studies of the maintenance and obsolescence aspects of the B-36 and B-52 airplanes revealed the desirability of changing to a B-52 carrier airplane. In September 1957, Air Force approval was received for this new effort. The X-15 will be mounted under the right wing of the B-52 on a pylon between the fuselage and the inboard engine nacelle as shown in figure 4. Clearance requirements and fuel plumbing of the X-15 necessitated elimination of the inboard flaps of the B-52. A large cutout in the wing trailing edge was also required to accommodate the upper vertical tail of the X-15 airplane.

The flaps-up take-off ground rolls of the B-52 do not appear to be of great concern (being about 11,000 feet on a 100° day at Edwards Air Force Base) and the B-52 has the ultimate structural capability of carrying approximately 65,000 pounds of weight in this location. The 31,275-pound X-15 airplane, therefore, does not seriously tax the B-52 wing structure.

One item which caused considerable concern in the early evaluation was the fact that in this installation, the pilot could not enter the X-15 in flight as had been possible in the B-36. This limitation was of concern from both the fatigue and safety aspects; however, the time from take-off of the B-52 to launching of the X-15 is about $1\frac{1}{2}$ hours, and considerable effort has been expended in plans for making the pilot comfortable during this time. In the event of an emergency, the configuration permits the pilot to eject safely while the X-15 and B-52 are still connected.

Wind-tunnel tests have been conducted to determine the static aerodynamic parameters of both the X-15 and the B-52 (and their mutual interferences), the launching characteristics of the X-15, the flutter characteristics of the B-52 with the X-15 installations, and also the B-52 buffet tendencies. No serious problems are expected in these areas. The effect of B-52 engine noise on the X-15 structure, however, during ground run-up and take-off has been shown to be a problem. Empennage components have failed after 5-minute exposure to simulated B-52 engine noise, and no solution has been reached as yet. Further discussion of these subjects are to be given in subsequent papers.

Next, a very superficial examination of some of the subsystems which make up the air vehicle is appropriate. The inboard profile of the airplane is shown in figure 5, wherein the major compartments are denoted. The intent here is to call attention to areas which will be more completely discussed in subsequent papers and to show how they compliment each other. The reaction-control rocket nozzles are located in the nose for the pitch and yaw attitude control. The reaction controls for roll

are located in the wing tip. Dual systems have been provided. Another paper reports on some aspects of the reaction controls and on the design and operation of the APU (auxiliary power unit).

The pilot's compartment and equipment bay shown in figure 6 are in a single sealed and insulated compartment, the environmental control of which warrants some discussion. The pilot has been provided with an ejection seat which is fin and shock-wave generator stabilized and in which the pilot is restrained against high load factors at the various points on his body. He is also provided with a full pressure (MC-2) suit which affords very good protection, yet imposes minimum restrictions on pilot mobility. The pilot's working area also has been given careful design with regard to the primary flight instruments, switches, the aerodynamic and reaction controllers, and pilot protection. All major components which have a primary effect on the pilot and his performance have been coordinated into an integrated system which is reported upon in detail in another paper. Furthermore, the physiological and psychological aspects which will be investigated in the X-15 program are discussed.

Figure 7 presents a view of the actual forward fuselage as well as a typical propellant tank which forms the main portion of the center fuselage. This particular tank will bear considerable scrutiny in papers dealing with the propellant system, structural design criterion and testing, material selection, and development of welding techniques, as well as the forming and manufacturing of the actual tanks.

One of the intricate points in the structural design has been the attachment of the wing and fuselage, especially since the main spar attachments have to be made to the integral-tank part of the fuselage. Figure 8 shows the actual wing in the construction jig and shows the root (A frame) attachments to the fuselage. The leading edges of the Inconel-X wing can be subjected to 2,100° F (well beyond the design value of 1,200° F) while nonload-bearing Inconel-X skin panels just rearward of the leading edge also have been satisfactorily tested to 1,800° F. Also shown in this figure is a panel of the horizontal stabilizer with instrumentation installed. This surface provides both a roll and pitch control and is supported by a spindle-type arrangement which has been the subject of considerable examination of flutter characteristics.

The engineering design considerations of the hydraulic system powering the horizontal- and vertical-tail control surfaces, the speed brakes, and the landing flaps will also be presented.

The rearward fuselage assembly shown in figure 9 provides the basic structure to which the horizontal tail panels, vertical tail, speed-brake panels, and main landing skids are attached. Details on the unique

landing-gear design are included in a paper on that subject. The aft fuselage also houses the rocket engine. Hydrogen peroxide is stored in the rearward fuselage compartment to power the rocket-engine turbopump, through which the desired rocket-engine chamber pressure is to be achieved.

An important redirection of the X-15 program in recent months is concerned with the status of the XLR99 engine, which will be completely discussed in a separate paper.. It is important to point out at this time that difficulties have been encountered in the development in the XLR99 thrust chamber. As a result of the associated delay, first flights of the Number 1 and Number 2 airplanes will be made with the interim engine (fig. 2) installation of two Reaction Motors XLR11-5 engines. The total of eight thrust chambers per airplane will deliver a thrust at 40,000 feet of 16,380 pounds.

The speed-altitude envelope of the X-15 when powered in its interim configuration by two Reaction Motors XLR11-5 engines is shown in figure 10. It will be noted that a maximum Mach number of approximately 4.0 can be achieved at approximately 100,000 feet. Maximum altitudes of around 180,000 feet can be achieved during the coasting phase of the flight testing.

The schedules of the phase of responsibility for the airplane assumed by North American Aviation, Inc. are shown in figure 11. The contract was initiated in December 1955, and a 2-year basic design period was spent prior to engineering release in December 1957. The major fabrication period has taken a 9-month period up to the present date. Approximately 3 months are expected to be required to make the major subassemblies and install the necessary equipment.

The airplane is scheduled to be delivered to the flight tests activity fully instrumented and put into test by November of this year for a 3-month period of instrumentation checkout, calibration ground testing, and captive flight tests of the various subsystems. Contractor type flight testing with the two RMI XLR11-5 engines is scheduled to start next February for an approximate 7 month period, after which installation of the XLR99 will be made. The second and third airplanes will be available at approximately the same time as the Number 1 airplane with the XLR99 engine. It is intended that the third vehicle will be delivered with the XLR99 engine installed.

In the discussion thus far, the individual subsystems which go together to make the research vehicle have been reviewed. Attention is now directed to the broad aspects of the whole research system which the NACA will ultimately operate. This system includes the carrier, the air vehicle, the support, and the research instrumentation.

The general features of the flight profiles of the airplane and the range through which the airplane is designed to fly are shown in figure 12. The B-52 carrier will operate out of Edwards Air Force Base and will fly to a drop area near Wendover, Utah, depending on the mission.

The airplane will be tracked by radar stations located at Ely and Beatty, Nevada, and at the NACA High-Speed Flight Station at Edwards. The details of this tracking range, called "High Range," are covered in another paper.

On the maximum performance missions, the airplane would be launched approximately midway between Wendover, Utah, and the Ely station. The X-15 will "light up" at an altitude of approximately 35,000 feet and a Mach number of 0.75. During the 88 second thrusting phase of the X-15 flight, the airplane will be accelerated to a velocity of 6,340 feet per second for the design altitude mission and 6,600 feet per second for the design speed mission. In the zero-lift coast after burnout, the airplane will reach a peak altitude of 250,000 feet on the altitude mission and 130,000 feet on the speed mission. Reentry into the atmosphere can be accomplished at altitudes as high as 115,000 feet by use of maximum available airplane lift. When the airplane is deliberately permitted to fall further into the atmosphere, a 7.33g pull-out at a dynamic pressure of 2,500 lb/sq ft could be experienced at an altitude as low as 65,000 feet. The time at which these recoveries are made is approximately 300 seconds after launch. Total free-flight time of the X-15 will be approximately 25 minutes with a maximum range of 400 nautical miles.

The performance and operational aspects of the stable platform system which will provide the pilot with inertial velocity, altitude, and angular information, as well as other aspects of the instrumentation, are to be discussed separately.

The techniques and characteristics associated with the landing phase of the flight are also to be presented in another paper.

The numbers quoted herein have represented values for the missions which were defined to give the contractor a firm basis for the design. They were intended to be typical, but it must be realized that there are numerous alternate missions which may and will be flown. Since the design and development phase of this program is now complete, the contractor and the staff of the NACA High-Speed Flight Station are engaged in analyses of various types of alternate missions. The contractor's part of this program is to evaluate the many possible missions in the light of the air vehicle's ability to operate under the prescribed environment.

The general features of the flight profiles of the airplane and the range through which the airplane is designed to fly are shown in figure 12. The B-52 carrier will operate out of Edwards Air Force Base and will fly to a drop area near Wendover, Utah, depending on the mission.

The airplane will be tracked by radar stations located at Ely and Beatty, Nevada, and at the NACA High-Speed Flight Station at Edwards. The details of this tracking range, called "High Range," are covered in another paper.

On the maximum performance missions, the airplane would be launched approximately midway between Wendover, Utah, and the Ely station. The X-15 will "light up" at an altitude of approximately 35,000 feet and a Mach number of 0.75. During the 88 second thrusting phase of the X-15 flight, the airplane will be accelerated to a velocity of 6,340 feet per second for the design altitude mission and 6,600 feet per second for the design speed mission. In the zero-lift coast after burnout, the airplane will reach a peak altitude of 250,000 feet on the altitude mission and 130,000 feet on the speed mission. Reentry into the atmosphere can be accomplished at altitudes as high as 115,000 feet by use of maximum available airplane lift. When the airplane is deliberately permitted to fall further into the atmosphere, a 7.33g pull-out at a dynamic pressure of 2,500 lb/sq ft could be experienced at an altitude as low as 65,000 feet. The time at which these recoveries are made is approximately 300 seconds after launch. Total free-flight time of the X-15 will be approximately 25 minutes with a maximum range of 400 nautical miles.

The performance and operational aspects of the stable platform system which will provide the pilot with inertial velocity, altitude, and angular information, as well as other aspects of the instrumentation, are to be discussed separately.

The techniques and characteristics associated with the landing phase of the flight are also to be presented in another paper.

The numbers quoted herein have represented values for the missions which were defined to give the contractor a firm basis for the design. They were intended to be typical, but it must be realized that there are numerous alternate missions which may and will be flown. Since the design and development phase of this program is now complete, the contractor and the staff of the NACA High-Speed Flight Station are engaged in analyses of various types of alternate missions. The contractor's part of this program is to evaluate the many possible missions in the light of the air vehicle's ability to operate under the prescribed environment.

Perhaps the most serious unknown area reported in the October 1956 conference was in the field of aerodynamic heating. However, much progress has been made in the specific X-15 model testing with the 1/15-scale heat-transfer pressure distribution model shown in figure 13. Heat-transfer data have been obtained in the Langley Unitary Plan wind tunnel at Mach numbers of 2.88 and 4.65 and recently in the Arnold Engineering Development Center B-minor wind tunnel at a Mach number of 7.0. The AEDC installation is shown in figure 13. It will be noted that the model is initially surrounded by "shoes" to keep it cool until the tunnel flow is established. The shoes are then retracted, and the model is exposed to large differential temperatures whereby potentially more accurate heat-transfer data are available.

Because so much was to be learned, it is not surprising that there are still some inconclusive concepts in this field. Papers will be presented on the correlation of theory and experiment and on the effects of experimental results on the anticipated skin temperatures of the actual air vehicle. It will be one of the primary objectives of the flight research program to obtain correlation with these data. Therefore, the contractor's present program has now been directed to the evaluation of the limiting temperature conditions to be expected in off-design missions.

As time has progressed during the design of the X-15, analog simulators with varying degrees of sophistication have been used to evaluate the airplane (fig. 14). Currently full six-degree-of-freedom simulators are being used at Langley, Johnsville, and Los Angeles. With the exception of the incorporation of the centrifuge in the Johnsville installation, these simulators differ only in the speed range covered.

Actual pilot instruments and controllers, actual primary flight control hardware, and the very latest aerodynamic parameters are incorporated. The Los Angeles installation can give speed simulation from launch to landing. The capability of the entire simulator has recently been expanded to include airplane skin-temperature prediction from approximately 15 critical locations on the airplane.

The load factors to which the pilot will be subjected have been of great interest as regards whether or not ±4g axial acceleration combined with, say, 7.33g normal acceleration will impose additional limitations on the operational flight envelope. Centrifuge testing at the Johnsville facility has shown that no additional limits are imposed. This tool is now being used to obtain an allowable flight operating envelope where all the transient parameters are taken into account. North American Aviation, Inc. considers the establishment of such an envelope to be their obligation to the USAF and NACA so that the X-15 can really be used to explore space quickly and safely.

The operating flight envelope of the X-15 airplane with full burning is shown in figure 15. The envelope is limited by the basic structural design dynamic pressure of 2,500 lb/sq ft. It is modified at altitudes lower than 30,000 feet to 1,600 lb/sq ft for maximum structural maneuvers. The shaded area of the curve represents the attainable combinations of speed and altitude for 88 seconds of burning at full thrust. The left-hand side of the shaded area has been established as the speed and altitude combination encountered in the thrusting phase of a vertical ascent mission. The coasting speeds after burnout, at approximately 250,000 feet, are shown in the upper part of the curve. Flights into the unshaded "island" at low dynamic pressures have not been defined as yet, but these will primarily be determined by coasting after partial throttle or short burning times.

This figure indicates that altitudes as high as 700,000 feet can be accomplished for the design weight and engine performance conditions. The peak altitude of practical importance is approximately 600,000 feet, being primarily influenced by the dynamic stability characteristics at high angles of attack, the heating rates and structural temperatures, and the pilot tolerance of the sustained load factors imposed.

Pertinent aerodynamic stability and heating data have been obtained at Mach number 6.86 up to angles of attack of only 20°, and estimates have been made up to angles of attack of 35°. Another model has been fabricated for the purpose of evaluating the estimates. This model should provide test data from 30° to 55°. These data will be used to formulate a more exact estimation of the maximum permissible altitude.

These studies are providing a definition of the flight regimes where the handling qualities and structural temperatures of the airplane can be described as satisfactory for flight research. In the last paper of the conference, the "Flight Research Objectives of the X-15 Airplane" will be described, indicating how the airplane will actually be put into the NACA flight test program, the research goals, and how they will be achieved.

The X-15 research vehicle has progressed through a $2\frac{1}{2}$ year development period. A tremendous amount of experience has been obtained in hypersonic aerodynamics, in structural design at elevated temperatures and also in material fabrication for these temperatures. On the basis of this experience, it appears that:

(1) The design velocity of 6,600 feet per second can be achieved, although success in this area will be largely determined by the accelerated development work that is now being conducted with the XLR99 engine.

(2) Predicted airplane handling qualities or skin temperatures are not expected to limit the achievement of the maximum speed capability of the airplane.

(3) The design altitude of 250,000 feet can easily be attained.

(4) The structure can be heated to the desired temperature of 1,200° F without significant structural distortion and a heating rate of 30 Btu per square foot per second can be tolerated.

As a result of these conclusions, it has been mutually agreed by all concerned that the X-15 air vehicle can be successfully used to extend our manned flight experience to approximately Mach number 7.0 in the near future. As in the past, studies are being conducted to explore the possibilities of extending the X-15 research capability beyond that point.

X-15 RESEARCH AIRPLANE

Figure 1

THREE VIEW

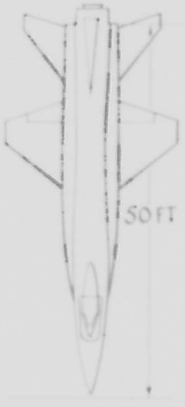

PERFORMANCE -	MAX VELOCITY	6,600 FT/SEC
	DESIGN ALTITUDE	250,000 FT
	LANDING SPEED	164 KTS
POWER PLANT RMI -	INTERIM (TWO XLR11-5)	
	MAX THRUST	16,380
	BASIC (XLR99-RMI)	
	MAX THRUST	57,000
	MIN THRUST	17,000
WING -	AREA	200 SQ FT
	SWEEP C/4	25 DEGREES
	THICKNESS	5 PERCENT
	ASPECT RATIO	2.5
WEIGHT -	LAUNCHING	31,275 LB
	BURN-OUT	12,971 LB
	PROPELLANT (USABLE)	18,304 LB

Figure 2

REVISED CONFIGURATION

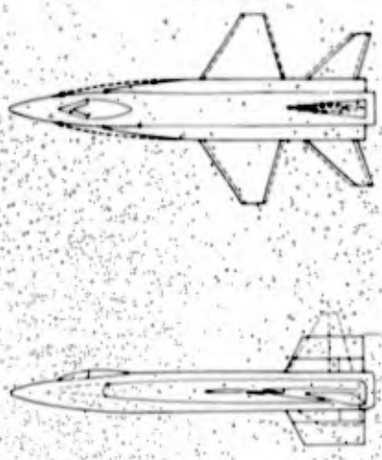

CONFIGURATION 2
— CONFIGURATION 3

- LONGITUDINAL
  - MOVED WING FORWARD 3.64 IN.
  - MOVED TAIL REARWARD 5.4 IN.
  - SHORTENED SIDE FAIRINGS
- LATERAL-DIRECTIONAL
  - VERTICAL TAIL MADE NEARLY SYMMETRICAL
  - VERTICAL AIRFOIL SECTION MADE A 10° SINGLE WEDGE
  - DIRECTIONAL CONTROLS LOCATED ON UPPER AND LOWER VERTICALS
  - SPEED BRAKES RELOCATED IN FIXED VERTICAL TAILS

Figure 3

X-15/B-52 INSTALLATION

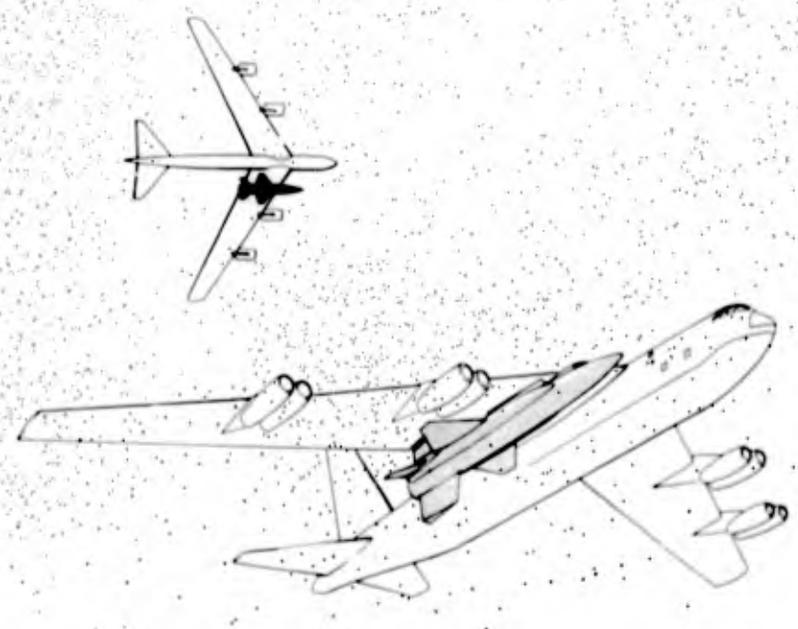

Figure 4

INBOARD PROFILE

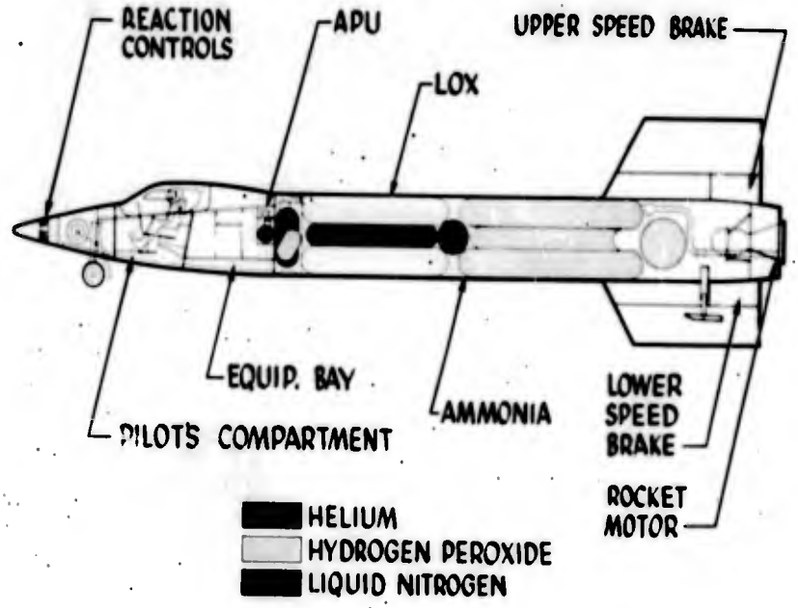

Figure 5

PILOT CONSIDERATIONS

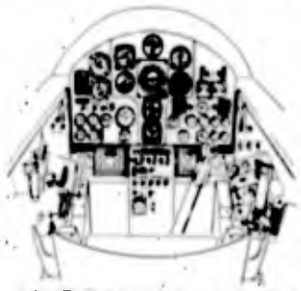

WORKING AREA

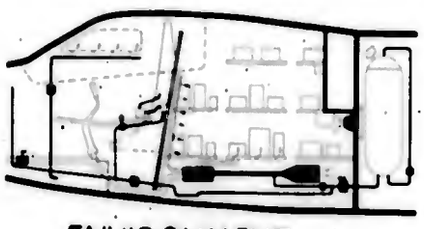

ENVIRONMENT

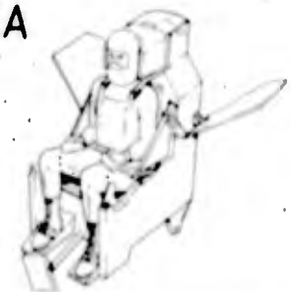

RESTRAINT & ESCAPE

Figure 6

FORWARD FUSELAGE & TANK

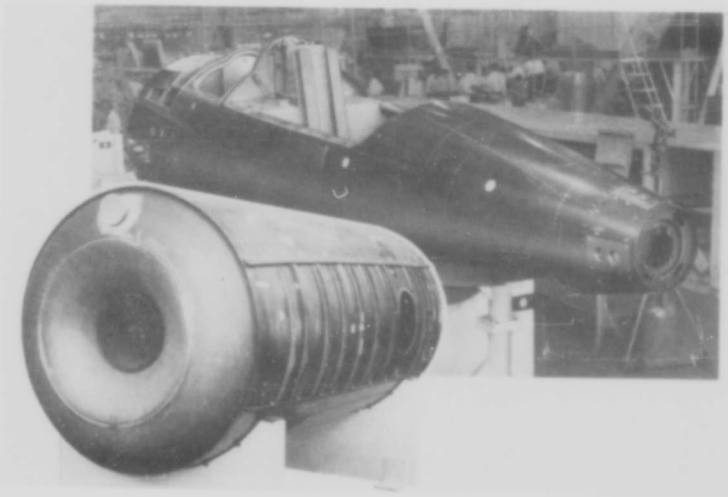

Figure 7

HOR STABILIZER AND WING

Figure 8

AFT FUSELAGE & VERTICAL STABILIZER

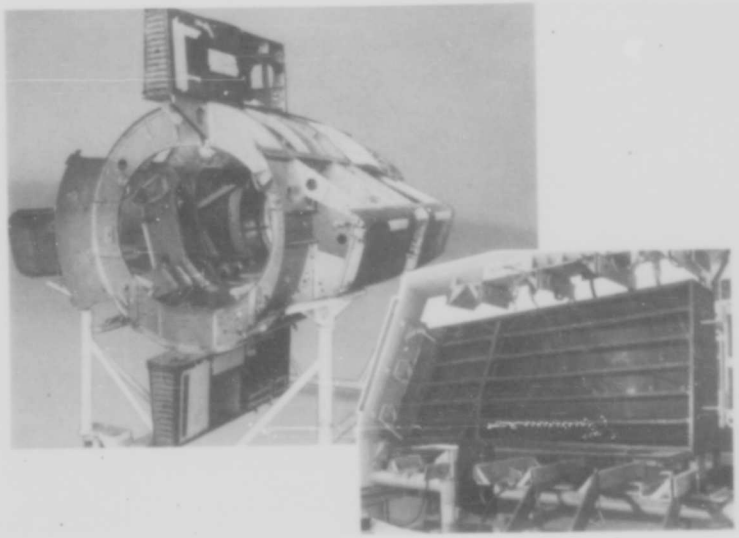

Figure 9

SPEED-ALTITUDE ENVELOPE
TWO RMI-XLR 11-5 ENGINES

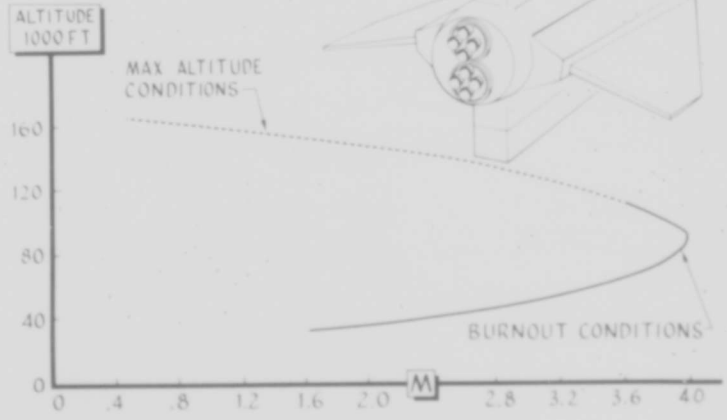

Figure 10

SCHEDULES

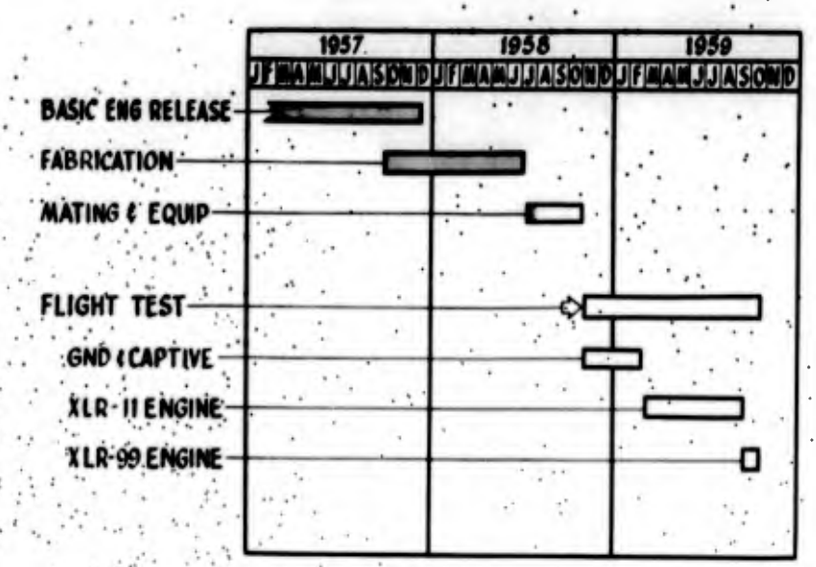

Figure 11

X-15 RESEARCH SYSTEM
TYPICAL MISSION

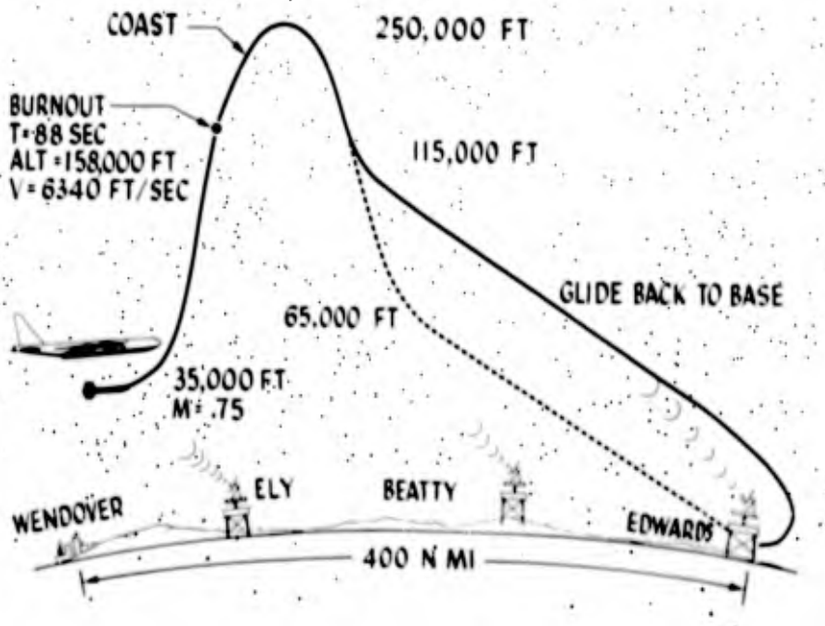

Figure 12

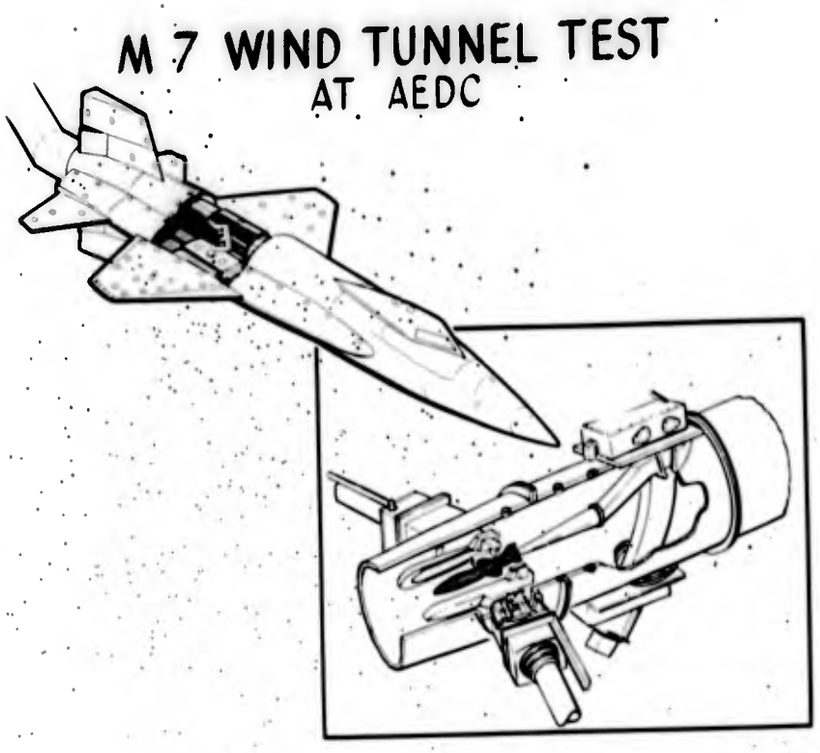

Figure 13

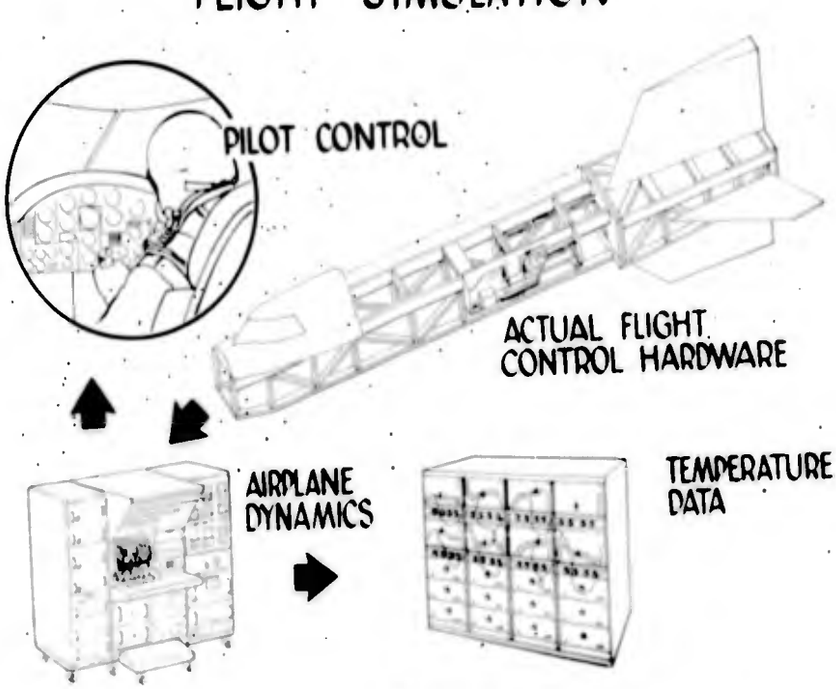

Figure 14

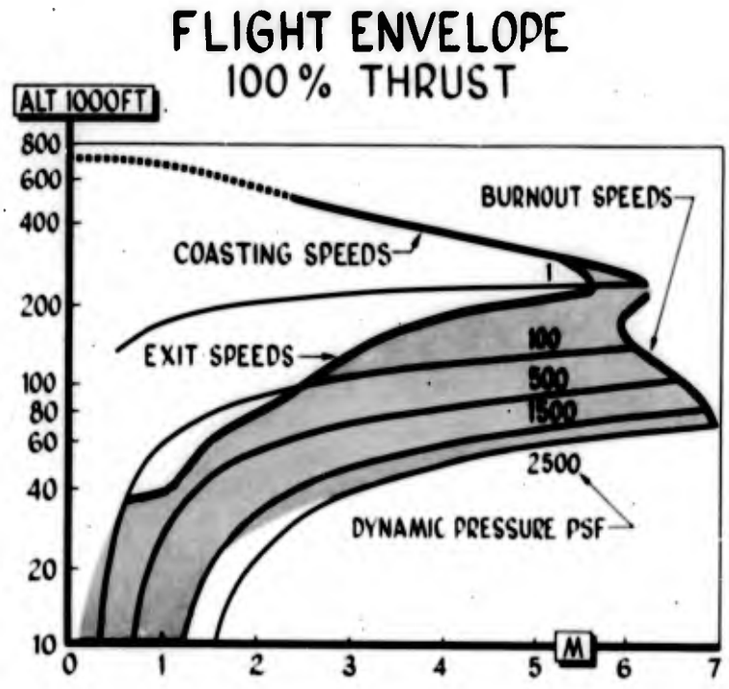
FLIGHT ENVELOPE
100% THRUST
ALT 1000FT
800
600
400
200
100
80
60
40
20
10
0
1
2
3
4
5
6
7
M
BURNOUT SPEEDS
COASTING SPEEDS
EXIT SPEEDS
1
100
500
1500
2500
DYNAMIC PRESSURE PSF

Figure 15

HIGH-SPEED STATIC STABILITY CHARACTERISTICS OF THE X-15 AIRPLANE

By Jim A. Penland and David E. Fetterman, Jr.

NACA Langley Aeronautical Laboratory

INTRODUCTION

At the time of the last conference on the X-15 Project in 1956, the configuration had been found to be aerodynamically deficient in several important regions. Both the longitudinal and directional stability were inadequate in the high Mach number region. The directional control parameter $C_{n_{\delta v}}$ approached zero at 20° angle of attack, an angle well within the contemplated flight attitude regime. The roll due to sideslip C_{l_β} and the roll due to yaw control $C_{l_{\delta v}}$ were large at near-zero angles of attack due to vertical-tail geometry. This configuration, which was designated configuration 2, is shown on the left of figure 1. Since the 1956 conference, the configuration has gone through a series of changes and appears as configuration 3 on the right of this figure.

SYMBOLS

C_m pitching-moment coefficient about center of gravity, $\frac{\text{Pitching moment}}{qS\bar{c}}$

C_n yawing-moment coefficient about center of gravity, $\frac{\text{Yawing moment}}{qSb}$

C_l rolling-moment coefficient about center of gravity, $\frac{\text{Rolling moment}}{qSb}$

C_L lift coefficient, $\frac{\text{Lift}}{qS}$

$\frac{\partial C_m}{\partial C_L}$ rate of change of pitching moment with lift coefficient

$$C_{n_\beta} = \frac{\partial C_n}{\partial \beta}$$

$$C_{l_\beta} = \frac{\partial C_l}{\partial \beta}$$

$$C_{n_{\delta v}} = \frac{\partial C_n}{\partial \delta_v}$$

$$C_{l_{\delta v}} = \frac{\partial C_l}{\partial \delta_v}$$

$$C_{n_{\delta h'}} = \frac{\partial C_n}{\partial \delta_{h'}}$$

$$C_{l_{\delta h'}} = \frac{\partial C_l}{\partial \delta_{h'}}$$

α angle of attack, deg

α_{trim} angle of attack at trim, deg

β angle of sideslip, deg

δ_h horizontal-tail deflection, deg

$\delta_{h'}$ differential horizontal-tail deflection, deg

δ_v vertical-tail deflection, deg

δ_b speed-brake deflection, deg

S wing area

$\bar{c}$ mean aerodynamic chord of wing

b wing span

q free-stream dynamic pressure

M free-stream Mach number

CONFIGURATION CHANGES

Details of the two configurations of the X-15 airplane are shown in figure 2, where configuration 2 is represented by the dashed lines and configuration 3 by the solid lines. The configuration changes that directly contribute to the variation of the longitudinal stability characteristics are the reduced length of the side fairings, the forward shift of the wing, the rearward shift of the horizontal tail, the increased size of the vertical tails, and the 10-inch forward shift of the center of gravity.

Changes that affect the lateral-directional stability characteristics are the increased area of the vertical tails from 50 square feet to 75 square feet, the use of full 10° included-angle wedge airfoils for the vertical tails in place of the double-wedge airfoils, and redistribution of the area to 55 percent for the dorsal fin and 45 percent for the ventral fin instead of the original 73 percent and 27 percent, respectively, on configuration 2. The selection of these particular tail areas and wedge airfoil sections was made on the basis of obtaining the needed directional stability with a minimum of weight and a minimum drag penalty.

In addition to the improved airfoil section and an increase in area, the directional control was altered by a redesign of the control surfaces. On configuration 2 only the upper vertical tail was controllable, the lower remaining fixed (fig. 2). Directional controls designed for configuration 3 consist of the outer panels of both upper and lower vertical tails. The inside portion of each tail is fixed and supports the speed brakes. These upper and lower controls are nearly symmetrical and operate together at all times except in landing, at which time the lower movable control is jettisoned to allow ground clearance.

LONGITUDINAL STABILITY

One of the major adverse stability characteristics of configuration 2 was the decrease of longitudinal stability with increasing Mach number. This deficiency is shown in figure 3, where the trim angle of attack for the exit and approximate reentry conditions and the static margin $\partial C_m/\partial C_L$ at trim are shown for the design flight Mach number range. The curves in this figure and all following figures represent faired experimental data unless otherwise specified. During the exit or powered part of the X-15 flight after the initial pull-up, it is proposed that the pilot will attempt to fly at essentially zero angle of attack. Since the powered phase of the flight will be quite

complicated from the pilot's standpoint, the airplane should have good flight characteristics at low angles of attack.

The stability of configuration 2 with zero horizontal-tail and speed-brake deflection was unsatisfactory since the static margin decreased to zero at the peak test Mach number of almost 7. Configuration 3 has improved stability throughout the Mach number range as compared with configuration 2 for $\delta_h = 0^\circ$, but due to the related loss in horizontal-tail lift effectiveness with increasing Mach number, there is still a gradual decrease in stability in the supersonic speed range. These data are for a center-of-gravity location at 20 percent of the mean aerodynamic chord, and therefore show only the effects of the configuration changes. The stability of configuration 2 would appear even worse with its original center-of-gravity location of $0.25\bar{c}$. This improved longitudinal stability of the final design is due primarily to the decrease in length of the side fairings. This fairing modification was made possible by a redesign of the plumbing and wiring in and around the cockpit area.

During the reentry phase of the flight program high angles of attack will be intentionally encountered; furthermore, during the exit phase high angles of attack can also be encountered.

Shown also in figure 3 is the stability that might be expected for configuration 3 at a high angle of attack. The static margin for trim with a horizontal-tail deflection equal to -20° is shown by the dashed curve for the speed brakes closed and the dashed-dot curve for the brakes deflected 35°. The curves of trim angle of attack correspond to the trimmed stability curves. For the condition of retracted speed brakes $(\delta_b = 0^\circ)$ there is a marked increase in the longitudinal stability in the high Mach number range with no loss in stability at lower Mach numbers. For the constant $\delta_h = -20^\circ$ it may be seen that the trim angle of attack, which is relatively constant at high Mach numbers, decreases considerably at lower Mach numbers. The deflection of the speed brakes to their maximum of 35° decreases the stability somewhat at the peak Mach number due to the resulting reduction of the trim angle of attack, as seen in the upper portion of figure 3.

A more detailed study of the pitching-moment variations with angle of attack for configuration 3 is shown in figure 4. The pitching moment C_m about $0.20\bar{c}$ is plotted against angle of attack α for various elevator deflections δ_h from 0° to -35°. It should be noted that the stability decreases with increasing Mach number at low values of α and that the curves become increasingly nonlinear with increasing Mach number. The marked nonlinearities at the peak Mach number at low angles of attack are caused by the wing-wake impingement on the horizontal tail and those at moderate angles of attack by the increased

dynamic-pressure field over the horizontal tail. For a given elevator deflection, such as $\delta_h = -20^\circ$, the trim angle of attack decreases with Mach number, being near 23° at $M = 6.86$ and decreasing to about 10° at the lower Mach numbers. This airplane has the capability of trimming at an angle of attack of 32° at the peak Mach number, with the maximum elevator deflection of -35°.

LATERAL-DIRECTIONAL STABILITY

The effects of the design alterations on the lateral and directional stability parameters, which are presented in the body-axis system, will now be discussed. The characteristics of the 1956 configuration 2 are illustrated in figure 5, which presents the directional-stability parameter C_{n_β} and the effective dihedral C_{l_β} for the flight Mach number range. Curves are shown for horizontal-tail deflections of 0° for configuration 2 and 0° and -20° for configuration 3 with the speed brakes retracted and deflected to 35°. The data presented for configuration 2 are for the upper and lower speed brakes extended 5° and 7.5°, respectively, thereby making the airfoil sections full wedges. This figure illustrates the insufficient directional stability of configuration 2 at $\delta_h = 0^\circ$, which decreased with increasing Mach number to zero at a Mach number of 7, and the large amount of roll due to sideslip, or positive dihedral effect, which presents a stability problem during the exit phase, as discussed by Lawrence P. Greene. This lack of directional stability was caused by insufficient vertical-tail effectiveness, and the large amount of roll due to sideslip was caused by the nonsymmetrical area distribution between the upper and lower vertical tails. Although the actual values of C_{l_β} are small, they have been shown by simulator tests to have an appreciable effect. The curve for configuration 3 shows, as expected, that the directional stability was increased by the modification in the vertical tail - in fact, at low angles of attack (that is, where $\delta_h = 0^\circ$) where the flow fields about the tail are known, the change in effectiveness is well predicted. Furthermore, the directional stability improves at high trim angles of attack $(\delta_h = -20^\circ)$ and is further increased by deflecting the speed brakes 35°. The extension of the speed brakes in effect increases the wedge angle of the vertical tails and thereby increases their effectiveness.

On the lower portion of figure 5 it may be seen that a reduction of the dihedral effect C_{l_β} at low angles of attack has been accomplished, as intended, by the design of the nearly symmetrical vertical tails. The effective dihedral at zero lift has been reduced to small values throughout the Mach number range, thus satisfying the specification of good static stability at low angles of attack during the exit

phase. As expected, this symmetrical tail arrangement was not without disadvantages, for at high trim angles of attack the large lower vertical tail operating in the high-dynamic-pressure region behind the bow shock from the fuselage causes a large and undesirable negative-dihedral effect $\left(\text{positive } C_{l_\beta}\right)$ throughout the high-angle-of-attack reentry, and this condition is further aggravated by deflecting the speed brakes.

DIRECTIONAL CONTROL

The directional control is presented in figure 6. The yaw due to yaw control is shown at the top of this figure and the roll due to yaw control at the bottom. Both are plotted against Mach number for $\alpha = 0^\circ$ and 20° with zero horizontal-tail deflection. The solid line for configuration 2 on the upper portion of figure 6 shows that it had adequate directional control at an angle of attack of 0°, but this decreased greatly at an angle of attack of 20°, as shown by the dashed line, and approached zero at the peak design Mach number. This was due to the characteristic loss in effectiveness at high Mach numbers of the upper vertical tail, the only movable surface, with increasing angle of attack. The lower portion of figure 6 shows another adverse characteristic caused by the fact that the upper vertical tail was the only movable control; that is, the large amount of roll due to yaw control for configuration 2 at an angle of attack of 0°. This effect is reduced to small values at an angle of attack of 20°. The curves presented for configuration 3 with the enlarged symmetrical vertical tails show that the directional control has been improved, especially at the higher angles of attack, there now being little difference between results for angles of attack of 0° and 20° throughout the high speed range. This is due to the movable lower vertical tail, which increases in effectiveness with increasing angle of attack at the same time that the upper vertical tail loses effectiveness. At the bottom of figure 6 is seen a reduction of the roll due to yaw control to the usual small positive values at 0° angle of attack which, like the effective dihedral, was particularly desirable during the exit phase. However, as expected, the roll due to yaw control increased to large negative values at an angle of attack of 20°.

The directional control and the effects of the speed brakes at trim for configuration 3 are presented in figure 7. A comparison of these data at trim with those in figure 6 shows that the elevator deflection and speed-brake extension have only a secondary effect on either yaw or roll due to yaw control. The directional control at trim remains at essentially the same high level and the roll due to yaw control at high trim angles of attack shows the same trend as in figure 6, namely, an excess of roll due to yaw control. This effect is reduced somewhat with speed-brake deflection. This excess of roll due to yaw control

presents a problem of stability and control that has been studied on the flight simulator. These characteristics have been responsible for some of the complexities of the damper system.

LATERAL CONTROL

The rolling tail effectiveness at trim is shown in figure 8 for configuration 2 at high Mach numbers for a mean deflection of $\delta_h = 0^\circ$ and for configuration 3 throughout the flight Mach number range for mean deflections of $\delta_h = 0^\circ$ and -20°. The roll and yaw due to differential tail deflection are shown plotted against Mach number. There were no configuration changes made to alter the lateral control, and therefore little change is seen between configurations 2 and 3. The positive values of $C_{l_{\delta h}}$, are normal and indicate good effectiveness, needed particularly for control at the high speeds and high angles of attack, and at low landing speeds. The small positive values of $C_{n_{\delta h}}$, for a mean deflection of $\delta_h = 0^\circ$ indicate good response and slight favorable yaw; that is, the plane will yaw in the direction in which it is being rolled.

The increase of yaw due to lateral control at the higher trim angles of attack shown on the curve for a mean deflection of $\delta_h = -20^\circ$ again presents a slight problem, inasmuch as this parameter should be small for all angles of attack. This increase in yaw due to lateral control at the higher angles of attack is caused by an increase in pressure on the side of the vertical tail on which the leading edge of the horizontal tail is deflected downward and the increase in drag due to this deflection.

LIFT AND DRAG

Although these several configuration changes have considerable effect on the stability, they have very little effect on the variation of lift with angle of attack or with Mach number, and the lift-curve slopes at $\alpha = 0^\circ$ remain unaltered from configuration 2 to configuration 3. The enlarged wedge-airfoil vertical tails have increased the overall drag for configuration 3 by about 10 percent, as expected, throughout the Mach number range.

CONCLUDING REMARKS

It can be seen that the modifications in the configurations since the last conference have given the X-15 the desirable static longitudinal and directional characteristics required at low angles of attack for the exit phase of the trajectory. Furthermore, at high angles of attack the latest configuration has good longitudinal characteristics as well as a reasonable amount of directional stability and control. However, the large lower tail has caused some undesirable lateral stability and control characteristics at these high angles of attack. The significance of these characteristics have been determined by means of flight simulator tests. The results of some of these simulation tests based on these data are presented in subsequent papers.

X-15

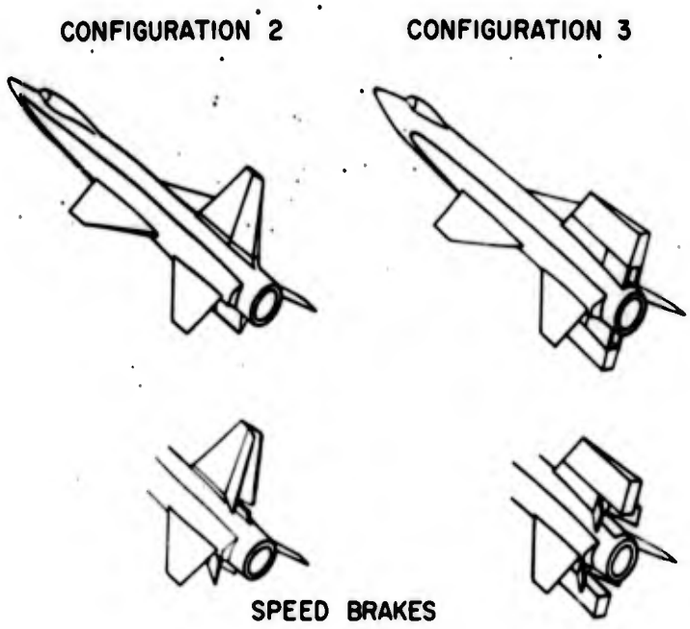

Figure 1

X-15

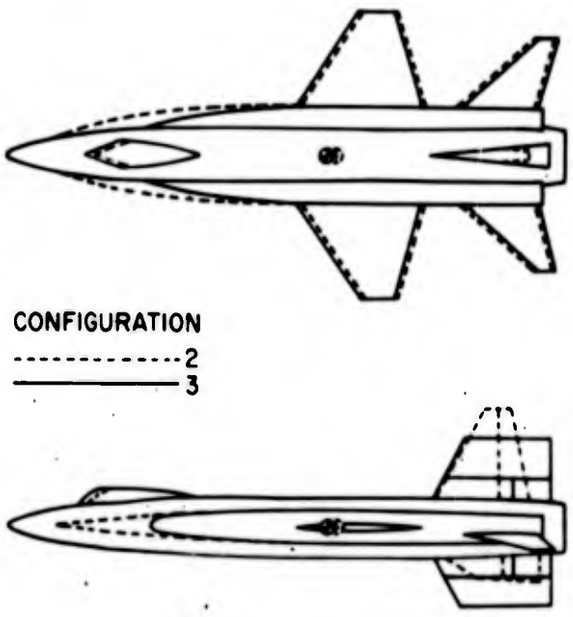

Figure 2

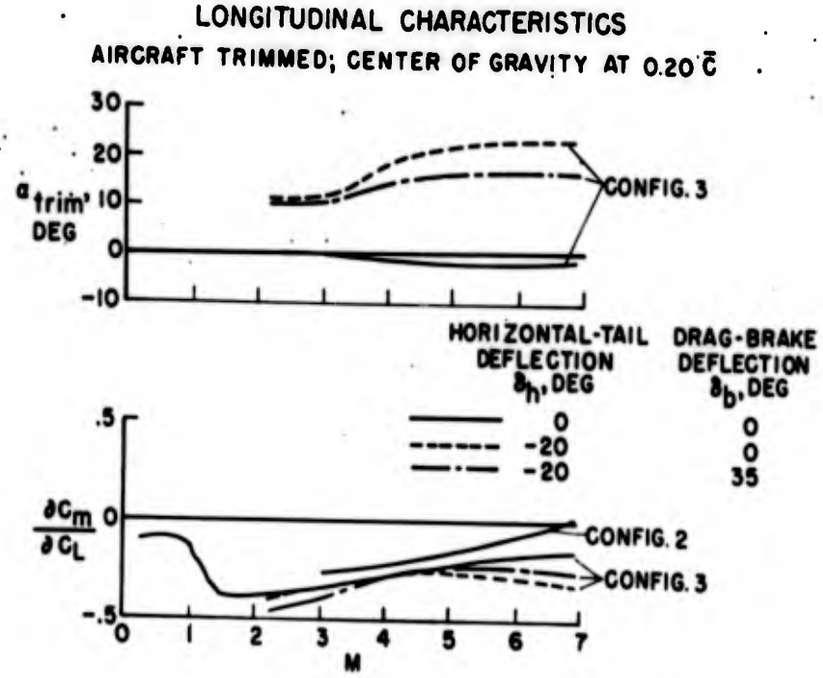

Figure 3

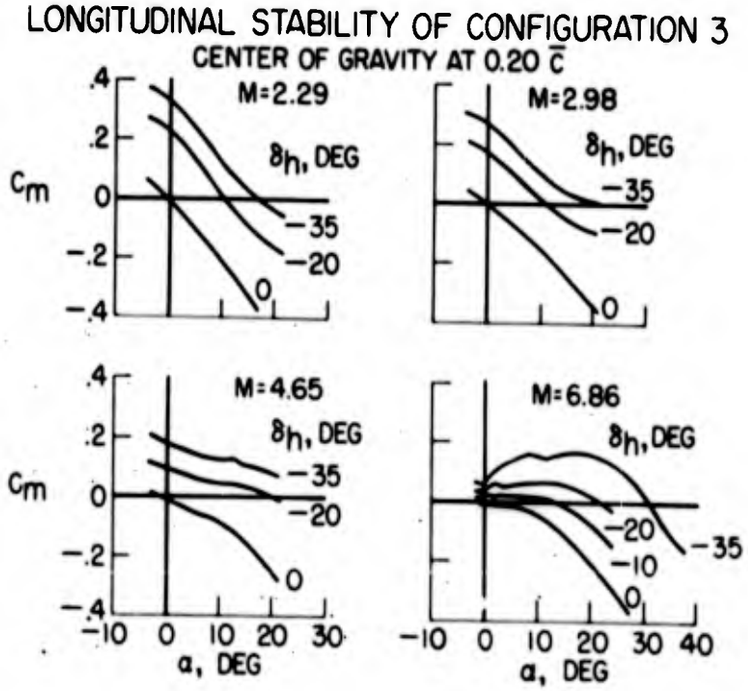

Figure 4

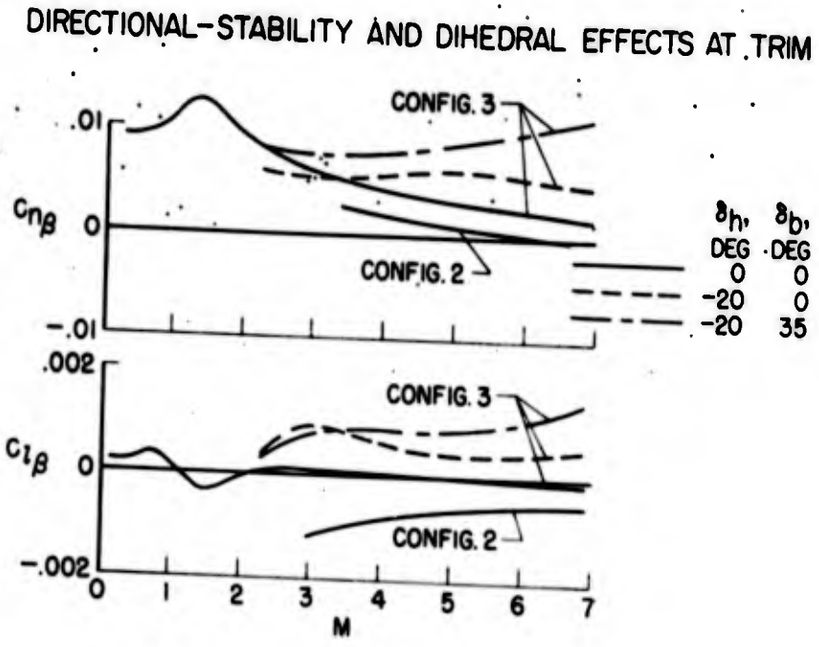

Figure 5

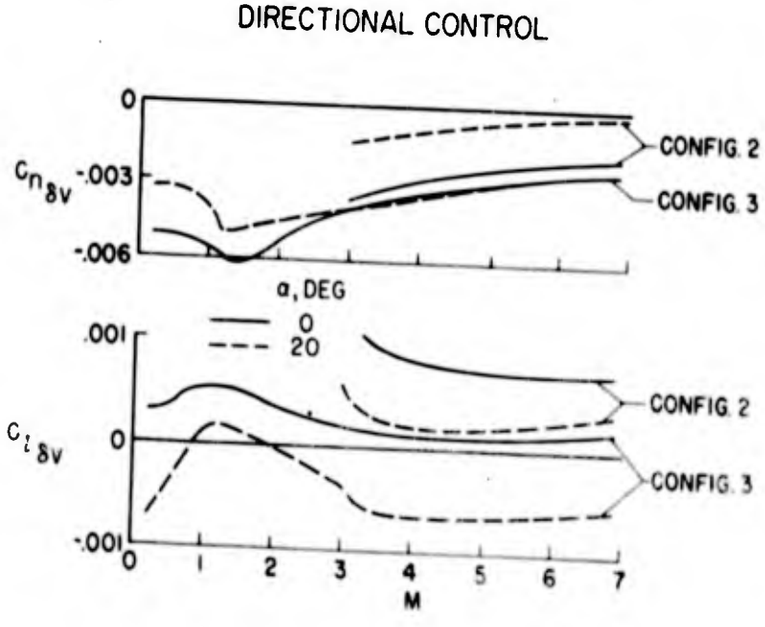

Figure 6

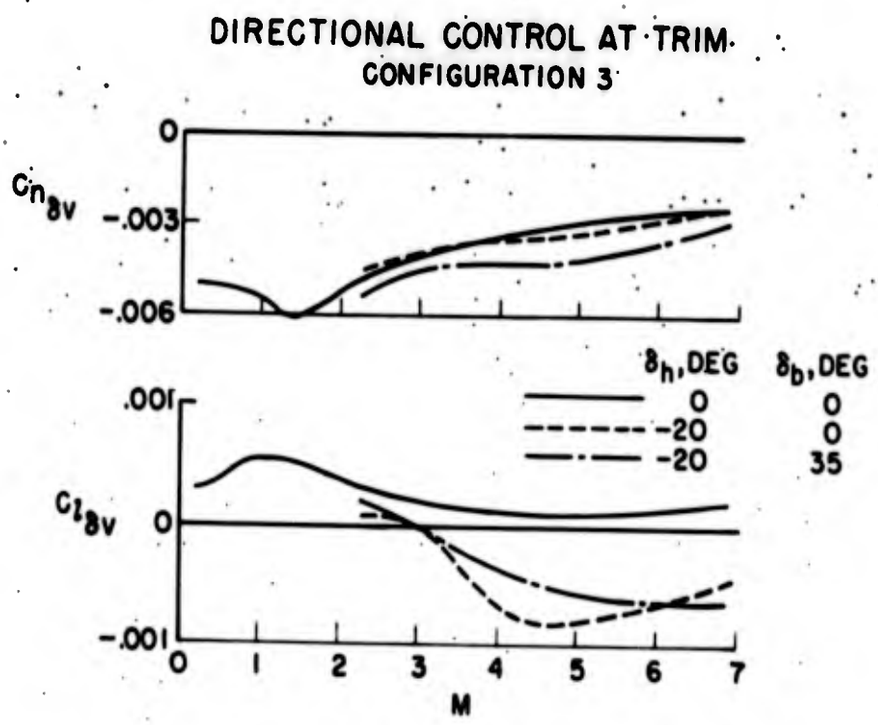

Figure 7

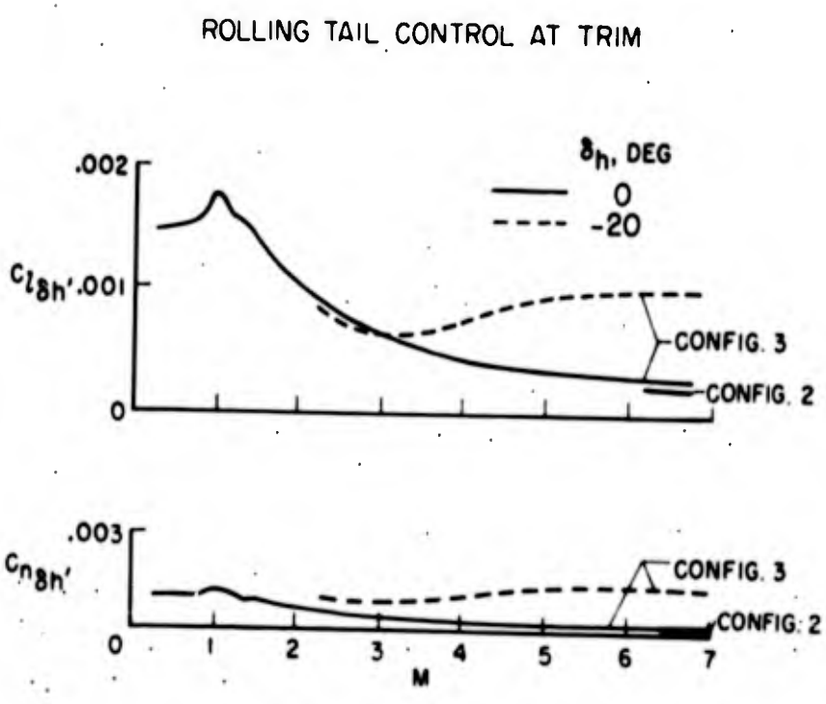

Figure 8

EFFECTS OF ROCKET JET ON STABILITY AND CONTROL AT HIGH MACH NUMBERS

By David E. Fetterman, Jr.

NACA Langley Aeronautical Laboratory

INTRODUCTION

Previous investigations have shown that a jet exhausting from the base of the fuselage may alter the base drag, the afterbody pressure distribution, and also the aerodynamic characteristics of the test configurations. (For example, see refs. 1 to 5.) The X-15 airplane will be subjected to these effects, but during the lower altitude portions of its trajectory the magnitudes of these effects should be relatively small and no difficulties during this flight regime are anticipated. As the X-15 approaches the burnout altitudes for either the speed or altitude missions, however, jet static-pressure ratios greatly exceeding those considered in previous investigations will be encountered. In order to determine the jet-interference effects which may occur at these high jet static-pressure ratios and high Mach numbers, an investigation was undertaken in the Langley 11-inch hypersonic tunnel at a Mach number of 6.86. This paper presents the results of this investigation.

SYMBOLS

$p_{t,j}$	jet total pressure (combustion chamber pressure)
γ_j	jet specific-heat ratio
p_j	jet static pressure at nozzle lip
p_∞	free-stream static pressure
M_∞	free-stream Mach number
α	angle of attack
z	vertical distance from bottom of fuselage

z_t	vertical tail height from bottom of fuselage
$R_{\bar{c}}$	Reynolds number, based on mean aerodynamic chord
h	altitude
x_b	axial distance from base of fuselage
l	fuselage length
C_L	lift coefficient
C_m	pitching-moment coefficient
C_{n_β}	rate of change of yawing-moment coefficient with sideslip angle
δ_h	horizontal-tail deflection
C_{l_β}	rate of change of rolling-moment coefficient with sideslip angle
$C_{n_{\delta v}}$	rate of change of yawing-moment coefficient with vertical-tail deflection
$C_{l_{\delta v}}$	rate of change of rolling-moment coefficient with vertical-tail deflection
$C_{l_{\delta h'}}$	rate of change of rolling-moment coefficient with differential horizontal-tail deflection
$C_{n_{\delta h'}}$	rate of change of yawing-moment coefficient with differential horizontal-tail deflection

DISCUSSION

The following discussion deals with the X-15 flight conditions at burnout for the speed and altitude missions. These flight conditions are shown in the following table:

Mission	h, ft	Mach number	R_c
Speed	137,000	6.15	1.0×10^6
Altitude	158,000	5.90	0.4×10^6

In figure 1 the increase in the jet static-pressure ratio p_j/p_∞ that the X-15 will encounter with increasing altitude is presented for the design jet chamber pressure of 600 pounds per square inch and an assumed specific-heat ratio γ_j of 1.25 for the exhaust gas. Three rocket-nozzle configurations are considered. The original design nozzle had an exit static pressure equal to ambient pressure at about 20,000 feet and will hereinafter be referred to as the 20,000-foot nozzle. The 40,000- and 50,000-foot nozzles are merely extensions of the divergent section of the original nozzle and are included to show the effects of nozzle extensions.

The jet static-pressure ratios for all three nozzles increase rapidly with altitude. For the 20,000-foot nozzle, values of p_j/p_∞ at burnout of 180 on the speed mission and 420 on the altitude mission are obtained. With the extended nozzles, lower jet static-pressure ratios are obtained at all altitudes.

The combination of these high jet static-pressure ratios and the low ratio of specific heats of the exhaust gases will cause the jet boundary to expand considerably after leaving the nozzle. If inviscid conditions are assumed, a strong jet exit shock would be present and the ratio of the pressure immediately behind the shock to the pressure in front of the shock has been calculated to be between 30 for the 50,000-foot nozzle at the speed-mission burnout altitude and 55 for the 20,000-foot nozzle at the altitude-mission burnout altitude.

At the high altitudes and speeds under consideration the character of the boundary layer may be such that pressure ratios in this range could cause a separated-flow region to occur ahead of the jet boundary in the vicinity of the tail surfaces, and changes in the stability and control characteristics of the X-15 may result.

In order to determine whether these separated-flow regions did exist, the flow field produced by a cold air jet exhausting into a Mach number 6.86 hypersonic air stream was observed in the NACA 11-inch hypersonic tunnel by means of a schlieren system. Since air, instead of hot gases, was used as the exhaust medium, equivalent jet static-pressure ratios were used during the tests so that the initial jet-boundary slope could be duplicated. The effects of specific-heat ratio on this initial jet-boundary slope and the details of obtaining these

equivalent jet static-pressure ratios for simulating effects of specific-heat ratio were determined in the investigations reported in references 6 and 7.

Figure 2 presents a typical schlieren photograph of the flow field produced by the air jet from the 20,000-foot nozzle exhausting into the Mach number 6.86 air stream. Indicated in the figure are the jet boundary, the jet-exit shock, and the jet-induced separated-flow region.[1]

In figure 3 the extent of these separated-flow regions with increasing equivalent air jet static-pressure ratios is indicated in terms of the parameter z/z_t where z is the height of the separated-flow region at the base of the fuselage and z_t is the height of the vertical tail. At the lower Reynolds numbers the separated-flow regions increase rapidly with jet static-pressure ratio and under certain low Reynolds number conditions could cover the entire vertical tail. With increasing Reynolds number, however, a reduction in z/z_t occurs, especially at the higher jet static-pressure ratios.

Since the jet air supply was inadequate to permit testing at both the required equivalent jet static-pressure ratios and also at the full-scale Reynolds number, extrapolations of the available data were made, with the lower Reynolds number variation as a guide, to determine the separated-flow conditions that would exist for the 20,000-foot nozzle on the speed mission (indicated by the flagged solid circle symbol at a p_j/p_∞ of 500) and for all nozzles during the altitude mission (indicated by the unflagged solid symbols). As might be expected the extent of the separated-flow regions is greater for all three nozzles during the altitude mission than during the speed mission. Therefore during the remaining part of this discussion, only the data pertaining to the altitude mission are considered.

For the 20,000-foot nozzle, the equivalent air jet static-pressure ratio of 1,200 for the altitude mission corresponds to the hot-jet value of 420 seen in figure 1; and, as indicated by the extrapolation, a determination of the separated-flow region induced by this nozzle could not be obtained experimentally at this jet static-pressure ratio and Reynolds number combination. However, experimental data were available at $p_j/p_\infty = 528$ and a Reynolds number of 0.25×10^6 which figure 3 shows closely approximated the desired separated-flow conditions and the schlieren photograph at this condition was used for defining the separated-flow regions induced by the 20,000-foot nozzle during the altitude mission.

[1]A motion-picture film supplement (L-372) showing the jet-exhaust test is available on loan from NACA Headquarters, Washington, D.C.

In order to duplicate these established separated-flow regions for the altitude mission on a force model of the X-15, axisymmetric metal jet-boundary simulators were machined to the jet-boundary shapes determined from the compressed-air tests at an angle of attack of 0° and then were attached to the wind shield of the force balance just aft of the model. These metal fairings were then modified by reducing the length of the duplicated jet boundary, if necessary, to produce approximately the same separated-flow regions, at an angle of attack of 0°, as those obtained from air tests. In figure 4 a schlieren photograph of the flow field produced by one of these jet-boundary simulators is shown. The jet-boundary simulator shown in this figure has been modified to produce approximately the same separated-flow region as that produced by the air jet in figure 2 and is the only one of the three jet-boundary simulators tested which needed modification.

At angles of attack the actual jet boundary becomes asymmetrical; however, for these tests the zero-angle-of-attack jet-boundary simulators were used throughout the small angle-of-attack range investigated.

Figure 5 shows a comparison of the separated-flow regions on the high-pressure side of the configuration induced at different angles of attack by the air jet and the comparable zero-angle-of-attack jet-boundary simulator. At $\alpha = 0^\circ$ the separated-flow region induced by the jet-boundary simulator is almost identical with that induced by the air jet. As the angle of attack is increased, however, the jet-boundary simulator induces a progressively larger separated-flow region than the air jet. On the low-pressure side a reversal of this trend would occur. In view of these results, the angle-of-attack range for the force tests was limited to $\pm 4^\circ$.

The effects produced by this simulated jet-exhaust technique on the longitudinal stability and control of the X-15 are shown in figure 6 where the variation in pitching-moment coefficient with lift coefficient is presented with the jet off and with the 20,000-foot, 40,000-foot, and 50,000-foot nozzle jet-boundary simulators in place. First, consider the curves for zero-horizontal-tail deflection, $\delta_h = 0^\circ$. With the jet off the configuration is longitudinally stable. Because of the large separated-flow region from the 20,000-foot nozzle, however, considerable instability occurs over a small positive and negative lift-coefficient range. Since the separated-flow regions produced by the extended nozzles are smaller, less loss in stability is indicated; however, at zero lift coefficient the configuration is still only neutrally stable.

The jet-exhaust effects on the control power of the horizontal tail is indicated by the difference in the curves for $\delta_h = 0^\circ$ and $\delta_h = -20^\circ$. With the jet off some loss in control power occurs at small negative lift coefficients because of wing wake effects. The combination of the wing

wake and the jet-induced separated-flow region from the 20,000-foot nozzle causes a large loss in control power, and at negative lift coefficients the horizontal tail becomes almost ineffective. With the extended nozzles the control power is only slightly reduced from the jet-off condition.

The effect of the simulated-jet exhaust on directional stability and control is indicated in figure 7, where the variations of the directional-stability parameter C_{n_β} and the directional-control parameter $C_{n_{\delta v}}$ with angle of attack are shown. Here again some loss in both the directional stability and control is indicated with the 20,000-foot nozzle in operation. With the extended 40,000- and 50,000-foot nozzles a small reduction in $C_{n_{\delta v}}$ is noted; however, no significant change is indicated for C_{n_β}.

The lateral stability and control results are shown in figure 8. No jet-exhaust effects from any of the nozzles under consideration on the lateral stability parameter C_{l_β} are noticeable; however, a loss is again evident in the lateral-control parameter $C_{l_{\delta h}}$ for all three nozzles, and at negative angles of attack, roll control is almost nonexistent.

The data of figures 6, 7, and 8 summarize the significant jet-exhaust effects observed during this investigation. Additional results indicated no noticeable change in the cross control derivatives $C_{l_{\delta v}}$ and $C_{n_{\delta h}}$, due to jet exhaust effects. The model was also tested with the speed brakes open 35°; however, the data also showed no significant change in the static longitudinal, directional, or lateral stability characteristics between the simulated jet-on and jet-off conditions.

One question which might naturally arise at this time is whether or not these simulated jet-exhaust effects are truly representative of those which may be encountered during an actual flight. In answering it must be noted that even though, during these tests, the flight Reynolds numbers in all cases but one were duplicated, boundary-layer transition very likely will occur farther forward on the full-scale vehicle; thus the jet-induced separated-flow regions and, consequently, the jet interference effects would be expected to be smaller. Therefore, although this simulated jet-exhaust technique may not predict the exact magnitude of these jet effects, it is believed that these results are useful for indicating trends and pointing out problem areas.

From consideration of the compressed-air test results and the altitude mission trajectory, the time for the jet-exhaust effects to develop from zero to the maximum effects shown herein prior to burnout was estimated to be 14 seconds on the altitude mission. Flight simulator tests then indicated that, over this relatively short time duration, little difficulty was experienced in overcoming these jet-exhaust effects.

Since the altitude capabilities of the X-15 are much greater than those obtained during the design altitude mission, higher burnout altitudes than 158,000 feet may be encountered and the jet-exhaust effects may become more serious. It is anticipated that an extensive investigation into these jet effects over a range of Mach numbers and Reynolds numbers will be carried out during the flight-program missions of the X-15.

REFERENCES

1. Cortright, Edgar M., Jr., and Schroeder, Albert H.: Investigation at Mach Number 1.91 of Side and Base Pressure Distributions Over Conical Boattails Without and With Jet Flow Issuing From Base. NACA RM E51F26, 1951.

2. Cortright, Edgar M., Jr., and Kochendorfer, Fred D.: Jet Effects on Flow Over Afterbodies in Supersonic Stream. NACA RM E53H25, 1953.

3. Love, Eugene S.: Aerodynamic Investigation of a Parabolic Body of Revolution at Mach Number of 1.92 and Some Effects of an Annular Supersonic Jet Exhausting From the Base. NACA TN 3709, 1956. (Supersedes NACA RM L9K09.)

4. Bromm, August F., Jr., and O'Donnell, Robert M.: Investigation at Supersonic Speeds of the Effect of Jet Mach Number and Divergence Angle of the Nozzle Upon the Pressure of the Base Annulus of a Body of Revolution. NACA RM L54I16, 1954.

5. Grigsby, Carl E.: An Investigation of the Effects of Jet Exhaust and Reynolds Number Upon the Flow Over the Vertical Stabilizer and Rudder of the Douglas D-558-II Research Airplane at Mach Numbers of 1.62, 1.93, and 2.41. NACA RM L54E03, 1954.

6. Love, Eugene S.: Initial Inclination of the Mixing Boundary Separating an Exhausting Supersonic Jet From a Supersonic Ambient Stream. NACA RM L55J14, 1956.

7. Love, Eugene S., Woodling, Mildred J., and Lee, Louise P.: Boundaries of Supersonic Axisymmetric Free Jets. NACA RM L56G18, 1956.

EFFECT OF ALTITUDE ON JET STATIC-PRESSURE RATIO

$p_{t,j}$ = 600 LB/SQ IN.; γ_j = 1.25

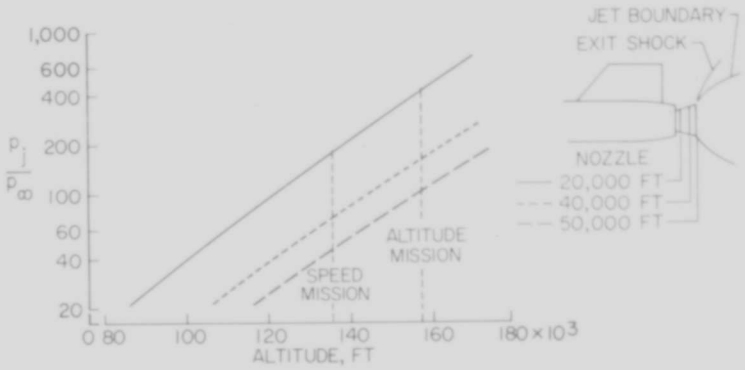

Figure 1

FLOW FIELD PRODUCED BY COMPRESSED-AIR JET

M_∞ = 6.86; $R_{\bar{c}}$ = 0.25 × 10⁶; $(p_j/p_\infty)_{\gamma=1.4}$ = 528; α = 0°

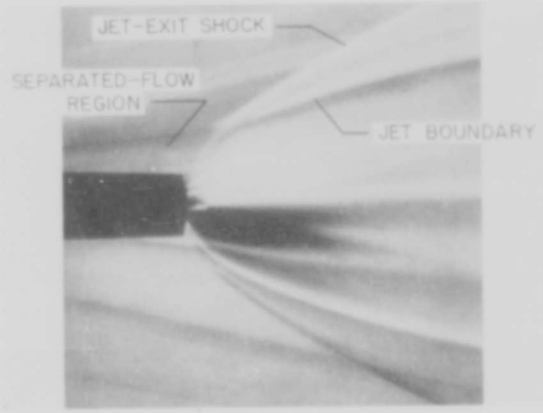

L-58-2526

Figure 2

EFFECT OF JET STATIC-PRESSURE RATIO AND REYNOLDS NUMBER ON SEPARATED-FLOW REGION

$\alpha = 0°$; $M_\infty = 6.86$

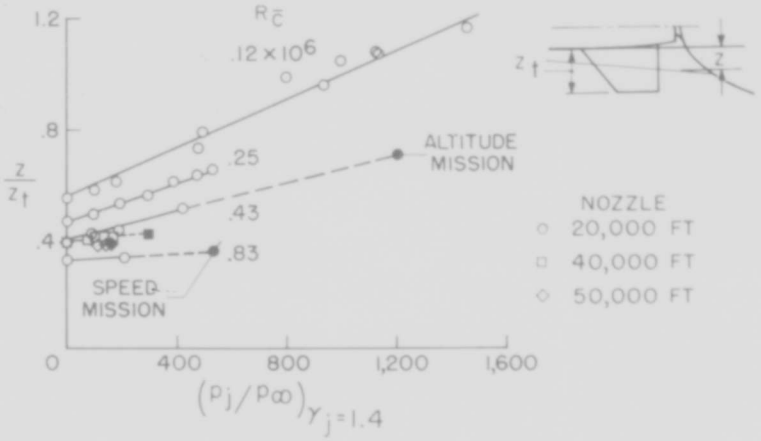

Figure 3

FLOW FIELD PRODUCED BY JET-BOUNDARY SIMULATOR

$M_\infty = 6.86$; $R_{\bar{c}} = 0.25 \times 10^6$; $\alpha = 0°$

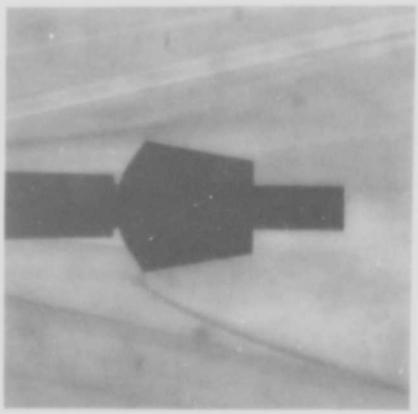

L-58-2527

Figure 4

SEPARATED-FLOW REGIONS FROM AIR JET AND JET-BOUNDARY SIMULATOR

$M_\infty = 6.86$; $R_{\bar{c}} = 0.25 \times 10^6$; $(p_j/p_\infty)_{\gamma_j=1.4} = 528$

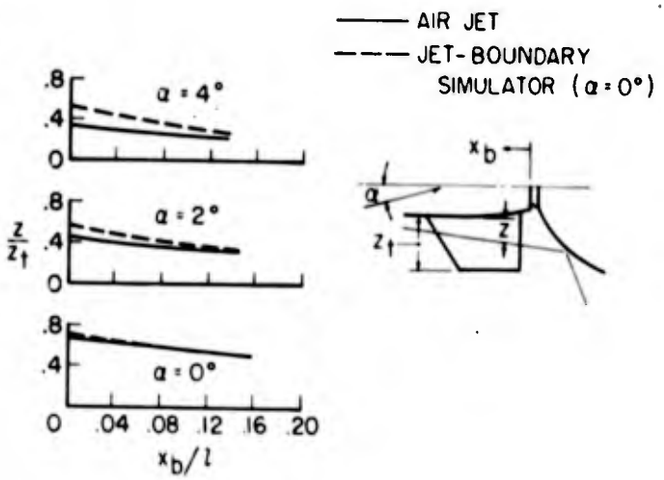

Figure 5

EFFECT OF SIMULATED JET EXHAUST ON LONGITUDINAL STABILITY AND CONTROL

ALTITUDE MISSION

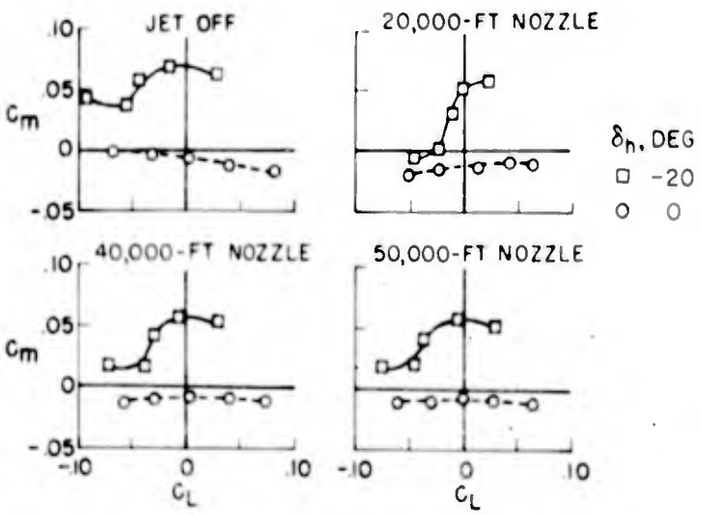

Figure 6

EFFECT OF SIMULATED JET EXHAUST ON DIRECTIONAL STABILITY AND CONTROL

ALTITUDE MISSION

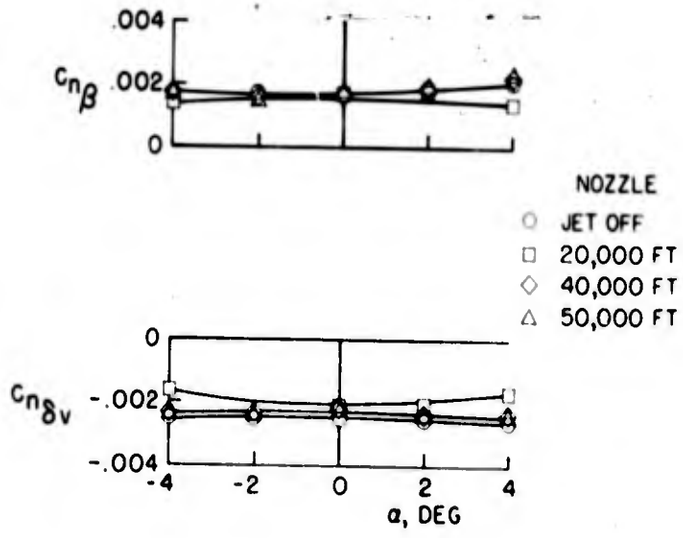

Figure 7

EFFECT OF SIMULATED JET EXHAUST ON LATERAL STABILITY AND CONTROL

ALTITUDE MISSION

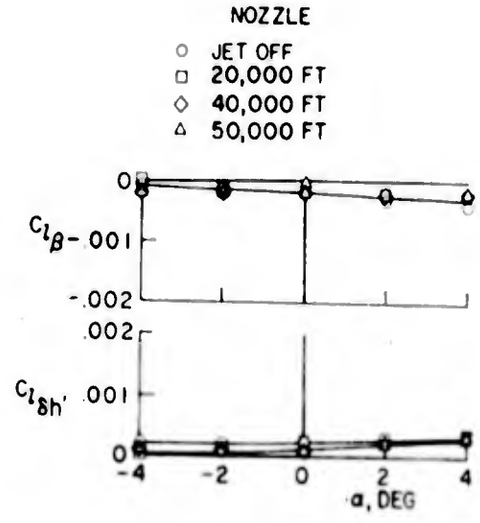

Figure 8

THE MEASURED AND ESTIMATED ROTARY STABILITY DERIVATIVES OF THE X-15 AIRPLANE

By Bruce Tinling
NACA Ames Aeronautical Laboratory

True Surber
North American Aviation, Inc.

Phillips J. Tunnell, and Armando Lopez
NACA Ames Aeronautical Laboratory

INTRODUCTION

Analysis of the dynamic motion of an airplane flying within the atmosphere depends upon a knowledge of the aerodynamic stability derivatives. Those derivatives which represent moments caused by rotational velocities are known as the rotary stability derivatives and contribute to the damping of the airplane motions. Once the derivatives have been evaluated, airplane motions can be computed or simulated, and the need for artificial stability augmenters or dampers can be determined.

The results of many theoretical studies directed toward estimating the rotary derivatives for isolated surfaces have been published in the last five to ten years. (See, for example, refs. 1 to 8.) Measurement of the derivatives in the wind tunnel or in flight is difficult and only a few experimental results are available from which to verify the estimation techniques and to extend them to airplane-like configurations for which the effects of a fuselage and the interference of one surface upon another must be considered. In this respect, the X-15 configuration might be considered to be an extreme example. It has large tail surfaces close to the wing and a fuselage which covers roughly 30 percent of the wing span. These factors contribute to the uncertainty of estimating the rotary derivatives by theoretical methods.

Measurements of the rotary derivatives of the X-15 have been made in several of the wind tunnels of the National Advisory Committee for Aeronautics (refs. 9, 10, and 11). The speed range was from landing speeds up to a Mach number of 3.5. The measurements were made on the steady-state, forced-oscillation equipment described by Beam in reference 12. This apparatus measures the rotary derivatives during small-amplitude, single-degree-of-freedom oscillations.

In this paper, the results of the wind-tunnel tests are compared with the values of the rotary derivatives estimated by the available procedures. Wherever possible, the results of wind-tunnel measurements of the static forces and moments on the X-15 have been utilized in the estimation procedures to obtain lift-curve slopes and centers of pressure

of the tail surfaces. In this way, at least a partial account is taken of the effects of the fuselage and wing downwash and pressure field on the tail surfaces.

SYMBOLS

$C_{1/2}$	cycles to damp to half amplitude
$C_{l_{\dot{\beta}}}$	rolling-moment coefficient due to sideslip acceleration
C_{l_p}	damping-in-roll coefficient
C_{l_r}	rolling-moment coefficient due to yawing velocity
$C_{m_{\dot{\alpha}}}$	pitching-moment coefficient due to plunging acceleration
C_{m_q}	pitching-moment coefficient due to pitching velocity
C_{N_α}	slope of normal-force coefficient with angle of attack
$C_{n_{\dot{\beta}}}$	yawing-moment coefficient due to sideslip acceleration
C_{n_p}	yawing-moment coefficient due to rolling velocity
C_{n_r}	yawing-moment coefficient due to yawing velocity
C_{Y_β}	rate of change of side-force coefficient with sideslip
V_e	equivalent airspeed
α	angle of attack, deg
ϕ	angle of roll, deg

DISCUSSION

The experimental technique employed permits measurements of the derivatives over a fairly wide range of angle of attack. The damping derivatives measured at the highest test Mach number, 3.5, are presented in figure 1. For the benefit of those not familiar with the measurement technique, both the moments due to pitching velocity C_{m_q} and plunging acceleration $C_{m_{\dot{\alpha}}}$ are measured simultaneously in the case of damping in pitch. In the case of the lateral derivatives, the moments due to rotational velocities C_{l_p} or C_{n_r} are measured along with a component

due to sideslipping acceleration. The lateral results shown are referred to a body system of axes. In the figures which follow, the damping measured at zero angle of attack has been selected to demonstrate the effects of Mach number, the contributions of the various airplane components to the damping, and the accuracy to which these contributions can be estimated.

The unexpected importance of the contribution of the fuselage to the pitch and yaw damping at supersonic speeds is one of the principal results of recent research on the rotary derivatives. In figure 2 the damping in pitch and yaw measured for several fuselage arrangements is compared with the damping predicted for bodies of revolution by slender-body theory. The experimental results in this figure are for the fuselage alone or in combination with the wing. The wing is not considered to contribute to the damping in yaw. A few points have also been included from pitch tests of the wing-fuselage combination at Mach numbers greater than 2, where the pitch damping of the wing is presumed to be small compared with the fuselage damping. The measured damping has been divided by the estimated value so that perfect correlation is indicated by unity. The estimated damping can be derived from slender-body theory (ref. 13) or from analyses using unsteady source-sink potentials for compressible flows where the wave length is long compared with the body length (ref. 14). The result from these analyses is that damping of a pointed body of revolution is independent of Mach number and dependent only on the base area and the square of the distance from the moment center to the base. It is obvious from the data points shown that slender-body theory grossly underestimates the fuselage damping at supersonic speeds. The two fuselages for which damping information is available, the X-15 and the F-104, bear only a faint resemblance to a body of revolution to which the theory applies. However, the same trend with Mach number exists for both fuselages and for both pitching and yawing motions. It is expected that the same trend will prevail for all slender, pointed bodies.

A possible explanation for the differences between the predicted and measured fuselage damping is found in a study of the limitations of slender-body theory in predicting the normal-force characteristics of elongated bodies at small angles of attack. In figure 3, slender-body theory has again been used as a standard of comparison - this time to compare the normal-force characteristics. The experimental results shown are for bodies of revolution having ogival noses and cylindrical afterbodies. The fineness ratio of the afterbodies was 6 (ref. 15). The effects of viscosity on the normal forces which may be significant at higher angles of attack are negligible for the data shown here. These results, then, indicate the differences which may be anticipated between measured normal-force characteristics and those predicted from slender-body theory. Syvertson and Dennis (ref. 16) have had good

success in accounting for these differences on the basis of second-order effects. Second-order calculations of the damping in pitch and in yaw have not been made. At speeds beyond the range of measured fuselage damping, it is anticipated that the damping will gradually approach the value given by Newtonian impact theory. This trend has been used in extrapolating the measured damping of the X-15 to higher Mach numbers. (See fig. 2.)

The measured damping in pitch of the wing-fuselage combination and of the complete airplane is shown in figure 4. The measured damping is indicated by the symbols. The damping derivative for the complete airplane reaches a maximum at about a Mach number of 1 and diminishes markedly with increasing supersonic Mach number. The average fuselage damping from figure 2 has been repeated in figure 4. It is obvious that at the higher Mach numbers more than one-half of the damping in pitch is contributed by the fuselage.

The damping of the wing was estimated from theoretical procedures for isolated surfaces. The estimated damping of the wing was small except at transonic speeds. The peak near a Mach number of 1.0 was not predicted by the estimation procedure.

Estimates of the pitch damping contributed by the horizontal tail agreed well with the measured increment. It is usually adequate when estimating tail damping to consider only those moments resulting from the angle of attack of the tail caused by rotation about the center of gravity and downwash lag. The horizontal tail of the X-15, however, is large and the tail length is short. Consequently, the moments caused by rotational velocity of the tail about its aerodynamic center during the pitching motion should be included in the estimate. These moments account for roughly 20 percent of the tail damping at subsonic speeds and less than 10 percent at supersonic speeds.

The total estimated damping in pitch matches the experimental trend at supersonic speeds. Extrapolation of these results through the use of the estimation procedures seems warranted.

The damping-in-yaw derivative $C_{n_r} - C_{n_{\dot{\beta}}}$ varies with Mach number in a manner similar to damping in pitch. (See fig. 5.) A maximum is reached near a Mach number of 1 and the damping is reduced with increasing supersonic speed. The contribution of the fuselage is again a large portion of the damping at supersonic speeds. The damping of the wing is considered to be negligible. Most of the subsonic measurements were made on a model of an earlier version of the X-15 which had fuselage side fairings extending well forward of the cockpit. These results are indicated by the flagged symbols. Removal of these fairings forward of the cockpit improved the fuselage yaw damping. The contribution of

the tail was about the same with the fairings either on or off. It is expected, therefore, that the yaw damping coefficient at the higher subsonic speeds for the X-15 will be 10 to 20 percent greater than indicated by the flagged symbols and will reach a value of about -2.0 near a Mach number of 1.0. In the estimates of the yaw damping of the vertical tail, it was possible to estimate only the coefficient due to yawing velocity C_{n_r}. The coefficient due to sideslipping acceleration, $C_{n_{\dot{\beta}}}$, is dependent upon the variation of sidewash with sideslip. Unfortunately, there is no reliable way to estimate the sidewash or to derive it from available static wind-tunnel test results. The estimated value of C_{n_r} of the tail has been added to the measured damping of the wing-fuselage combination in figure 5. The resulting total is less than the measured damping of the complete airplane at subsonic speeds and fails to follow the experimental trend at supersonic speeds. Extension of the estimates to higher supersonic speeds appears to yield unconservative results.

The derivatives due to rolling velocity were the most difficult to measure by the experimental technique employed. In this technique, single-degree-of-freedom oscillations are forced about axes lying in the plane of symmetry midway between the axes for rolling and yawing motions. Thus, the damping moment measured during these oscillations contains components of all of the rolling and yawing rotary derivatives. These measurements and those made separately of the yawing derivatives are used to formulate a determinate system of simultaneous equations from which the rolling derivatives are extracted algebraically. For the complete airplane, the damping-in-yaw derivative was of the order of -1 and appeared to have an experimental scatter of about 0.1. Obviously, since the measurements of damping in yaw are utilized to extract the rolling derivatives from the measurements made about inclined axes, the rolling derivatives must also have a scatter of at least 0.1. The results for the damping-in-roll derivative at an angle of attack of 0° are shown in figure 6. The data are shown to be scattered and one should probably turn to estimations of the damping of isolated surfaces as a guide for fairing the results. The measurements made at Mach numbers slightly less than 1.0 are particularly anomalous. The flagged symbols indicate data obtained with the lower tip of the vertical tail removed which is required for landing. This should not cause any significant changes in roll damping. Also included is a low-speed measurement (solid test point) obtained during a pure rolling oscillation in the Langley free-flight tunnel.

The estimated damping in roll of the isolated wing approximates the experimental results obtained at supersonic speeds with the tail off. No measurements of the roll damping with the tail removed were made at subsonic speeds.

Estimates of the contribution of the tail surfaces to the damping in roll require more careful consideration of the X-15 airplane than for more conventional configurations. The damping of geometrically similar surfaces varies as the fourth power of a typical dimension. For conventional airplanes, therefore, the tail damping in roll is usually negligible compared with the damping contributed by the wing. For the X-15, this is not true, and the damping of its isolated tail surfaces is significant compared with the wing damping. The damping estimated for isolated tail surfaces will not be realized because of the wash from the rolling wing. For the estimates presented, the downwash and sidewash due to the local wing angle of attack caused by rolling velocity were taken to be identical to the wing downwash induced by a uniform angle of attack. This quantity can be derived from static wind-tunnel test results. This method of accounting for the flow rotation from the rolling wing is crude but is thought to be as accurate as any of the theoretical techniques. The resulting estimates follow the trend of the experimental results. Extrapolation to higher supersonic speeds, using the estimated derivatives for isolated surfaces, indicates the damping-in-roll derivatives at a Mach number of 7 to be about 30 percent of the value measured at low supersonic speeds.

The cross derivatives as well as the damping derivatives can be measured by the experimental techniques employed. Results of measurements of these derivatives at a Mach number of 3.5 are presented in figure 7. These data are referred to the body system of axes. Calculations were made of the short-period lateral dynamics or Dutch roll characteristics in which these derivatives were varied from the most positive to the most negative values measured (0.2 to -0.2). These calculations indicated no important effect of these derivatives on the short-period dynamics.

The results of the research on the rotary derivatives of the X-15 can be best summarized by examining the effect of these derivatives on the dynamics of the airplane. As an illustration, the Dutch roll characteristics for the gliding flight following the entry maneuver are presented in figures 8 and 9. Plotted is a damping parameter, the reciprocal of cycles to damp to 1/2 amplitude for Mach numbers from 0.6 to 6. Included for reference are the minimum acceptable damping boundaries from the current Air Force specifications (ref. 17). For the roll-yaw coupling encountered, that is $\left|\frac{\phi}{V_e}\right|$ less than 0.4, these boundaries are constant. The calculations were made for dynamic pressures of 200 and 1,500 lb/sq ft, which correspond to altitudes near the upper and lower boundaries of the Mach number-altitude flight envelope. Calculations were made with the rotary derivatives set equal to zero and set equal to the estimated and measured derivative at the angle of attack for a 1 g glide. When the rotary derivatives are set equal to

zero some damping is indicated which is contributed by the large value of the sideforce due to sideslip derivative C_{Y_β}. At the lower dynamic pressures, which correspond to high altitudes, the rotary derivatives have little effect at a Mach number of 6. Simulated piloted entries from the ballistic phase of flight have also demonstrated the unimportance of the rotary derivatives in the high altitude-high Mach number part of the flight envelope. Little or no difference in the handling characteristics during the entry was noted when the rotary derivatives were varied from 0 to twice the estimated values. As the Mach number is reduced, the magnitude of the derivatives increases and the altitude decreases for a given dynamic pressure. These two factors increase the importance of the rotary derivatives at the lower Mach numbers. At the higher dynamic pressure (or lower altitude) the derivatives have a significant effect at all Mach numbers. Comparison of the damping calculated for the measured and for the estimated derivatives indicates the estimation procedure to be adequate. The differences in damping shown would probably have little effect on the pilot's opinion of the flying qualities. It should be borne in mind, however, that the estimate of yaw damping was made by adding the estimated tail damping to the measured fuselage damping. This estimate, therefore, is not truly representative of the estimate one would arrive at if he were to start from "scratch" without benefit of experimental data. At the present time, there are no procedures available to reliably estimate the damping of fuselages which, for the X-15, is indicated to contribute 50 percent or more of the total pitch and yaw damping at high supersonic speeds.

REFERENCES

1. Campbell, John P., and McKinney, Marion O.: Summary of Methods for Calculating Dynamic Lateral Stability and Response and for Estimating Lateral Stability Derivatives. NACA Rep. 1098, 1952. (Supersedes NACA TN 2409.)

2. Jones, Arthur L., and Alksne, Alberta: A Summary of Lateral-Stability Derivatives Calculated for Wing Plan Forms in Supersonic Flow. NACA Rep. 1052, 1951.

3. Malvestuto, Frank S., Jr., Margolis, Kenneth, and Ribner, Herbert S.: Theoretical Lift and Damping in Roll at Supersonic Speeds of Thin Sweptback Tapered Wings With Streamwise Tips, Subsonic Leading Edges, and Supersonic Trailing Edges. NACA Rep. 970, 1950. (Supersedes NACA TN 1860.)

4. Harmon, Sidney M.: Stability Derivatives at Supersonic Speeds of Thin Rectangular Wings With Diagonals Ahead of Tip Mach Lines. NACA Rep. 925, 1949. (Supersedes NACA TN 1706.)

5. Margolis, Kenneth, and Bobbitt, Percy J.: Theoretical Calculations of the Pressures, Forces, and Moments at Supersonic Speeds Due to Various Lateral Motions Acting on Thin Isolated Vertical Tails. NACA Rep. 1268, 1956. (Supersedes NACA TN 3373 by Margolis and TN 3240 by Bobbitt.)

6. Harmon, Sidney M., and Jeffreys, Isabella: Theoretical Lift and Damping in Roll of Thin Wings With Arbitrary Sweep and Taper at Supersonic Speeds - Supersonic Leading and Trailing Edges. NACA TN 2114, 1950.

7. Martin, John C., Margolis, Kenneth, and Jeffreys, Isabella: Calculation of Lift and Pitching Moments Due to Angle of Attack and Steady Pitching Velocity at Supersonic Speeds for Thin Sweptback Tapered Wings With Streamwise Tips and Supersonic Leading and Trailing Edges. NACA TN 2699, 1952.

8. Harmon, Sidney M., and Martin, John C.: Theoretical Calculations of the Lateral Force and Yawing Moment Due to Rolling at Supersonic Speeds for Sweptback Tapered Wings With Streamwise Tips - Supersonic Leading Edges. NACA TN 2156, 1950.

9. Tunnell, Phillips J., and Lathem, Eldon A.: The Static and Dynamic Rotary Derivatives of a 0.09-Scale Model of the X-15 Research Airplane at Mach Numbers From 1.55 to 3.50. (Prospective NACA paper.)

10. Lopez, Armando E., and Tinling, Bruce E.: The Static and Dynamic-Rotary Stability Derivatives at Subsonic Speeds of a Model of the X-15 Research Airplane. (Prospective NACA paper.)

11. Beam, Benjamin H., and Endicott, Kenneth C.: Wind-Tunnel Data on the Longitudinal and Lateral-Directional Rotary Derivatives of a Straight-Wing, Research Airplane Configuration at Mach Numbers From 2.5 to 3.5. NACA RM A58A14, 1958.

12. Beam, Benjamin H.: A Wind-Tunnel Test Technique for Measuring the Dynamic Rotary Stability Derivatives at Subsonic and Supersonic Speeds. NACA Rep. 1258, 1956. (Supersedes NACA TN 3347.)

13. Sacks, Alvin H.: Aerodynamic Forces, Moments, and Stability Derivatives for Slender Bodies of General Cross Section. NACA TN 3283, 1954.

14. Dorrance, William H.: Nonsteady Supersonic Flow About Pointed Bodies of Revolution. Jour. Aero. Sci., vol. 18, no. 8, Aug. 1951, pp. 505-511, 542.

15. Grimminger, G., Williams, E. P., and Young, G. B. W.: Lift on Inclined Bodies of Revolution in Hypersonic Flow. Jour. Aero. Sci., vol. 17, no. 11, Nov. 1950, pp. 675-690.

16. Syvertson, Clarence A., and Dennis, David H.: A Second-Order Shock-Expansion Method Applicable to Bodies of Revolution Near Zero Lift. NACA Rep. 1328, 1957. (Supersedes NACA TN 3527.)

17. Anon.: Flying Qualities of Piloted Airplanes. Military Specification, MIL-F-8785 (ASG), Sept. 1, 1954; Amendment-1, Oct. 19, 1954.

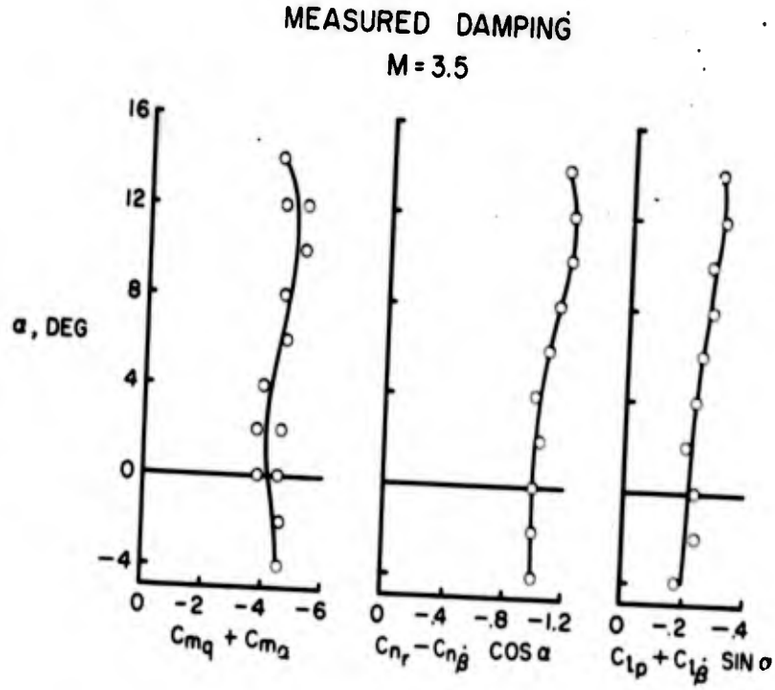

Figure 1

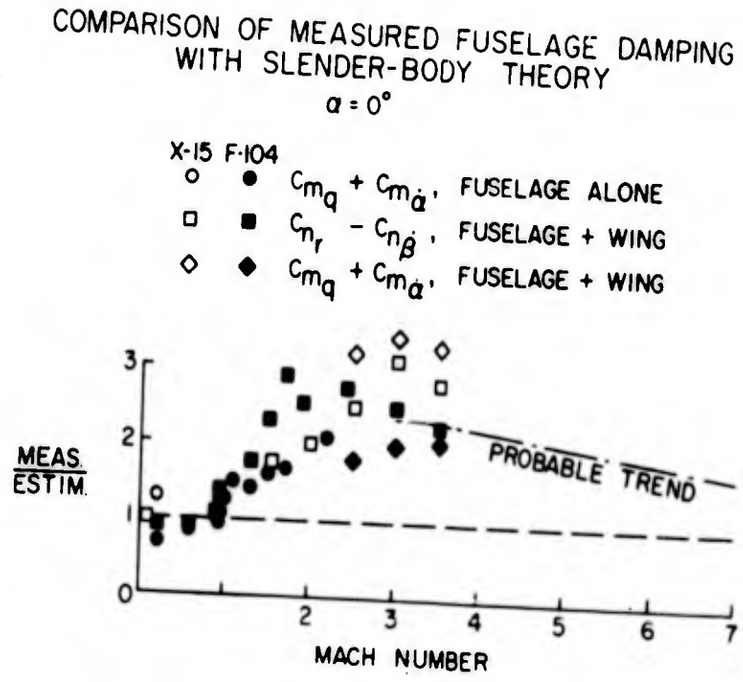

Figure 2

COMPARISON OF MEASURED FUSELAGE NORMAL-FORCE WITH SLENDER-BODY THEORY

OGIVE CYLINDER, $\alpha = 0°$

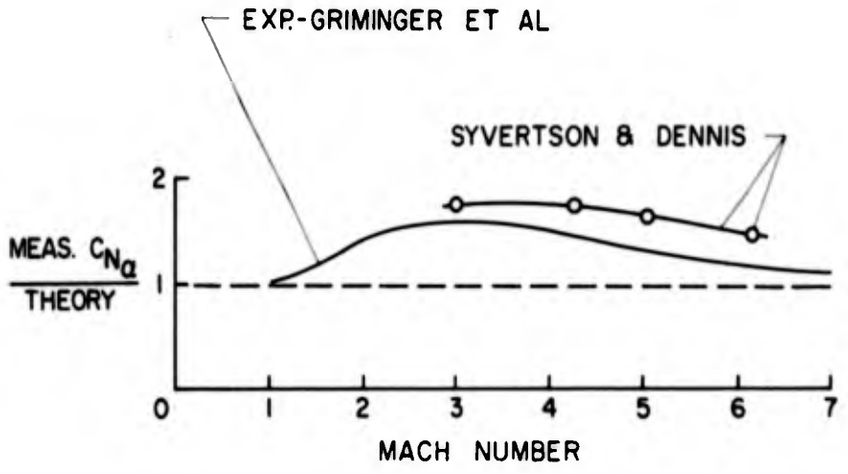

Figure 3

DAMPING IN PITCH

$\alpha = 0°$

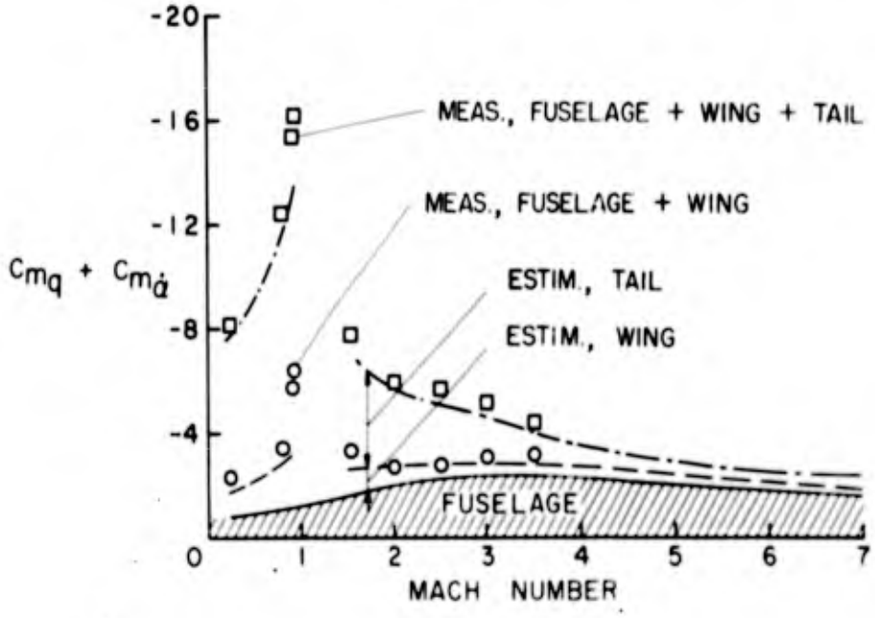

Figure 4

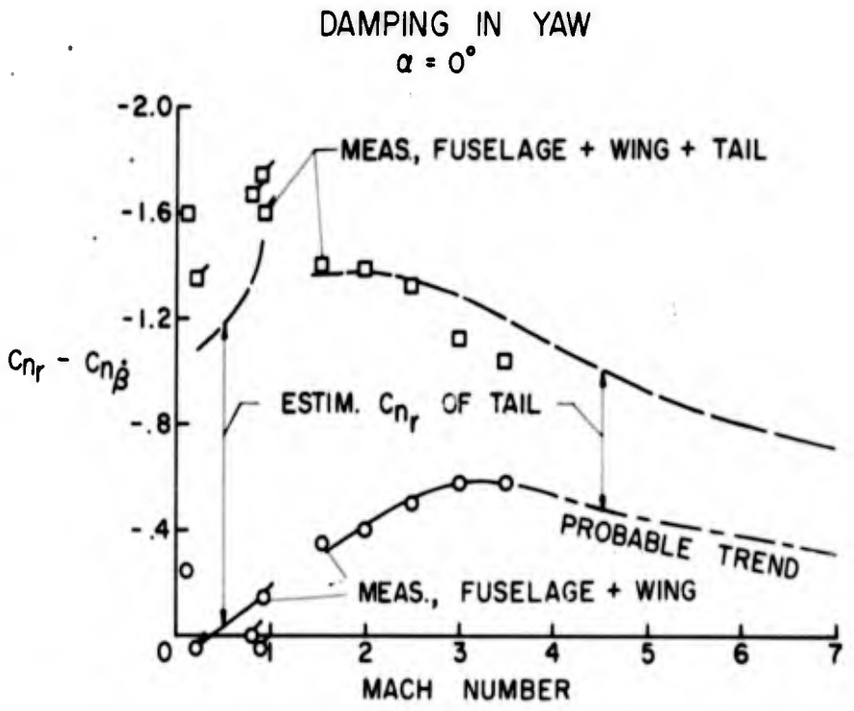

Figure 5

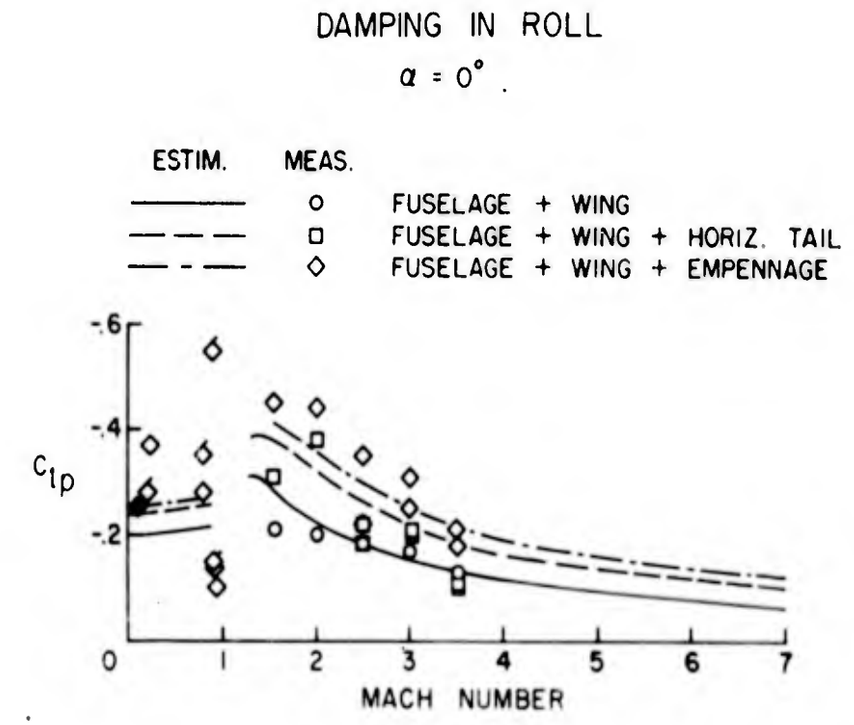

Figure 6

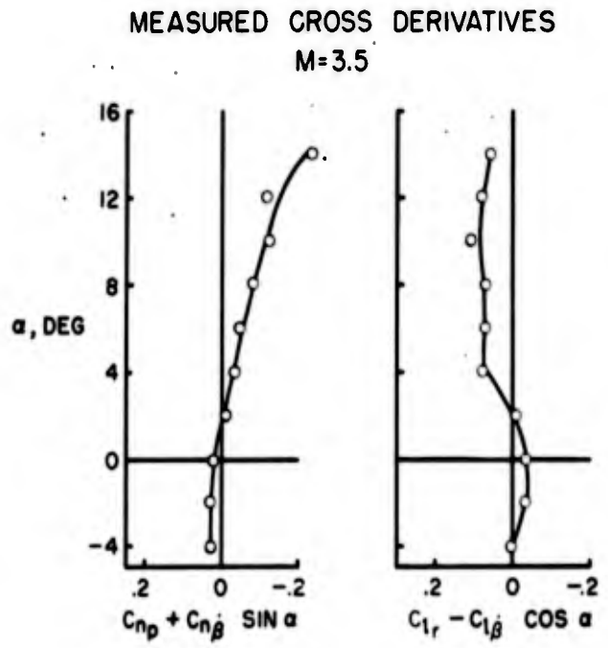

Figure 7

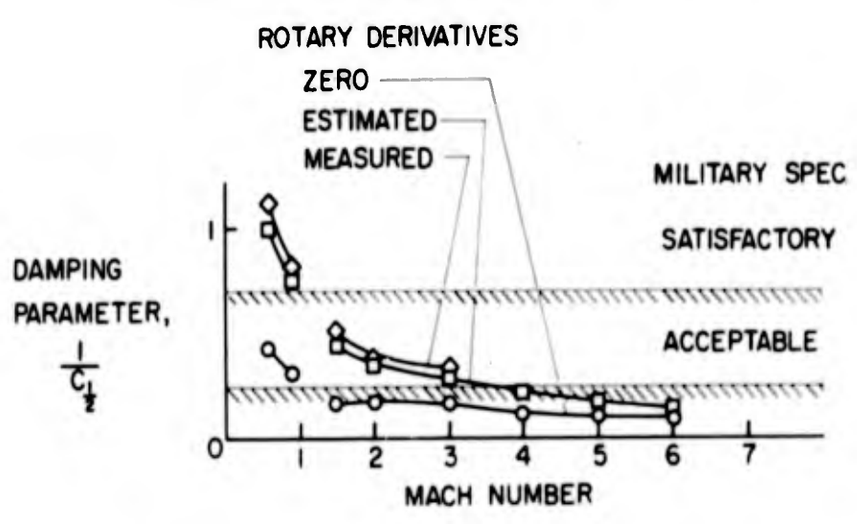

Figure 8

DAMPING OF THE DUTCH ROLL MODE

DYNAMIC PRESSURE = 1500 psf, $\left|\frac{\phi}{V_e}\right| < 0.4$

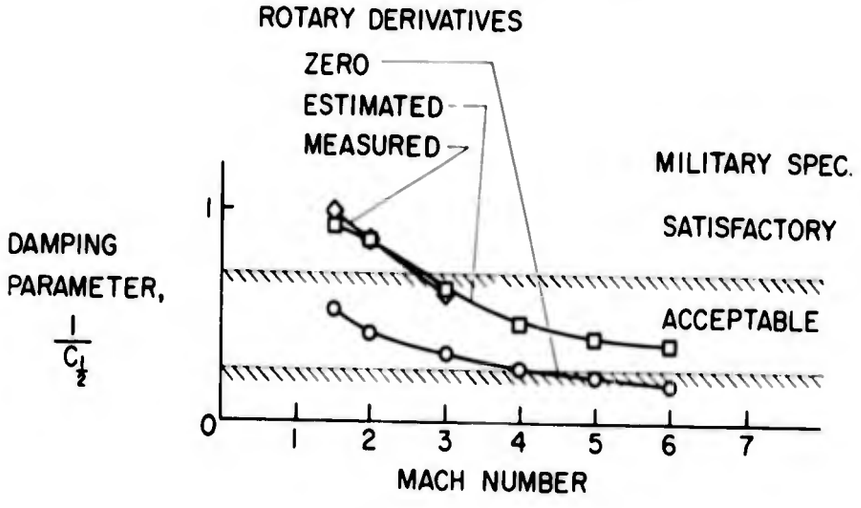

Figure 9

LOW-SPEED STABILITY AND CONTROL AND SPINNING CHARACTERISTICS OF DYNAMIC MODELS OF THE X-15 AIRPLANE

By Donald E. Hewes, James S. Bowman, Jr., and James L. Hassell, Jr.

NACA Langley Aeronautical Laboratory

INTRODUCTION

One of the papers presented at the X-15 conference in 1956 discussed the low-speed flight characteristics of a dynamic-scale model of the original configuration and placed particular emphasis on the novel use of the horizontal tail for roll control. The purpose of the present paper is to summarize results of more recent low-speed dynamic-model studies of the final configuration designated as configuration 3 in a previous paper by Jim A. Penland and David E. Fetterman, Jr.

The scope of this investigation as related to the flight program of the X-15 airplane is illustrated by use of figure 1 which shows the variation of lift coefficient and lift-drag ratio with angle of attack for the airplane at subsonic speeds with flaps and landing gear retracted. During the final glide and landing phase which will begin at about 30,000 feet, the airplane will normally be flown at maximum L/D, which occurs at an angle of attack of about 6° or 7°. Throughout the turning and flare maneuver for landing, it is expected that the angle of attack will be held below 15° or 20° and will be approximately 6° at touchdown. However, the airplane could reach angles much higher than those intended for normal operation since the pitch control is capable of trimming the airplane at angles of attack as high as 40°. The results of this investigation indicated generally satisfactory stability and control characteristics for the airplane for the relatively low angles of attack at which the airplane will normally be flown. The emphasis of this paper will therefore be on the flight characteristics of the airplane in the high-angle-of-attack range where stalls, directional divergences, and spins may be encountered.

The investigation included flight tests of a 1/7-scale model in the Langley full-scale tunnel and also in free-gliding flight using a recently developed radio-control technique. In order to interpret and evaluate some of the flight-test results, static and dynamic force tests were conducted to determine the low-speed stability and control parameters for angles of attack from 0° to as high as 90°. Preliminary

tests also have been made in the Langley 20-foot free-spinning tunnel to determine the developed spin and recovery characteristics. Inasmuch as the lower rudder will be jettisoned sometime during the subsonic glide, the investigation has included tests with the lower rudder both on and off.

SYMBOLS

C_L	lift coefficient
C_l	rolling-moment coefficient
C_m	pitching-moment coefficient
C_n	yawing-moment coefficient
C_{l_β}	effective-dihedral parameter, per deg
C_{n_β}	directional-stability parameter, per deg
L/D	lift-drag ratio
α	angle of attack, deg
β	sideslip angle, deg
δ_h	horizontal-tail deflection, deg
δ_h'	differential horizontal-tail deflection, deg
δ_v	rudder deflection, deg

DISCUSSION

Some of the significant stability and control parameters for the model used in the flight tests are illustrated in figures 2 to 5.

Figure 2 shows static longitudinal stability and control data. Variation of pitching-moment coefficient with angle of attack is shown for the model with four different horizontal-tail settings. These data

indicate that the model was longitudinally stable and trim angles of attack as high as 40° could be obtained.

The variations of the lateral control effectiveness with angle of attack for longitudinally trimmed conditions are shown in figure 3. The control moments are shown for the maximum control deflections used in the model flight tests, that is 14° for roll control and 5° for yaw control. Rolling effectiveness of the horizontal tail was maintained to angles of attack above 40°. Yawing moments produced by the roll control, expressed as the ratio of yawing-moment coefficient to rolling-moment coefficient, are favorable over the complete angle-of-attack range. Yawing effectiveness of the rudders decreases with increasing angle of attack and becomes zero at $\alpha \approx 40°$. Rolling moments produced by the yaw control are small for all angles of attack.

The variations with angle of attack of the static directional-stability parameter C_{n_β} and effective-dihedral parameter C_{l_β} for the complete model and for the model without the lower rudder are shown in figure 4. These data show that the static directional stability decreases with increasing angle of attack for both configurations and becomes zero at an angle of attack of about 18° or 20°. Effective dihedral becomes zero at about the same angle.

Some additional points regarding directional stability C_{n_β} for both configurations are illustrated by figure 5 which shows the variation of the yawing-moment coefficient with sideslip angle for two angles of attack, 15° and 25°. Curves of this type were used to obtain the values of C_{n_β} shown in the previous figure. At $\alpha = 15°$, the yawing-moment curves are nearly linear and the slopes indicate directional stability. At $\alpha = 25°$, the curves are nonlinear and indicate directional instability for small sideslip angles for the complete configuration as well as directional instability for much larger angles for the model with the lower rudder off. With a condition such as this, the airplane would tend to fly in a sideslipping attitude, either to the left or right, where the yawing-moment curve indicates both trim and stability. For the model with the lower rudder off, it is doubtful that steady trimmed flight could be obtained at sideslip angles as large as the 20° indicated.

Additional static force tests of the landing configuration have been completed only recently, but these indicate that there are only relatively minor changes in the static stability and control characteristics when the flaps and landing gear are extended, particularly for the angles of attack required for landing.

Motion pictures were made of the model flight tests in the full-scale tunnel. The low-speed flight characteristics were shown for both configurations at an angle of attack of 15° and at an angle of attack of about 25° to 30°. Since the model exhibited good low-speed longitudinal stability and control characteristics in all the test conditions, the following discussion of the motion pictures will be devoted to the lateral characteristics.

At an angle of attack of 15° and a speed of 55 knots, which corresponded to about 150 knots for the full-scale airplane, the flight characteristics of the model with both the lower rudder on and off were considered very good. At an angle of attack of 25° to 30°, the complete model had a tendency to fly in a sideslipping attitude, either to the left or right, due to directional instability at small angles, as discussed previously. Although the model could be flown successfully, the flight characteristics were considered unsatisfactory because of the sideslipping condition. Without the lower rudder, the flight characteristics of the model were considered to be worse than those for the complete model at the same angle of attack.

Although the flight characteristics were found to be unsatisfactory for angles of attack higher than 20°, they appeared to be satisfactory for the angle-of-attack range in which the airplane will normally be flown. In an effort to improve the flight characteristics at the higher angles of attack, the model was tested with a type of fuselage nose strake or fence which has shown beneficial effects on the directional stability of other configurations. (See refs. 1 to 3.) These strakes were attached to the nose of the fuselage as shown in figure 6. On the airplane, this strake would correspond to a strake 2 inches wide and 6 feet long.

The effects of these strakes on directional stability at an angle of attack of 25° are illustrated in figure 7. The nonlinearity for the complete configuration is reduced by the use of the strakes so that directional stability exists at zero sideslip angle. Addition of strakes with the lower rudder off produced a similar beneficial effect but the resulting stability increment was sufficient to produce only neutral or a very small amount of stability at small sideslip angles.

Motion pictures illustrated the beneficial effect of these strakes on the flight characteristics of the model. The complete model with strakes was photographed at an angle of attack of about 25° to 30°, the same angle as in the previously mentioned motion pictures where the model was flying in a sideslipping attitude. In this case the model showed no tendency to fly in a sideslipping attitude, and the flight characteristics were considered very good. A marked improvement was also noted for the model with the lower rudder off. The resulting

flight characteristics in this case were not quite so good as for the complete model with strakes.

As a direct result of adding strakes, the model could be flown satisfactorily at angles of attack as high as 30° with the lower rudder off and 40° with it on.

Additional tests were made on a 1/50-scale model in the Langley 11-inch hypersonic tunnel and in the Langley 4- by 4-foot supersonic pressure tunnel to determine the effects of strakes of this type on directional stability at supersonic speeds. The results of these tests indicated a decrease in the effectiveness of the strakes with increasing Mach number. The effects were small at a Mach number of 2.01 and negligible at a Mach number of 6.86. The effect on longitudinal stability appeared to be small or negligible for all speeds. At the present time, there are no plans to install strakes on the airplane because the directional stability appears to be adequate without the strakes for the normal subsonic flight conditions; also, additional studies will be required to evaluate the structural and heating problems imposed if strakes are added.

The preliminary studies of the developed-spin and recovery characteristics of the X-15 airplane were made with a 1/30-scale dynamic model, which was the largest properly ballasted model that could be tested in the spin tunnel. For this size model, it appeared that Reynolds number effects would have to be considered before a proper interpretation of dynamic spin-tunnel results could be made. (See ref. 4.) Results of force tests indicated that at spin angles of attack there were appreciable differences between model and airplane in both the aerodynamic pitching and yawing moments. As a preliminary attempt to compensate for the pitching-moment differences, the center of gravity was moved forward; and in an effort to compensate for the yawing-moment differences, a strake was added to the fuselage near the canopy on the left side for a right spin, and vice versa. For the complete configuration, fully developed spins were not obtainable. However, with the lower rudder off, spins were readily obtainable and recoveries from these spins were unsatisfactory or impossible. Tests are still being made to evaluate more fully the full-scale airplane spin and recovery characteristics.

The preliminary results just discussed were illustrated by a movie made from the test records. As shown in the movie, the model was launched into the tunnel with an initial rotation. The model with the lower rudder on lost this launching rotation and entered a glide indicating that a fully developed spin was not obtained. Without the lower rudder, sometimes the model would spin and sometimes it would not. In one movie sequence where a spin was obtained, the model was seen to recover in 3 turns after the rudder was moved against and the roll

controls moved with the spin; in another case, the model did not recover although recovery was attempted.

The testing technique in the spin tunnel involves launching the model with initial spinning rotation. (See ref. 4.) It is recognized that obtaining a spin in this manner does not necessarily mean that the airplane will enter a spin from normal-flight conditions. In order to simulate more closely possible spin-entry conditions, a few flight tests were made in which the 1/7-scale model was dropped from a helicopter and flown in free-gliding flight by radio control. This technique also afforded the opportunity to study the recovery of the airplane from incipient spins, that is, the transient spinning motion which precedes a fully developed spin and which cannot be evaluated in a conventional spin tunnel.

The results of these tests showed that the model could develop spinning motions from a normal-flight condition by applying full up pitch control and attempting to correct any rolling or yawing motions with an opposing roll control movement. These tests also showed that satisfactory recovery could be achieved when attempted during the incipient phase of the spin by applying roll control in the direction of rotation.

A motion picture of a flight record from one of these glide tests was made in which the model with the lower rudder off was seen to enter a spin inadvertently. A satisfactory recovery from the incipient spin was achieved in less than half a turn.

On the basis of the preliminary results obtained from the spin tunnel tests and from the radio-controlled flight tests, it appears that the airplane will not enter a fully developed spin with the lower rudder on. However, after the lower rudder has been jettisoned, the airplane can spin and care should be exercised to avoid allowing the spin to develop. If any yawing or rolling motion is experienced at angles of attack above about 20° where directional divergences and spins may be encountered, the stick should be moved with and the rudder against the direction of rotation during the incipient phase. The pilot should be warned particularly against attempting to level the wings immediately by moving the stick against the direction of rotation. Attempts for recovery which are delayed until after the spin has fully developed may be difficult or impossible to achieve. Some auxiliary device such as reaction rockets therefore may be required in order to insure a satisfactory recovery from developed spins.

CONCLUDING REMARKS

The flight characteristics of the X-15 model were found to be generally satisfactory for angles of attack up to about 20°. Although the controls were effective at much higher angles of attack, the low-speed flight characteristics became unsatisfactory because of directional instability. Addition of small fuselage strakes provided a definite improvement in the flight characteristics for both configurations at these higher angles of attack.

Since spins may be encountered after the lower rudder has been jettisoned and satisfactory recoveries may be difficult or impossible to obtain if the spin is allowed to develop fully, it is strongly recommended that the lower rudder be retained on the airplane as long as possible.

REFERENCES

1. Klinar, Walter J.: A Study by Means of a Dynamic-Model Investigation of the Use of Canard Surfaces as an Aid in Recovering From Spins and as a Means for Preventing Directional Divergence Near the Stall. NACA RM L56B23, 1956.

2. Sleeman, William C., Jr.: Investigation at High Subsonic Speeds of the Effects of Various Horizontal Fuselage Forebody Fins on the Directional and Longitudinal Stability of a Complete Model Having a 45° Sweptback Wing. NACA RM L56J25, 1957.

3. Driver, Cornelius: Wind-Tunnel Investigation at a Mach Number of 2.01 of Forebody Strakes for Improving Directional Stability of Supersonic Aircraft. NACA RM L58C11, 1958.

4. Neihouse, Anshal I., Klinar, Walter J., and Scher, Stanley H.: Status of Spin Research for Recent Airplane Designs. NACA RM L57F12, 1957.

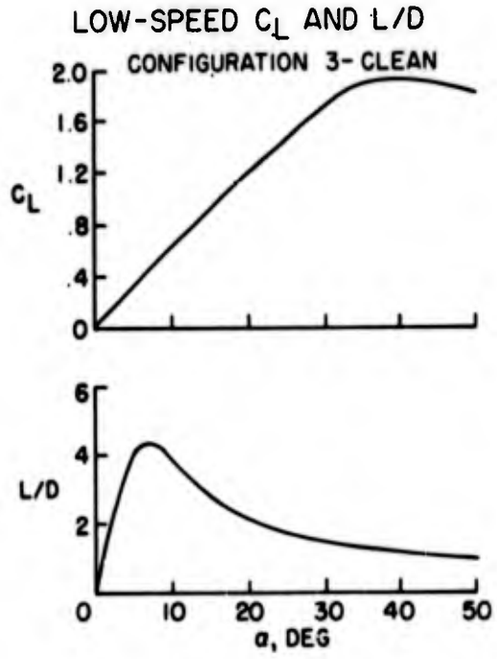

Figure 1

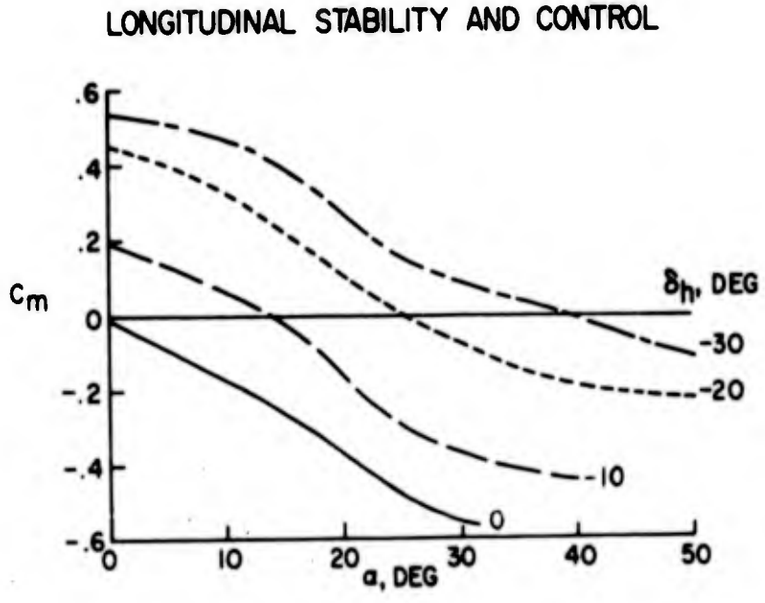

Figure 2

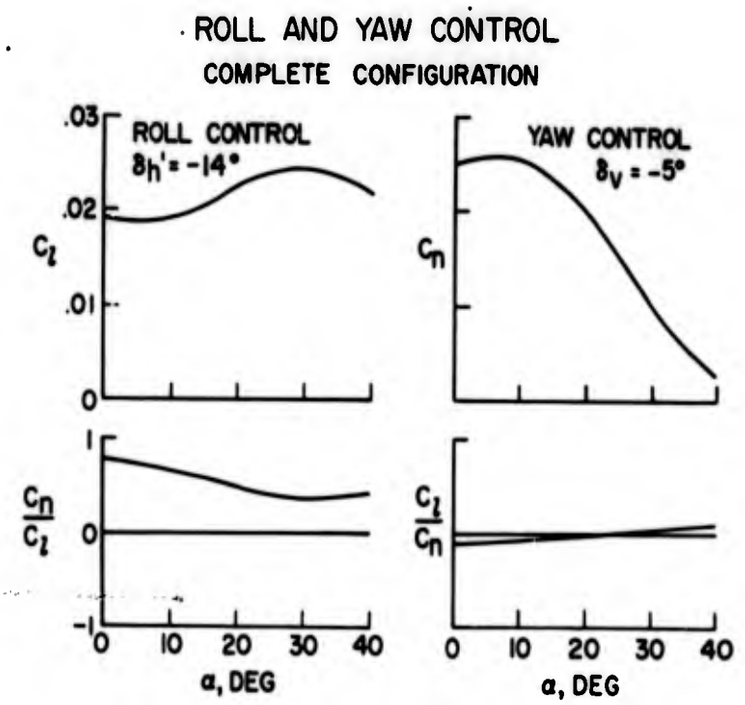

Figure 3

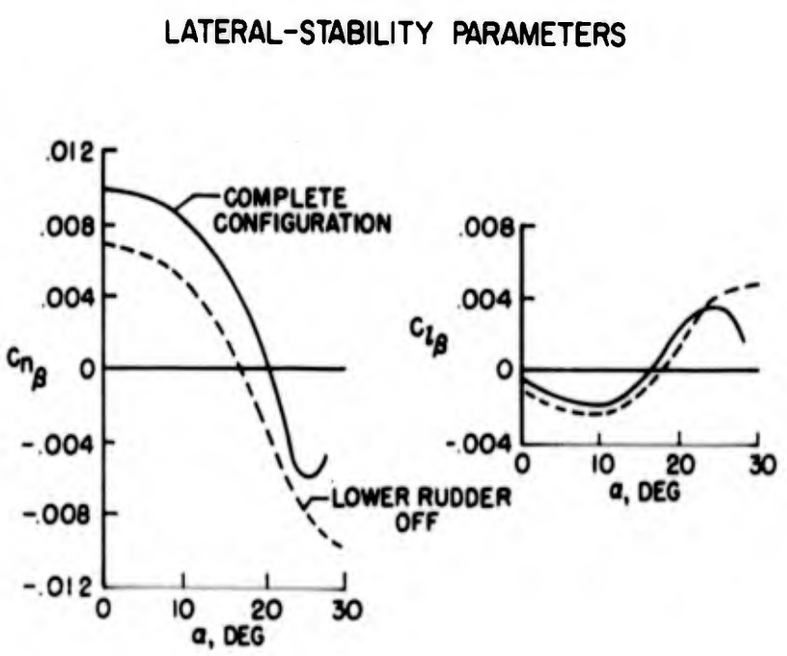

Figure 4

DIRECTIONAL STABILITY

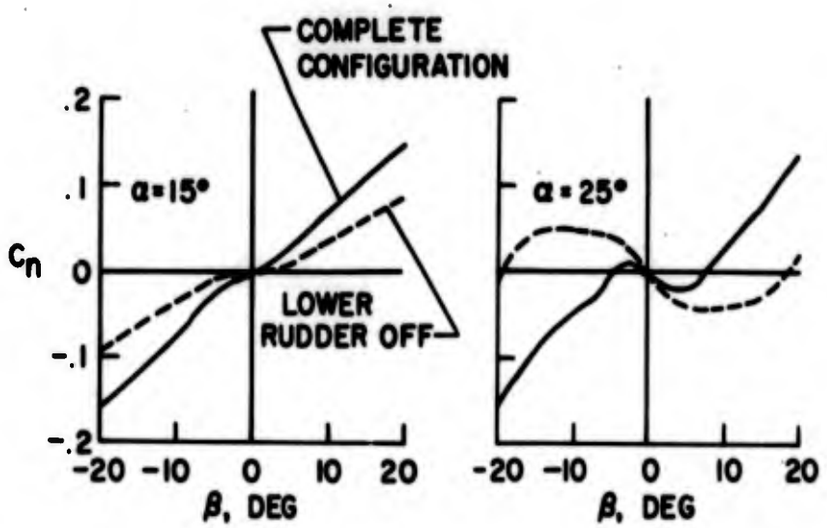

Figure 5

STRAKE INSTALLATION USED ON MODEL

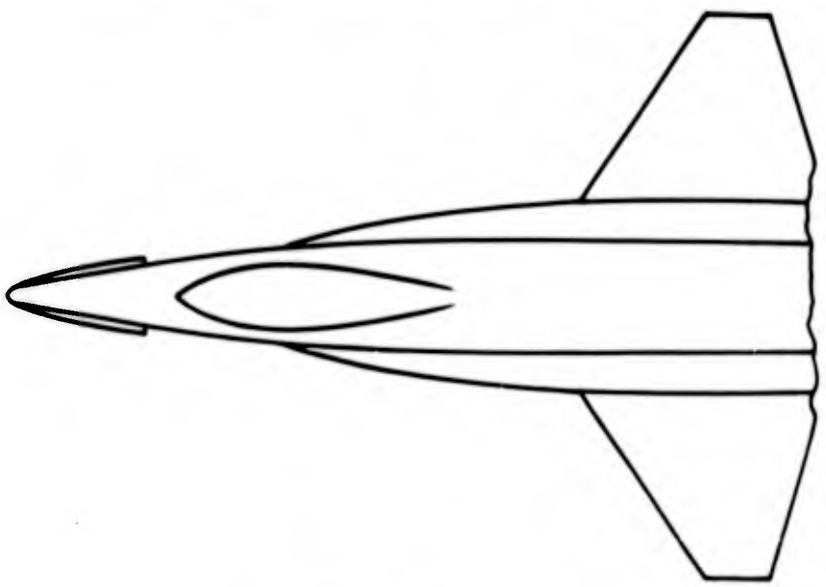

Figure 6

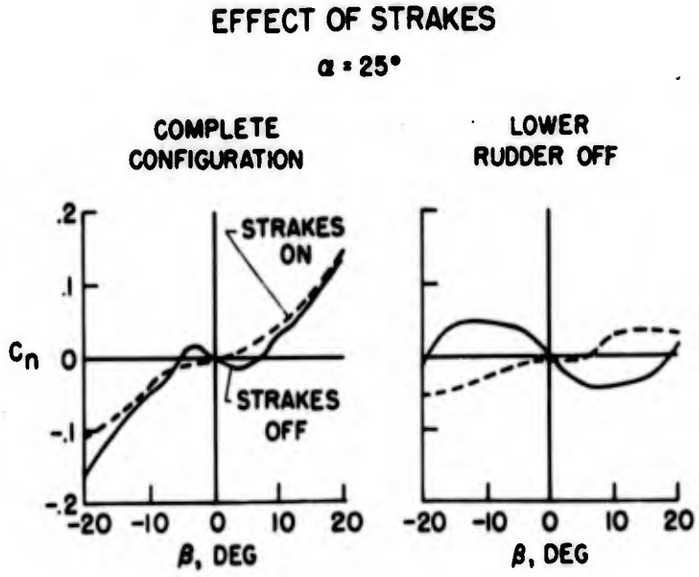
EFFECT OF STRAKES
α = 25°
COMPLETE CONFIGURATION
LOWER RUDDER OFF
STRAKES ON
STRAKES OFF
C_n
.2
.1
0
-.1
-.2
-20 -10 0 10 20
β, DEG
-20 -10 0 10 20
β, DEG

Figure 7

AERODYNAMIC CHARACTERISTICS OF THE X-15/B-52 COMBINATION

By William J. Alford, Jr., and Robert T. Taylor

NACA Langley Aeronautical Laboratory

INTRODUCTION

Past aerial launchings of research airplanes have been made from the center-line location of the carrier airplane. In the case of the X-15/B-52 combination the carry location chosen is beneath the 18-percent-semispan station of the right wing between the fuselage and the inboard engine nacelle. The reason for the choice of this location has been stated previously in the "X-15 Research Airplane Development Status" paper. With such an asymmetrical location, questions immediately arise as to the carry and launching safety and the aerodynamic-loads problems confronting the combination.

Investigations were therefore undertaken by the National Advisory Committee for Aeronautics to determine (1) the carry loads and mutual aerodynamic interference effects from high-speed wind-tunnel tests and (2) the drop characteristics of the X-15 through the B-52 flow field from low-speed dynamic-model drop tests and six-degree-of-freedom calculations. The purpose of this paper is to present briefly the major results of these investigations.

SYMBOLS

α_{B-52}	angle of attack of B-52 water line, deg
α_{X-15}	angle of attack of X-15 center line, deg
$C_{D,trim}$	drag coefficient that corresponds to zero pitching moment (trim)
R	Reynolds number
M	Mach number
C_l	rolling-moment coefficient
C_n	yawing-moment coefficient

h	altitude, ft
C_L	lift coefficient
C_m	pitching-moment coefficient
L	lift, lb
M_Y	pitching moment, ft-lb
M_Z	yawing moment, ft-lb
M_X	rolling moment, ft-lb
q	dynamic pressure
z	distance along Z-axis, ft
α_o	initial angle of attack of X-15, deg
W	weight, lb
θ	pitch angle, deg
V	velocity, ft/sec
Ψ	yaw angle, deg
ϕ	roll angle, deg

HIGH-SPEED TUNNEL TESTS AND RESULTS

A drawing of the X-15/B-52 combination is presented in figure 1. Here the X-15 is shown pylon mounted on the B-52 in the carry location. The detail sketch shows the outline of the B-52 wing cut out to accommodate the X-15 vertical tail and the three points of suspension. The top and front views show the longitudinal and spanwise relative location of the two airplanes. A photograph of the 1/40-scale models of the combination mounted in the Langley high-speed 7- by 10-foot tunnel is shown in figure 2. Both models were internally instrumented with six-component strain-gage balances, with the B-52 model having additional strain gages and a pressure gage located in the right horizontal-tail panel to obtain a qualitative measure of tail buffet as affected by the X-15 installation. Some results of these buffet

tests will be presented subsequently in the paper by Messrs. Runyan and Sweet. The parameters varied in these wind-tunnel tests were: Mach number, angles of attack and sideslip, and control deflections of both models. In addition, tests were made with the X-15 model mounted in the presence of the B-52 by means of a sting so that the effects of separation distance between the airplane models could be determined.

Presented in figures 3 and 4 are the effects of the X-15 on the B-52 aerodynamic characteristics for longitudinal trim at a Mach number of 0.75 and a Reynolds number of 2.25×10^6. Figure 3 presents the lift and drag coefficients and figure 4 presents the rolling- and yawing-moment coefficients plotted against the angle of attack of the B-52 fuselage waterline. The solid curves represent the B-52 alone (with wing cutout) and the dashed curves represent the combination of the B-52 and the X-15. It should be noted that the B-52 wing has a root incidence of 6° relative to the fuselage and hence the angle of attack for zero lift (fig. 3) is approximately -6° on the α-scale. The cruise angle-of-attack range to be studied is indicated in both figures 3 and 4 by the arrows. The addition of the X-15 produced essentially no change in the pitching-moment characteristics, and pitching-moment data therefore are not presented. The most noteworthy effect of the X-15 is an increase of approximately 30 percent in minimum trim drag and 15 percent in the cruise range. The cutout in the B-52 wing to accommodate the X-15 vertical tail caused small right-wing-down rolling moments and small nose-right yawing moments. The addition of the X-15 reduced both the rolling and yawing moments. The maximum rolling moment indicated would require less than 0.1 percent spoiler deflection for trim, and the yawing moments correspond to less than 0.1° in sideslip angle.

The effects of Mach number on the X-15 aerodynamic characteristics are presented in figures 5 and 6. The lift and pitching-moment coefficients are presented in figure 5 and the rolling- and yawing-moment coefficients are presented in figure 6. All coefficients are plotted against angle of attack of the combination with the lower α-scale referred to the X-15 center line and the upper α-scale referred to the B-52 waterline. As would be surmised from past flow-interference experience (ref. 1), the effect of increasing Mach number generally caused larger magnitudes and variations with α for all aerodynamic coefficients. Note that the rolling-moment coefficient usually decreases with increasing angle of attack.

The effects of the B-52 flow field on the X-15 aerodynamic loads for a Mach number of 0.75 and an assumed altitude of 38,000 feet are presented in figures 7 and 8. In these figures the lift in pounds and the pitching, rolling, and yawing moments in foot-pounds are plotted as functions of the angle of attack of the combination. The solid curves are the free-stream loads and the dashed curves represent the

X-15 loads in the carry location. The B-52 flow field reduced the lift load to approximately one-third of the free-stream level and produced large nose-down pitching moments throughout the angle-of-attack range. This lift and moment variation for the carry location indicate a load-center movement from 145 percent mean aerodynamic chord ahead of the center of gravity at $\alpha = -4^{\circ}$ to 110 percent mean aerodynamic chord behind the center of gravity at $\alpha = 4^{\circ}$. The negative moment at $\alpha = -4^{\circ}$ is as would be expected to result from downflow on the fore-body of the X-15. At $\alpha = 4^{\circ}$, however, theoretical studies indicate that the pitching moments should be or tend to be positive because of downflow on the X-15 tail induced by the B-52 wing. The large negative moment is therefore presumed to result from a localized upflow induced by the cutout in the B-52 wing to accommodate the vertical tail of the X-15. Additional data obtained with a larger cutout indicate such a "flow-sink" effect. Although sizable yawing moments are in evidence at the extreme angles, the moment is small at $\alpha = 1^{\circ}$, which is the design drop angle. A particular point to note is the large right-wing-down rolling moments that decrease with increased angle of attack.

The effects of separation distance between the X-15 and B-52 airplanes are presented in figures 9 and 10. The abscissa for these curves is the separation distance z in feet. The ordinates are lift in pounds and the pitching, rolling, and yawing moments in foot-pounds. The conditions shown are for design launch conditions, that is, an altitude of 38,000 feet, a Mach number of 0.75, and an X-15 center-line angle of attack of 1°. Although large initial inputs are indicated for all components except the yawing moment, these inputs diminished rapidly with small changes in distance. An interesting point to note is the initial decrease in the lift. The reason for this decrease is not completely understood, although it is presumed to be associated with the movement of horizontal tail out of the localized region of upwash generated by the cutout in the B-52 wing.

DYNAMIC-MODEL DROP TESTS AND RESULTS

The dynamic-model drop tests made to determine launch safety and drop characteristics utilized the constant Froude number similarity technique (ref. 2). In this procedure the models are ballasted and the free-stream velocity is reduced so that model and prototype translational accelerations are equal, whereby similar trajectory time histories are produced. The effects of Mach number cannot, however, be determined from this simulation because of incompatible velocity

criteria. Motion-picture records were obtained to show the results of the drop tests for both the empty-weight and the full-weight conditions.[1]

Drop tests made to determine the effect of sideslip indicated that significant rolling motions were induced but were not considered to be critical. Photographic records of the X-15 vertical-tail motions in the B-52 wing cutout indicated adequate clearance for all conditions investigated. The drop-tests results indicated that safe drops should be expected for all fully loaded conditions. The same is true for the weight-empty condition if nose-up pitch control is avoided.

DROP TRAJECTORY CALCULATIONS

In order to determine the effects of Mach number and altitude at the higher Mach numbers, six-degree-of-freedom calculations were made on the IBM 704 electronic computer. The static aerodynamic inputs for these calculations were obtained from the high-speed tunnel results. The natural first inclination in such a program is to compare calculated drop motions with the dynamic-model drop-test results. Figures 11 and 12 present such a comparison. The abscissas are full-scale time in seconds and the ordinates are separation distance z in feet and pitch angle θ, roll angle ϕ, and yaw angle ψ in degrees. The solid curves represent the experimental drop characteristics and the dashed curves represent the calculated results. The calculated results underpredict the variations in separation distance; agree well with the experimental pitch and yaw angles; and, initially underpredict and then overpredict roll angle. The roll time histories indicate rolling velocities of approximately 15° and 20° per second for the calculated and experimental results, respectively. Consideration of the parameters to be estimated in calculations such as these indicates that the correlation of the results of the best available techniques and the experimental results is acceptable.

The calculated X-15 drop motions for two Mach numbers are presented in figures 13 and 14. Again, the separation distance and pitch, roll, and yaw angles are plotted as functions of time. The assumed conditions are an altitude of 38,000 feet and full-weight characteristics. The solid curves represent motions at $M = 0.60$ and the dashed curves represent motions at $M = 0.75$. It should be noted in this and the remaining figures that the B-52 airplane is assumed in straight and level flight and therefore the effect of changing the primary variable produced attendant changed in others. In this case changing Mach number caused changes in α and q. The initial X-15

[1]These results are presented in film L-344, which is available on loan from NACA Headquarters.

angle of attack α_o and the B-52 trim angles of attack α_{B-52} are listed for reference in the legend. Increasing Mach number caused only small changes in z and ψ, reduced the θ-motion somewhat, but reversed the rolling motion ϕ. The initially smaller roll angle existing at M = 0.60 is due primarily to the higher angle of attack and therefore lower rolling-moment input.

Presented in figures 15 and 16 are the calculated X-15 drop motions at two altitudes. The parameters shown are the same as for the previous figures. The assumed conditions are the full-weight characteristics and a Mach number of 0.75. The solid curve represents 30,000 feet and the dashed curve represents 38,000 feet. The effect of increasing altitude is to reduce the intensity of the motions, particularly roll. This result is due to the lower dynamic pressure associated with and the higher angle of attack required at the higher altitude.

CONCLUDING REMARKS

In summary, results of high-speed wind-tunnel tests indicate that the X-15 installation increases the B-52 drag at cruise conditions by approximately 15 percent. The B-52 flow field induces sizable changes in the X-15 aerodynamic loads. These loads are increased with Mach number and have steep gradients with separation distance. The results of low-speed dynamic-model drop tests and six-degree-of-freedom calculations indicated that safe drops should be obtained.

REFERENCES

1. Alford, William J., Jr.: Theoretical and Experimental Investigation of the Subsonic-Flow Fields Beneath Swept and Unswept Wings With Tables of Vortex-Induced Velocities. NACA Rep. 1327, 1957. (Supersedes NACA TN 3738.)

2. Scherberg, Max, and Rhode, R. V.: Mass Distribution and Performance of Free Flight Models. NACA TN 268, 1927.

X-15/B-52 COMBINATION

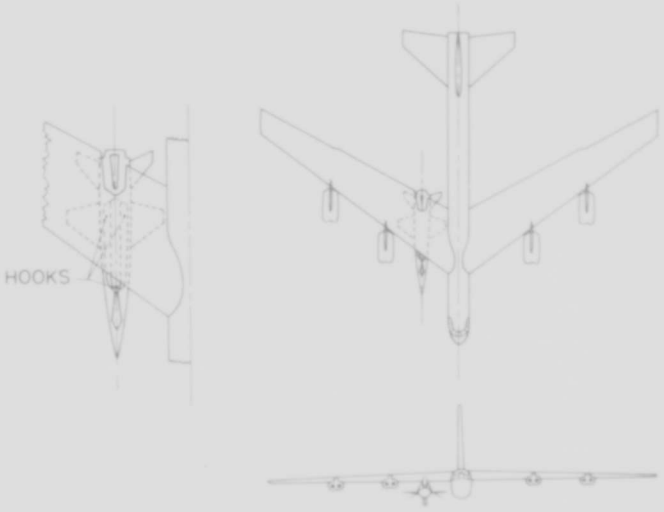

Figure 1

X-15 AND B-52 MODELS IN LANGLEY HIGH-SPEED 7- BY 10-FT WIND TUNNEL

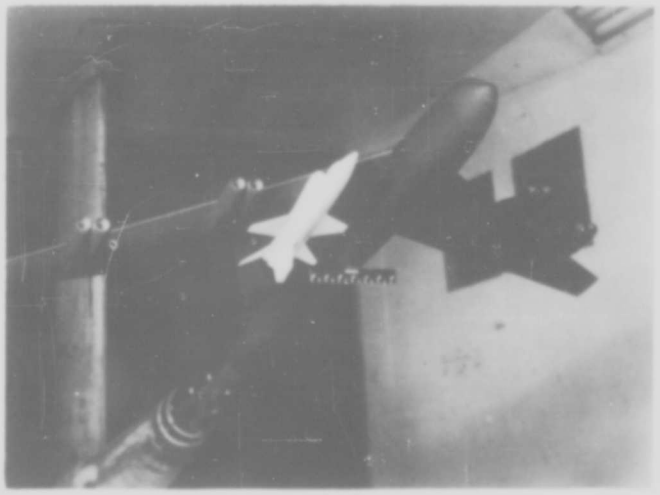

Figure 2

EFFECT OF X-15 ON B-52 AERODYNAMIC CHARACTERISTICS

LONGITUDINAL; M = 0.75; R = 2.25×10^6

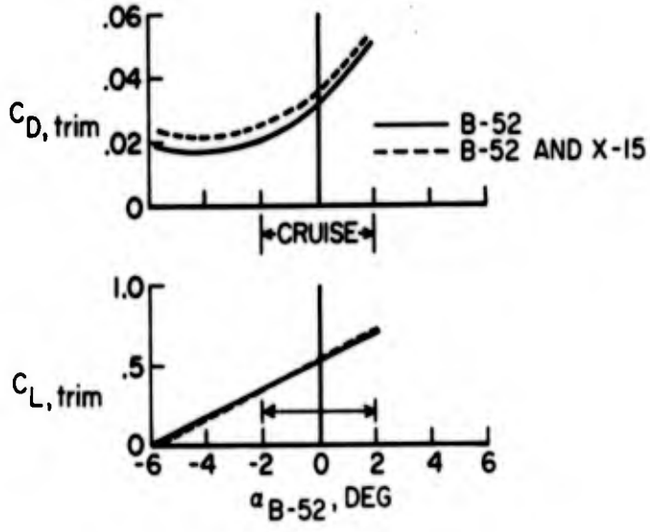

Figure 3

EFFECT OF X-15 ON B-52 AERODYNAMIC CHARACTERISTICS

LATERAL ; M = 0.75 ; R = 2.25×10^6

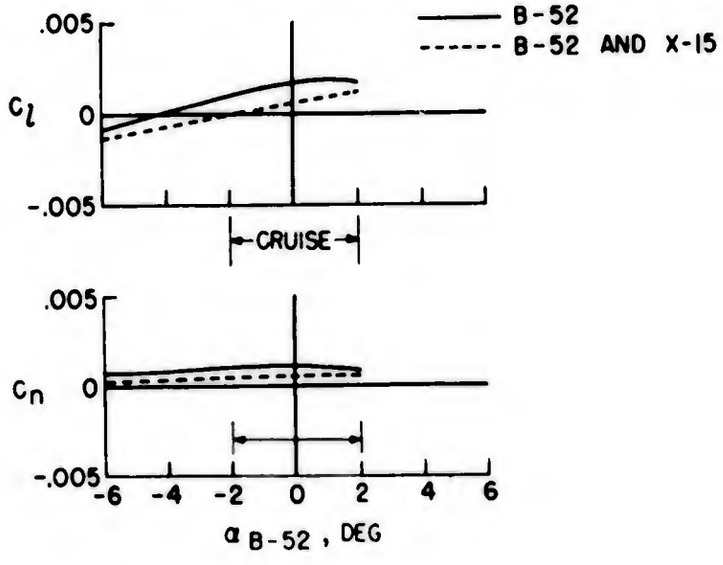

Figure 4

EFFECT OF MACH NUMBER ON X-15 AERODYNAMIC CHARACTERISTICS
LONGITUDINAL; CARRY POSITION

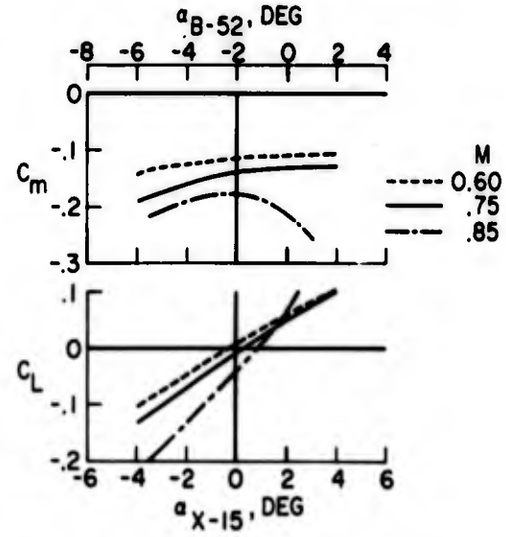

Figure 5

EFFECT OF MACH NUMBER ON X-15 AERODYNAMIC CHARACTERISTICS
LATERAL; CARRY POSITION

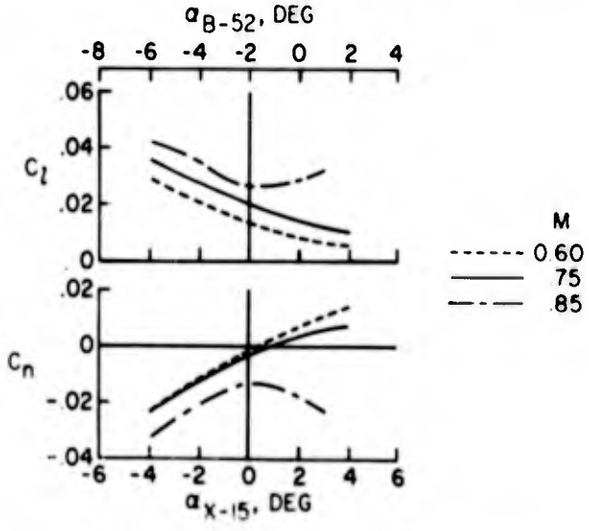

Figure 6

EFFECT OF B-52 ON X-15 AERODYNAMIC LOADS

LONGITUDINAL; M=0.75; h=38,000 FT; R=0.92 x 10^6

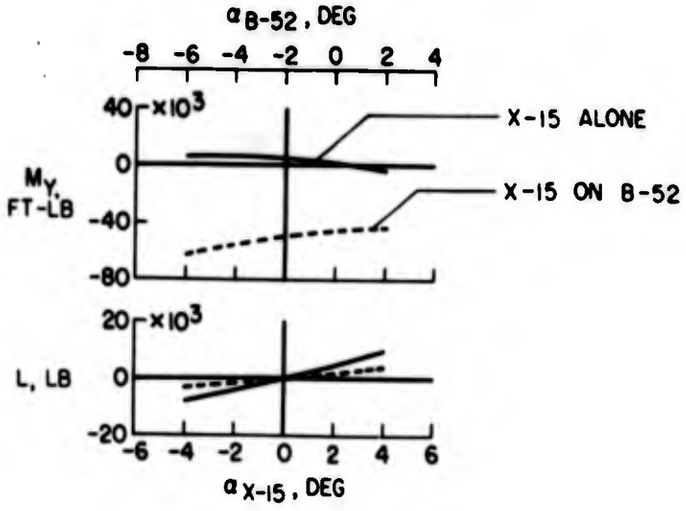

Figure 7

EFFECT OF B-52 ON X-15 AERODYNAMIC LOADS

LATERAL; M=0.75; h=38,000FT; R=0.92x10^6

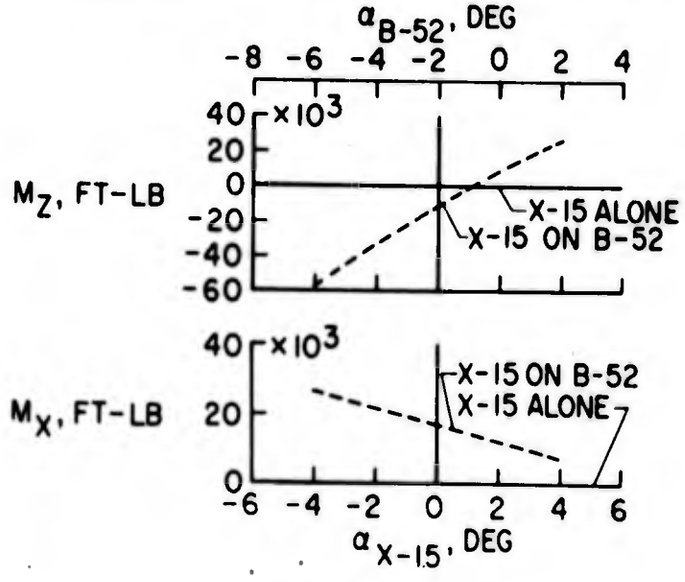

Figure 8

EFFECT OF SEPARATION DISTANCE ON X-15 AERODYNAMIC LOADS
LONGITUDINAL; M = 0.75; h = 38,000 FT; α_0 = 10°

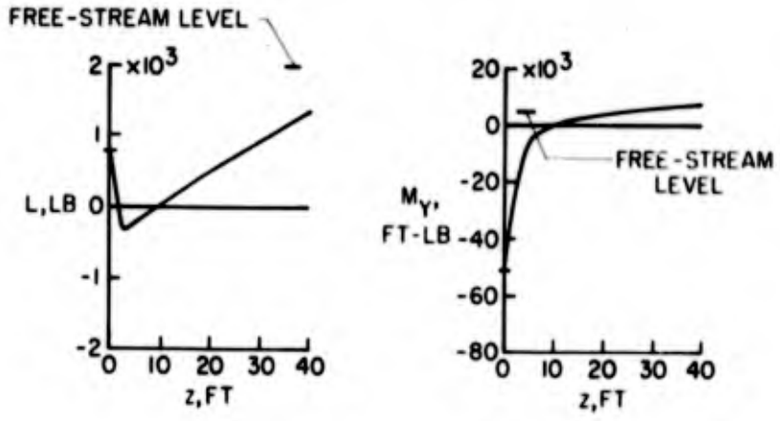

Figure 9

EFFECT OF SEPARATION DISTANCE ON X-15 AERODYNAMIC LOADS
LATERAL; M = 0.75, h = 38,000 FT; α_0 = 10°

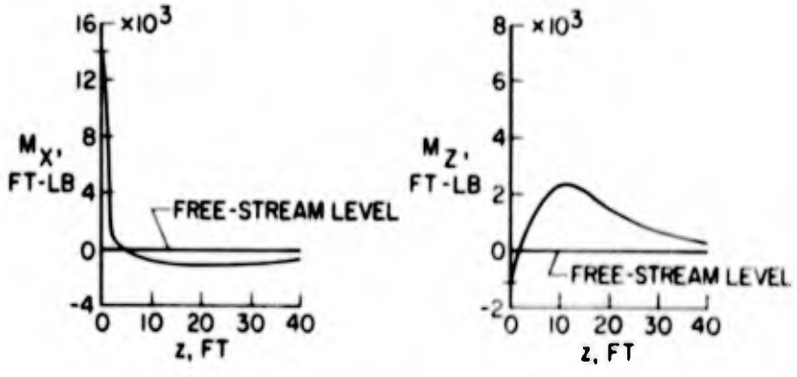

Figure 10

COMPARISON OF CALCULATED AND EXPERIMENTAL DROP MOTIONS

LONGITUDINAL; V CORRESPONDS TO M=0.60; h=30,000 FT; α_0=1.8°; W=12,366 LB

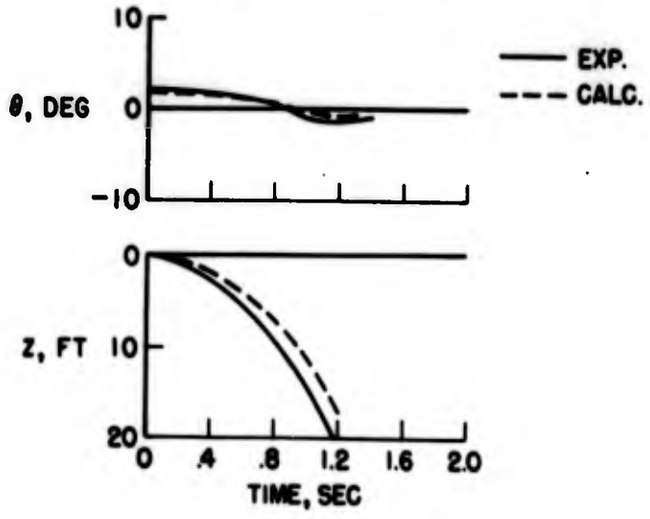

Figure 11

COMPARISON OF CALCULATED AND EXPERIMENTAL DROP MOTIONS

LATERAL ; V CORRESPONDS TO M=0.60 ; h=30,000 FT ; α_0=1.8° W=12,366 LB

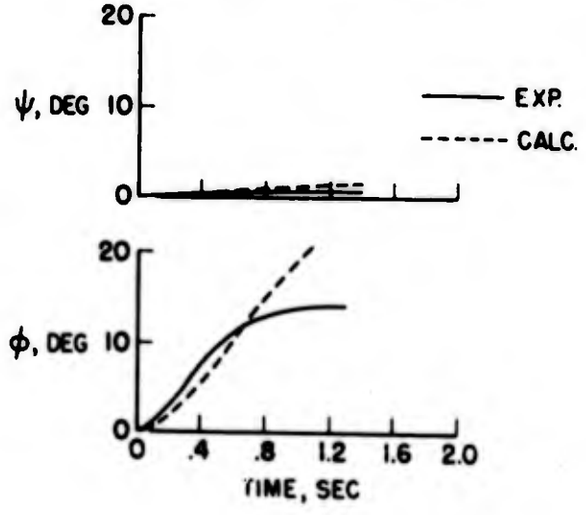

Figure 12

CALCULATED X-15 DROP MOTIONS
FOR TWO MACH NUMBERS
LONGITUDINAL; h = 38,000 FT; W = 31,635 LB

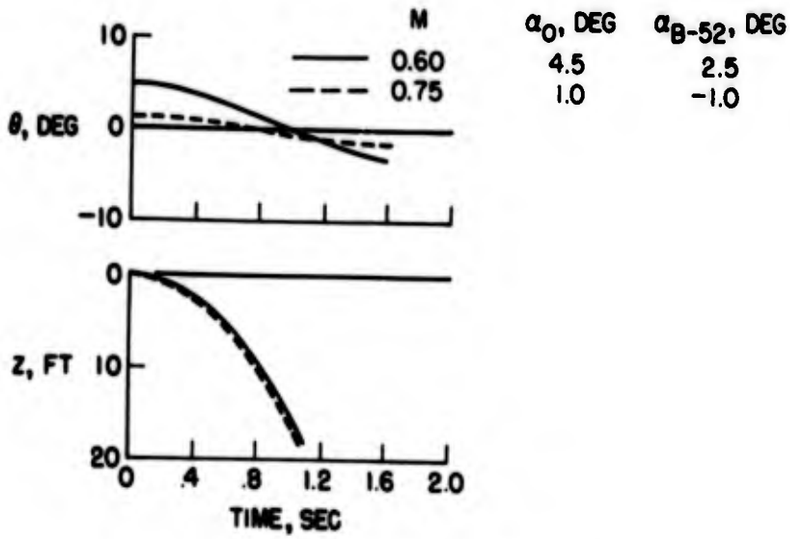

Figure 13

CALCULATED X-15 DROP MOTIONS
FOR TWO MACH NUMBERS
LATERAL; h = 38,000 FT; W = 31,635 LB

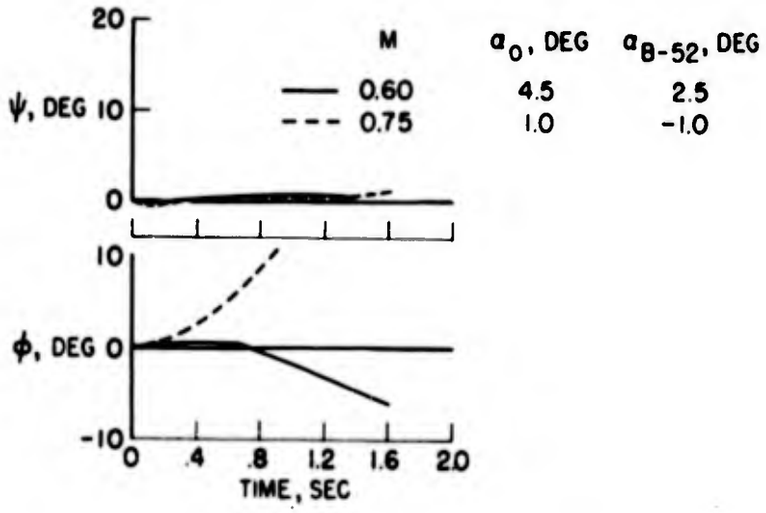

Figure 14

CALCULATED X-15 DROP MOTIONS AT TWO ALTITUDES
LONGITUDINAL; M = 0.75; W = 31,635 LB

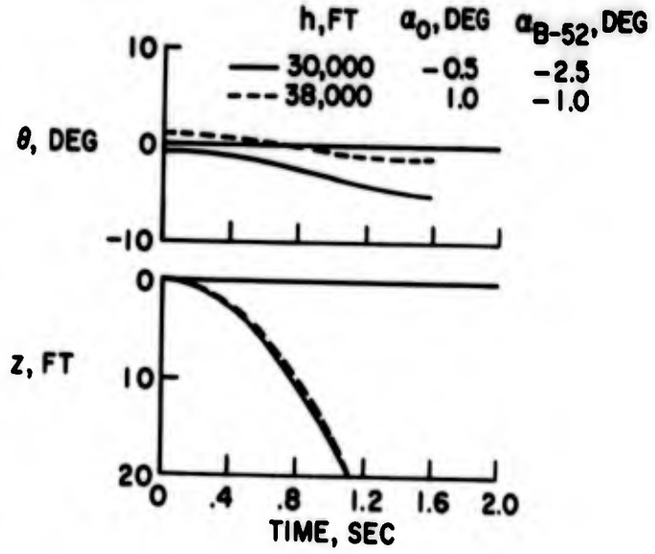

Figure 15

CALCULATED X-15 DROP MOTIONS AT TWO ALTITUDES
LATERAL; M = 0.75; W = 31,635 LB

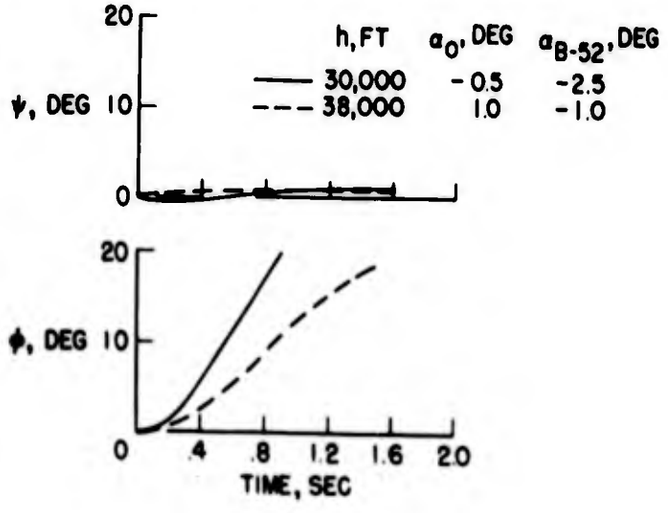

Figure 16

FLIGHT AND ANALOG STUDIES OF LANDING TECHNIQUES PERTINENT TO THE X-15 AIRPLANE

By Thomas W. Finch, Gene J. Matranga, Joseph A. Walker, and Neil A. Armstrong

NACA High-Speed Flight Station

INTRODUCTION

The approach and landing operation of unpowered rocket airplanes has always required considerable pilot concentration but has been completed without undue demands on piloting technique. The X-15 airplane will land in a range of lift-drag ratio L/D markedly lower than previous rocket airplanes have used. In order to assess the potential difficulty of landing the X-15 at low L/D and to determine whether different techniques would be required in the landing maneuver, a flight and analog study of landing was initiated at the NACA High-Speed Flight Station.

DISCUSSION

Figure 1 shows the variation of lift-drag ratio L/D with lift coefficient C_L for the X-15 in the clean configuration and in the flap-and-gear-extended configuration estimated from wind-tunnel results. The shaded area represents the L/D range (flap and gear down) utilized in the approach and landing of several previous rocket airplanes. The L/D curve for the D-558-II airplane forms the top of the envelope, and the curves for the X-1E airplane forms the lower edge of the envelope. It should be noted that the L/D level for the X-15 with gear and flap down is appreciably lower than the values used in landing the earlier airplanes. It may also be noted that the wing loadings W/S for all airplanes described are of the same general order of magnitude.

Shown in figure 2 is a typical X-1E landing pattern which is representative of the lowest L/D experienced in rocket-airplane landings. The plan and profile views of the landing are presented in terms of distances away from the touchdown point. The landing approach is set up in a conventional manner except that the altitudes and speeds are higher than those for a powered airplane. The landing gear and partial flaps are deployed at about 12,000 feet and at a speed of 240 knots in a position 180° from the touchdown point. Full flaps are usually

deflected on the final approach whenever the pilot feels that the landing can be accomplished at the desired touchdown point. It may be noted that the pilot has 180 seconds to complete the landing. During the final turn to the runway heading, the pilot gradually reduces the rate of sink from a maximum of about 100 feet per second to about 15 feet per second at an altitude of 50 feet. It is important to note that the pilot appreciated the additional 30 seconds available to reduce the sinking rate to zero at touchdown, which occurred at about 140 knots.

A landing program was initiated for a modified F-104A test vehicle to obtain flight experience in an L/D range that would be directly applicable to that expected for the X-15 landing operation. This airplane was selected since by changing configuration and thrust an L/D range similar to that with the X-15 could be attained. Figure 3 compares the L/D curves for the X-15 in the clean and in the landing configurations with the flight L/D attained with two configurations tested on the F-104A. The upper dashed line represents the curve for the F-104A with gear and trailing-edge flaps deflected. The lower dashed curve was attained for the configuration with speed brakes deflected, in addition to the deflected gear and trailing-edge flaps. The leading-edge flaps were undeflected for both configurations, and the landings were performed with idle power where there was approximately 200 to 300 pounds of negative thrust. An $(L/D)_{max}$ of about 4 was attained with only gear and flaps down, and the $(L/D)_{max}$ with configuration utilizing gear, flaps, and speed brakes was slightly under 3.

In figure 4 is illustrated a representative flight path of the F-104A in the configuration in which the L/D varied from 2 to 3 (the configuration with the gear, trailing-edge flap, and speed brake down). This figure permits some interesting comparisons to be made with the previous results for the X-1E. It is obvious from a cursory inspection that the lower L/D landing pattern (F-104A) is characterized by a marked increase in initial altitude, a shrinking of the lateral and longitudinal distances involved, and a critical decrease in time available for completion of the landing.

The low L/D approach was initiated from the 270° position over the runway at an indicated airspeed of about 280 knots and at an altitude of 21,000 feet about 90 seconds prior to touchdown. The pilots felt that a 270° approach was preferred to position the airplane in the required pattern and to maintain visual contact with the landing point. During the turn to the base leg, sinking speeds of the order of 300 to 400 feet per second were encountered with the F-104A as compared with a maximum of about 100 feet per second with the X-1E. At this point the pilot's main concern was not one of missing the desired

landing spot, but of hitting it too hard. By the time the final runway heading was approached at an altitude of 2,500 feet, the sinking rates were reduced to less than 200 feet per second. Inasmuch as the flare is the most critical part of the approach, the effect of L/D on the flare characteristics will now be examined in some detail.

Figure 5 presents the landing characteristics of the F-104A in the L/D range from 3 to 4 (the configuration with the gear and trailing-edge flap deflected). Presented are altitude h, sinking speed V_v, indicated airspeed V_i, normal acceleration a_n, and L/D as a function of time to touchdown. The pilot did not feel it necessary to reduce sink rate below 100 fps until the altitude was reduced to about 500 feet at 275 knots. The sink rate was then progressively decreased to about 5 fps at an altitude of 20 feet with an airspeed of 235 knots. Excess speed at this point was sufficient to permit the pilot to delay touchdown until, 8 seconds later, the speed had reduced to 185 knots.

In figure 6 a similar summary of landing characteristics is presented for the F-104A in the L/D range from 2 to 3 (the configuration with the gear, trailing-edge flap, and speed brake down). In this instance a gradual flare was accomplished above an altitude of about 2,000 feet, but in order to maintain a reasonably high airspeed of 290 knots, the pilot accepted the high rate of sink of 160 feet per second. However, by the time the altitude had decreased to about 1,300 feet, the pilot's chief concern was whether the available lift capabilities of the airplane would enable a successful flare to be made. The pilot's feeling can be appreciated by noting the sink rates of 35 feet per second at an altitude of 50 feet and of 14 feet per second at an altitude of 6 feet. The reason for the pilot's concern is indicated by the normal acceleration which had to be held for a longer period of time and to a lower altitude. Maximum angles of attack reached during this landing were about 8° to 10° as compared with about 6° to 8° on the landing previously described (fig. 5) for the L/D ranges from 3 to 4. It was felt that such high sinking rates in close proximity to the ground imposed excessive demands on the pilot's judgment so that it would be dangerous to repeat landings in this configuration. It should be noted that although touchdown speed was about 185 knots in both landings, the time to touchdown from an altitude of 20 feet was reduced from 8 to 5 seconds with reduction in L/D.

In general, the pilots felt that it was desirable to have a landing test vehicle in which the L/D could be progressively reduced by variations in configuration and thrust. Experience from such tests led to an appreciation of the problems and procedures involved in landing at low L/D.

As a result of the F-104A low L/D landing study, it was deemed desirable to conduct a preliminary analog program to determine the probable landing characteristics of the X-15 airplane by using various techniques. Accordingly, a simplified six-degree-of-freedom analog setup was mechanized on the basis of X-15 inertia and aerodynamic characteristics. The presentation used is shown in figure 7. A short bar on an oscilloscope represented the airplane. The vertical displacement of this bar above a horizontal reference was indicative of altitude, while the rate of closure gave an indication of sinking speed. In addition, normal acceleration a_n, angle of attack α, sensitive vertical velocity V_v, indicated airspeed V_i, and sensitive altitude h_p were shown on dials. A center control stick having about the same force gradient as contemplated for the X-15 was used. The pilot used the scope presentation for initial flare and control down to an altitude of about 400 feet, below which he used the sensitive altimeter and rate-of-sink indication in trying to meet the touchdown conditions of less than 9 fps rate of sink, a ground attitude of 8°, and an airspeed above 175 knots. Admittedly, the setup left much to be desired as a simulator. The scope and dials did not enable the pilots to achieve the "feel" for the problem that is present in flight where the pilot primarily uses visual cues. However, the simulator did enable a number of performance variables to be assessed in a fairly systematic manner and, as such, the simulation was found to be a useful tool. Only the results of the final approach phase of the landing are presented in this paper.

As shown in figures 1 and 3, there is a large reduction in L/D for the X-15 when the flap and gear are down. Figure 8 shows the effect of flap and gear deployment technique on the X-15 landing characteristics. With the flaps and gear deflected at altitudes above 2,000 feet, as was general practice on previous research airplanes, a very high initial sinking speed is present which requires an exceedingly careful technique in programing the flare so that a successful landing can be assured. If both the gear and flap deflection are delayed, the higher values of L/D in the clean configuration can be used to reduce initial rates of sink and increase the time available to complete the landing. The solid line represents a typical run made with this technique. The initial vertical velocity was reduced by 50 percent from 280 fps to 140 fps. The flare was initiated near an altitude of 800 feet and at an altitude of about 350 feet, a speed of 295 knots, and about 15 seconds prior to touchdown, the flap and gear extension was initiated. The flaps and gear were full down at 7 seconds prior to touchdown with vertical velocity essentially zero and the airspeed 240 knots. The pilots had little difficulty with this technique and completed nearly all of the attempts, which is felt to be within the limitations of the simulator. It is obvious that this technique is an improvement over the one with the gear and flaps down all the way. It

should be mentioned that the success and relative ease of making the landings were not too sensitive to the altitude at which flap and gear deployment were initiated in the altitude range of about 200 to 500 feet. Additional calculations are being made to optimumize the flap and gear extension technique with particular emphasis on the effects of transients in trim caused by the extension of flaps and gear at low altitude.

The results shown were made by assuming an initial approach speed of 300 knots. However, calculations were also made to determine the landing characteristics from initial speeds of from 250 to 350 knots. It would appear that the lower rates of sink associated with a substantially lower initial speed might be outweighed by the lack of sufficient excess speed near the ground for minor height corrections prior to touchdown. At an airspeed approaching 350 knots the landing may be more difficult because of higher initial rates of sink.

These preliminary results may indicate a more restrictive technique than is necessary, since the nose-gear design limits of a rate of sink of 9 fps at a ground attitude angle of 8° pose rather stringent requirements at touchdown. Additional studies may indicate somewhat less stringent requirements.

It should be pointed out that the X-15 landing characteristics in the configuration with the gear and flap down all the way would in some respects be similar to those of the modified F-104A in the L/D range of from 2 to 3 that were considered marginal by the pilots. The characteristics of the X-15 with gear and flap extension delayed to a lower altitude were comparable in many respects to those of the F-104A in the L/D range of 3 to 4 which the pilots considered reasonably conventional.

CONCLUSIONS

In conclusion, it can be said that flight tests of a configuration having a moderately high wing loading indicated, for the technique employed, relatively conventional approach and landing procedures in the L/D range from 3 to 4. Because of the relationship of vertical velocity, forward speed, and time, approach and landing at values of L/D of 2 to 3 was considered hazardous, since it was difficult to achieve a decrease in vertical velocity while still retaining a speed margin for minor height corrections prior to touchdown.

Since a higher L/D is safer from the standpoint of lower vertical velocity and more time available after initiation of flare, it

appears most advantageous to delay extension of landing gear and flap on the X-15 to a minimum altitude - perhaps less than 500 feet.

It is also highly desirable to use a vehicle which enables achievement of a progressive buildup to low L/D landings as a means of attaining pilot experience prior to X-15 flights.

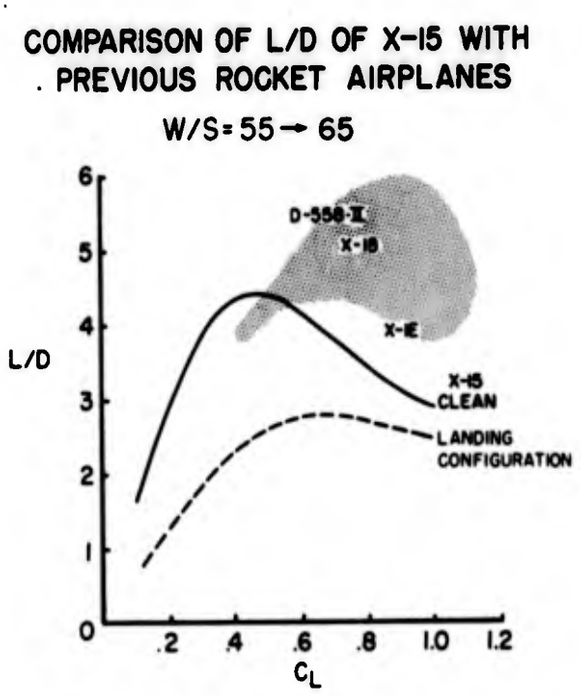

Figure 1

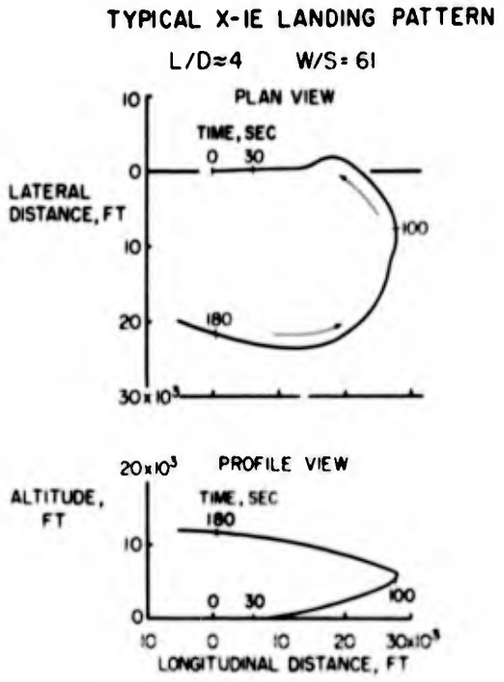

Figure 2

COMPARISON OF L/D OBTAINED IN MODIFIED F-104A LANDING TESTS WITH X-15

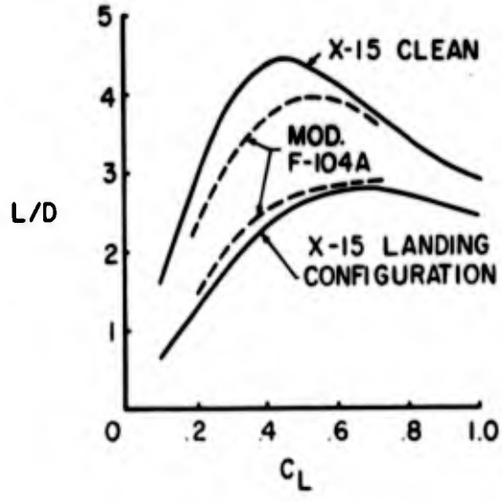

Figure 3

MODIFIED F-104A LANDING PATTERN AT LOW L/D

L/D=2→3 W/S=81

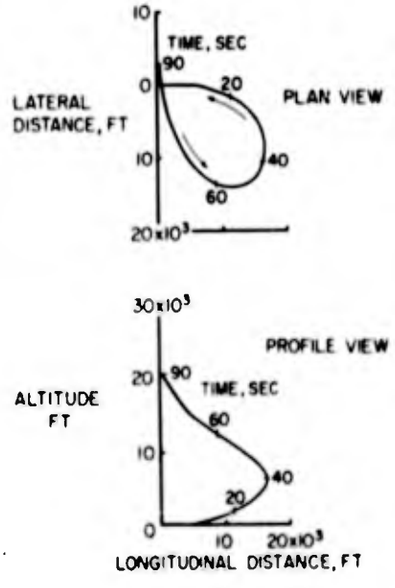

Figure 4

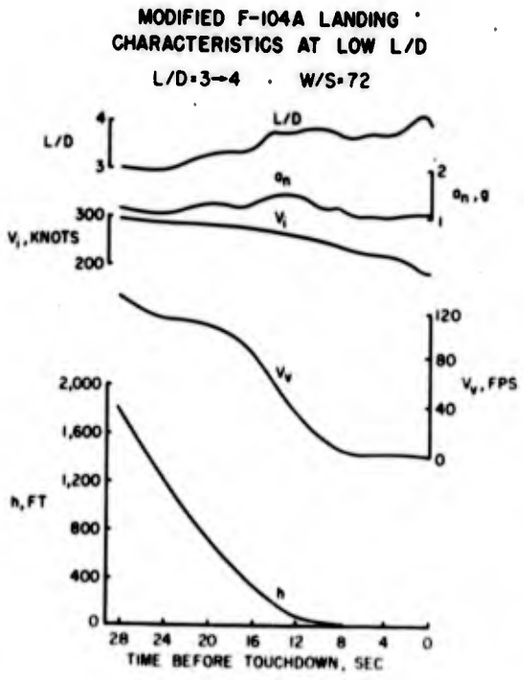

Figure 5

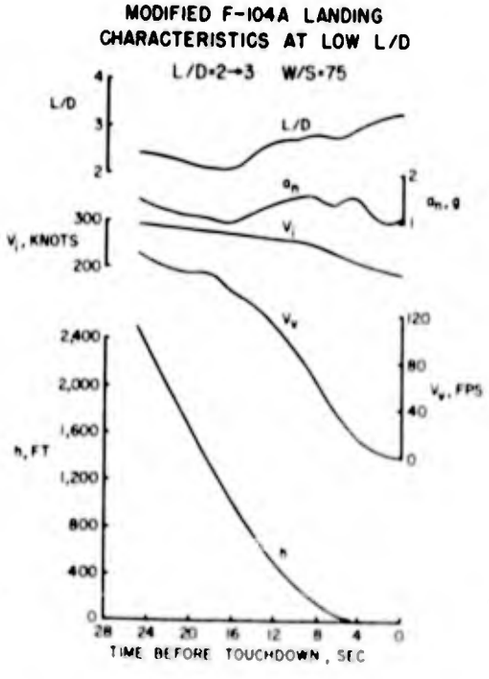

Figure 6.

X-15 ANALOG PRESENTATION

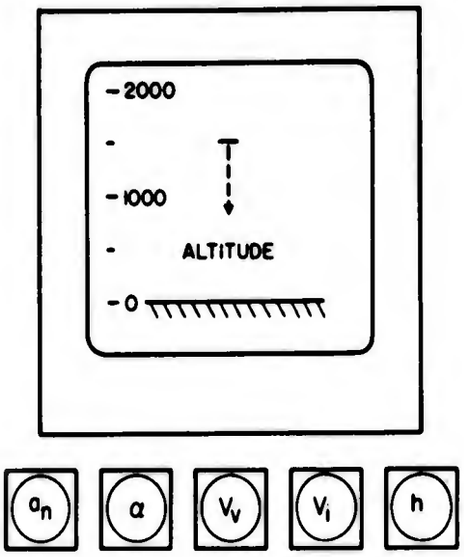

Figure 7

EFFECT OF FLAP AND GEAR DEPLOYMENT TECHNIQUE
ON X-15 LANDING CHARACTERISTICS

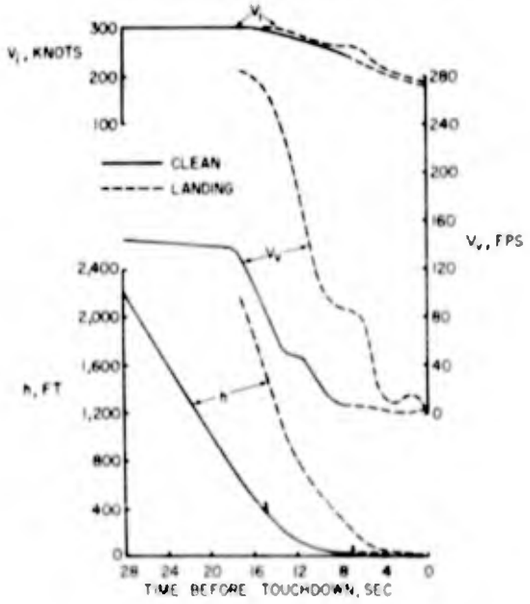

Figure 8

X-15 FLIGHT SIMULATION STUDIES

By George B. Merrick
North American Aviation, Inc.

and C. H. Woodling
NACA Langley Aeronautical Laboratory

INTRODUCTION

The vast flight regimes to be explored by the X-15 research vehicle and the rapid rate at which these regimes are traversed make an extensive flight-simulation program imperative and an integral part of the vehicle development. At the 1956 conference on the X-15, results were presented of individual flight-simulation studies covering the exit phase, the high altitude or reaction control phase, and the reentry phase of the X-15 mission. Since then, the scope of these simulations has been expanded to cover the entire flight regime so that it is now possible to fly, in essence, the entire mission from launch to landing approach. This paper describes briefly the flight-simulation studies carried out on the X-15 since the 1956 conference, the capabilities of current simulations, and some of the significant results of these studies.

SYMBOLS

V_o	velocity
q	dynamic pressure
h	altitude
β	angle of sideslip
α	angle of attack
n_z	normal acceleration
n_y	lateral acceleration
θ	pitch angle
ϕ	roll angle

DISCUSSION

Figure 1 presents a time schedule of the various simulation activities covering the period from October 1956 to the present date. It is of interest to note the increasing sophistication of these studies. Initial work allowed study at only one flight condition. Later, complete freedom was allowed over a limited portion of the mission, and finally unlimited freedom was allowed over the complete flight regime. A detailed description of each of these studies is not practical for this presentation; however, several significant results from earlier work can be summarized.

Initial exit studies indicated the need for a more symmetrical tail to reduce aerodynamic coupling tendencies at low angles of attack. This resulted in the present tail configuration, referred to in previous papers as configuration 3. Reentry studies at high angles of attack indicated that the original rate-feedback-damper configuration was not adequate for the symmetrical tail and an additional feedback of yaw rate to roll control was required for stability in the high angle-of-attack range. These are two configuration changes which resulted from early simulation work.

Since there was some concern as to the pilot's ability to control the airplane under certain dynamic loading conditions of exit and reentry, a simulation at the U. S. Naval Air Development Center, Johnsville, Pa. utilizing the human centrifuge was also accomplished. In this work the pilot was subjected to the actual flight loads during each run.

Next consideration is given to the capability of current simulations. The six-degree-of-freedom mechanizations listed in figure 1 allow complete freedom of motion of the airplane, include the variation of all significant derivatives with angle of attack and Mach number, and vary only in the range of Mach numbers covered. The complete six-degree-of-freedom mechanization at North American Aviation, Inc., Los Angeles, Calif. covers Mach numbers from 0.2 to 7.0 from sea level to an altitude of 200 miles. Currently, a real time solution is also included of temperature at any one of numerous points on the fuselage and wing.

A typical simulation flight of the design altitude mission is shown in figure 2. The flight begins at drop conditions of Mach number 0.8 at approximately 40,000 feet.

At this point thrust is on, and the pilot makes an abrupt pull-up by using an angle of attack of 15° until the proper initial climb angle is established. For the design mission, this climb angle is 50°. At that point, a zero g trajectory is maintained throughout the exit

phase. This technique provides control of the exit path by establishing the initial trajectory angle, the altitude, and the speed.

During the period of engine burning, pitch and yaw control is required to correct for thrust misalinement. Burn-out occurs at approximately 90 seconds from drop as shown at a velocity of 6,200 feet per second and at an altitude of 160,000 feet. At this point the effects of thrust misalinement are seen in the oscillations in angle of attack and sideslip. At burn-out the pilot begins use of the reaction control system and this system is used throughout the rest of the high-altitude phase to maintain angle of attack and sideslip zero. Peak altitude reached is slightly over 250,000 feet. The recovery used for this particular flight was an angle of attack of 15° established at approximately 200,000 feet on the way down. The required trim for this angle of attack can be set at any time near peak altitude, and the reaction control system is used to establish this angle of attack. As the dynamic pressure builds up at reentry at approximately 150,000 feet, the load factor increases, and for this mission the pilot allowed the load factor to build up to 5g and then maintained this 5g recovery until completion of pull-out. The simulation just shown is also typical of those in operation at Langley and Johnsville. Consider next what this complete flight simulation allows in the way of system development. Since the pilot can essentially fly the mission, a complete evaluation of controls and display is possible, in this case some 8 months prior to the time for first scheduled flight. In past research-aircraft development, only qualitative evaluation was possible before the flight program. In the case of the X-15 on the basis of simulation work, changes were made in the display; most significant was the addition of the cross pointer indication of angle of attack and sideslip in the attitude indicator. A redesign of the right console grip was found necessary only after the system was operational on the simulator, and pilots had had the opportunity to evaluate the grip under operation conditions. The Johnsville program indicated a deficiency in control system mass balance and the critical nature of this consideration. These are typical of some of the problems discovered and solved in the area of system development by use of the flight simulator.

In order to accomplish this simulation, an extensive mechanization including actual control system equipment is utilized. A complete operational mock-up of the flight control system as shown in figure 3 provides system characteristics under operating conditions. Actual production design components, including cables, push rods, bellcranks, hydraulic system, artificial feel, and so on as installed in the actual airplane, are utilized. The electronic equipment such as the stability-augmentation system is also included. The cockpit area shown in figure 4 is a realistic simulation of the airplane configuration. The controllers as found in the airplane are shown, with the reaction control on

the left console providing pitch, roll, and yaw control inputs. The aerodynamic-control surfaces are actuated by a conventional center stick and rudder pedals and, in addition, by a right-hand console stick which provides pitch and roll control inputs to the horizontal all-movable tails. The instrument panel provides working models of all significant flight instrumentation. These models include the attitude indicator, the altimeter, rate-of-climb meter, inertial velocity meter, angle of attack and sideslip, roll rate indicator, and normal accelerometer.

The mechanization of the aerodynamic six-degree-of-freedom equations of motion are mechanized on an analog computer. The mechanization required 330 computing amplifiers, 35 computing servos, and 70 arbitrary function generators. The nonlinear variations of derivatives with Mach number are accomplished on special interpolating servos which provide 17 interpolating points for each of 16 parameters throughout the Mach number range. Nonlinear variation of derivatives with angle of attack and other required nonlinearities are accomplished on diode function generators. Currently, a real time solution is also included of temperature at any one of numerous points on the fuselage and wing. This complete simulation has been in operation the major part of this year and will be utilized continuously in support of the future flight test program.

In addition to the usefulness of the simulator for system development the actual performance capability of the vehicle is also more completely defined by inclusion of the pilot in the control loop. In this area, the various phases of the X-15 mission and the significant simulation-test results are discussed. Figure 2 presents a time history of the simulation flight for the altitude mission. Shown is a typical pull-up made by a technique whereby a specified initial climb angle was established and the rest of the burning accomplished at zero angle of attack. Variation in the time required to establish this initial climb angle results in considerable variation in the peak altitude, obtained primarily because of the variations in the initial altitude and speed of the trajectory. Figure 5 shows the results from numerous flights made by using this technique, where the time to establish this initial climb angle varied from less than 20 seconds to 40 seconds. The data show some spread in the results for repeated runs. When a constant pitch angle during exit was utilized for obtaining accurate altitude, the variation of peak altitude with pitch angle for several runs at each pitch angle was obtained and is also shown. The data indicate considerable improvement in the ability to obtain a specified peak altitude by using this constant-pitch-angle exit.

The zero g trajectory is used to obtain maximum speed performance, and the constant-pitch-angle exit is used where specific peak altitudes are desired.

From consideration of the high-altitude portion of the design mission, the ability of the pilot to maintain proper angle of attack and sideslip by use of the reaction control was greatly improved with time on the simulator. Figure 6 shows a time history, during high-altitude portions of the flight, of angle of attack and pitch-control input for the first and the seventh runs of a particular test pilot. For the first run, considerable excursions are seen for angle of attack with relatively large control inputs. Total control impulse used was over 2,000 pound-seconds. The control used in the seventh run was less than 500 pound-seconds. With the dual reaction control systems a total of 10,000 pound-seconds is actually available.

Since a given pilot makes hundreds of simulator runs, this is considered to be a relatively short learning time. Considerable work has been accomplished in the comparison of an on-off type control with the proportional system in the X-15. Pilots have indicated a preference for the proportional system in accuracy of control and total impulse used.

The reentry from the design mission shown in figure 2 was a 15° initial angle of attack held at 5g. Considerable variation is available in reentry flight procedure. Figure 7 shows three typical reentry flight plans. The solid line is a constant zero-pitch-angle reentry which results in a peak g of slightly over 4 and a peak dynamic pressure of 1,100 lb/sq ft. A lower dynamic-pressure recovery by using a higher initial angle of attack and load factor is shown by the dotted reentry time history. Here an angle of attack of 25° was held throughout the reentry and resulted in a peak load factor of 6g and a dynamic pressure of 500 lb/sq ft. For a recovery at minimum load factor and maximum dynamic pressure, the dashed time history traces show an initial angle of attack of 15° held at 3g and then the load factor held constant at 3g. This recovery results in a peak dynamic pressure of 2,500 lb/sq ft. The zero pitch-angle reentry is of interest in that it appears to be a technique the pilot could use without the use of flight instruments.

Recovery can be made from altitudes considerably in excess of the design altitude of 250,000 feet. Figure 8 shows the minimum angle of attack required for recovery from peak altitudes with and without speed brakes limited by a load factor of 7g and a dynamic pressure of 2,500 lb/sq ft. An angle of attack of 30° is required for a recovery from 500,000 feet with speed brakes closed. By use of the speed brakes, this minimum required angle of attack is reduced to 18°. Recovery is shown as a function of angle of attack because of the effects on controllability of this parameter.

A broad picture of controllability as a function of angle of attack is indicated in figure 9. This figure gives a qualitative idea,

based on pilot comment during reentry, of the effects of angle of attack on controllability. The results indicate that satisfactory control is available to angles of attack greater than 25° with dampers. With all dampers off, control is satisfactory at small angles of attack and is acceptable for emergency conditions at angles of attack up to 18°. The damper system improves control sensitivity, and provides coupling stability at high angles of attack. Here the damper configuration change required by the symmetrical tail is most evident. The dashed line indicates controllability without the yaw rate to roll control crossfeed (referred to as yar damper). At angles of attack above 15° the increase in roll due to sideslip and roll due to directional control results in dynamic instability with only direct rate feedback dampers Most important effect here is the action of the yaw damper, which in damping yaw motion induces rolling moments from rudder inputs. Cancellation of these rolling moments by the crossfeed is necessary for stability and greatly increases usable range of angle of attack.

These results, together with those shown in figure 8 indicate that recoveries can therefore be made from altitudes in excess of 500,000 feet. At this point it is of interest to note the results of the dynamic simulation made at Johnsville and their effects on this information. For the high-altitude recoveries the physiological tolerances of the pilot were in question. Recoveries were accomplished at Johnsville from as high as 550,000 feet, where the normal load factor reached 7g and the longitudinal deceleration reached 4g, and lasted as long as 25 seconds, during which time the pilot was able to maintain adequate control. It was generally concluded that the flight envelope was not limited by pilot considerations. The work at Johnsville considering reentries from the design altitude mission provided comparable results as those shown in figure 9. That is, when the pilot was subjected to the dynamic loads of the reentry, although additional concentration and minor changes in technique were required, the dynamic simulation did not significantly alter pilot comment regarding controllability as a function of angle of attack.

More descriptive of the controllability as a function of angle of attack are actual reentry time histories flown on the simulator. Figure 10 shows three time histories for various angle-of-attack reentries. The first at 15° was adequately controlled by the pilot, and comment indicated only minor difficulties. As the angle of attack was increased, as shown in the second reentry at approximately 19°, considerably more difficulty in maintaining wings level was experienced. When the pilot attempted a reentry at angles of attack above 20° as shown in the third reentry time history, control was unacceptable and recovery was possible only when the angle of attack was abruptly reduced below 20°. At this point the pilot was able to complete the reentry successfully. The symmetrical tail actually provides an "island of safety" so to

speak, of such nature that if coupling difficulties are experienced at high angles of attack, control can be regained by pushover to lower angles.

A comparison of some typical traces from the centrifuge simulation indicates the effect of dynamic loads on the pilot. Figure 11 shows four consecutive runs made by one pilot at Johnsville for a dampers-off reentry from 250,000 feet. The first two runs are static runs, the last two runs are dynamic runs where the pilot was actually subjected to the accelerations shown.

Up to this point in the development of the airplane, extensive and continuous use has been made of the several static simulations covering the complete flight control picture. Design of the system had been based on previous knowledge of the effects of load factor and related human-factors aspects of these loadings. The pilot restraint and control system provisions for these loadings were developed without actual test evaluation. There were, however, certain areas felt to be critical with regard to the effects of dynamic loads on the pilot, and the centrifuge was used to evaluate these areas. In the case of the X-15 configuration the centrifuge tests verified the final design. A confidence has thus been established in the combined simulation work which will allow the flight test program to proceed at a more rapid pace.

CONCLUDING REMARKS

In summary, the flight simulation studies have shown the advanced status of simulation work and the effective tools available for system development and evaluation. Results of these simulation studies have indicated that, with the unaugmented airplane, pilots are capable of successfully completing design missions with adequate margins. The damper system is found to provide improved control characteristics and to extend mission capability. Recoveries can be made from altitudes considerably in excess of the design altitudes. Adequate control of peak altitude is obtainable by several exit techniques. Considerable flexibility is available for reentry in required load factors and dynamic pressures. The symmetrical tail provides desirable stability and control characteristics as a function of angle of attack over the complete Mach number range.

Emphasis at the present time is being placed on integration of all flight control equipment into the flight simulator. Simulation of the actual research flights prior to and during the flight program will be accomplished to optimumize various trajectories and thus to obtain maximum data points per flight, as well as to develop and maintain pilot technique throughout the program.

FLIGHT SIMULATION STUDY SCHEDULE

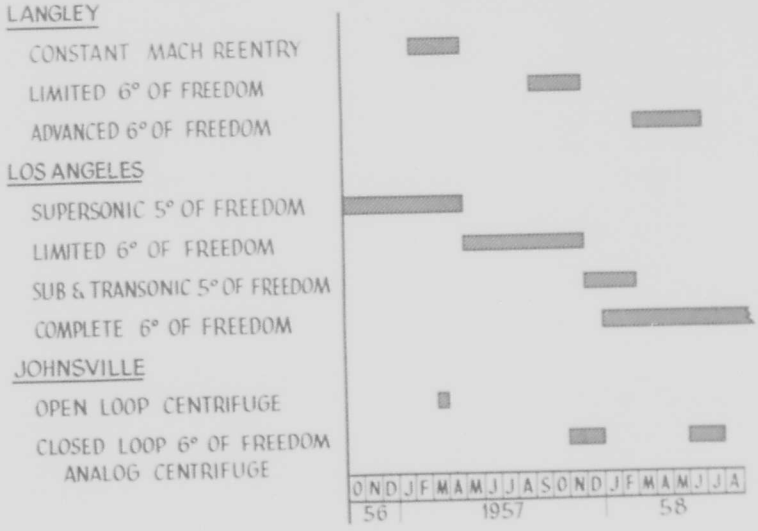

Figure 1

DESIGN ALTITUDE MISSION

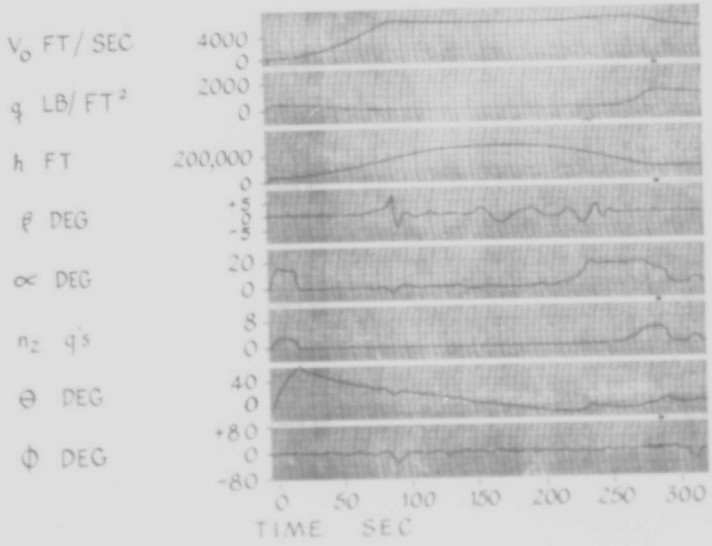

Figure 2

FLIGHT SIMULATOR

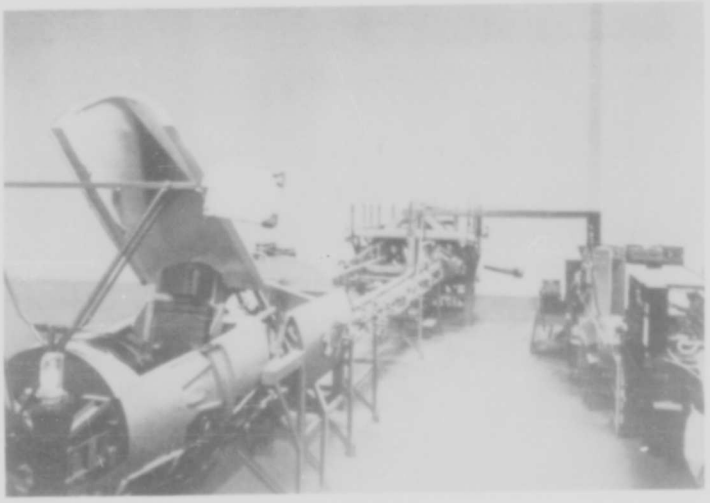

Figure 3

FLIGHT SIMULATOR CONTROLS

Figure 4

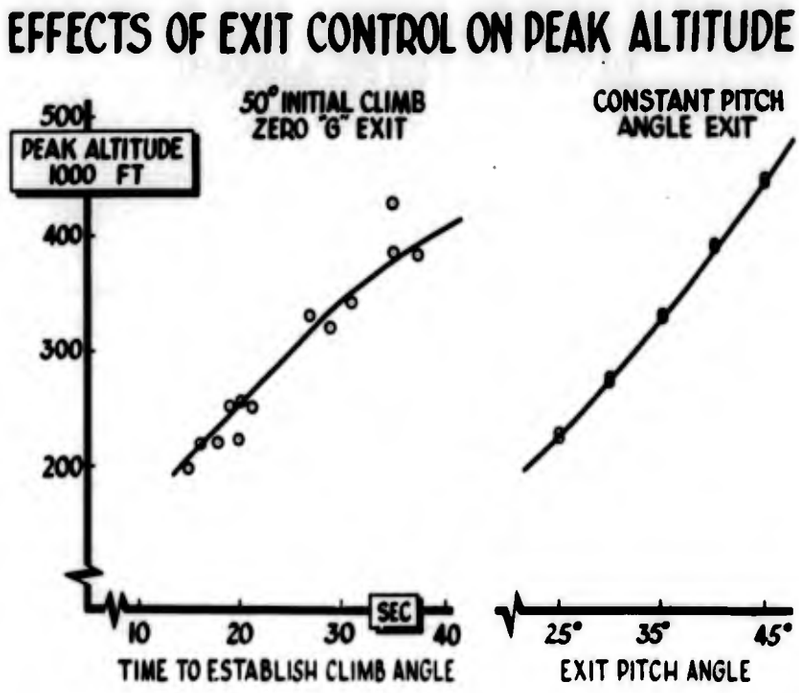

Figure 5

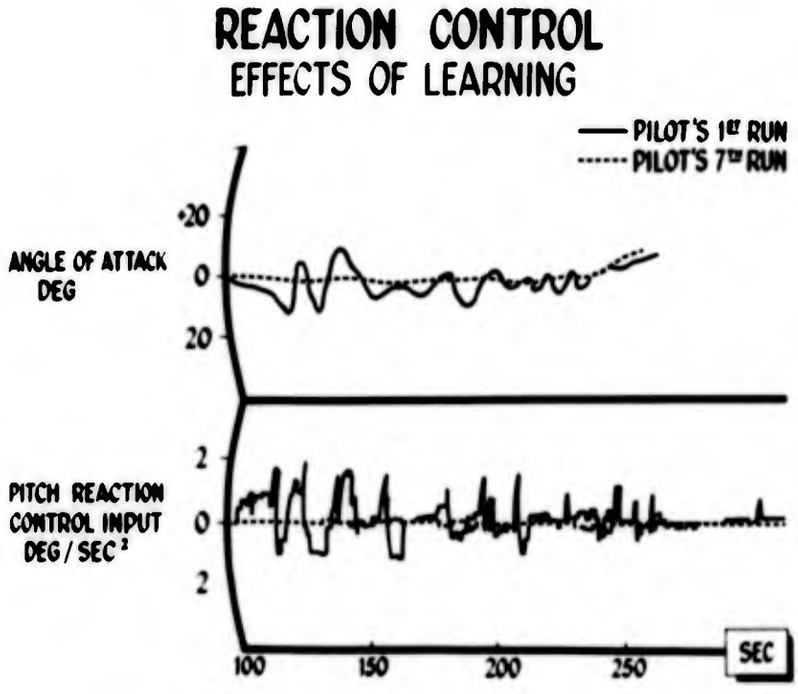

Figure 6

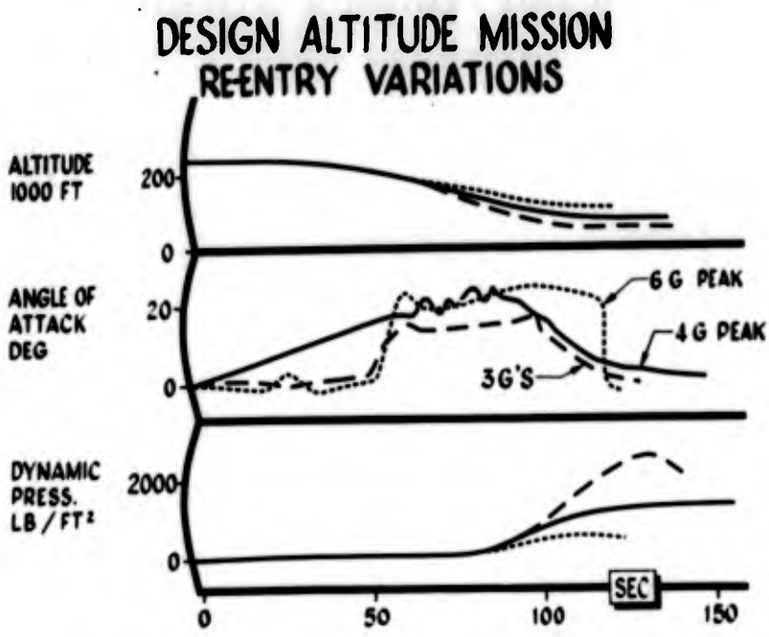

Figure 7

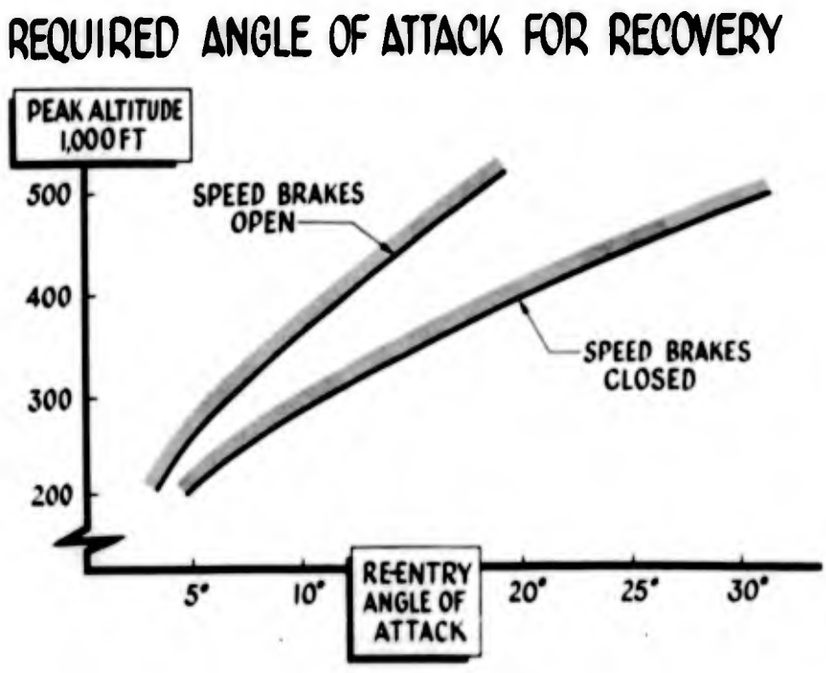

Figure 8

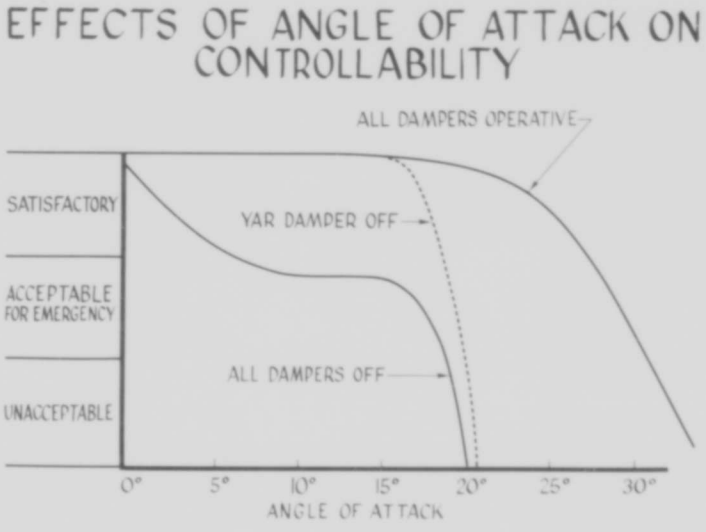

Figure 9

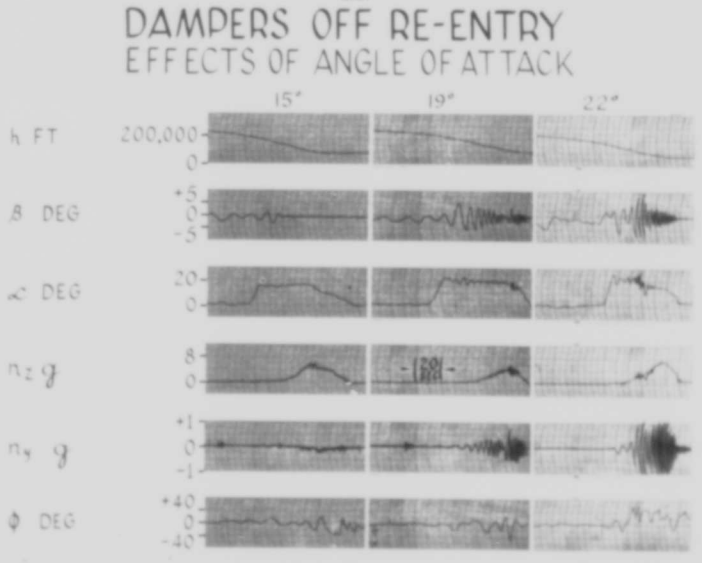

Figure 10

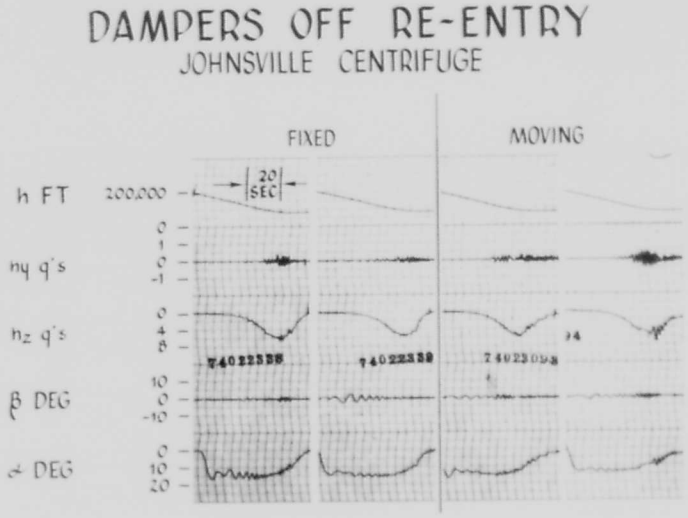
DAMPERS OFF RE-ENTRY
JOHNSVILLE CENTRIFUGE
FIXED
MOVING
h FT
200,000
20 SEC
n_y q's
n_z q's
β DEG
α DEG
74022338
74022338
74023038

Figure 11

CENTRIFUGAL SIMULATION OF THE X-15

By Carl Clark

Aviation Medical Acceleration Laboratory,
Naval Air Development Center

The physiological tolerance of the pilot to the oscillating accelerations of large amplitude and long duration which might occur as a result of aircraft heading errors during reentries from the altitude mission in the X-15 without control augmentation was not known. North American Aviation, Inc. (NAA) therefore approached the U. S. Navy for use of the Johnsville human centrifuge (fig. 1) to determine this tolerance. In the past 16 months, three X-15 centrifuge programs have been carried out as a cooperative effort of NAA, NACA, USAF, and USN, to investigate under dynamic conditions the medical tolerance of the pilot, adequacy of pilot restraint, adequacy of the X-15 cockpit display, and adequacy of the pilot controls and control techniques during simulated flight of the fully augmented, partially augmented, and unaugmented X-15. The first X-15 centrifuge program utilized cam control of the centrifuge to demonstrate physiological tolerance and tracking capability of the pilot through the maximum accelerations which might occur during emergencies (ref. 1). The second and third X-15 centrifuge studies utilizing the newly developed technique of centrifuge dynamic control simulation (fig. 2 and ref. 2) followed extensive NAA and NACA static simulator studies, and particularly emphasized those conditions which had been found marginal in the static studies. In this technique, signals proportional to pilot control motions pass to a computer, which drives the pilot display instruments to represent the changing flight conditions of the simulated aircraft. This part of the centrifuge simulator is equivalent to the usual fixed-base control simulator. But, in addition, in the centrifuge simulator the three linear acceleration components computed for the aircraft pass through a "coordinate converter" circuit to generate the three centrifuge drive signals to the centrifuge arm, the outer gimbal, and the inner gimbal.

The success of the acceleration simulation is illustrated in figure 3, in which the accelerations computed for the X-15 for the particular pilot control motions during a reentry from 250,000 feet without control augmentation and with the speed brakes closed are compared with the accelerations actually measured in the centrifuge gondola during this reentry simulation. The most serious inaccuracy of linear-acceleration simulation is in the measured a_x component, which, as a_z oscillations reach 1 cps, may oscillate with an amplitude of ± 1 g.

The Johnsville human centrifuge is in the Aviation Medical Accelcration Laboratory at the Naval Air Development Center (NADC), Johnsville, Pa. This centrifuge has an arm of 50-foot radius directly mounted on the armature shaft of a vertical 4,000-horsepower DC motor. Radial acceleration can attain a peak value of 40g in 7 seconds. At the end of the centrifuge arm is a gondola within a power-driven double-gimbal system. As shown on the left in figure 1, the outer gimbal has a sector gear of 90°. The inner gimbal may rotate continuously, but in order to prevent exposure of the pilot to "physiologically negative" acceleration that would force blood into his head, the inner gimbal motions were limited in these programs by limit microswitches to ±97°. The angular velocities of the gimbals can reach 2.8 radians/sec and the angular accelerations can reach 10 radians/sec^2. When radial accelerations do not exceed 25g, the gimbals may be driven with gondola loads up to 600 pounds (ref. 3).

The centrifuge gondola has three degrees of freedom of control of its motion, as compared with the six degrees of freedom of motion of an aircraft. In the recent X-15 centrifuge programs, the attempt has been made to simulate the three linear acceleration components of the aircraft. The angular accelerations of the centrifuge are therefore not comparable to those of the aircraft. For successful reentries, these centrifuge angular accelerations did not produce pilot nausea and the pilots quickly learned to ignore their sensations of centrifuge angular motions. Results obtained on the centrifuge concerning pilot physiological tolerance; adequacy of restraint, controls, and display; and even suitable pilot control techniques are considered indicative of results that would be obtained in the X-15.

During the X-15 Centrifuge Program 2 (ref. 4) it was found that the pilot could maintain adequate control of the centrifuge simulator when in the inflated or uninflated X-15 pressure suit (fig. 4). A rearrangement of some of the display instruments to reduce the required eye motions was recommended. Under "greyout" conditions or whenever head motions reduce vision during normal accelerations experienced in certain of the simulation runs, instrument deflections which may seem prominent on the static simulator may not be noticed by the pilot. The program results indicated the critical control by the pilot required for successful "reentries" with dampers off in the centrifuge simulator.

Certain inadequacies in the simulation of the X-15 during program 2 were recognized: inadequacies in the computation of aircraft responses at high frequencies, in the pilot restraint, in the lack of simulated speed brakes, and in the control mechanizations. The X-15 Centrifuge Program 3 was therefore carried out in June and July of 1958, with an improved cockpit mockup and improved computer simulation. Detailed plans of this program are reported in reference 5. A final report and a motion-picture report of the results are in preparation. Figure 5

shows the pilot in the centrifuge simulator of program 3. Figure 6 shows the instrument panel assembled by the NADC Aeronautical Instruments Laboratory. This program entailed 2 weeks of computer preparation; 3 weeks of gondola installation, centrifuge and computer checks, and preliminary flights; and 3 weeks of flights by 7 men who may fly the X-15 and by 15 others. A work week of 68 hours was utilized. During this last program 755 piloted static flights (with the centrifuge at rest) and 287 piloted dynamic flights (with the centrifuge in motion) were made and recorded.

The NADC Aeronautical Computer Laboratory analog mechanizations for six-degrees-of-freedom simulation of the X-15 and for control of the centrifuge, developed with the cooperation of their University of Pennsylvania consultants, consisted of 370 operational amplifiers, 21 servos, 8 resolvers, and 1 electronic multiplier. In this program, 51 continuous and 6 binary variables were recorded on 8 recorders to describe the pilot control motions, the computed aircraft responses, the centrifuge command signals, the measured centrifuge responses, the antiblackout-suit pressure, and the pilot's electrocardiogram. The centrifuge was viewed by the project officer, who coordinated the conditions for the run, and the centrifuge operator, whose primary function was to synchronize the centrifuge with the computer. The medical officer viewed the pilot's electrocardiogram and control motions on a recorder. All sites were in an open communication system, and the centrifuge could be rapidly brought to rest from each site, as well as by the pilot himself.

During an altitude-mission exit and reentry, the simulation commenced after the pilot had attained the exit flight path and a speed of Mach 2, and terminated after the pilot had brought the aircraft back to level flight after reentry. During powered flight, the thrust acceleration gradually built up to 4.5g and the pilot was forced against the seat back. He could keep his feet on the rudder pedals, but this required some effort. He could still reach the instrument panel to operate switches if required. The consequences of thrust misalinement were simulated, so that during powered flight the pilot had to apply aerodynamic control corrections with the right-hand console stick and with the rudder pedals. He attempted to hold zero angle of attack as shown on his instrument panel.

At burnout the a_x acceleration component dropped to zero and the pilot's head came off the back rest. The pilot attempted to hold the aircraft heading on the ballistic path by the use of the ballistic control, for the aerodynamic control surfaces rapidly lost their effectiveness as the air density decreased. In design altitude-mission flights, which reach a peak altitude of 250,000 feet, the aircraft would have

had a resultant acceleration of less than 0.1 g for a total of 150 seconds. The centrifuge simulator remained at rest, at 1 g, during this period.

As the aircraft descended the pilot actuated the pitch trim knob and the aerodynamic control stick at about 200,000 feet to attain the desired angle of attack. He continued to use the ballistic control until the aerodynamic control became effective. As the dynamic pressure built up, the pullout acceleration commenced and the centrifuge began to turn. If the speed brakes were closed, the drag deceleration reached about 1g. With the speed brakes open, the drag deceleration would increase to 2.8g for the design altitude mission and 4g for the reentry from 550,000 feet. The pilot gradually reduced the angle of attack to maintain the desired g value until the aircraft was level, at which time the simulation was completed. For the major part of the centrifuge program, only the reentry was simulated.

The results from these three X-15 centrifuge programs may be summarized as follows:

With proper restraint and proper operation of the antiblackout protective equipment, the pilot of the X-15 can tolerate the expected accelerations, including such oscillating accelerations as 5g ± 2g at 1 cps for 10 seconds which might occur during a reentry from 250,000 feet without control augmentation as a result of a gross aircraft heading disturbance, and 7g normal and 4g onto the straps for 25 seconds which might occur during a reentry from 550,000 feet. Pilot tolerance to the oscillating accelerations was unknown prior to this program.

The trained pilot not only can tolerate these accelerations; he also can continue to carry out the required control tasks with a minimum of involuntary pilot control inputs. This is largely due to the NAA design of the pilot supports and restraints and of the right-hand console control stick. A bucket seat without padding adjusted in height for the particular pilot, arm and elbow rests fitted for the particular pilot, an integrated harness with the lower ties lateral to the hips to minimize pilot "submarining" and rolling in the seat, a helmet "socket" to limit motion posteriorly, laterally, and at the top, and a retractable front "head bumper" which can be swung down to limit forward motion of the head are notable features. When speed brakes were used or dampers were off, the pilot generally found it desirable to use the front head bumper. Two kinematic designs and three grip designs of the right-hand console stick were tested on the centrifuge in perfecting this control. Under dynamic conditions, the pilots generally preferred this stick to the center stick. The importance of careful dynamic balancing and suitable breakout and friction forces of the control stick were emphasized by the centrifuge program. A few

flights with roll and roll-to-yaw-interconnect dampers off were made with one-half the usual roll control gain. There was some indication of improved controllability. This will be further examined on the static simulators.

Due to the rare involuntary pilot inputs by trained pilots in the X-15 cockpit, flight technique in the centrifuge simulator with the pilot experiencing the flight loads was quite similar to flight technique in the static simulator for pilots who were suitably fitted in the centrifuge simulator, who had had at least 15 previous hours of static practice, and who had had previous high-acceleration experience. For pilots who did not meet these conditions, flights made under the dynamic loads were notably less well controlled than flights made with the centrifuge at rest. To illustrate this point, the X-15 pilots who met these conditions made 6 successful static reentries (with the centrifuge at rest) in 6 attempts with all dampers off, using an angle of attack of 13°. They made 5 successful dynamic reentries (with the centrifuge in motion) in 5 attempts. Other X-15 pilots, with 4 to 10 hours of static practice, made 24 successful static reentries under these conditions in 24 attempts, but they made only 7 successful dynamic reentries in 15 attempts. The other pilots, with less static practice or little acceleration experience, made 18 successful static reentries in 21 attempts but made only 2 successful dynamic reentries in 14 attempts. Unintentional pilot control inputs which occurred during acceleration consisted of the use of the rudder pedals during drag deceleration, 0.5° of roll input due to the dynamic unbalance of the right-hand stick, pitch inputs while making roll corrections with the right-hand stick due to its breakout and friction characteristics, roll inputs while making pitch corrections with the center stick due to the large control forces required and lack of arm support, and ballistic inputs due to leaving the left hand on the ballistic control during acceleration. The trained pilots would detect the consequences of these unintended control inputs more rapidly than the other pilots, and so would make the required control corrections in time.

With dampers off, the pilots utilized the reentry techniques developed on the static simulator: to hold an angle of attack below 15°, not to attempt to correct for each oscillation but to control only the mean value of angle of attack or normal load, and to be particularly careful not to establish a roll angle which would make the pullout of longer duration and higher dynamic pressure. The use of speed brakes made reentries with dampers off easier to control.

The drag decelerations of the speed brakes, when combined with the pullout normal loads, increase the blood pressure in the limbs. When the resultant acceleration was below 5g there was no discomfort, but

when the resultant acceleration was above 7g, including a drag component of more than 3g, petechiae (small skin hemorrhages) were noted on the forearms and ankles and tingling with subsequent numbness, and in a few cases definite pain, was noted in the limbs. This numbness became more severe when several runs were made in succession. In one case of a pilot with a poorly fitted harness, severe groin pain was the reason for stopping the centrifuge. In two cases of brakes-open reentries, the pilots reported pronounced oculogravic illusions, with the visual field seeming to oscillate vertically and appear doubled vertically for a few seconds at the end of the reentry.

One pilot made nine dynamic runs in one 2-hour period on the centrifuge, but in general two periods on the centrifuge per day, each of 1 hour's duration or less, were utilized to reduce pilot fatigue. To establish technique, static flights preceded dynamic flights for each new flight condition.

The pilots agreed on the acceptability of the final cockpit instrument panel. Two arrangements of the instruments and three forms of the attitude indicator were studied during the centrifuge programs in reaching such agreement.

Two additional centrifuge programs should be mentioned. The Centriguge Flight Validation Program will compare pilot tracking performance in the centrifuge simulator for a particular aircraft with pilot tracking performance in that aircraft, to determine the limitations of the centrifuge technique. NADC has a program to develop the ability to utilize the fixed-base aircraft-simulator computers anywhere in the country to drive the centrifuge. The centrifuge in Johnsville, Pa., has already been under "real time" control of the X-15 computer of the NACA Laboratory at Langley Field, Va., through telephone-line links.

It is expected that the centrifuge simulator will find further use in the X-15 program, particularly after preliminary flights by the aircraft have established its actual aerodynamic coefficients. Future simulations could begin at the time of drop from the carrier aircraft, to include the control problem of attaining the initial flight path and to include some effects of turbulence and high-altitude winds. It might be possible to simulate the pilot's visual field through the aircraft windows. Emphasis might be on the practice of emergency techniques previously worked out on the static simulators. With the centrifuge simulator it should be possible to extend the flight envelope of the aircraft more rapidly, for the consequences of small extrapolations beyond the confirmed flight envelope could be determined on the centrifuge in addition to the static simulator. Moreover a larger group of pilots experienced in the control techniques and expected flight loads could be available. Tasks too hazardous to attempt initially in

the air should be attempted first statically and then on the centrifuge. As an example, the author has already made a number of reentries utilizing reverse thrust.

In conclusion, centrifuge dynamic control simulation has been applied to the X-15. Pilots in the centrifuge simulator have carried out altitude-mission flights utilizing various control techniques, with and without automatic control augmentation, while receiving the flight loads continuously computed for such control techniques. The present form of the X-15 cockpit instrumentation, controls, and restraints is such that trained pilots can control the X-15 through that part of its design flight envelope above Mach 2 while receiving the expected flight loads.

REFERENCES

1. Brown, John Lott: Tracking Performance During Simulated Exit and Reentry Flights of the X-15 Research Aircraft. Project TED ADC AE-1406, Aviation Medical Acceleration Lab., U. S. Naval Air Dev. Center (Johnsville, Pa.), Jan. 15, 1958.

2. Clark, Carl, and Crosbie, Richard: Centrifuge Simulation of Flight Accelerations. Project TED ADC AE-1410 (NM 11 02 12.6), Aviation Medical Acceleration Lab., U. S. Naval Air Dev. Center (Johnsville, Pa.), Sept. 17, 1957.

3. Crosbie, Richard J.: Utilization of a System of Gimbals on the Human Centrifuge for the Control of Direction of Acceleration With Respect to the Subject. Rep. No. 4, Project NM 001 100 303, Aviation Medical Acceleration Lab., U. S. Naval Air Dev. Center (Johnsville, Pa.), Aug. 2, 1956.

4. Woodling, C. H., Whitten, James B., Champine, Robert A., and Andrews, Robert E.: Simulation Study of a High-Performance Aircraft Including the Effects on Pilot Control of Large Accelerations During Exit and Reentry Flight. NACA RM L58E08a, 1958.

5. Clark, Carl: Plans for the June Centrifuge Simulation of the X-15. Project TED ADC AE-1406, Aviation Medical Acceleration Lab., U. S. Naval Air Dev. Center (Johnsville, Pa.), May 27, 1958.

THE HUMAN CENTRIFUGE

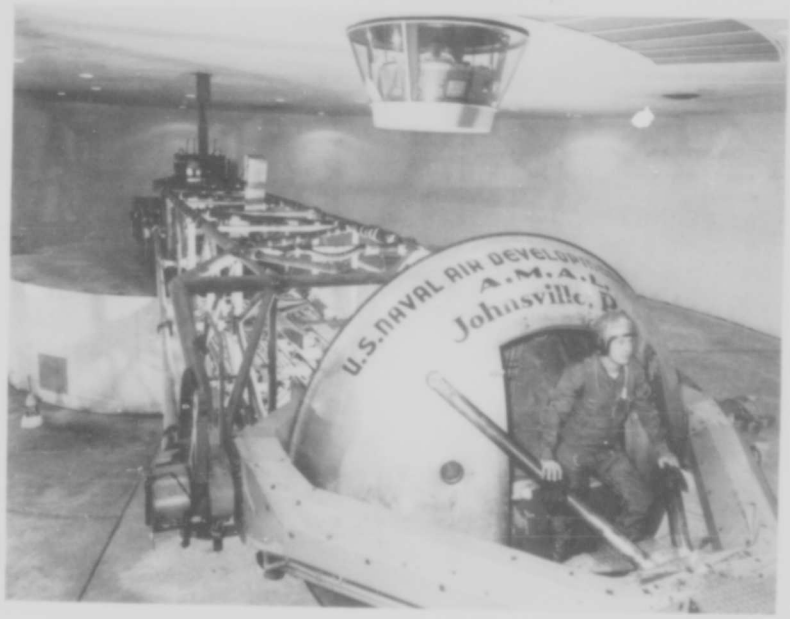

Figure 1

CENTRIFUGE DYNAMIC SIMULATION
"CLOSED LOOP" PILOT-COMPUTER CONTROL

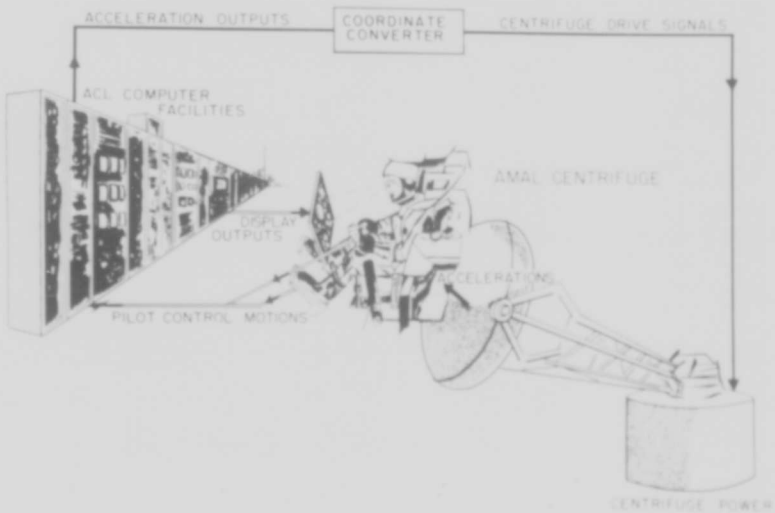

Figure 2

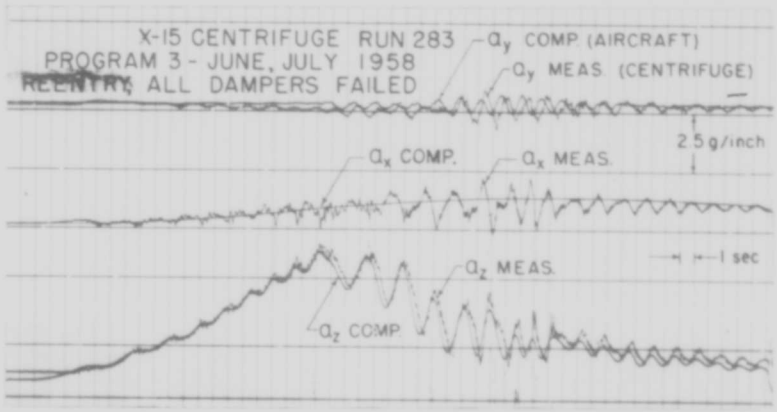

Figure 3

CROSSFIELD IN THE X-15 PRESSURE SUIT
IN THE CENTRIFUGE SIMULATOR, PROGRAM 2

Figure 4

THE SEAT AND PILOT CONTROLS OF THE
CENTRIFUGE SIMULATOR, PROGRAM 3

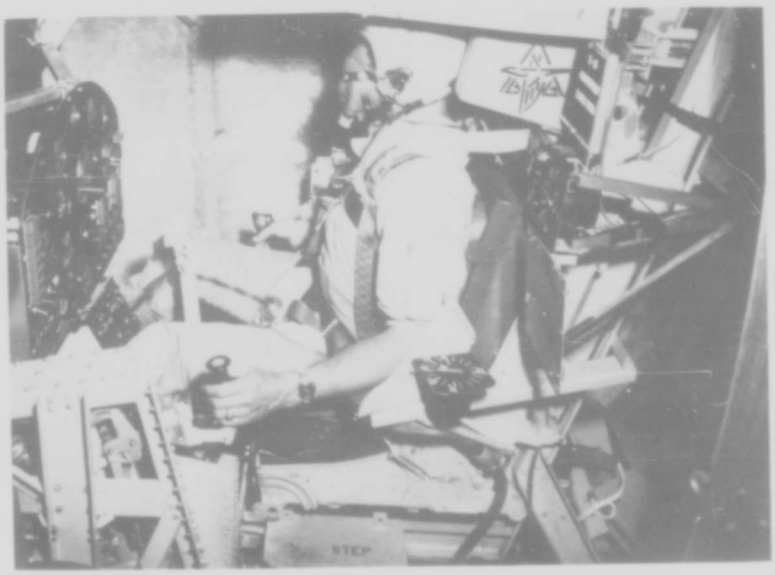

Figure 5

THE INSTRUMENT PANEL OF THE
CENTRIFUGE SIMULATOR, PROGRAM 3

Figure 6

PILOT PROTECTION FOR THE X-15 AIRPLANE

By Edwin G. Vail and Richard G. Willis

Wright Air Development Center

Development of a full-pressure altitude suit was initiated during the early part of World War II, but an unsatisfactory garment resulted in the termination of this undertaking. Following the war, tactical operations dictated aircraft performance at higher and higher altitudes, thereby necessitating the theoretically superior protective properties afforded by this type of suit. The project was therefore reopened in May of 1954 with a directed requirement to provide a minimum of 12 hours' protection above 55,000 feet for strategic bombers. The objective of this program was to construct a fully mobile suit weighing less than 30 pounds, operating with an internal pressure of 5 lb/sq in., and providing the user with sufficient oxygen partial pressure for breathing, adequate counterpressure over the body, and suitable ventilating properties. Based on these requirements, a research program was initiated utilizing experience gained in the development of partial-pressure suits and certain principles embodied in the Navy full-pressure suit. The first suit developed under this program (on the right in fig. 1) possessed limited mobility under pressure, and the use of convoluted joints and metal bearing rings resulted in a heavy, bulky, unwieldy garment. These joint bearings also produced painful pressure points on the body and were considered hazardous during bailout.

In the spring of 1955, a flight surgeon with the Fifteenth Air Force came to the Aero Medical Laboratory with several ideas for a new joint system. One of these ideas, subsequently known as the distorted-angle fabric, was successfully incorporated into the development of a new and greatly improved garment by the David Clark Company and possessed many of the desired characteristics. The concurrent development of the Aero Medical Laboratory of a lightweight ventilating assembly and integrated harness provisions also solved heretofore perplexing problems in these areas.

The MC-2 suit described here (shown on the left in fig. 1) is a lightweight, nonrigid omnienvironmental garment. It consists of a number of integrated layers, each performing a specific function in the complete assembly. The suit assembly to be used in the X-15 research vehicle includes a modified MA-3 helmet and a suit-helmet controller in a back-pack configuration.

The first part donned is a one-piece suit of lightweight cotton underwear (fig. 2). The function of this layer is to allow a full

circulation of ventilation air over the body and to provide an evaporation site for body perspiration.

The second layer donned is the ventilation suit (on the left in fig. 3) which provides for a flow of conditioned gas over the body at flows up to 10 cu ft/min selected by the user. Integrating with the ventilation suit and donned at the same time is a porous wool insulation garment (figs. 3 and 4) which also provides space for the return flow of the ventilation gas to the suit exhaust port. In this assembly, the even air distribution over the ventilated body surface is possible only when careful attention is paid to equal resistance of the airflow channels. The present design is approximately 7 inches of water back pressure at 12 cu ft/min. A new concept has been adopted in ventilating full-pressure suits. This is the principle of the counterflow heat exchanger. Briefly, this is described as follows: Incoming ventilating air is delivered equally over the body surface in its original cool condition. The returning ventilating air, after it has picked up heat and moisture from the body surface, can be further heated without detriment to the subject. This is accomplished by flow of the return air external to the wool insulation suit and just under the pressure shell. Environmental chamber tests were conducted at 165° F, with ventilating air of 10 cu ft/min at 85° F. In early tests, the index of strain was 4.1 with time to reach tolerance being 45 minutes (the index of strain is a ratio of change in heart rate to change in rectal temperature with time). Redesign and later tests brought the index of strain below 2.0, with time to reach tolerance in excess of 90 minutes. Information indicates that the index of strain can be lower with an infinite time tolerance if insulating material is added under the aluminized coverall external to the pressure shell. Total clo value of the complete suit for the X-15 is 2.6.

The third layer to be donned is the gas-retaining layer (fig. 5). This is donned in two pieces and is sealed at the waist by means of a roll-up seal. The lower half of this layer contains an anti-g suit which is similar in design to the standard cutaway anti-g suit but is an integral part of the gas-retaining layer. Centrifuge evaluation indicates good "g" protection up to 7g with good control performance above 5g while pressurized.

The restraint layer (fig. 6), also separating at the waist into two pieces, is donned over the gas-retaining layer and is zipped together. The upper half of this layer (fig. 7) is permanently joined at the neck to the upper half of the gas-retaining layer by the helmet-separating ring. Thus, in practice, the upper halves of the restraint and pressure layers are donned together.

This restraint layer is constructed of a unique distorted-angle material, called link-net by the manufacturer, which gives the suit its lightweight, nonrigid characteristic. The ballooning and elongating usually associated with an inflated pressure suit are controlled in the MC-2 suit by this material. The so-called "breakthrough in pressure-suit design" achieved by this suit is a direct result of using the link-net material. The link-net material might be best described as a slipping torsion net which acts something like the old Chinese finger puzzle in that as it elongates, its circumference becomes smaller. As internal suit pressure increases, it tends to shorten the longitudinal dimension. Control of the suit's ballooning and elongation tendencies are achieved by a careful balance of the link-net material so that any tendency for the suit to elongate is offset and balanced by its tendency to increase in size circumferentially; thus the suit remains nearly the same size whether pressurized or unpressurized.

The detachable gloves and boots are donned and zipped to the restraint layer. With the helmet, this completes the assembly of the functional full-pressure suit.

The last garment to be donned (fig. 8), while not required for altitude protection, is an important part of the assembly. It contains an integrated parachute-restraint harness. It also (1) protects the basic pressure suit during routine use, (2) serves as a sacrifice garment during high-altitude, high-speed bailout, and (3) provides additional insulation for protection against extremes of high or low ambient cockpit temperatures. The MC-2 suit assembly withstood a wind blast of 2,200 lb/sq ft on the Phase-A sled tests.

The donning of such a multilayer garment is naturally time consuming, requiring about 15 minutes from start to finish. Although this donning time is not a serious objection for use in the X-15, it is objectionable for routine operational use. Future development plans are to integrate the various layers into one garment so that the donning time will be reduced to a minimum.

The helmet (fig. 9) consists of a Fiberglas shell with a molded full head liner. The visor is a conductive-coated lens which by means of electrical resistance heating provides excellent defogging characteristics with good light transmission. The communications provisions consist of liquid-seal ear cups and miniature AIC/10 earmotors and microphone. All helmet services (oxygen and electrical) are internal within the helmet; thus the helmet presents a "clean" profile for minimum blast effects during high-speed bailout. The helmet is joined to the suit by means of a lightweight, quickly detachable, positive-locking, free-swiveling ring which allows full head mobility at any pressure.

The helmet is separated from the rest of the suit by a neck seal which contains the exhalation valves. Pressurization and oxygen concentration for this area are controlled by the suit-helmet pressure regulator which delivers 100-percent dry oxygen gas to the helmet automatically at the correct pressure for the ambient altitude. The suit is pressurized by the ventilation gas, which flows at a rate of 1 to 10 cu ft/min as selected by the user. The suit-helmet regulator automatically maintains the correct pressure in the suit for the ambient altitude by control of the suit ventilation-gas exhaust. In normal use, with the man ventilating, either pressurized or unpressurized, a constant flow of oxygen and ventilating gas is exhausted from the suit. The man breathes in oxygen and exhales it through the exhalation valves into the suit, where it exits through the suit exhaust valve.

In emergency use (during bailout) the ventilation-gas flow is stopped. The suit and helmet are automatically pressurized for the ambient altitude by the emergency oxygen supply and controller. During such emergency use, oxygen is exhausted only as the man exhales. The back pack (fig. 10) contains the emergency oxygen supply and regulator, the anti-g valve, the suit helmet regulator, and the inlet line for the ventilation gas.

For X-15 use, the suit controller has only one pressure schedule which maintains the suit at an isobaric pressure corresponding to the ambient altitude until the absolute pressures fall to 3.5 lb/sq in. abs (35,000 feet). At this point, the suit is maintained at an absolute pressure of 3.5 lb/sq in. abs.

The MC-2 performance capabilities have been evaluated on a workspace apparatus and the centrifuge, using a basic task program (fig. 11). The task selected was one of operating a lever, a continuous rotary control, a push button, or a toggle switch to extinguish a light adjacent to the control operated. The measure of performance selected was the time required to reach, grasp, and manipulate the appropriate control. The four control boxes used were essentially identical (except for location) in that each contained two levers, one rotary control, one push-button control, and a toggle switch. The location of the boxes was selected for one-arm operation simulating front- and side-console operation. Each subject served as his own control. The evaluations were based upon the additional time in seconds required to operate thirteen controls over a street-clothes baseline. Tests were conducted in street clothes, in the suit unpressurized, and in the suit pressurized at 0.75 lb/sq in. and 3 lb/sq in. Additional performance time for the MC-2 suit at 0.75 lb/sq in. was 1.37 seconds and at 3.0 lb/sq in., 7.42 seconds. Other suit scores ranged from 8 to 13 seconds in additional time. The centrifuge time performance up to 5g with the MC-2 suit was not significantly different.

Supersonic tests on eight types of pressure-suit material components were conducted in the preflight jet of the Langley Pilotless Aircraft Research Station at Wallops Island, Va. The components were tested under the following conditions: (1) Test arm in vertical position, no skip flow device, (2) sleeve inflated to 5 lb/sq in., (3) dynamic pressure, 2,200 lb/sq ft, (4) Mach number 1.4, and (5) time of test runs, 8 to 10 seconds.

Flight tests and training of pilots with MC-2 full-pressure suits at Edwards Air Force Base, Calif., will be discussed in a subsequent paper by Lt. Col. Rowen.

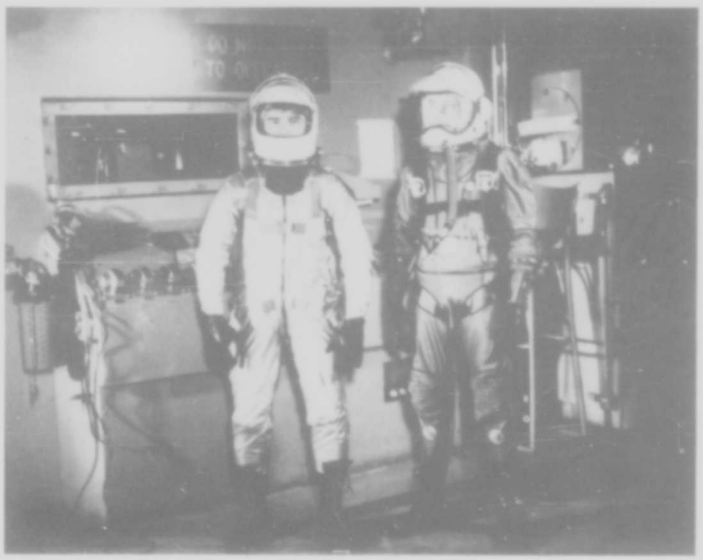

Figure 1

Figure 2

Figure 3

Figure 4

Figure 5

Figure 6

Figure 7

Figure 8

Figure 9

Figure 10

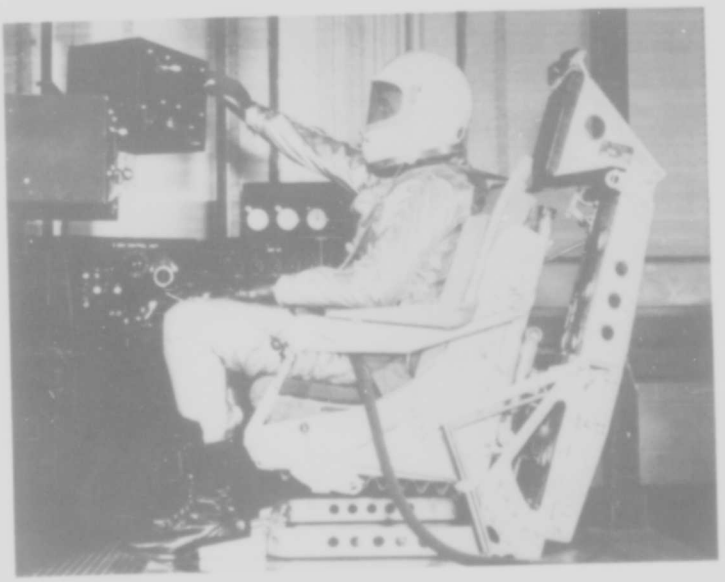

Figure 11

DEVELOPMENT OF X-15 ESCAPE SYSTEM

By J. F. Hegenwald

North American Aviation, Inc.

INTRODUCTION

The X-15 research airplane is designed to explore high-speed, high-altitude performance and to approach the maximum attainable performance by a single-stage vehicle. By a detailed analysis of representative X-15 mission profiles accident potential is determined as a function of mission progress. The basis for this evaluation was the predicted flight time in each mission stage, with accident potential during that stage being used as a weighting factor. The results thus obtained indicated that 98 percent of the total accident potential is contained within the envelope bounded by the following flight conditions:

(a) Dynamic pressures up to and including 1,500 pounds per square foot

(b) Mach numbers up to 4.0

(c) Altitudes up to 120,000 feet.

With the foregoing results serving as criteria, a comparison of various escape-system configurations was conducted. Systems considered for X-15 application included:

(a) Fuselage-type capsule

(b) Cockpit capsule

(c) Encapsulated seat

(d) Open ejection seat (fig. 1).

For the purpose of determining the suitability of the above systems, a comparison was made which included such factors as cockpit mobility, escape potential, mechanical reliability, post-separation performance, and airframe compatibility. Integrating the results of the various studies led to the conclusion that the pressure suit in combination with the open ejection seat (fig. 2) would best satisfy the X-15 emergency-escape requirements by virtue of elimination of

capsule-imposed penalties on aircraft performance and significant reduction in development time.

The content of this presentation is concerned primarily with the developmental testing of the subject system, and design factors will be considered only when influenced by results obtained during the test program.

AERODYNAMIC TESTING OF WIND-TUNNEL MODELS

The wind-tunnel facilities of the Massachusetts Institute of Technology, Naval Supersonic Laboratory, were used in a preliminary evaluation of the aerodynamic characteristics of the ejection seat. In the previous X-15 conference of October 1956, the supersonic longitudinal trim position was at a positive angle of attack of approximately 120°. This design attitude would considerably reduce wind blast effects and aerodynamic heating of the pilot's protective gear. In the wind-tunnel testing of the 0.10-scale isolated seat-pilot model (fig. 3), it was observed that adequate directional stability of the seat could not be achieved by practical means through the angular displacement of 120°. As a result, the supersonic trim attitude was revised to a design angle of attack of 30° which, relative to the ejection attitude, reflects an appreciable reduction in head, shoulder, chest, and torso wind-blast exposure (fig. 4). The magnitude of the pitching moment in the ejection attitude was subsequently adjusted to insure that the combined load factor at the pilot's head would be within acceptable limits.

In addition to moment coefficient, drag and lift coefficients and lateral directional parameters were established as a function of Mach number and angle of attack. The wind-tunnel data and an I.B.M. 704 high-speed digital computer have been utilized in effecting a complete dynamic analysis of the ejection seat throughout the probable escape envelope.

The basic wind-tunnel tests on the isolated seat-pilot model have been completed. However, supplemental testing is scheduled in the Southern California Co-Operative Wind Tunnel in Pasadena, California. These tests are expected to develop the final stabilization-system configuration and, in addition, to determine the influence of the forward fuselage without the cockpit canopy. The wind-tunnel effort described has been basically substantiated by full-scale testing on a high-speed track, which will be discussed subsequently in more detail.

RECOVERY PARACHUTE SYSTEM

Testing of the personal parachute system was accomplished in stages consisting of component evaluation and culminating in tests of the complete system.

Bench Testing of Aneroid Release

The automatic aneroid release (fig. 5) incorporated in the system for initiation of the recovery sequence was bench-tested to verify conformance to functional requirements. The unit utilizes a powder-train time delay with an aneroid override. The unit was installed on a seat in the operational configuration and actuated by manual extraction of the arming device. The attached initiator in turn energized the pilot restraint system which operated in complete conformance to design principles.

Bench Extractions of Recovery Parachute

During the course of the parachute deployment sequence, the seat headrest is ballistically removed. The kinetic energy of the jettisoned headrest is salvaged and used to augment pilot chute extraction of the main parachute canopy. In order to determine the magnitude of this effect, a complete parachute system was installed on an anthropomorphic dummy with the dummy in turn positioned in an ejection seat (fig. 6). A headrest was installed in an operational configuration and subsequently jettisoned. The kinetic energy of the headrest, when fired statically, is capable of deploying the pilot chute and approximately 75 percent of the canopy material not contained in the skirt bag.

Wind-Tunnel Force Measurements of Pilot Parachute

Inherent characteristics of the parachute pack demand efficient pilot-chute performance. Attachment of the headrest and replacement of the coil spring necessitated minor modifications to the standard A-3 pilot-chute configuration. As assurance against undetected sacrifices in drag and performance characteristics, the modified pilot-chute was tested in the wind tunnel and the results were compared to available data on an unmodified version (fig. 7). There were no significant differences.

Whirltower Testing of Parachute System

The parachute-pack configuration is such that the standard quarter-deployment-bag is not compatible with the system. With the canopy material and the suspension lines stowed, the bag is too thick and the friction between the fiberglass pack and the deployment bag is excessive. To alleviate the problem, a smaller bag was designed which contains approximately 5 inches of the canopy skirt and is therefore termed a "skirt-bag."

Whirltower tests (fig. 8) were made to verify the design of the skirt-bag, the optimum pilot-parachute bridle length, and the effect of having the seat headrest permanently attached to the pilot chute. The suspension line stowage flutes are parallel to the line of deployment and as such are susceptible to line spillage, which was observed on successive tests. A retainer flap was added to alleviate the situation. The effect of the attached headrest was determined to be negligible.

The system was successfully whirltower-tested at speeds from 100 to 300 knots with snatch force, opening shock, and opening times being recorded. Evaluation of the fiberglass pack was not a parameter during this series; therefore, the components to be tested were packed in a B-5 pack and fitted to a 200-pound torso-type dummy. Data gathering facilities included a self-recording potentiometer positioned between the harness and risers for recording force as a function of time. A Hulcher camera with a time-base generator installed, in addition to motion-picture cameras, provided the photographic records. Design changes dictated by these tests necessitated changing from a standard C-9 28-foot canopy to a special 24-foot canopy. The whirltower tests were successfully repeated for the new configuration.

Airplane Drop Testing of the Parachute System

To supplement whirltower testing of the parachute system and to determine deployment characteristics from the hard pack during free fall, a series of airplane drops (fig. 9) was successfully accomplished. The complete system was fitted on an anthropomorphic dummy and released from a C-119 aircraft at 125 knots and at an altitude of 1,200 feet. During the initial tests the dummy was in a head-down attitude and the pilot chute, in the wake of the dummy, was not capable of effecting the rotation necessary to allow deployment from the aperture in the top of the pack. The bridle length was increased to 70 inches for subsequent tests, all of which were successful.

Photographic coverage was provided from air-to-ground, air-to-air, and ground-to-air vantage points. Hulcher cameras with a time base

generator incorporated, provided an accurate history of the deployment sequence.

BENCH EXTENSION OF SEAT-STABILIZATION FINS

As an operational check of the actuating system of the seat-stabilization fins, the system was fired statically and the rate and degree of fin extension recorded. All components functioned properly. Superimposing anticipated airloads on the statically derived data permits a more accurate prediction of fin performance under dynamic conditions.

POST-STRUCTURAL-LOAD OPERATIONAL CHECKS

Numerous seat components are required to fulfill structural requirements during the initial ejection sequence and subsequently to perform a critical function. To insure that the components are structurally adequate to resist deformations which would inhibit post-load functioning, these items were subjected to predicted loads and actuated after load relief. (See fig. 10.) Items included in this test are as follows:

(a) Leg manacle

(b) Lap belt

(c) Shoulder harness

(d) Arm retention

(e) Head rest

(f) Manual jettison handle

(g) Manual leg-manacle release

All items were tested to 90 percent of design load; all were structurally adequate and all operated satisfactorily after load relief.

STRAIN-GAGE CALIBRATIONS FOR DYNAMIC TESTS

A primary reason for conducting full-scale dynamic tests is to obtain conclusive data relative to airloads encountered. The procedure utilized most extensively is to provide the item in question with strain gages, in conjunction with on-board telemetering equipment. For adequate interpretation of the recorded data, the strain gages must be accurately calibrated prior to the test (fig. 11). This is accomplished by applying a series of known loads and noting the resultant variation in electrical resistance. Having established a load-delta resistance relationship for a given gage, loads encountered during the dynamic test can be accurately determined from telemetered data. Strain-gaged seat components for sled testing are as follows:

(a) Stabilization fins

(b) Ejection handles

(c) Shock-wave generator

(d) Primary roller support structure

(e) Arm retention

WINDSTREAM EXPOSURE SLED TESTS

As was mentioned earlier, wind-tunnel data on the ejection seat were supplemented by full-scale tests on a high-speed track. For this test series, the seat was mounted on a truss assembly which positioned the item considerably forward of the vehicle in an area of minimum airstream disturbances (fig. 12). The truss assembly was completely equipped with strain gages and provided a means of determining the aerodynamic loadings on the seat. Data were recorded continuously during acceleration to maximum speed (approximately Mach number 1.25) and during the subsequent deceleration. The seat was in a fixed position for each test; therefore, for that particular angle of attack, lift, drag, and moment coefficients were obtained as a continuous function of Mach number. Three tests, one of which was a check run, were conducted with the seat in the ejection attitude of 13°. One test had the seat positioned in a -10° attitude. In tests 2 and 3 the stabilizing fins were actuated, as was a prototype shock-wave generator on run 4. The fins functioned properly, although on an initial run, one failed structurally upon locking in the extended position. The shock-wave generator failed during initial extension on the highest speed test and inflicted damage to basic seat structure. Both fin and

generator designs were subsequently corrected. Another reason for conducting the tests was to obtain data on the wind-blast resistance capabilities of the pilot's protective clothing. This is discussed in another paper and will not be restated here.

GROUND JETTISONING OF COCKPIT CANOPY

A functional check of the canopy remover system was effected by statically jettisoning the canopy from the seat-ejection test vehicle (fig. 13). In addition to the operational check, canopy separation and trajectory characteristics were determined. To effect recovery of the canopy, a prestressed bungee assembly was attached. All components of the system fulfilled design objectives.

SEAT-EJECTION STATIC TESTS

As a preliminary to sled track testing, a complete operational check of the integrated system was accomplished by statically ejecting the seat from the track test vehicle (fig. 14). Of equal importance, however, was an evaluation of rocket catapult performance, the effect of rocket thrust misalinement, and a determination of system capabilities under zero-airspeed—zero-altitude conditions.

The stabilization fins, shock-wave generator, parachute recovery system, and pilot restraint mechanism are initiated by interference between a seat-mounted lever and a bulkhead-mounted tripper. On test 1 catapult-imposed loads caused seat and sled structural deflections which were apparently sufficient to allow the seat to pitch forward. As a result, the tripper mechanism was not engaged and the aforementioned systems were not actuated. The seat and dummy struck the ground as a unit after having attained a trajectory zenith of approximately 235 feet. The seat-mounted lever was redesigned to correct the conditions noted in test 1. A second static ejection was accomplished, during which all systems were actuated. The seat experienced 4.0 rotations in pitch prior to reaching trajectory zenith of 240 feet, at which time the headrest fired, partially deploying the personal parachute. Rocket catapult performance in each case was considered to be within acceptable limits.

SLED EJECTION TESTS

The development program culminates in full-scale dynamic testing of the integrated system. Use is made of the Edwards Air Force Base high-speed track facilities in conjunction with a test vehicle simulating the airplane's cockpit and forward fuselage, from which escape-system ejections are effected at representative airspeeds. The objectives of this phase of the test program are primarily derivation of data in the following areas:

(a) Structural and functional integrity of the seat and canopy installations and the pilot's pressure suit and personal equipment

(b) Post-ejection trajectories of the seat and canopy

(c) Aerodynamic characteristics of the seat-dummy unit

(d) Stability of the seat-dummy in free flight

(e) Very low altitude parachute recovery of the dummy at low and high airspeeds

(f) Acceleration patterns at the dummy's head and center of gravity during ejection

(g) Post-ejection separation of the seat and dummy

(h) Cockpit noise level and pressure variations subsequent to canopy jettison.

Two sled ejection tests have been conducted. During the initial test (fig. 15) the system was proven satisfactory at an ejection airspeed of 230 knots. The canopy and seat-dummy were ejected from an unpressurized cockpit with the dummy attaining a trajectory zenith of 145 feet. Parachute recovery of the dummy was successful with full canopy inflation occurring 120 feet above the terrain. (See fig. 16.) All seat components and systems functioned properly. The anthropomorphic dummy was equipped with telemetering equipment which relayed data from rate gyros, accelerometers, and pressure transducers to trackside receiving and recording facilities. An accurate analysis of the reduced data revealed the acceleration histories, as a function of time and seat dynamics, were within acceptable limits.

The second test (fig. 17) was conducted to prove the system at an airspeed of 620 knots ($M = 0.91$; $q = 1{,}130$ lb/sq ft). The canopy and dummy, clothed in a full pressure suit, were ejected from a cockpit pressurized to a 3.5 lb/sq in. differential. The canopy and seat-dummy

separated cleanly from the test vehicle, the dummy attaining a trajectory zenith of 60 feet before recovery by the parachute (fig. 18). The rates of angular displacement and combined load factors were within the limits of human tolerance. All seat components were structurally adequate and operated according to design objectives.

CONCLUSIONS

The X-15 emergency-escape-system development program included those tests outlined by this paper, all of which were considered necessary to support the design effort adequately, to evaluate individual components completely, and finally to determine the functional and structural integrity of the entire system under full-scale dynamic conditions. Although only partly complete, the test program to date has demonstrated that the aerodynamic, mechanical, structural, propulsive and survival aspects of the X-15 emergency escape system are proper in concept and implementation.

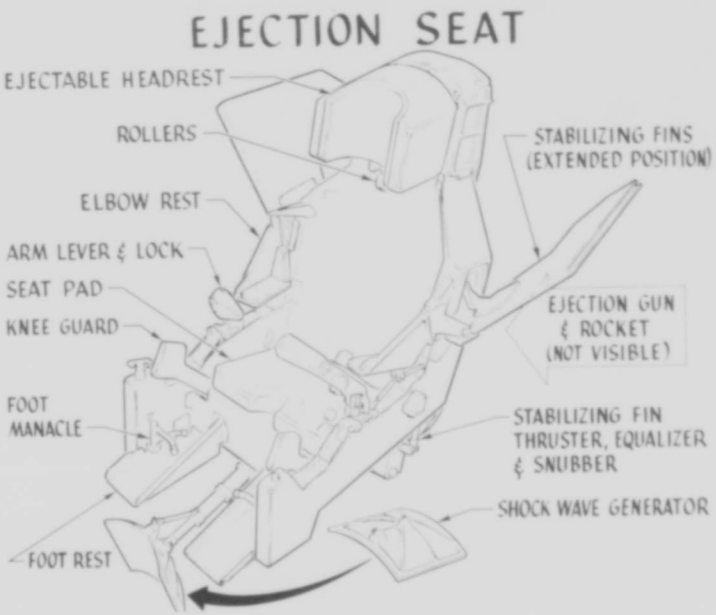

Figure 1

EJECTION SEAT

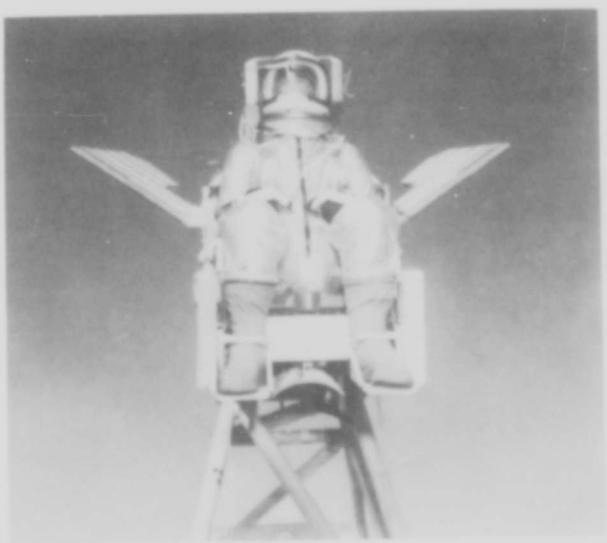

Figure 2

WIND TUNNEL TEST
SEAT-PILOT MODEL

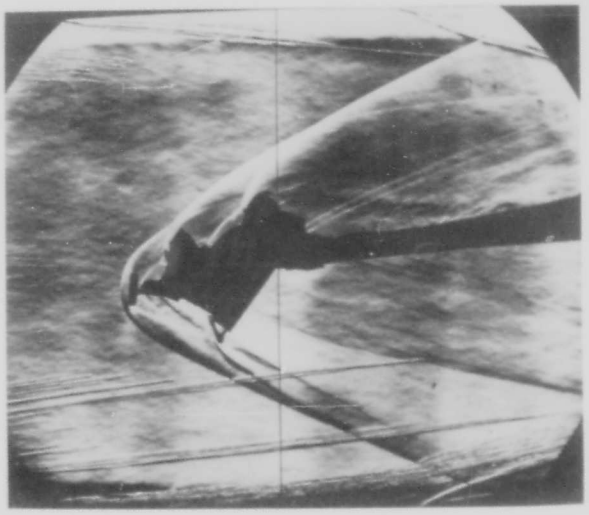

Figure 3

SEAT STABLE ATTITUDE

Figure 4

ANEROID ACTUATOR FOR RESTRAINT RELEASE & PILOT RECOVERY SYSTEM

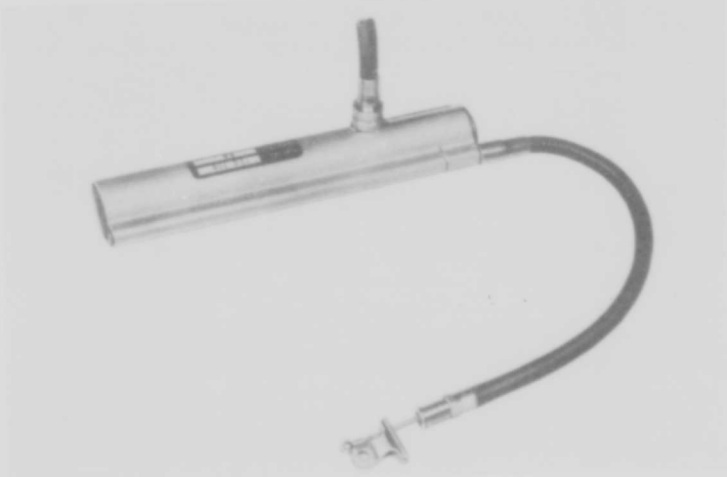

Figure 5

HEADREST JETTISON & CHUTE DEPLOYMENT - STATIC

Figure 6

PILOT CHUTE
WIND TUNNEL

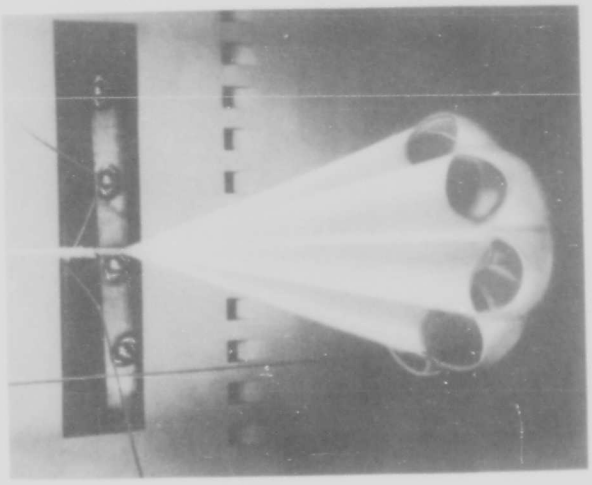

Figure 7

WHIRLTOWER TEST

Figure 8

PARACHUTE DEPLOYMENT-FREE FALL

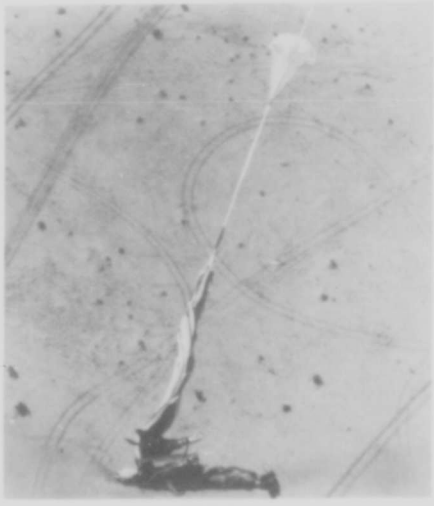

Figure 9

POST-LOAD OPERATIONAL CHECK

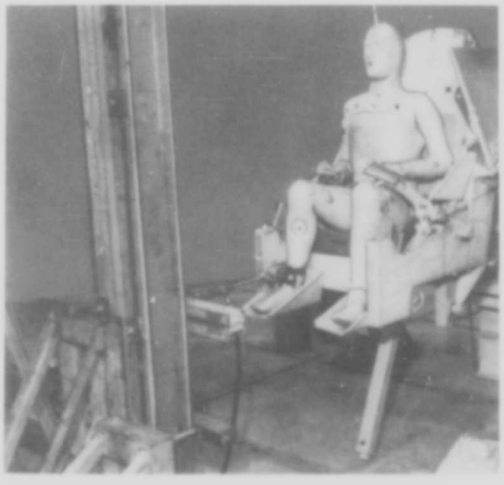

Figure 10

STRAIN GAGE CALIBRATION

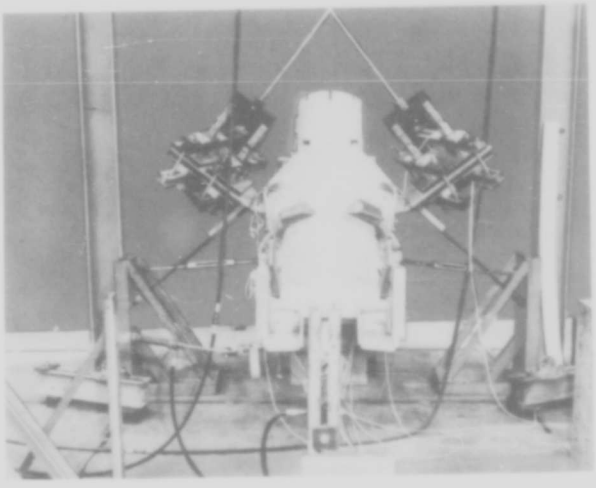

Figure 11

WINDSTREAM EXPOSURE TEST

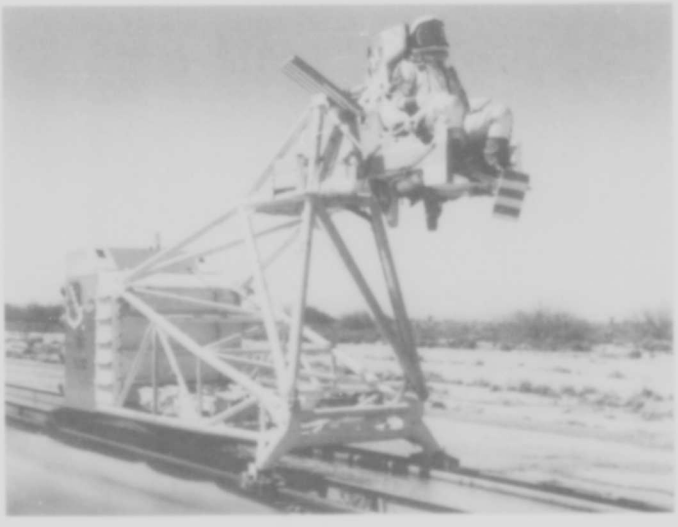

Figure 12

CANOPY JETTISON - STATIC

Figure 13

SEAT-DUMMY EJECTION-STATIC

Figure 14

SLED TEST-LOW SPEED
SEAT-DUMMY EJECTION

Figure 15

SLED TEST-LOW SPEED
PARACHUTE RECOVERY

Figure 16

SLED TEST - HIGH SPEED
SEAT DUMMY EJECTION

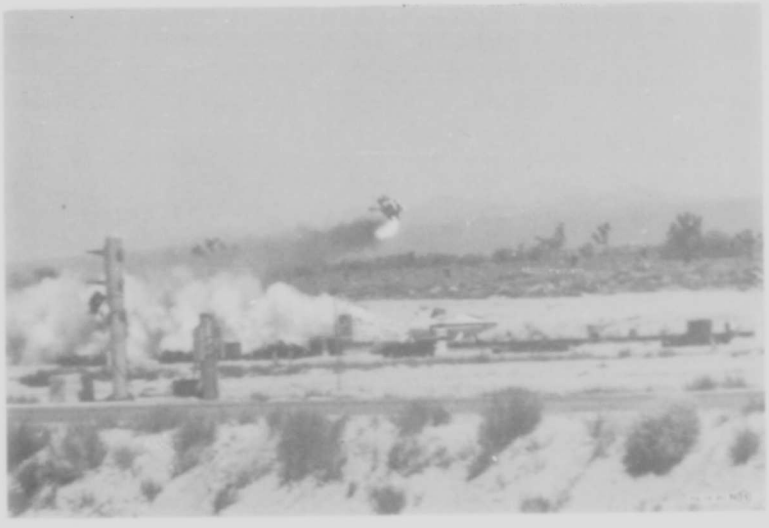

Figure 17

SLED TEST - HIGH SPEED
PARACHUTE RECOVERY

Figure 18

AEROMEDICAL SUPPORT OF THE X-15 PROGRAM

By Burt Rowen

Air Force Flight Test Center

For approximately 10 years aeronautical engineers have been recording in-flight data from instrumented aircraft on ground read-out indicators through telemetry. In the past, when a research aircraft arrived at its flight phase of development and began flying, the pilot's physiological status was never recorded during flight. This was the situation during the X-2 program. During the flight phase of the X-15 aircraft, physiological data will be telemetered so that a flight surgeon observing the ground read-out can tell when the pilot is approaching the limit of his physiological tolerance. This will quantitatively identify the most stressful portion of a particular mission profile.

The full-pressure suits to be worn during the X-15 program were specifically designed with 12 electrical contact points to facilitate the necessary connections between the telemetering sensors and transmitters.

With current techniques of closed-loop dynamic simulation, it is possible to record additional physiological data during simulated flight trajectories. During the dynamic simulation at the Aviation Medical Acceleration Laboratory of the Naval Air Development Center, Johnsville, Pa., electrocardiographic data were recorded but not telemetered.

Before the date of the first flight of the X-15 in 1959, pilot's physiological data will be telemetered to ground recording stations to evaluate and prove this technique, using a TF-102 aircraft specifically assigned to the Air Force Flight Test Center for this project. Physiological data will be recorded at Edwards Air Force Base, Calif., by means of currently operational NACA High-Speed Flight Station and USAF telemetering receivers.

Such items as (1) differential between cockpit pressure and suit pressure, (2) differential between helmet pressure and suit pressure, (3) pilot's body-surface temperatures, and (4) electrocardiographic data will be monitored by a flight surgeon at the ground receiving station during flight. The body-surface temperatures will be correlated with recorded cockpit temperatures. This is an extension of the electrocardiographic recording system monitored by a physician during the centrifuge simulation program at the Naval Air Development Center at Johnsville, Pa. This system has a growth potential for additional data recording. For certain missions specific data can be collected,

permitting flexibility of operation. The objectives of the TF-102 program at the Air Force Flight Test Center are: (1) training and familiarization for X-15 pilots; (2) physiological instrumentation research and development, and establishment of criteria for future crew selection; (3) standardization of the MC-2 suit; (4) product improvement of the MC-2 suit assembly for future weapon systems; and (5) operational capability of the MC-2 suit. The transducers for these measurements are all miniaturized and will not hinder pilot performance in any way. The flat electrocardiographic pickups, for example, are approximately the size of small dental X-ray films.

Another interesting aspect of physiological monitoring of pilots associated with the X-15 program is their whole-body radiation levels. The University of California operates a whole-body radiation counter for the Los Alamos Scientific Laboratory about 70 miles north of Albuquerque in the Los Alamos airspace prohibited area. This device is shielded by 20 tons of lead and has been used as an investigative tool in measuring whole-body radiation levels of more than 3,000 people. This gamma counter measures radioactive potassium 40 K_{40}, a constituent of muscle tissue, and identifies radioactivity as so many counts per second. (See fig. 1, where male subjects are identified by circles and female subjects by triangles.) Preflight baseline K_{40} activity will be obtained from pilots in this program and later correlated with postflight levels. The anticipated increased activity represents a quantitative increment of cosmic-radiation effects which will be available for the first time from a human subject flying a research aircraft. This program, using the only known whole-body radiation counter, is easy to implement. The only portion that needs to be hurried is the trip back to the Los Alamos Scientific Laboratory after landing from a high-altitude flight. Since the induced whole-body radioactivity of K_{40} has a half-life of 12.8 hours, the pilot's postflight radioactivity therefore returns to normal in about 3 days. The technique of performing the whole-body count is very simple, requiring only 3 minutes, and does not involve the use of drugs. The Los Alamos Scientific Laboratory will obtain a newer whole-body radiation counter in December of 1958. The Air Research and Development Command is currently trying to obtain the original whole-body radiation counter for transportation to and installation at the Air Force Flight Test Center.

The Air Force Cambridge Research Center, upon inquiry, has expressed a position of interest and complete cooperation regarding assistance in obtaining quantitative data of cosmic-ray activity on the surface of the X-15 itself. These results, compared with the pilot's whole-body activity, should be extremely informative regarding the relation between pilot and aircraft exposure to cosmic-ray activity. The initial proposals include (1) an abrasion detector to measure crater erosion, (2) cosmic radiation by emulsion, and (3) micrometeorite detection.

This briefly is the Human Factors or Aeromedical Support Program for the X-15. The overall objective is to obtain quantitative physiological data and to make the pilot's actual flight task a realistic continuation of previous experience and training. The procedures for accomplishing these goals are in existence today; they need only further refinement in an operational aircraft to make their use a reality when the X-15 begins its scheduled flight program.

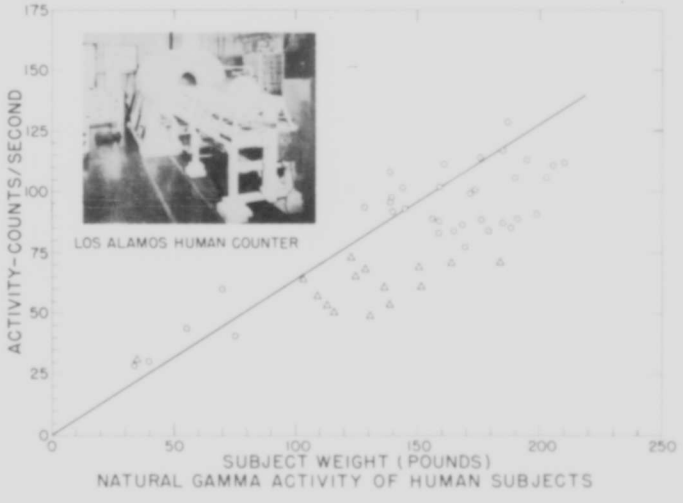
175
150
125
100
75
50
25
0
ACTIVITY-COUNTS/SECOND
LOS ALAMOS HUMAN COUNTER
0
50
100
150
200
250
SUBJECT WEIGHT (POUNDS)
NATURAL GAMMA ACTIVITY OF HUMAN SUBJECTS

Figure 1

STATUS OF HIGH-RANGE AND FLOW-DIRECTION SENSOR

By G. M. Truszynski
NACA High-Speed Flight Station

and W. D. Mace
NACA Langley Aeronautical Laboratory

INTRODUCTION

The performance capabilities of the X-15 airplane, particularly in terms of the altitudes reached and distances traveled during many of the flights planned, are such that the use of certain systems are required to assure accomplishment of the desired mission. One of these systems, the inertial platform, is required to provide certain critical information that will enable the pilot to fly the airplane satisfactorily and safely throughout its trajectory; this system is described in a subsequent paper by Lipscomb and Dodgen. In addition to the inertial platform, two additional systems will be required to supply further information necessary in carrying out the flight program and to provide certain research measurements. These systems are:

(1) A probe and associated system that will be capable of operating throughout the extreme temperature environment encountered on reentry to provide a measure of the angle of attack and sideslip to the pilot

(2) An instrumented ground range capable of monitoring the flight of the airplane throughout its entire trajectory.

DISCUSSION

Some of the requirements to be met by the ground range are as follows:

(1) To aid in the initial guidance and vectoring of the launching airplane to the required heading

(2) To monitor the initial climb of the research airplane

(3) To provide a "backup" for altitude and velocity information to the pilot in the event of on-board equipment failure

(4) To monitor the flight path as an aid in homing or vectoring to a suitable intermediate emergency landing area, if required

(5) To provide information for chase airplane rendezvous

(6) To provide final approach and landing information to the pilot

(7) To provide reliable long-range communications capability

(8) To provide accurate space-trajectory data for research purposes.

In order to meet these requirements, a ground range has been designed and is presently under construction. Figure 1 illustrates the geographical location of the three stations comprising the range. The stations at Edwards and Beatty are essentially complete and are presently undergoing check-out. Present plans call for these two stations to be operational by September 1958, and completion of the third station at Ely is scheduled for December 1958. Many considerations entered into the choice of the specific locations for the down-range sites including items such as the required radar overlap capabilities, the power balance in the radar-to-beacon loop, the requirement of a maximum omnidirectional seeing angle, and the overall logistic problem. The locations and elevations of the sites are such that omnidirectional tracking can be accomplished down to an altitude of at least 10,000 feet. The distances between sites are such that overall trajectory control can still be maintained in event of failure of any one of the radars. Also illustrated in figure 1 are the specific emergency landing areas which are intended for use during remote drops. The spacing of these emergency areas allows a logical buildup of the flight program.

The equipment installed at each site to provide the range functions are as follows:

(1) Radars - AFMTC Model II

(2) Plotting boards

(3) Velocity computer

(4) Telemeter receiver

(5) Data monitor

(6) Communications

(7) Data transmission and receiving equipment.

The tracking radars used are type AFMTC Model II and are similar to those in use on the Canaveral range. These radars operate on S-band and have a 400-mile ranging circuit capability. Statistical angular

accuracies expected are of the order of 1 mil with a range accuracy of 10 to 15 yards. The plan is to utilize a beacon transponder in the airplane; this unit will be capable of responding to coded interrogations in order to minimize interference from radar equipment of the Air Defense Command and other installations.

Plotting boards are being installed at each site to provide for the monitoring of trajectory data. These units will plot information from the respective local radar; however, at the Edwards site, an additional plotting board is provided to allow monitoring of the full-length trajectory. Trajectory data available on these units in the form of instantaneous airplane plan position and altitude, together with airplane velocity, will be utilized for ground monitoring and controlling the aircraft to a landing at Edwards or for terminal guidance to one of the emergency landing areas if required. The velocity computer, operating from radar-data input, allows for the monitoring of either the individual component or the total flight-path velocity.

The telemetering planned for use is a standard pulse-duration-modulation system with the capability of receiving up to 90 channels of information. Both engine and aircraft operational parameters will be telemetered to the ground, where they will be monitored as an aid to the pilot in performing the overall flight mission and will be recorded in permanent form on magnetic tape. Real-time information can be observed in various forms at the data monitor. All the channels transmitted will be presented in vertical bar-graph form on two oscilloscopes. Of these, any forty channels can be observed as meter presentations calibrated in the respective quantity. Finally, when a time-history presentation is required, up to twelve channels can be plotted in real time on a strip-chart recorder.

Communication with the aircraft will be accomplished through the use of standard military ground UHF equipment, network connected by ground telephone lines, such that two-way conversation with the aircraft is possible from the Edwards site, regardless of the location of the aircraft in its flight path. The transmission and reception of radar-acquisition information is accomplished through equipment that converts analog data to digital data, with distribution between sites again performed through the use of ground telephone lines.

A photograph of the station at Beatty is shown in figure 2; the isolation of the area is fairly evident.

As has been indicated at the 1956 conference on the X-15, the measurement of angles of attack and sideslip at extreme altitudes and the consequent regions of low dynamic pressure will be obtained through the use of a null pressure seeking nose sphere.

Figures 3 and 4 illustrate the configuration and essential features of the system. As shown, the system takes the form of a sphere-cone combination, which makes up approximately the first 18 inches of the airplane fuselage. The unit operates in such manner that differential pressures sensed at orifices located at 42° from the sphere stagnation point in both the pitch and yaw planes are utilized through a servosystem to maintain the sphere in alinement with the relative wind. Synchro pickoffs attached to the sphere will then reproduce the sphere position in terms of angles of attack and sideslip for use by the pilot, and the flow-angle data will be also recorded for research purposes. Both sphere and cone are fabricated from Inconel X. The sphere itself is $6\frac{1}{2}$ inches in diameter. The configuration of the external components, particularly in the region of the lip, is based on tests made in the Langley 11-inch hypersonic tunnel for the purpose of obtaining the necessary heat-transfer data. The skin thicknesses provide a sufficient heat sink to limit their temperature to 1,200° F for all design missions with the exception of the cone extension, which may approach 1,800° F for some missions. The skin of the sphere and cone have now been tapered, and this change resulted in a considerable weight saving while still providing an adequate heat sink. The sealing in the region of the cone-sphere junction is accomplished through the use of a steel ring which is kept in contact with the sphere by means of a preloaded steel bellows. This seal ring is protected from direct aerodynamic heating by the replaceable extension of the conical afterbody. The internal temperatures are controlled through the use of insulation, radiation shields, and a coolant in the form of expanded liquid nitrogen.

The sphere and its supporting, sealing, and hydraulic-actuating mechanisms are designed as an integral assembly. The electronic amplifiers, power supplies, and control valves are mounted in the conical afterbody. The electrical, hydraulic, and pneumatic connections between the sphere and the cone pass through the single central supporting member. The rotary hydraulic actuators provide the two degrees of freedom required.

Two independent servosystems, each composed of a pressure transducer, servoamplifier, and electrohydraulic actuator, will be used for rotating the sphere in the pitch and sideslip axes. The design approach for this system has been finalized and its development and construction is being accomplished by the Nortronics Division of Northrop Aircraft Company. Tests on a prototype sensor are scheduled to begin in the latter part of August 1958. These tests will consist, in part, of determining the sensor's operating characteristic while it is in the exhaust of a turbojet engine. This test approximates the heating rates to be encountered during some typical X-15 missions. The completed sensor is scheduled for delivery by December 1958.

The anticipated overall accuracy of the sensor is presented in figure 5. The results indicate the error in angle of attack (or sideslip) as a function of dynamic pressure, and the data are based on tests performed on some of the sensor components and on other anticipated system characteristics. The design missions of the X-15 will involve a range of dynamic pressure from about 2,500 lb/sq ft down to about 1 lb/sq ft. The lower limit corresponds to the design condition of Mach number 5 at an altitude of about 250,000 feet. As indicated in figure 5 the error for this condition is about 2.8°. This is a sufficiently accurate indication to allow the pilot enough time to aline the airplane with the flight path that he wishes to follow during reentry. For an extreme altitude mission it is interesting to note that if the airplane experienced free fall from 500,000 feet, the sensor would have this same accuracy at an altitude of about 240,000 feet. This still allows the pilot enough time to aline the airplane properly to a reasonable flow angle.

Some of the pertinent performance characteristics of the system are as follows:

(a) Angle-of-attack range: 40° to -10°

(b) Angle-of-sideslip range: ±20°

(c) Dynamic response: 20° maximum phase shift at 1.5 cps

(d) Actuation capability: 60°/sec minimum with no more than 2° velocity error.

The sensor design is flexible in that equipment improvements resulting from advancements in the state of the art may be incorporated. Such improvements may include the use of ionization gages and alphatron or other vacuum gages to extend the useful range of the sensor to even higher altitudes to keep pace with the ever increasing performance capabilities of research airplanes.

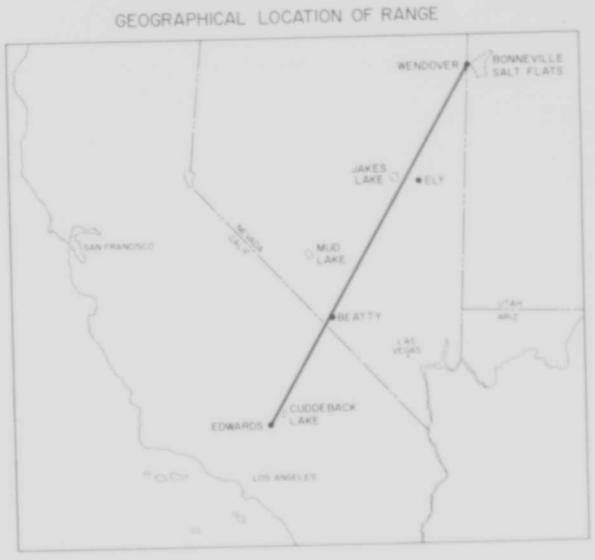

Figure 1

Figure 2

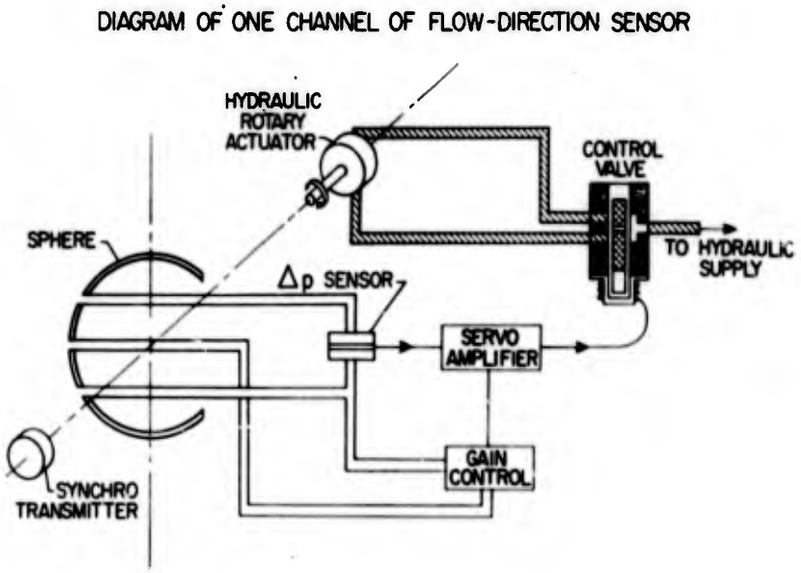

Figure 3

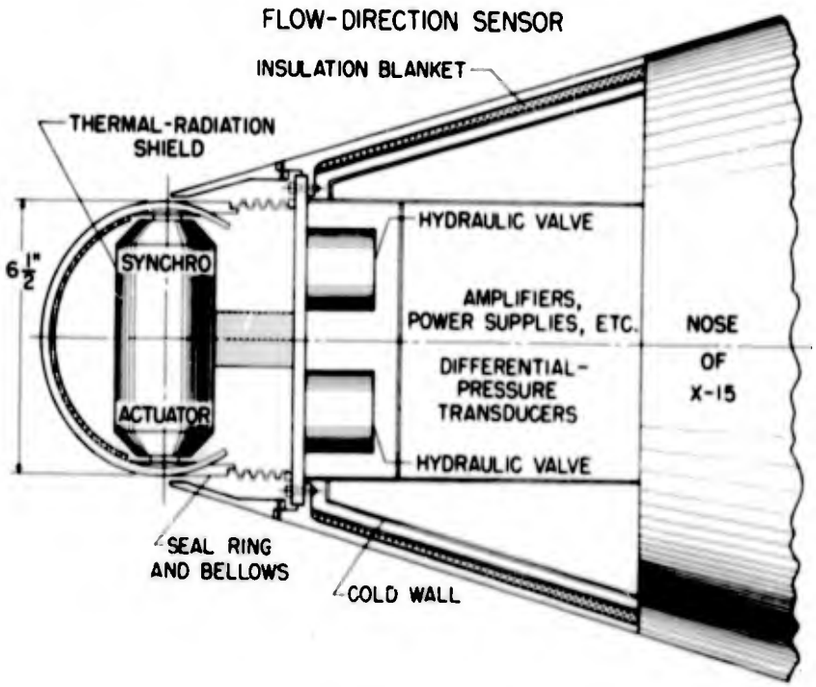

Figure 4

ACCURACY OF FLOW-DIRECTION SENSOR

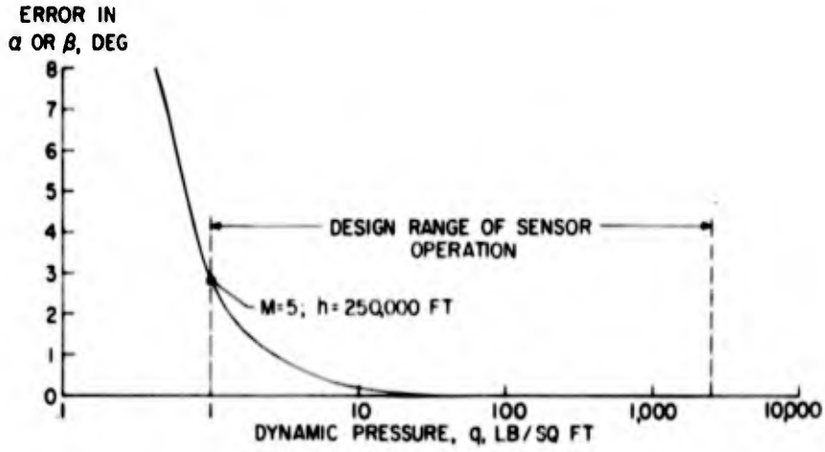

Figure 5

ALL-ATTITUDE FLIGHT-DATA SYSTEM FOR THE X-15 RESEARCH AIRPLANE

By M. L. Lipscomb
Wright Air Development Center

and J. A. Dodgen
NACA Langley Aeronautical Laboratory

This paper is intended to review briefly the data requirements leading to the selection of an inertial-type flight-data system for use in the X-15, and to describe the system now being constructed to meet the requirements.

A talk given at the X-15 conference in 1956 presented some material leading to the selection of an inertial-type system to supply flight data for display to the pilot and for recording as research data. To review, the following table shows the measurements desired of the system, as well as the required ranges and the intended use of the data:

Measurement	Range	Use	
		Pilot's display	Research data
1. Velocities:			
(a) Along-range	±7,000 fps		✓
(b) Across-range . . .	±3,000 fps		✓
(c) Vertical	±5,000 fps	✓	✓
(d) Trajectory	0 to 7,000 fps	✓	
2. Altitude	0 to 500,000 ft	✓	
3. Attitude angles:			
(a) Pitch	360°	✓	✓
(b) Roll	360°	✓	✓
(c) Yaw	360°	✓	✓

It is seen that the eight quantities desired may be classified in three general groups: (1) velocities, (2) altitude, and (3) attitude angles. The four velocities are the three component velocity vectors and the scalar total, or "trajectory," velocity. The "along-range" and "across-range" velocity vectors coincide with the velocity data obtainable from the ground-radar range which was described in the preceding paper.

This will facilitate the combination of the velocity data from the airborne and the ground equipment so that refined trajectory velocity data can be obtained for research purposes. (That is, the ground range data can be used as a long-term reference for correcting the data from the airborne system.) The altitude and the attitude angles are defined according to conventional aerodynamic practice.

The following table illustrates the reasons for the selection of an inertial approach to obtain these data:

	Pressure	Doppler or radio	"Simple" Gyroscopic	Inertial
Measurements required:				
Velocities	✓	✓		✓
Altitude	✓	✓		✓
Attitude angles			✓	✓
Limiting factors:				
Accelerations			×	
Velocity range	×			
Altitude range	×			
Attitude range		×	×	
Flight range			×	
Flight duration			×	×*
Power required		×		
Cooling required		×		

*For extended duration.

The vertical columns show the various available methods which were considered for measuring the quantities listed in the first group on the left. The lower half of the table is a listing of the factors which limit the use of these methods. It can be noted that all of the methods except the inertial approach are eliminated for basic reasons established by the mission, whereas the limiting factor for the inertial approach is "flight duration." Since the flight time of the X-15 is within the acceptable operating time of existing inertial components, this limitation will not present a problem. It appears, then, that the X-15 requirement is uniquely suited to an inertial-system approach.

The inertial flight-data system for the X-15 is being procured from Sperry Gyroscope Co. Figure 1 is a functional schematic of the system as it evolved from design. It can be seen that the system is

divided into two groups. The first group is carried in the X-15 and consists basically of the stabilizer and the computer. This equipment supplies all of the required data after the X-15 is launched. The second group, carried in the B-52, is used to supply the proper initial conditions to the computer and thus aline and stabilize the platform prior to launch.

Figure 2 shows the perspective outlines of the basic flight-data system components mounted in the X-15. They are estimated to weigh approximately 160 pounds, displace a volume of approximately 3 cubic feet, and require a peak electrical load of 600 watts. The component configuration, particularly the computer, is tailored to the space available in the X-15. Heat exchangers, incorporated in the cases, will use the aircraft cooling gas to maintain the equipment at an operating temperature which will assure proper performance.

Figure 3 is a photograph of the stabilizer, which consists of a stabilized platform mounted in a four-gimbal arrangement. This gimbal system provides unlimited angular freedom about all axes, and also yields the pitch-, roll-, and heading-angle outputs free of unwanted interactions. The electronic circuitry necessary to operate the various platform components is mounted within the stabilizer case. Where possible, the amplifiers are mounted on the gimbals to reduce the slipring requirements and allow use of the gimbal structure as a heat sink.

Figure 4 is an exploded view of the stabilizer and gives some appreciation of the various components used in constructing the unit. The stabilized element carries three integrating gyros which serve as stabilizing elements and three force-restrained linear accelerometers which are the inertial sensors. The gimbals are actuated by direct torquers. The attitude-angle pickoffs are gimbal-mounted pancake synchros.

The computer receives the acceleration signals from the stabilizer and performs the necessary computations, which include:

(1) Integration to obtain velocity

(2) Integration of velocity to obtain displacement

(3) The trajectory velocity summation

(4) The "earth's-rate" computation

(5) The acceleration corrections which are required because of kinematic velocities and changes in mass attraction

This unit furnishes the torquing signals to the platform gyros to maintain the platform vertical with respect to the local earth. It also supplies the velocity and altitude outputs to the indicators and recorders. Prior to launch, the computer receives the initial condition data from the control panel in the B-52, and serves as a Doppler-inertial velocity mixer and a barometric-inertial velocity mixer to aline the platform and integrators and to determine a gyro "drift" correction.

The computer is connected to the control panel in the B-52 through the umbilical connector. This panel provides the necessary controls and indications to perform:

(1) The system mode selection

(2) Manual insertion of initial altitude and position data

(3) System performance monitoring prior to launch

It also contains the converters and couplers necessary to introduce the initial velocities and heading angle into the system for alinement purposes. The initial horizontal velocity is determined by means of the AN/APN-81 Doppler radar and is transformed into along-range and across-range components in the control panel through use of the N-1 compass data. The barometric rate-of-climb transducer furnishes the initial vertical velocity component to the control panel. The three velocities are then furnished to the mixers in the computer. It should be noted that the control panel operator in the B-52 has the responsibility of making the initial settings and mode selections, as well as that of monitoring the alinement process to assure proper operation, thus relieving the X-15 pilot of these responsibilities. The B-52 portion of the system is disconnected at launch and the flight-data system operates throughout the X-15 flight as a pure inertial system.

The system is designed to operate over a limited portion of the earth's surface. It is set up to accept a launch point anywhere in a corridor extending 540 nautical miles up-range of Edwards Air Force Base and 180 nautical miles down-range. The corridor has a width of ±120 nautical miles about the reference course, which is a great circle lying in close proximity to the radar-tracking stations described in the preceding paper.

Operation of the system can best be illustrated by following a typical mission from ground checkout at Edwards through launch. The system has three modes of operation: (1) Standby, (2) Erection, and (3) Inertial. The system is started by placing the mode selector in "standby." This initiates an alinement cycle during which the platform is crudely erected to the vertical and alined in azimuth to point

down-range. After warmup, a preflight check is completed and the selector is switched to the "erection" mode. In this mode, the velocity mixers previously mentioned normally operate to perform their alinement functions; however, the design is such that when the Doppler is turned off, or when the signal return is too low for proper operation, the flight data system automatically reverts to a pure inertial mode. Thus, when the X-15/B-52 combination is ready for take-off, the system is crudely erected and operating as an earth's radius pendulum. After take-off, the Doppler is turned on, and the system now begins the job of refining the "vertical" and adjusting the velocity integrators. The control-panel operator can monitor the alinement process and perform certain "confidence" checks on the system during the flight up-range to the drop point. Just prior to launch, with the mode switch still in the "erection" position, final values of range, cross-range, and altitude are set into the system. The mode switch is now turned to the "inertial" position. This causes the initial data values to be locked into their respective circuits, and a compensation circuit begins to supply gyro drift corrections. The X-15 is then released and the system operates as a pure inertial system until landing.

Table I shows a tabulation of the results of a theoretical error analysis of the system now being constructed. This error analysis is based on a 67-percent confidence limit, so that we may expect an error of no more than twice this magnitude 95 percent of the time. The estimated overall error is within the required accuracy and is acceptable for the X-15 flight program. The table indicates the error distribution due to the various error sources. The heading "Initial Conditions" covers errors caused by the inaccuracy, noise, and so forth, in the initial data supplied to stabilize the system. For this analysis the initial velocity accuracies were assumed to be 10 ft/sec rms in along-range and across-range velocities and 2 ft/sec rms in vertical velocity. The size of the errors due to the initial conditions emphasizes the necessity for good initial input data. As mentioned earlier, the initial along-range and across-range velocities are supplied by transforming the Doppler ground speed into the proper coordinates by means of the Doppler drift angle combined with the N-1 compass heading. The platform itself is alined in azimuth by reference to the N-1 compass. These facts, coupled with the distribution of the various components between the X-15 and the B-52, has introduced several alinement problems. Some of these problems are:

(1) The N-1 compass system alinement with the B-52 reference line and the calibration of the unit

(2) The APN-81 Doppler antenna alinement with the B-52 reference line and the calibration of the unit

(3) Stabilizer alinement relative to X-15 reference line

(4) Mounting alinement of X-15 reference line relative to the B-52 reference line

(5) Relative motion of X-15 reference line with respect to B-52 reference line

(a) Steady-state misalinement due to static aerodynamic loads

(b) Dynamic or fluctuating misalinements due to gust loads or X-15 prelaunch control checks

Procedures have been devised which will allow the various components to be alined within the airframes to acceptable accuracy. Instrumentation is being built into the B-52 which will allow the remainder of the misalinements to be measured in flight to an accuracy of 0.1^{o}. An "azimuth-error-synchro" is built into the B-52 control panel to allow corrections for the steady-state misalinements that are found. The X-15 prelaunch control checks will be programed and executed in a sequence that will cause the least disturbance to the platform system.

Figure 5 shows the basic flight instruments which are displayed to the pilot. Four of these indicators, those showing normal acceleration, angle of attack, angle of sideslip, and roll rate, are not supplied by the inertial system. The remainder derive their inputs from the system. They are: the trajectory velocity indicator; the inertial altimeter; the vertical velocity indicator; and a combined attitude indicator which displays roll and pitch on the center ball, turn and slip at the bottom, and a sensitive "command pitch" at the left side. This command pitch is a plus or minus error indication relative to a desired pitch angle which may be selected by means of the pitch-angle-set unit. Under the roll-rate indicator is a combined heading and radio direction indicator which displays heading on the dial and radio homing information by means of a pointer. It should be noted that the indicators here very closely resemble those currently used in operational aircraft. They differ in display only so far as required to satisfy the intended purpose. They are graduated and marked to be compatible with the range and accuracy of the data displayed. The combined attitude indicator will be the center of the display, and as was described in an earlier talk, has allowed considerable improvement to be made in the effectiveness of the display.

The inertial flight-data system must be well maintained and properly checked if delays to the X-15 flight program are to be minimized. Considerable planning has gone into the system design to allow convenient check procedures and parts replacement. Also, a suitable ground test facility is being procured. The system, particularly the

computer, is built in modular form, and grouped so that each of the basic functions is contained in a separate unit, thus allowing each unit to be checked as an entity. The ground checking equipment is designed to allow system testing all the way from the bench to the combined X-15/B-52 configuration. Means will be available to supply proper power and coolant to the system as required.

The first complete inertial system, including the ground checkout equipment, is scheduled for delivery in December 1958. An engineering model (prototype) has already been constructed and is under test at the contractor's plant. Theoretical error analyses and component testing to date indicate that the described inertial system will be satisfactory for the X-15 research program.

TABLE I

THEORETICAL ERROR ANALYSIS FOR TIME = 300 SECONDS AFTER LAUNCH

Error source	Root-mean-square error, σ, in -				
	Along-range velocity, V_R, ft/sec	Across-range velocity, V_X, ft/sec	Vertical velocity, V_H, ft/sec	Total velocity, V_T, ft/sec	Altitude, ft
Gyroscopes:					
1. Gyro acceleration drift	1.0	1.0	2.4	-----	530
2. Gyro random drift	1.5	1.5	2.5	-----	600
3. Azimuth gyro drift	-----	9.0	-----	-----	-----
4. Gyro torquer and torquer amplifier	1.3	1.3	2.0	-----	500
5. Line frequency	1.6	2.8	2.5	-----	625
Accelerometers:					
1. Linearity and scale factor	8.0	2.7	7.7	-----	2,000
2. Bias	-----	-----	1.2	-----	180
Computer:					
1. Coriolis computer	6.0	6.0	3.1	-----	350
2. Velocity integrator	.8	.8	2.0	-----	320
3. Position integrator	-----	-----	-----	-----	150
4. Summing circuit	-----	-----	-----	25.0	-----
Initial conditions:					
1. Initial vertical noise	4.3	4.3	4.4	-----	1,030
2. Initial azimuth alinement	-----	5.0	-----	-----	-----
3. Initial velocity data	10.0	10.0	2.0	-----	600
4. Initial position data	-----	-----	-----	-----	100
Overall rms error	15.05	16.78	10.95	35.50	2,645

FUNCTIONAL SCHEMATIC DIAGRAM OF ALL-ATTITUDE FLIGHT DATA SYSTEM

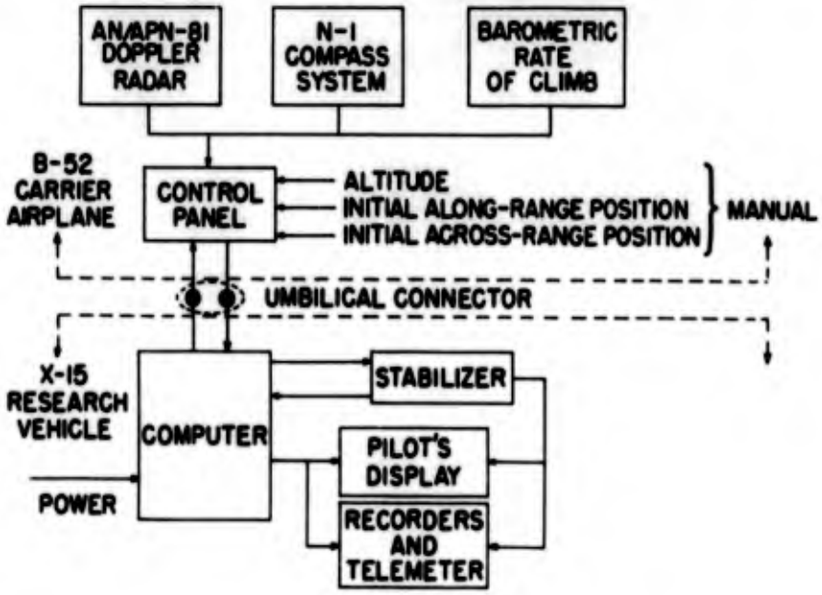

Figure 1

ALL-ATTITUDE FLIGHT DATA SYSTEM

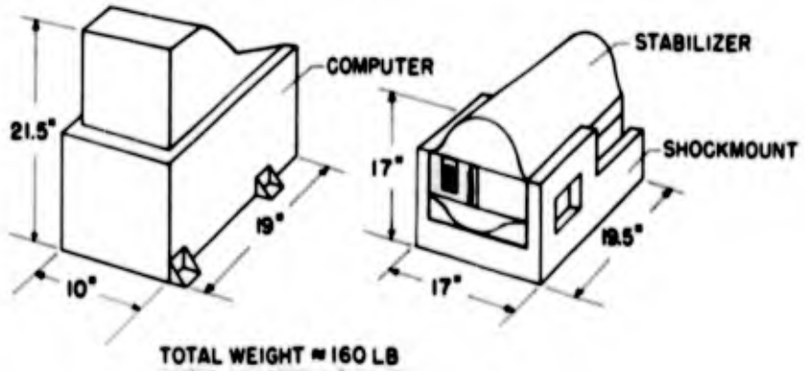

TOTAL WEIGHT ≈ 160 LB
TOTAL VOLUME ≈ 3 CU FT
POWER REQUIRED:
208 V, 3 - PHASE, "Y" WOUND
400 CPS A.C.
NORMAL ≈ 425 WATTS
PEAK ≈ 600 WATTS

Figure 2

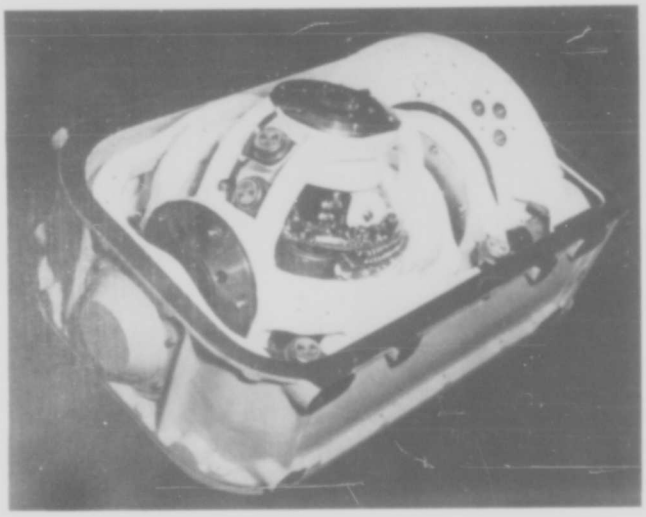

Figure 3

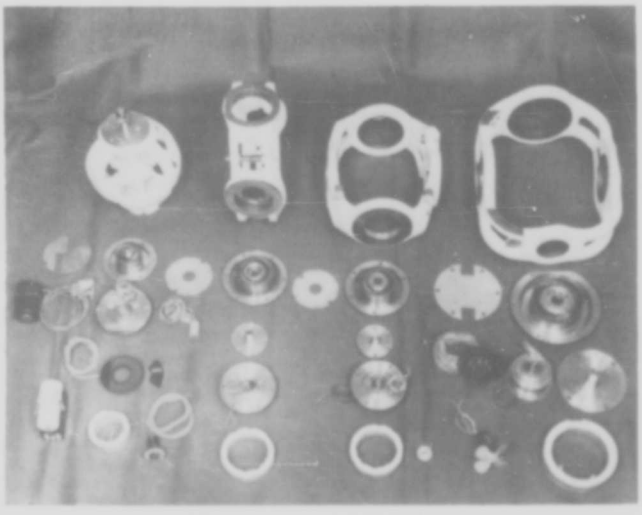

Figure 4

X-15 INSTRUMENT PANEL

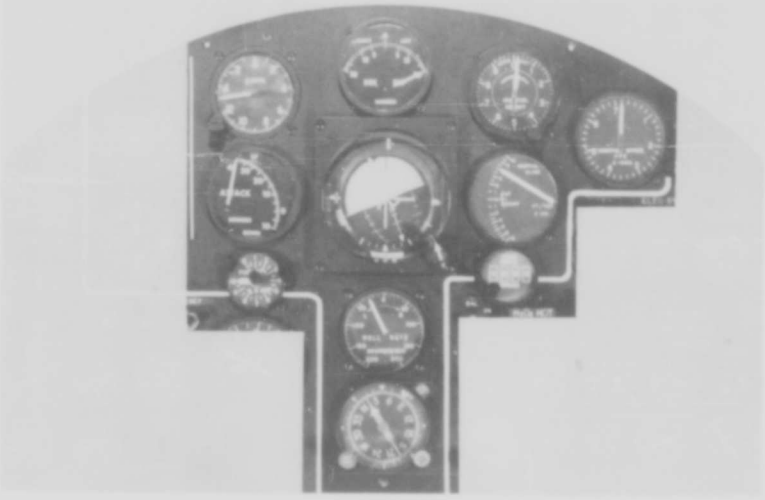

Figure 5

WIND-TUNNEL INVESTIGATION OF THE HEAT TRANSFER TO THE X-15 AIRPLANE

By William V. Feller and Paige B. Burbank

NACA Langley Aeronautical Laboratory

INTRODUCTION

At the X-15 conference in 1956, the heat-transfer coefficients expected on the X-15 airplane were discussed in terms of theories and experimental results then available for simple shapes that could represent isolated parts of the airplane. The complexity of the flow field around the complete airplane prevents accurate theoretical prediction of the local flow conditions everywhere for calculating heat transfer and makes an experimental study of the complete configuration essential. Such a test program has recently been completed on a 1/15-scale model in the Langley Unitary Plan wind tunnel (UPWT) and in the Arnold Engineering Development Center (AEDC) B-minor tunnel.

In order to orient the heat-transfer test program with respect to the full-scale airplane, figure 1 shows the envelope of the design missions for the airplane in terms of altitude and Mach number (shaded area). The symbols indicate the full-scale flight altitudes corresponding to the Reynolds numbers of the tunnel tests. The test program covers the Mach numbers for which aerodynamic heating is a major problem, at Reynolds numbers which duplicate the full-scale values for the upper part, at least, of the flight envelope. This is in contrast to past practice, where it has usually been necessary to make large extrapolations of Reynolds number effects.

In this paper only a small part of the available data can be presented. Study of the data at $M = 7$ from the AEDC tests is still under way so that the present discussion will be limited to the results of the Langley UPWT tests at $M = 4.65$ and 2.88.

SYMBOLS

b	wing span
c	local chord of wing

d	cylinder diameter
h	heat-transfer coefficient
$h_{inf.\ cyl.}$	heat-transfer coefficient for infinite cylinder
l	total length of body
M	free-stream Mach number
N_{St}	Stanton number
p	local surface static pressure
p_∞	free-stream static pressure
R_c	Reynolds number based on local wing chord
R_{c_t}	Reynolds number based on tail chord
R_D	Reynolds number based on maximum body diameter
R_d	Reynolds number based on cylinder diameter
R_l	Reynolds number based on body length
x	distance from nose of body or leading edge of surface
y	spanwise distance from plane of symmetry
α	angle of attack
β	angle of sideslip
Λ	sweep angle of cylinder
ϕ	meridian angle from lower-surface plane of symmetry

DISCUSSION

A sketch of the 1/15-scale tunnel model is shown in figure 2. The left sides of the fuselage, wing, and tails were made with uniform skin thicknesses and were instrumented with thermocouples. The right sides

were fitted with pressure orifices. In order to avoid the occurrence of large areas of laminar flow on the model which might not occur on the airplane, roughness strips were applied near the leading edges of the wings and tails and near the fuselage nose. In addition, two strips of roughness were applied down the length of the fuselage on either side of the bottom meridian to insure transition at angles of attack. The dashed lines in figure 2 indicate the stations on the fuselage, wing, and vertical tail for which the heat transfer will be discussed.

In the Langley UPWT tests, heat-transfer coefficients were determined from the transient temperatures of the model skin after a step increase in tunnel stagnation temperature. The temperature jump was about 100° F and was obtained by bypassing the last stage air coolers in the tunnel drive system. Recovery temperatures were determined from the values measured after thermal equilibrium was reached. The model was tested through an angle-of-attack range from -5° to 28° and at sideslip angles of 0° and 10°.

For the fuselage at zero angle of attack, figure 3 shows the distribution of the dimensionless heat-transfer coefficient, the Stanton number (based on free-stream conditions), for two meridian lines on the fuselage, along the bottom ($\phi = 0°$) and top ($\phi = 180°$). On the lower meridian, the data show some laminar flow near the nose, with transition starting at $x/l = 0.05$. The solid curve is the distribution calculated by the simple, often used, local flat-plate method. This curve is in good agreement with the measured values on the cylindrical part of the body but badly underestimates the heat transfer on the ogive. Refinement of the calculation by using the measured pressures and applying a correction for conical flow increases the values by only about 15 percent near the nose.

The dashed curve in figure 3 was calculated by assuming that the turbulent boundary layer started at station $x/l = 0.05$ (where the data indicate the start of transition) and using the measured pressures and a conical-flow correction to the flat-plate values. This curve is in fair agreement with the measured values. Even closer agreement could be obtained by choosing a more rearward starting point for the turbulent flow. However, the entire approach is unsatisfactory because it requires an experimental location of transition which would not necessarily be the same in flight as in a tunnel test. Prediction of the start of transition and the behavior of the boundary layer during and just after transition still requires a great deal of study.

On the upper meridian (fig. 3), the heat transfer on the canopy is high near the leading edge, as would be expected, and as the flow expands over the canopy falls rapidly to a value below that for the smooth body given by the lower meridian. Behind the canopy, however,

the heat transfer rises considerably above that found on the lower surface and remains higher all the way to the tail. This increased heat transfer in the wake of a protuberance on a smooth surface has been previously observed in tests of cylinders projecting from a plate in the Langley UPWT.

The effect of angle of attack on the heat transfer to the fuselage is most clearly shown by plots of the circumferential distribution. The circumferential distributions of Stanton number at angles of attack are presented in figures 4 and 5 for the stations indicated in figure 2: at $x/l = 0.13$, ahead of the canopy; $x/l = 0.40$, on the side fairing ahead of the wing; and $x/l = 0.71$, at the wing.

Figure 4 is a polar plot of Stanton number with meridian angle at $\alpha = 0^\circ$, 15°, and 28° for station $x/l = 0.13$, where the body is a smooth ogive with no protuberances. At the windward meridian the Stanton number increases rapidly with angle of attack, to about six times the value at zero angle of attack at $\alpha = 15^\circ$ and about ten times at $\alpha = 28^\circ$. From these values the Stanton number decreases around the circumference to about the same value as was found at zero angle of attack at the 90° meridian. The distribution is similar in shape to that measured on yawed cylinders. However, this station is too close to the nose to expect a theory for infinite circular cylinders to be applicable and, in fact, values calculated for an infinite cylinder tangent to the fuselage are less than one-third of the measured values at the windward meridian.

The effect of the side fairings and wing is shown in figure 5. The Stanton numbers are considerably lower than those at the forward station on the ogive and, therefore, the N_{St} scale has been changed. At zero angle of attack, the Stanton numbers are approximately constant around the body except for a bump on the edge of the side fairing associated with the inclination of this surface to the stream direction.

At angles of attack, the side fairing and wing modify the decrease of the Stanton number around the circumference, keeping the values higher than would be expected for a circular cylinder. On the leeward side, the values are low, decreasing as the angle of attack increases. As a matter of interest, the Stanton numbers calculated for an infinite circular cylinder of the basic body radius are only one-half of those measured on the windward meridian.

The pressures and heat transfer for an isolated wing have been extensively studied and can be calculated with reasonable confidence. Some parts of the X-15 wing, however, are behind the bow shock from the fuselage nose and, therefore, are influenced by the flow field of the fuselage. The location of the fuselage bow shock at $M = 4.65$ is

shown for zero angles of attack and sideslip in figure 6. On the left side in this figure is plotted the ratio of wing surface pressure to free-stream static pressure for a chordwise station approximately at the middle of the exposed wing panel. The measured pressures are compared with values calculated for an isolated wing by the shock-expansion method, shown by the solid curve. At 10 percent chord, the measured pressures are higher by 20 percent but decrease to about the isolated-wing values at 70 percent chord. The pressure ratio that would be expected on the wing at midchord from the pressure rise across the fuselage bow shock is about 2.2 if the bow shock were plane and were the only factor involved. The fact that the measured pressures are only slightly higher than those calculated for an isolated wing indicates that the pressure rise at the fuselage bow shock has been considerably attenuated between the shock and the wing position.

The Stanton numbers, shown in the right-hand plot in figure 6, like the pressures are about the same magnitude as those calculated for the isolated wing.

In order to show the behavior of the pressure and heat transfer close to the shock, the model was tested at 10° sideslip, as shown in figure 7. In this attitude the fuselage bow shock crosses the wing measuring station at about 30 percent chord. The measured pressures are shown by the circle symbols. For comparison, the measured and calculated values at $\beta = 0^{\circ}$ from figure 6 are also shown. The pressure rise across the shock is spread out by the boundary-layer interaction and is only about one-half of that calculated from the fuselage shock angle ahead of the wing, as shown by the tick.

The Stanton numbers show a somewhat sharper rise at the shock crossing than did the pressure. The dashed curve was calculated by using the measured pressures and the total pressure behind the fuselage bow shock, and is in very good agreement with the data behind the shock. There is no indication of any large local effect at the shock impingement point beyond that expected from the shock pressure rise.

The effect of angle of attack on the wing lower surface is shown in figure 8 for zero sideslip with the fuselage shock out near the wing tip. At zero angle of attack, as shown in figure 6, the pressures and Stanton numbers are close to the values expected for the wing alone. At angles of attack, however, the pressures near the leading edge of the wing are about $1\frac{1}{2}$ times those for an isolated wing at the same angle but decrease to about the values for an isolated wing near the trailing edge. This kind of pressure distribution has been observed on a different configuration at a Mach number of 6.86 at angles of attack and, therefore, is not a peculiarity of the X-15 geometry.

The changes in the heat-transfer distribution at angles of attack are even more pronounced than those in the pressures. The measured Stanton number at $\alpha = 15^{\circ}$ is nearly twice and at $\alpha = 28^{\circ}$ is more than twice the value for the wing alone at the 10-percent-chord station and decreases like the pressures to about the values for the isolated wing near the trailing edge. It is difficult to account for the high heat-transfer coefficients even when the measured pressures are used. The flow field around wing-body combinations at high angles of attack is a problem requiring further investigation.

The construction of the wing prevented installation of enough instrumentation to demonstrate any local effect at the shock impingement on the leading edge. However, several preliminary tests have been made on simple configurations in other facilities to study the problem. Results from one such study in the Langley gas dynamics laboratory are shown in figure 9. The configurations tested were circular cylinders swept 20° to the air flow projecting from a wedge with an 8° half-angle and from a plate parallel to the flow. The stagnation-line heat-transfer coefficients divided by the value for an infinite cylinder (which in this case was turbulent) are plotted as a function of distance away from the junction in diameters. The heat-transfer coefficient reaches a peak value of about 2.5 times the infinite-cylinder value behind the shock from the wedge. But the peak is not out near the shock-impingement location, about 1 diameter from the wedge, but somewhat inboard, at about 0.5 diameter.

Part of the increase is due to the increased pressure in the flow behind the wedge shock. An estimate of the magnitude of this effect is shown by the arrow. The peak occurs so close to the wedge that there is some influence of the cylinder-wedge boundary-layer interaction. Measurements made with the cylinder projecting from the flat plate are shown by the square symbols. The peak value is much lower than that found with the wedge, about 30 percent above the infinite-cylinder value, but the peak occurs at about the same distance from the juncture. In this test, it is not possible to separate clearly the effects of the wedge shock and the cylinder root, but the data do not suggest the existence of a large local effect due to shock impingement alone for the case of a turbulent leading edge. However, the shock impingement could produce transition on a laminar leading edge and thus produce a somewhat different pattern.

This kind of interference effect between a cylinder and plate can be expected to occur at several places on the airplane: at the roots of wings and tails and at protuberances like masts.

The effect of angle of attack on the lower vertical tail and speed brake is shown in figure 10 for a Mach number of 2.88. At zero angle of attack, the pressures calculated for the fixed tail without

considering the body influence, shown by the dashed curve, are in good agreement with the measured pressures. On the deflected speed brakes, the pressures decrease rapidly with distance from the hinge line because of the low aspect ratio of the brake but approach the calculated two-dimensional value near the hinge line.

The Stanton numbers calculated at zero angle of attack, neglecting the leading-edge blunting and the fuselage influence, somewhat overestimate the measured values on the fixed tail. On the speed brakes, the heat transfer can be closely estimated by assuming that the boundary layer starts at the hinge line. For an isolated tail the effect of changing angle of attack would be to change the sweep angle, which previous work has shown produces little change in pressure. The pressures on the tail, however, show a large increase as the angle of attack increases because of the changes in the pressure field of the fuselage and wing with angle of attack. It can be seen in figure 10 that the Stanton numbers follow the trend of the measured pressures with angle of attack.

CONCLUDING REMARKS

The tunnel test program has provided a picture of the general distribution of heat-transfer coefficients over the airplane. Martin R. Kinsler, in the next paper, will discuss the application of these results to the airplane. The tunnel tests have also emphasized the importance of the interactions of the flow fields of components and have shown that in some cases, where the local flow direction and total pressure can be reasonably closely inferred, use of experimental pressures to compute flow conditions yields very good predictions of heat-transfer rates.

There are still some regions of the airplane for which the heat transfer could not be adequately studied because of the size or construction of the model. Such local regions will not necessarily limit the operation of the airplane but will require evaluation in the full-scale tests.

X-15 WIND-TUNNEL TEST AND FLIGHT CONDITIONS
1/15-SCALE HEAT-TRANSFER MODEL

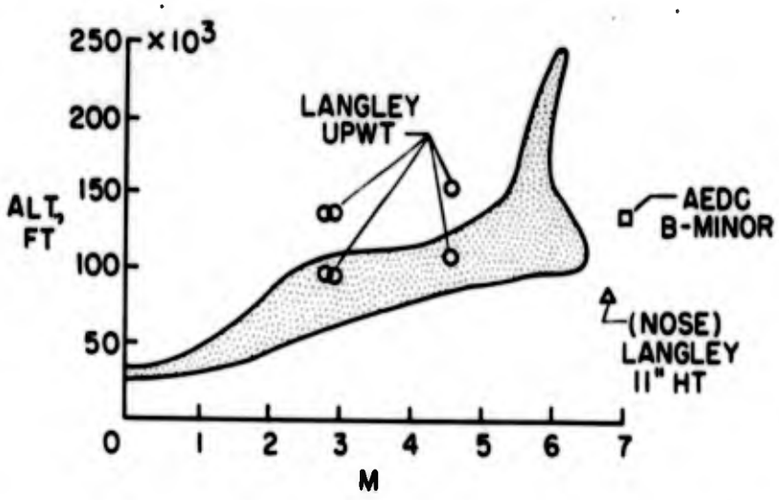

Figure 1

X-15 HEAT-TRANSFER AND PRESSURE MODEL
1/15 SCALE; LENGTH 39.2 IN.

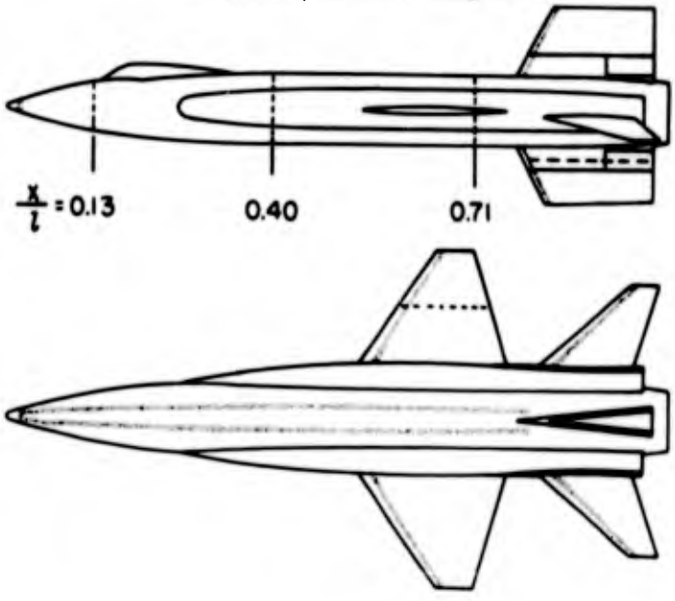

Figure 2

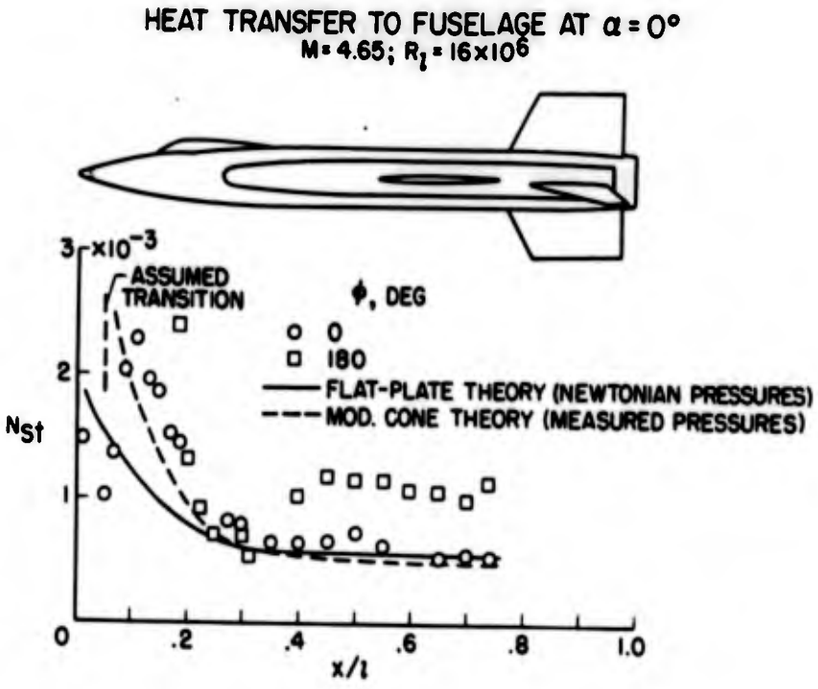

Figure 3

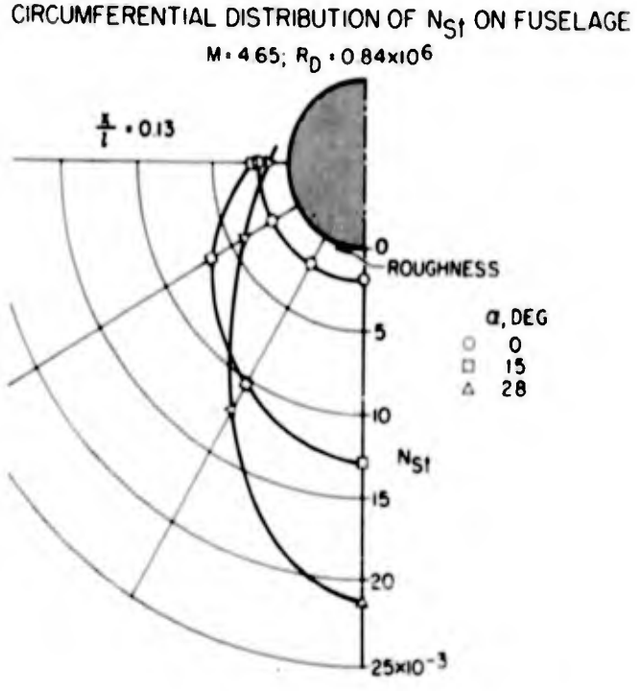

Figure 4

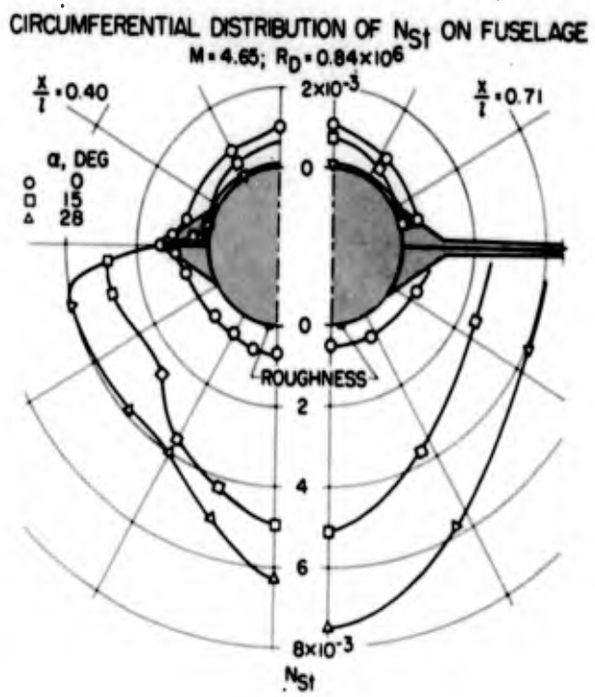

Figure 5

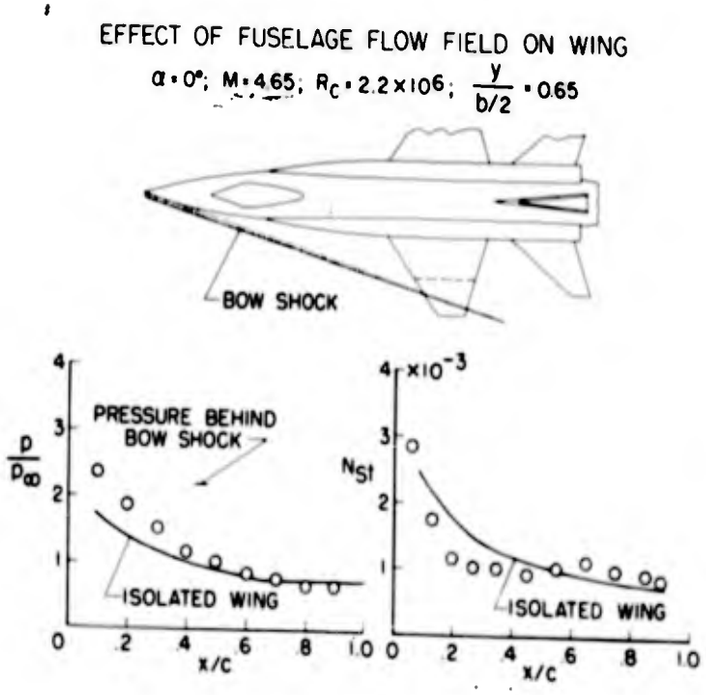

Figure 6

EFFECT OF FUSELAGE BOW SHOCK ON WING

$\alpha = 0°$; $\beta = 10°$; $M = 4.65$; $R_c = 2.2 \times 10^6$; $\frac{y}{b/2} = 0.65$

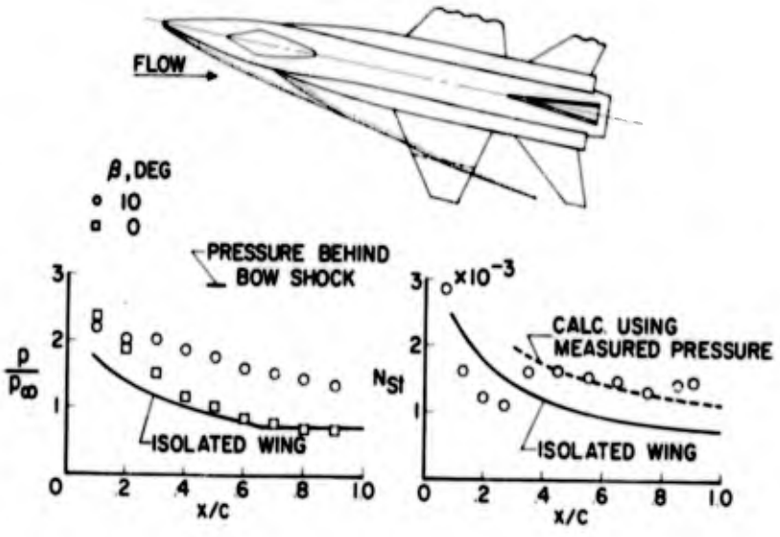

Figure 7

EFFECT OF ANGLE OF ATTACK AND FUSELAGE FLOW FIELD ON WING

$M = 4.65$; $R_c = 2.2 \times 10^6$; $\frac{y}{b/2} = 0.65$

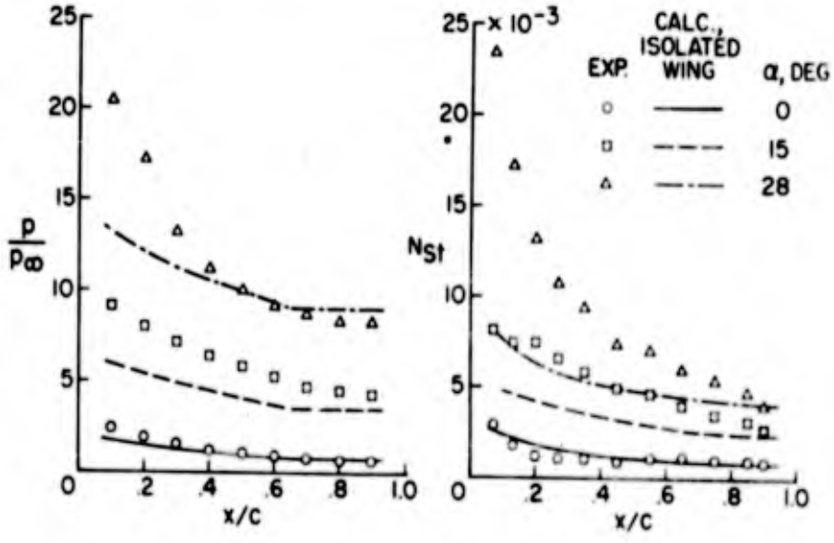

Figure 8

HEAT TRANSFER TO STAGNATION LINE OF INFINITE CYLINDER NEAR JUNCTION WITH PLATE

$M = 4.15$; $\Lambda = 20°$; $R_d = 1.7 \times 10^6$

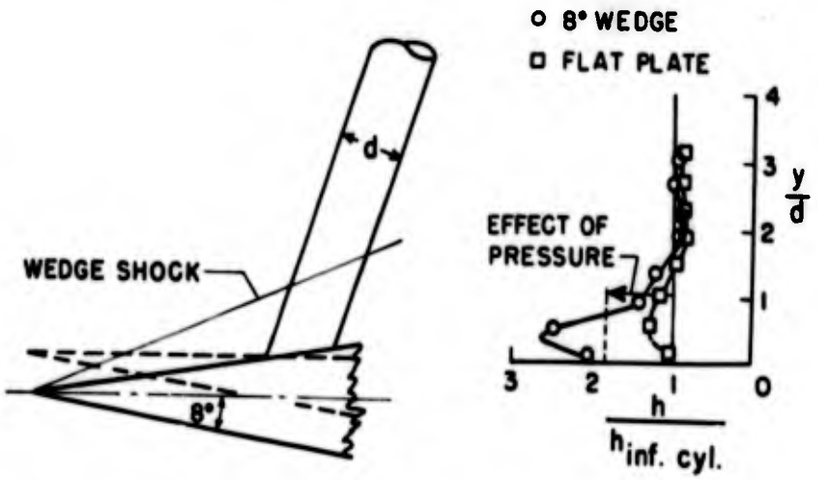

Figure 9

HEAT TRANSFER TO LOWER VERTICAL TAIL

$M = 2.88$; $R_{c_1} = 2.8 \times 10^6$; SPEED BRAKES DEFLECTED 35°

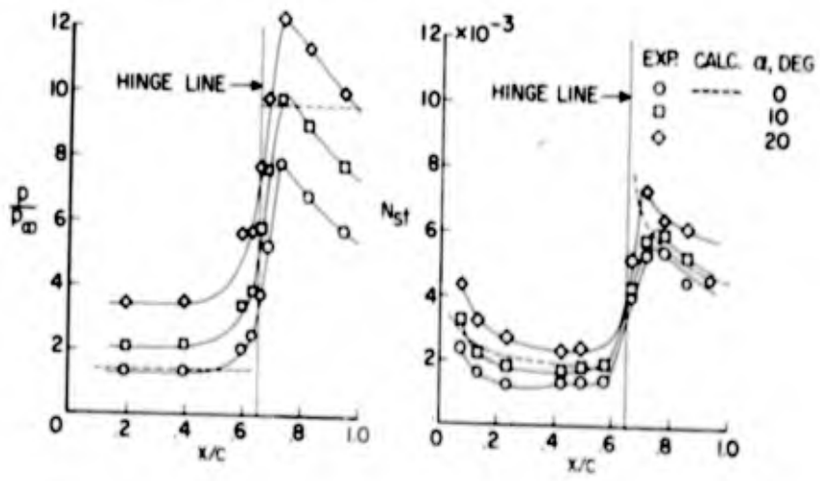

Figure 10

EFFECTS OF AERODYNAMIC HEATING ON X-15 TEMPERATURES

By Martin R. Kinsler

North American Aviation, Inc.

INTRODUCTION

The preceding paper by Feller and Burbank of the Langley Laboratory described the results of various model tests performed for the purpose of obtaining aerodynamic-heating rates. Included also was a description of the degree of agreement of several theories with the data. The present paper describes two primary effects of the aerodynamic heat input, as follows:

(1) The expected temperature levels that can be obtained for design missions making use of the best available heating data for the X-15 configuration

(2) Some off-design missions that the airplane can fly

In the process of indicating the expected temperatures, several phenomena of importance to the X-15 and similar aircraft are discussed.

SYMBOLS

c	wing chord
D	fuselage diameter
M_∞	free-stream Mach number
P_T	total pressure
$P_{T\infty}$	free-stream total pressure
P_{TNS}	total pressure behind normal shock
R_∞	Reynolds number based on free-stream conditions
R_l	Reynolds number based on local flow conditions

x	longitudinal station on wing
X	longitudinal station along fuselage
α	angle of attack

DESIGN TEMPERATURES

One of the problems of interest for X-15 design and the design of more advanced vehicles of this type is illustrated in the schlieren photographs of figures 1 and 2. These results were obtained from wind-tunnel tests of X-15 models at the NACA Langley Laboratory at Mach numbers of 4.65 and 6.86. Both models are shown oriented at zero angle of attack and zero yaw. Both photographs show shocks emanating from fuselage bow and fuselage side fairings. At Mach 4.65 the shocks intersect the wing leading edge near the tip, and at Mach 6.86, the shocks intersect very near the wing midspan. It might be expected, then, that the flow field in front of the wing will be considerably altered by this combination of moving shocks. In addition, the pressure field, and consequently the wing heating rates, would be expected to be affected throughout the flight. The strongest effects should be noted at the higher Mach numbers.

Situations such as the one presented in these figures are, at best, difficult to analyze. However, data such as that shown in figure 3 have made it possible to predict wing temperatures with some confidence in spite of the complicated flow expected. This figure presents the results from some recent data obtained in the AEDC B-Minor tunnel. Dimensionless heat-transfer coefficients (Stanton numbers) are shown for a spanwise location that is about halfway between the model wing root and the shock intersection at Mach number 7. This location was chosen because it is expected to be the one least likely to be affected by the local disturbances set up by the shock intersection and the one that probably would not be influenced by the side-fairing boundary layer.

The data were obtained with a line of thermocouples located about 20 percent out along the exposed wing span. Carborundum particles were cemented to the wing to form a boundary-layer trip as shown. The data were taken at Mach number 7 at angles of attack of 0°, 15°, and 24°. Also shown in this figure are Stanton numbers computed for the isolated wing at angles of attack of 0°, 15°, and 24°.

The trend of the data is similar to that shown at Mach 4.65, in the previous paper by Feller and Burbank. The data show a strong effect of angle of attack on local heat-transfer coefficient. The

magnitude of the variation is not predicted by the isolated-wing calculation.

These data, along with data at other Mach numbers and other angles of attack, were used to determine empirical factors that would correct flat-plate heat-transfer coefficients to those computed from the model data. These same factors were incorporated in high-speed digital computer programs to correct heat-transfer coefficients computed for the full-scale airplane flying assigned missions.

Figure 4 shows temperatures plotted against time from launch computed for a point on the wing at a station similar to the one for which data were shown in the previous figure. The point chosen is on the bottom of the wing at 20 percent chord and a spanwise station 59 inches from the center line. The skin-gage at this point is 0.069 inch.

The temperature computations were made for the speed design mission. This is a mission during which the aircraft would reach a peak altitude of 129,000 feet and a peak velocity of 6,600 feet per second and would pull out at 7.33g to 115,000 feet.

The bottom curve is an estimate of the temperature-time history at the point computed on the assumption of no fuselage shock effects; that is, the flow in front of the wing shock was assumed to be at the instantaneous flight velocity and at a pressure and temperature corresponding to the instantaneous altitude. The solid curve shows temperatures after the heat-transfer coefficients of the lower dashed curve have been corrected for the model data results. This solid curve includes all of the varied effects taking place in front of this portion of the wing at all Mach numbers and angles of attack expected in the speed mission.

Previous to receiving wind-tunnel data, estimates were made for wing temperatures which hypothesized various flow phenomena. Considerable uncertainty existed concerning these temperature estimates. However, as a result of the wind-tunnel heat-transfer tests on the actual configuration, flight temperatures for this and other wing points can be predicted with considerably increased reliability.

Another problem of interest in temperature prediction is that of estimating local total pressure. This total pressure, along with the local static pressure, permits one to obtain the local velocity which in turn is used for estimating heating rates.

Figure 5 shows values of the ratio of local total pressure to free-stream total pressure as obtained from measurements on the heat-transfer and pressure-distribution model in the AEDC B-Minor Tunnel at Mach 7 for angles of attack of 0°, 20°, and 24°. This ratio is plotted as a

function of distance along the fuselage in terms of the number of fuselage diameters. Total pressures were obtained from the outermost tube of total-pressure rakes attached to the fuselage. The dashed line shows the total-pressure ratio for normal shock at Mach number 7. This value is about the lowest value of the total pressure that can be expected. The reduction in total pressure from fuselage location $X/D = 8$ to that at $X/D = 9.5$ is probably due to the passage of the horizontal-stabilizer shock across the flow field between these two stations.

Model and airplane total-pressure distributions are the result of complicated flow phenomena and in order to attempt a prediction of local total pressure, it would be necessary to know the details of the local boundary-layer flow, to know details of the shock shape, and to know where various streamlines of the flow cross the shocks. For the routine job of predicting temperatures for design, this task is far too involved, and every effort should be made to avoid it. What can be done, however, is to make use of pressure data, such as are shown, or of measured heat-transfer coefficients, or to make some conservative assumptions concerning total pressure.

Figure 6 shows the effects, on the temperature-time history, of two widely different assumptions and the results of application of test data. This computation was made for a point on the bottom of the fuselage at longitudinal station 200 and for the speed design mission. The upper curve was computed on the assumption that the local total pressure would be equal to the free-stream total pressure. The peak temperature is seen to reach about 1,280° F. The lower curve was computed by assuming that the total pressure would be that behind one normal shock. The peak temperature is about 1,030° F. The solid curve was computed in the same way as the curve below it, except that the heat-transfer coefficients were corrected for the wind-tunnel results. The peak temperature is about 1,080° F.

The 200° F spread in peak temperature shown by the two dashed curves represented the uncertainty in the temperature prediction due to the total-pressure variations. However, as a result of the model tests, considerably greater insight into the mechanism of total-pressure variation has been obtained, and again temperature prediction has been put on a much more reliable basis.

Figure 7 describes the effect that variation in boundary-layer-transition point can have on X-15 skin temperature. Local peak skin temperature is shown plotted against wing station in percent chord from about the 10-percent chord position back to the trailing edge. This information is for the midspan region of the wing. Temperatures are shown for the cases of all laminar flow, all turbulent flow, and for four intermediate transition Reynolds numbers: 100,000, 500,000,

1,000,000, and 10,000,000. Transition Reynolds numbers were computed on the basis of local flow conditions and the distance back from the nose or leading edge.

It is seen that the boundary-layer-transition location, represented by the transition Reynolds number, will have a considerable effect on wing temperature. For design calculations, a transition Reynolds number of 100,000 was used to obtain a maximum temperature distribution as shown by the solid line. From an inspection of the literature, this value seemed to be about the lowest value that can be expected for a body in free flight. Higher transition Reynolds numbers than that used for design will mean that flight restrictions, imposed by high temperatures, will be considerably relaxed.

The information presented thus far has been concerned only with the effects of local aerodynamics on skin temperatures. An important part of the design job is that of supplying temperature distributions for interior structure. For this part of the work it has been necessary to consider the effects of heat conduction and internal radiation, as well as the heat storage ability of the structure.

Figure 8 shows a titanium web located about midspan near the Inconel X leading edge. The adjacent view shows this web connected to the Inconel X skins with Inconel X caps. The temperatures of this combination were predicted early in the structural analysis without consideration of interior radiation. These temperatures are shown (boxed in the figure) to be: About 1,250° F in the leading-edge region, 650° F in the web, 980° F for the lower skin, and about 830° F for the upper skin. Subsequent to these predictions the question arose as to whether radiation from the leading edge would have sufficient influence to raise the titanium web temperature above its limit of 1,000° F. The results of later calculations accounting for radiation are shown above the boxed temperatures. It is seen that because of the large mass, the inclusion of internal radiation had but a small effect on leading-edge temperatures. Estimates of web temperatures were raised about 250° F to a value of 900° F.

C. L. Davis of North American will discuss in a paper to be presented later the results of some very interesting transient leading-edge structural tests performed at these and higher temperatures.

Figure 9 presents in summary form the maximum skin temperatures predicted for the speed design mission. Maximum temperature isotherms are shown for the bottom of the fuselage, bottom of the wing, bottom of the side fairing, lower vertical, and top of the horizontal stabilizer. The maximum temperature for the fuselage is not expected at the nose or leading edge as one might first believe but at a point located approximately at station 100. This result is attributed to the particular

skin gage used in this region. Structural analyses have been made by using this temperature, and present design has been found satisfactory. The rise in temperature on the after portion of the fuselage is also attributable to a reduction in skin gage in this region as compared with the gage at the center of the fuselage. For the wing, temperatures are shown for isotherms passing through the leading edge and through points located at 10, 25, and 50 percent chord at midspan. The side fairing is shown to reach a relatively high temperature of about 1,200° F. The speed brake on the lower tail is expected to attain a temperature of 1,320° F when it is used for the speed brake open version of the speed mission. The peak temperatures for the horizontal stabilizer are experienced on the top skin for this type of mission because the deflections of the horizontal tail and the wake from the wing give an effective negative angle of attack.

OFF-DESIGN TEMPERATURES

So far, some of the design temperatures and design considerations have been presented for one of the four design missions developed as a result of the ground rules established for flight conditions of the X-15. The following part of this paper presents some of the results of a program to establish the off-design missions that the airplane can fly in addition to the present design missions. This program makes extensive use of the Six-Degree-of-Freedom Flight Simulator of North American Aviation, Inc. described in an earlier paper by G. B. Merrick and C. H. Woodling.

Figure 10 describes a group of high-altitude off-design missions that have been investigated on this simulator. In these missions an altitude of 400,000 feet is reached after engine burning times of 70, 80, and 88 seconds. Pull-out from a reentry is accomplished at a maximum of 7.33g and, for this case, at 60,000 feet. Peak Mach numbers of about 4, 5, and 7 are reached corresponding to the three engine burning times. The two Mach number peaks on the right are attributable to the variations in the speed of sound with altitude. From the angle of attack schedule, it is seen that burning occurred mainly at zero lift after the initial pull-up. Peak angles of attack up to about 20° are obtained.

These missions and other missions at different pull-out altitudes were then used as inputs to an analogue computer, which computed temperature-time histories for 12 critical points on the aircraft.

Figure 11 presents peak temperatures for one of the 12 points investigated. The abscissa here is the altitude at which the simulator pilot pulled out from the reentry. Pull-out altitudes ranged from

about 37,000 feet to 78,000 feet from the 400,000-foot peak altitude. The data are presented for station 100 on the bottom center line of the fuselage for engine burning times of 88, 80, and 70 seconds.

For the purpose of establishing permissible flight conditions the speed mission design temperature has been chosen as a nominal allowable peak temperature for this fuselage point. This temperature limit, 1,330° F, is shown by the dashed line. An examination of this plot reveals that, for the 88-second burning, the lowest altitude at which pull-out can be accomplished without exceeding the temperature limit is 71,000 feet.

In addition to the class of missions described here, other missions have been studied on the flight simulator and thermal analogue. At a later date, this information will be organized so as to present a more complete picture of the X-15 flight regime.

CONCLUDING REMARKS

Examples have been presented which show how wind-tunnel model tests of the actual configuration aid in aerothermodynamic analyses and how these tests have made possible increased accuracy in structural temperature prediction. Also, from this and other research, development and design work on the X-15 has been done to accomplish a design consistent with the specified flight requirements. In this work, structural temperatures have been held within acceptable limits by providing sufficient heat sink material. Limited areas of the skin and leading edges are expected to attain temperatures greater than 1,200° F. However, these areas have been carefully investigated for the effect of these higher temperatures on the structure and have been found to be satisfactory.

Furthermore, a program is now underway to determine missions that the X-15 can accomplish in addition to the present four design missions. Some investigations have been performed to establish these missions from a temperature point of view. The completion of this investigation will allow an estimation of the airplane flight envelope over the whole flight regime as defined by the engine and fuel load.

X-15 SCHLIEREN PHOTOGRAPH
LANGLEY 4X4 UPT

M_∞=4.65 ANGLE OF ATTACK=0 ANGLE OF YAW=0

Figure 1

X-15 SCHLIEREN PHOTOGRAPH
LANGLEY 11-INCH HYPERSONIC TUNNEL

M_∞ = 6.86
ANGLE OF ATTACK = 0
ANGLE OF YAW = 0

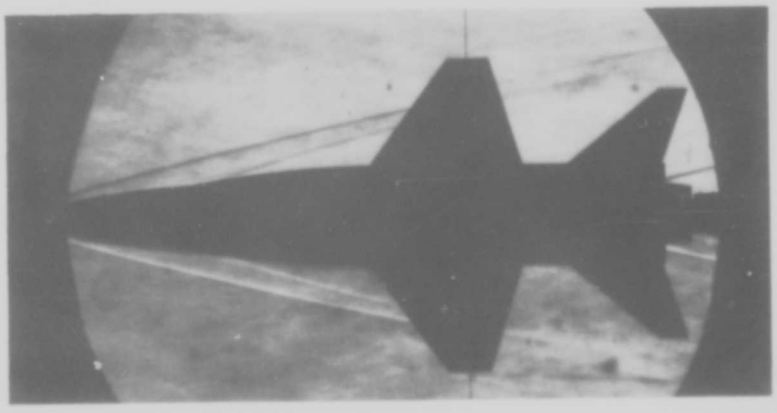

Figure 2

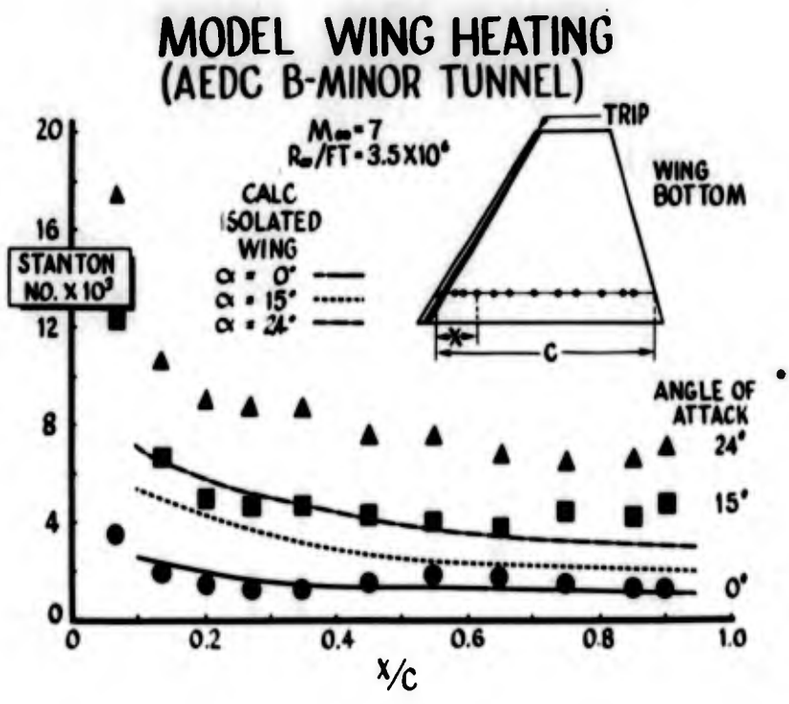

Figure 3

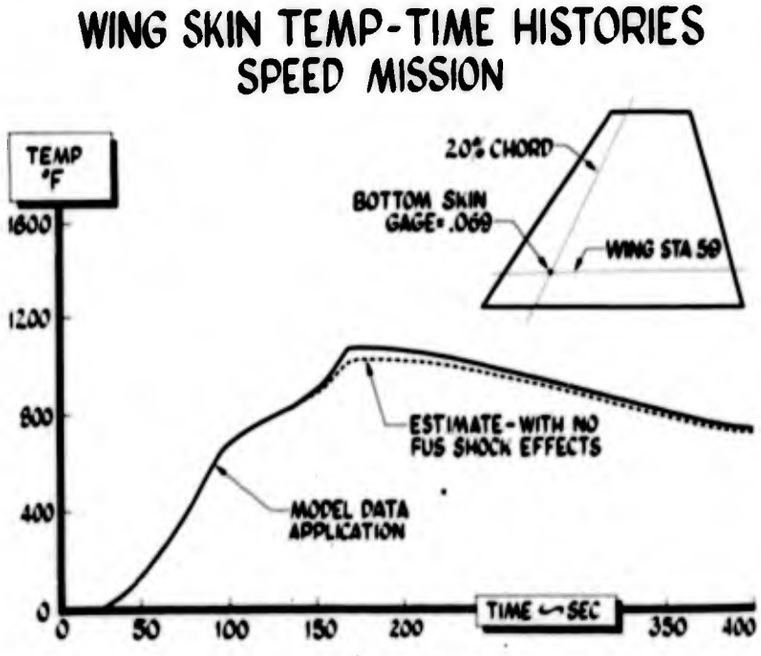

Figure 4

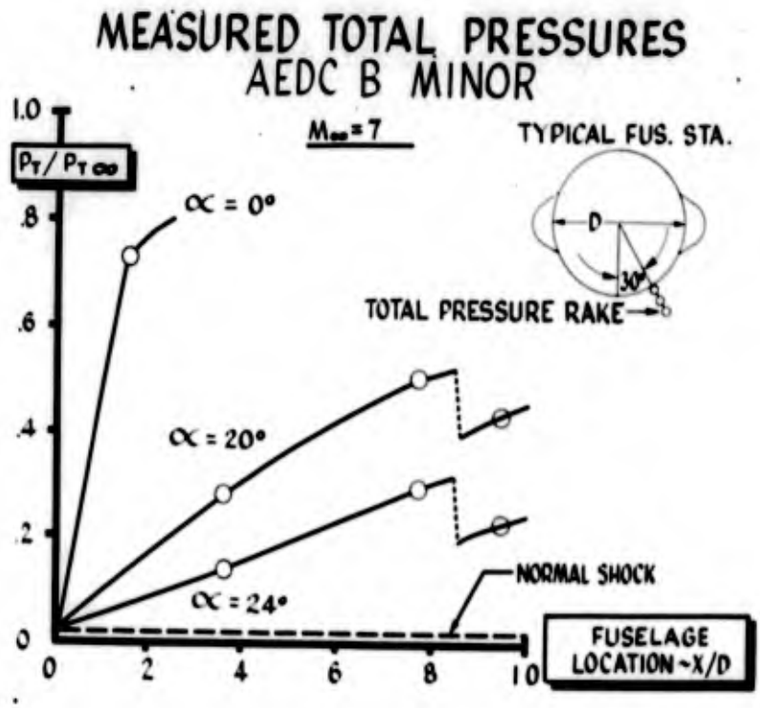

Figure 5

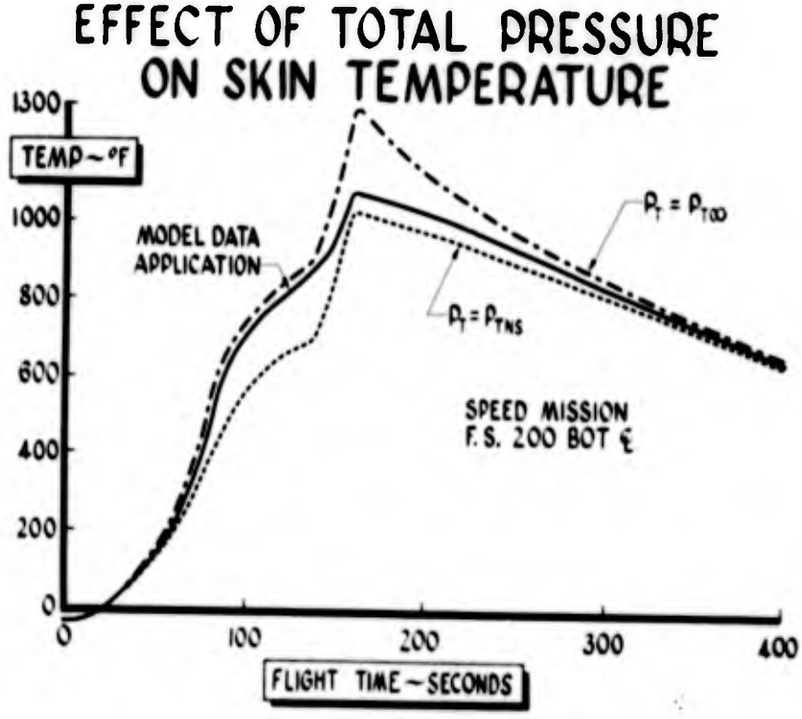

Figure 6

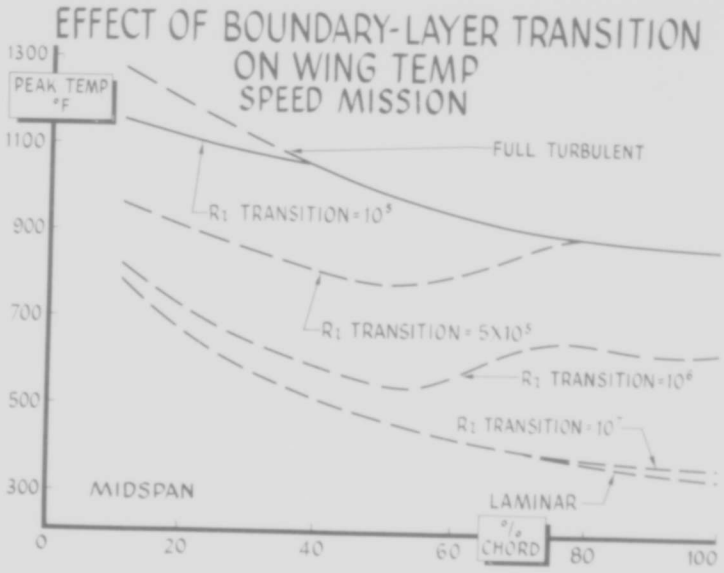

Figure 7

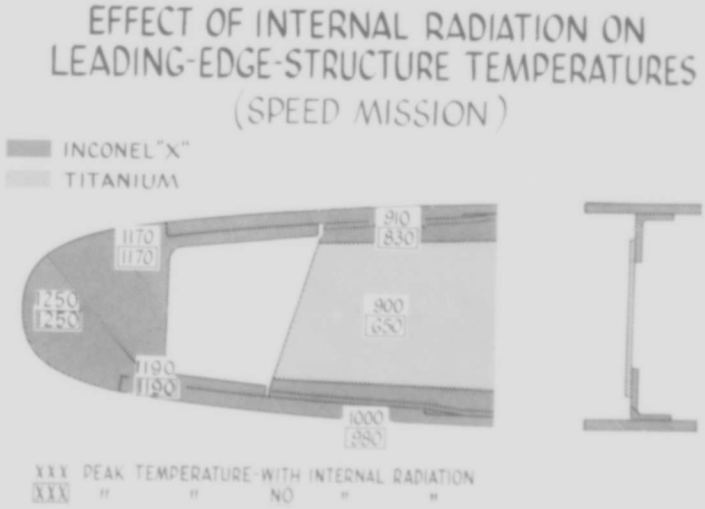

Figure 8

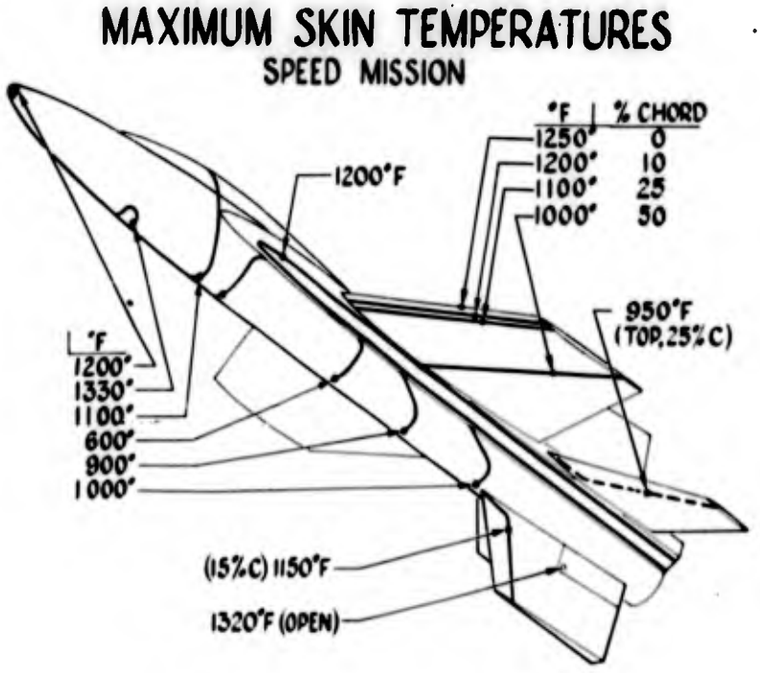

Figure 9

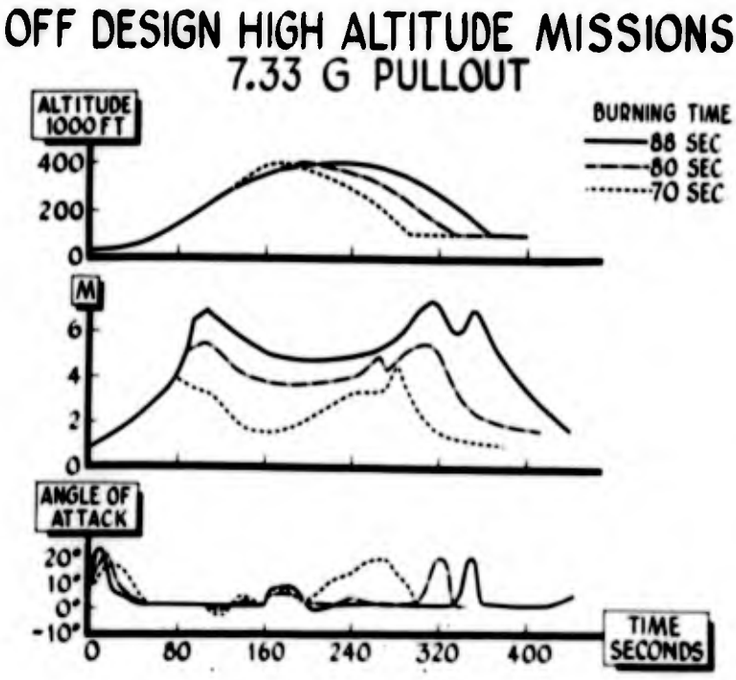

Figure 10

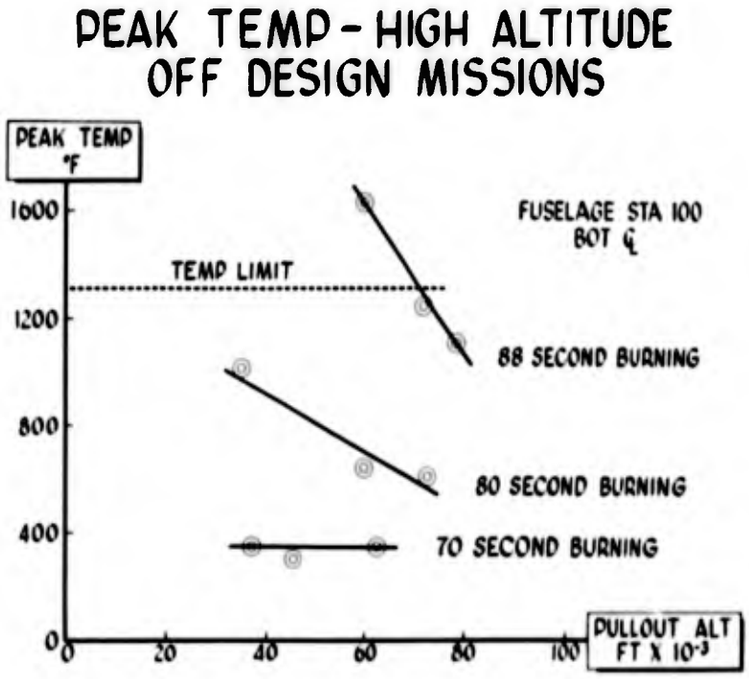
PEAK TEMP - HIGH ALTITUDE
OFF DESIGN MISSIONS
PEAK TEMP °F
1600
1200
800
400
0
TEMP LIMIT
FUSELAGE STA 100
BOT ℄
88 SECOND BURNING
80 SECOND BURNING
70 SECOND BURNING
0
20
40
60
80
100
PULLOUT ALT
FT X 10⁻³

Figure 11

X-15 STRUCTURAL LOADS

By Gerald H. Johnson

North American Aviation, Inc.

INTRODUCTION

One of the primary purposes of the X-15 manned research vehicle is to investigate flight regions which subject the airframe structure to extreme heating conditions. Design requirements specify that an altitude of 250,000 feet, a speed of 6,600 ft/sec, and structural temperatures on the order of 1,200° F shall be attained. An altitude mission and a speed mission were established to meet these requirements. The basic structural design criteria of Military Specification MIL-S-5700 for a class II fighter were applied to the environment encountered in these missions. Because of the high temperature level due to aerodynamic heating, coupled with aerodynamic and inertia loads, structural problems were encountered that do not normally have to be considered in contemporary manned aircraft. The reduction of material properties at elevated temperatures and the induced thermal stresses required an expanded search for critical load-temperature combinations.

DISCUSSION

After release from the B-52, the X-15 mission trajectories are entered at an altitude of about 30,000 feet and a speed of 600 ft/sec. A pull-up is made until the required initial flight-path angle is reached; then zero lift is established and maintained throughout the powered and ballistic phases.

In the design altitude mission shown in figure 1, the airplane reaches a height of 250,000 feet and a velocity of 6,300 ft/sec. Two types of reentries are considered for design; both maintain the zero-lift trajectory until time of pullout. One type uses a maximum-angle-of-attack reentry wherein the speed brakes remain closed and the pullout is initiated at a predetermined altitude which is the highest at which available lift and control power permit a 7.33g pullout. In the other type of reentry the speed brakes are opened at the peak altitude and a 7.33g pullout is initiated at a predetermined point such that the design limit dynamic pressure of 2,500 lb/sq ft is attained but not exceeded.

In order to attain the required true airspeed V_T of 6,600 ft/sec, as shown in figure 2, the pull-up after launch is made to a lower climb angle than for the altitude mission. The design speed is reached at burnout, from which point a zero-lift coast is made to the peak altitude of approximately 130,000 feet. Recoveries at high altitude or maximum dynamic pressure q similar to those of the design altitude mission are executed.

The structural design of the X-15 is primarily influenced by the exit and reentry phases. During the exit phase the airplane reaches an altitude of 112,000 feet at burnout in the speed mission and 154,000 feet at burnout in the altitude mission. Burnout time for these missions is 84 seconds. The design launch weight is 31,275 pounds and the design weight at all times after burnout is 12,970 pounds. The strength level of the structure is based on design limit maneuver load factors of 4.0g and -2g prior to burnout and 7.33g and -3g after burnout. Although the maximum product of load factor and weight nW occurs during the exit phase, the reentry conditions are the most severe because of the high-temperature effects.

The variations of maximum dynamic pressure and Mach number with altitude for the design speed and altitude missions are shown in figure 3. The peak values of dynamic pressure indicate approximately the minimum altitudes at which 7.33g pull-ups must be made to avoid exceeding the design limit dynamic pressure of 2,500 lb/sq ft. Above these altitudes the X-15 is capable of sustaining loads resulting from the typical fighter-type pitching, rolling, and yawing maneuvers for all combinations of Mach number and altitude consistent with these missions. Below these altitudes strength is provided for these same types of maneuvers but the dynamic pressure is limited to 1,600 lb/sq ft to avoid compromising the primary objectives.

Critical combinations of loads, temperatures, and temperature gradients for the wing structure are encountered in the speed mission during a 7.33g pullout at a Mach number of 3, an altitude of 40,000 feet, and a dynamic pressure of 2,500 lb/sq ft. The net limit load on the wing panel outboard of the fuselage side fairing is 26,000 pounds for this condition.

The horizontal-tail structure is critical for a 7.33g pullout at 80,000 feet and a Mach number of 5. The net tail load is 18,000 pounds.

The vertical-tail surfaces are critical for yawing maneuvers, with speed brakes extended, at a dynamic pressure of 2,500 lb/sq ft. The total load of the upper and lower surfaces is 7,700 pounds.

A comparison of wing chordwise pressure distributions for a pull-up at maximum dynamic pressure q and low supersonic Mach number and

a pull-up at a high Mach number and high angle of attack is shown in figure 4. The upper surface produces negligible lift for the Mach 6.0 condition because the vacuum limit is approached. Pressure distributions over the horizontal tail are similar to those for the wing.

The vertical tail is unusual in several respects, but the single-wedge airfoil shape is perhaps the most noticeable. The thickness of the trailing edge at the root of the all-movable part of the tail is 21 inches. Speed brakes are located on the trailing edge of the inner fixed portion of the tail and rotate about a vertical axis. The pressure distributions shown in figure 5 are representative of a supersonic steady yawed flight condition. The airplane is yawed 3° nose-left and the outer tail is deflected $7\frac{1}{2}^\circ$ nose-right. Most of the loading is from positive pressure. The negative pressure on the trailing edge contributes considerably to the airplane drag but the need for the increased directional stability furnished by this configuration offsets the cost of this drag.

Typical fuselage top and bottom center-line pressure distributions are shown in figure 6 for a condition corresponding to a 7.33g pullout at a Mach number of 5.0. The effect of the windshield and canopy can be seen. A cross section just aft of the canopy shows the typical variation of pressure around the fuselage and side fairings. The fuselage carries a large percentage of the aerodynamic lift in a maneuver, as might be expected from an examination of the plan form of the X-15. In the moderate angle-of-attack range from 0° to 10° the body carries 45 percent of the total wing-body load, and this increases to 65 percent at 20° angle of attack.

During a 7.33g recovery the X-15 fuselage, which has large masses at the extremities and empty tanks in the center, is subjected to exceptionally large inertia loads. The large fuselage airload therefore becomes very significant since it supports the fuselage somewhat uniformly throughout its length and thereby reduces the net bending moments considerably.

Roll, pitch, and yaw dampers are incorporated in the X-15 to improve the dynamic stability of the airplane so that accurate trajectories and recoveries can be more easily flown by the pilot.

The effects of these dampers on the rolling-tail displacement and the resulting airplane response during a typical rolling pullout maneuver are illustrated in figures 7(a) and 7(b) which show the time history of an abrupt roll superimposed on a 5.2g pullout. Figure 7(a) shows the antisymmetrical tail displacement corresponding to direct pilot input and the roll rate that would occur. With the dampers, the displacement δ_H' is 4° instead of 12°, and the roll rate p is

100 deg/sec instead of 600 deg/sec. Figure 7(b) shows that the sideslip angle is reduced from -14° to -2° and the change in angle of attack is reduced from -23° to -1° when the dampers are used. The design limit rate of roll is 100 deg/sec. The roll dampers, when operating at the full gain setting, will limit the rate of roll to this value. When the dampers are off, or operating at a low gain setting, the rate of roll must be limited by the pilot using the roll-rate indicator as a guide.

Although the comparison shows the effects with all dampers operating, small differences would be noted with only the roll damper operating, since the yawing and pitching effects are largely a result of the coupling associated with high rolling rates. Limiting the roll rate to the design value of 100 deg/sec either by damper action or by pilot action results in essentially the same rolling-maneuver responses. During abrupt pitching or yawing maneuvers the pitch and yaw dampers become effective in reducing large responses. For structural design purposes the pitch damper is assumed to be inoperative in pitching maneuvers and the yaw damper inoperative in yawing maneuvers.

The landing gear of the X-15 consists of a nose gear located well forward and a pair of main skids located under the tail. This configuration, with the main gear far aft of the airplane center of gravity, did not permit the gear loads to be computed in the normal manner. A dynamic analysis was made wherein the aerodynamic forces and moments, gear reactions, and resulting airplane motions were computed as a function of time. As might be expected, the nose-gear reaction was unusually large, being 50 percent greater than the sum of the main-gear loads.

A time history of the nose-gear vertical velocity for the design landing condition is given in figure 8. The vertical velocity increases from the initial sinking speed R/D of 9 ft/sec at the time of main-gear contact to a nose-gear-contact velocity of 18 ft/sec. The gear load factor is 3.9. It is anticipated that actual landings will be accomplished at higher landing speeds with lower sinking speeds and smaller ground angles, thus reducing the nose-gear-contact velocity and load factor. Nose-wheel drop tests have been successfully conducted at contact velocities up to this maximum.

Carrying the X-15 under the wing of the B-52 is comparable, loadwise, to carrying a large finned tank. The load problem consists of determining the aerodynamic interaction effects between the B-52 and the X-15.

The structural design of the X-15 attachment to the B-52, including fittings, pylons, and backup structure, is based primarily on the strength level of the B-52. This permits normal maneuvering

and does not unduly penalize the structural design of either aircraft. Strength is provided for checkout of X-15 control systems, individually, to full surface deflection at speeds up to the maximum design equivalent airspeed of 300 knots.

Static drop tests will be made to assure that the mechanism for the release of the X-15 functions properly, but no structural flight demonstration or static test is contemplated for the X-15/B-52 combination. Therefore, an 80-percent restriction will be in effect. This means that the maneuver load factor will be limited to 1.6g instead of the B-52 design limit load factor of 2.0g, as shown in figure 9. Gust intensities of 30 ft/sec can be encountered at speeds up to 300 knots without exceeding 1.6g. The controlled nature of this operation precludes thunderstorm flying, and the amount of clear-air turbulence encountered during the carrier missions is not expected to result in gust velocities greater than 30 ft/sec.

The operating limits for the X-15 are based on control capabilities and on the strength level established by the structural-load and temperature combinations corresponding to the design altitude and speed missions shown in figures 1 and 2.

Below 100,000 feet there is sufficient longitudinal control power to attain 7.33g. Above 100,000 feet the dynamic pressure is too low to permit attainment of the full load factor even with maximum horizontal-tail displacement.

As explained in connection with figure 3, which shows a plot of dynamic pressures, a limit q of 1,600 lb/sq ft is imposed below 36,000 feet. At these lower altitudes and Mach numbers the aerodynamic coefficients and their distribution to the components would result in excessive empennage loads without this restriction.

Between 36,000 and 60,000 feet it is possible to attain the maximum design q of 2,500 lb/sq ft. However, in this region another restriction, also imposed to avoid adding unnecessary weight, is required. A second 7.33g maneuver immediately following the first is prohibited. During the first pullout the airplane will slow down very rapidly but will remain at high temperature. If another pullout is then attempted at the reduced Mach number the aerodynamic characteristics may be such that load-temperature combinations more severe than the primary conditions can occur. The secondary pullouts can be made to lesser load factors or delayed to allow time for the structure to cool to a temperature consistent with the lower Mach number.

Recoveries from alternate missions which result in more critical temperatures must be made at lower load factors or lower dynamic

pressures in order that the strength level established by the design missions will not be exceeded.

Although from an available energy consideration the X-15 is capable of reaching an altitude of 700,000 feet in a vertical ascent, a mission which reaches a peak altitude of 620,000 feet (fig. 10) is the maximum altitude mission from which a recovery can be made without exceeding the limit load factor of 7.33g or the limit dynamic pressure of 2,500 lb/sq ft. This recovery maintains maximum lift throughout the reentry until the limit load factor is attained. However, structural temperatures and temperature gradients that would be encountered during this recovery do not permit such a mission. Alternate missions with peak altitudes between 250,000 and 620,000 feet are being studied to determine the maximum altitude to which the present X-15 airplane may be flown.

Since performance depends directly on weight, it is appropriate that a brief review of the weight status be presented. Table I shows a comparison between the basic specification as originally written and the authorized revised specification. The "Current weight" column shows the results of the effort spent in controlling the weight of each component.

The revised specification incorporates an increase in fuel, oxidizer, and hydrogen peroxide to regain performance, an increase in vertical-tail area to improve directional stability, and other miscellaneous changes. To support the additional weight, the structure of the wing, fuselage, and horizontal tail had to be strengthened, and the surface controls had to be strengthened to be compatible with the increased vertical-tail size. A total of 765 pounds was authorized in the revised specification: 184 pounds in weight empty and 581 pounds in useful load.

The current weight status shows a gross weight increase of 387 pounds over the revised specification weight. The weight empty increased only 61 pounds and the useful load decreased 196 pounds. Instrumentation increased 522 pounds.

The changes in weight empty consist of the following:

(1) The wing was changed from 7 to 15 intermediate spars, the skin gage was reduced, and the heat-sink material was changed from titanium carbide with a nickel binder to Inconel X, resulting in a net decrease of 131 pounds.

(2) A 17-pound net increase in the empennage resulted from a 58-pound increase to meet thermal requirements and a reduction of

41 pounds for changing the leading-edge heat-sink material from titanium carbide with a nickel binder to Inconel X.

(3) Chem-Milling pockets in the skin and reducing the skin gages by adding Z-stiffeners and substituting aluminum for Inconel X in a portion of the intermediate fuel- and oxidizer-tank bulkheads saved 102 pounds in the body group, but a 15-pound increase was caused by additional structure to accommodate the engine weight increase. The net fuselage change is a decrease of 87 pounds.

(4) The alighting-gear group was decreased 73 pounds by eliminating the shimmy damper and reducing the gage of the main-landing-gear skids.

(5) A reduction of 12 pounds in surface controls was realized by changing from four direct-acting speed-brake actuators to two actuators with a linkage arrangement.

(6) The engine dry weight increased 296 pounds.

(7) The addition of an engine purge system increased the propulsion group by 67 pounds. However, this was partially offset by a reduction in the internal liquid-oxygen system plumbing of 29 pounds, giving a net propulsion-system increase of 38 pounds.

(8) The 4-pound increase in the auxiliary powerplant group was due to an increase in the weight of the power units.

(9) Changes in the fixed equipment resulted in a net increase of 9 pounds, consisting of a 76-pound increase in the pilot's seat, an 11-pound increase in instruments, a 34-pound decrease in the nitrogen system, and a 44-pound decrease in the air-conditioning system.

The changes in useful load consist of the following:

(1) The fuel for engine pumps (H_2O_2) was reduced 196 pounds through a change in engine requirements.

(2) According to the latest information from the engine manufacturer, the trapped fuel and oxidizer in the engine has increased 70 pounds.

(3) The helium requirements for the fuel and oxidizer increased 13 pounds.

(4) The nitrogen requirements for cockpit pressure and cooling were reduced 82 pounds.

Although instrumentation is customarily included in the "weight empty" in weight reports, it is listed separately in table I. This is done because when maximum-performance missions are to be flown, 370 pounds of instrumentation can be removed, bringing the actual weight very close to the revised specification weight.

TABLE I

CURRENT WEIGHT STATUS

Item	Basic specification weight, lb	Revised specification weight, lb	Current weight, lb
Weight empty:			
Wing	1,258	1,271	1,140
Empennage	1,063	1,243	1,260
Body group	3,871	3,898	3,811
Alighting gear	427	447	374
Surface controls	1,057	1,152	1,140
Propulsion group:			
Engine	540	540	836
Propulsion systems	808	868	906
Auxiliary powerplant group	270	197	201
Fixed-equipment group	1,096	958	967
Total weight empty	10,390	10,574	10,635
Useful load:			
Pilot	290	290	290
Oxidizer (engine LOX)	9,755	10,080	10,080
Fuel:			
NH_3 (engine)	7,790	8,011	8,011
H_2O_2 (engine pumps)	854	889	692
H_2O_2 (APU and ballistic control systems)	268	268	268
Trapped oil, fuel, and oxidizer	82	82	152
Helium	49	49	62
Nitrogen (cockpit pressure and cooling)	232	232	150
Total useful load	19,320	19,901	19,705
Instrumentation	800	800	1,322
Total gross weight	30,510	31,275	31,662

DESIGN ALTITUDE MISSION

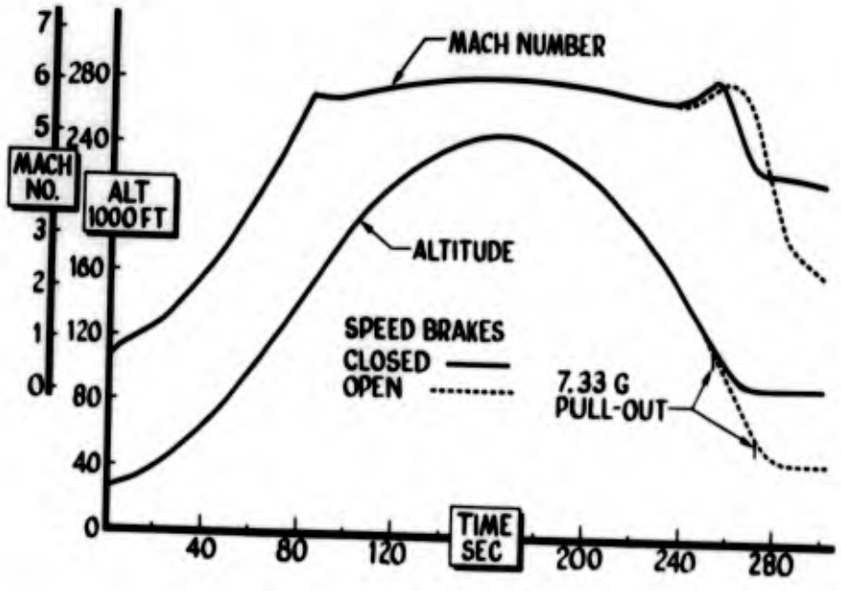

Figure 1

DESIGN SPEED MISSION

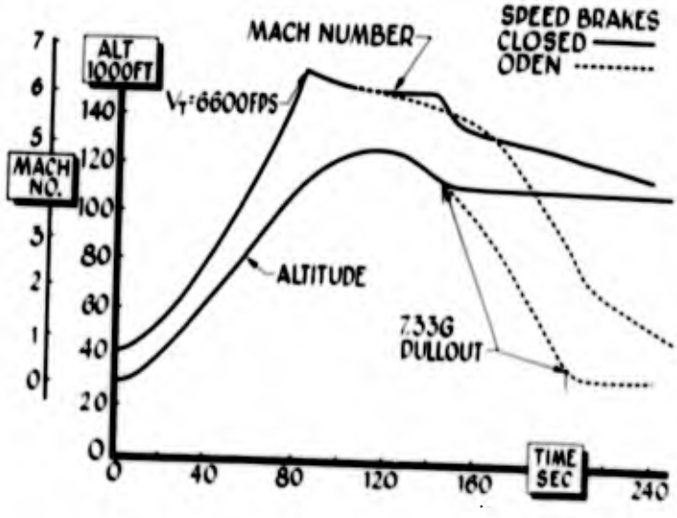

Figure 2

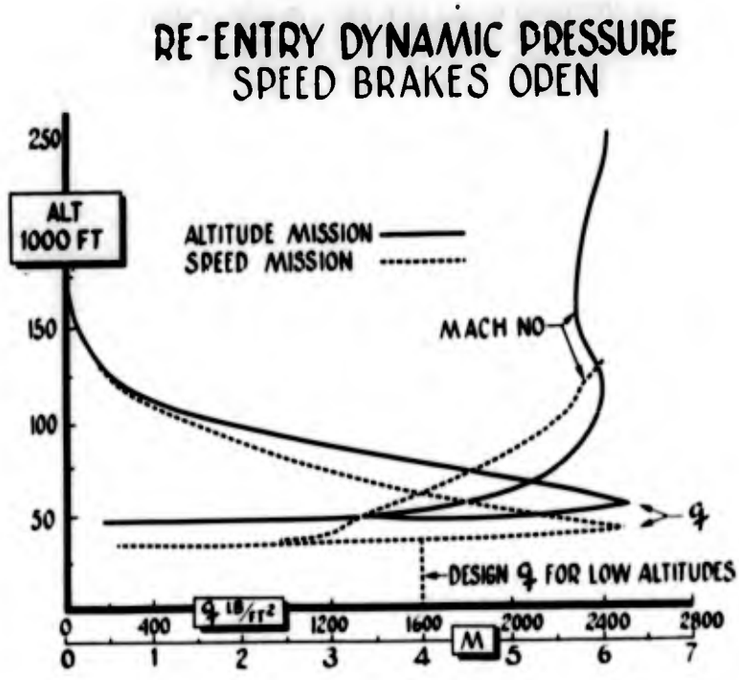

Figure 3

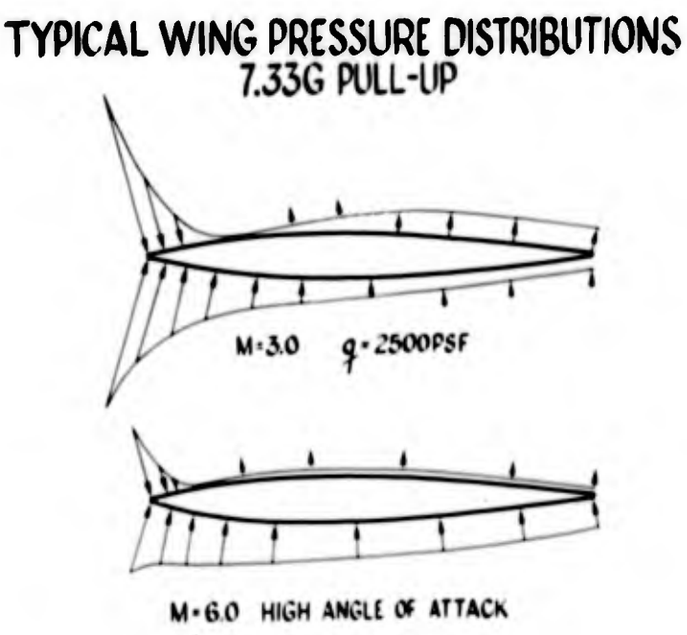

Figure 4

TYPICAL VERTICAL TAIL PRESSURE DISTRIBUTIONS

STEADY YAW M = 3.0

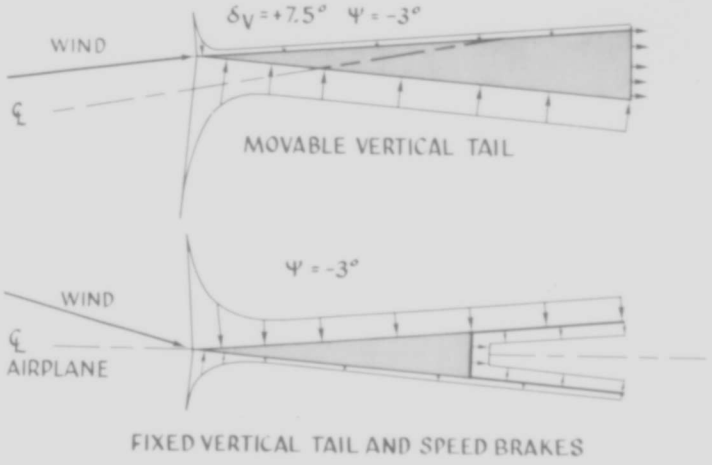

FIXED VERTICAL TAIL AND SPEED BRAKES

Figure 5

TYPICAL PRESSURE DISTRIBUTION OVER FUSELAGE

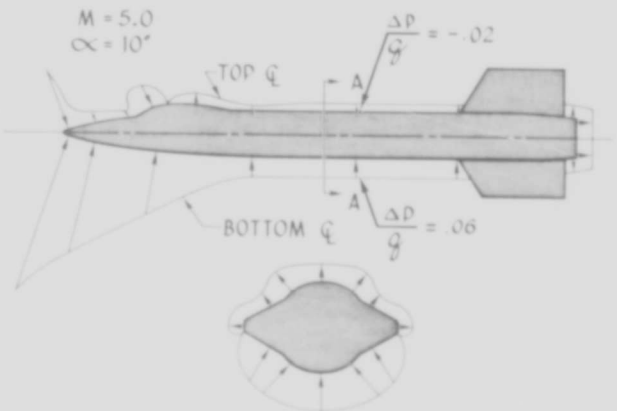

SECTION A-A
(SCALE: DOUBLED)

Figure 6

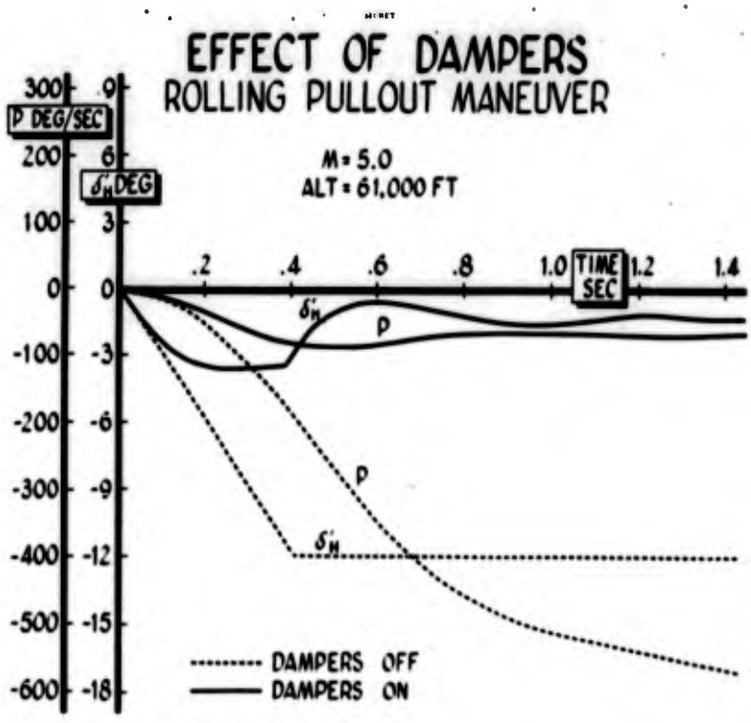

Figure 7(a)

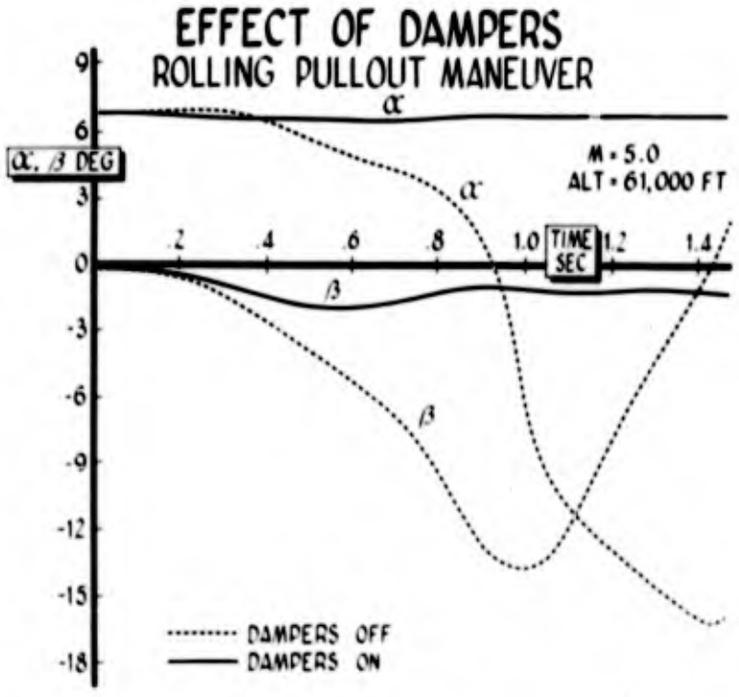

Figure 7(b)

NOSE GEAR VERTICAL VELOCITY DURING LANDING

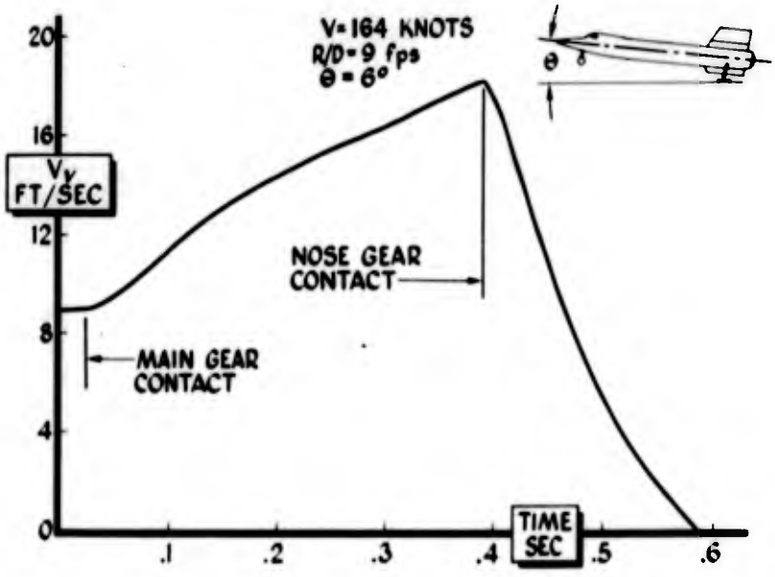

Figure 8

B-52 AND X-15 COMBINATION

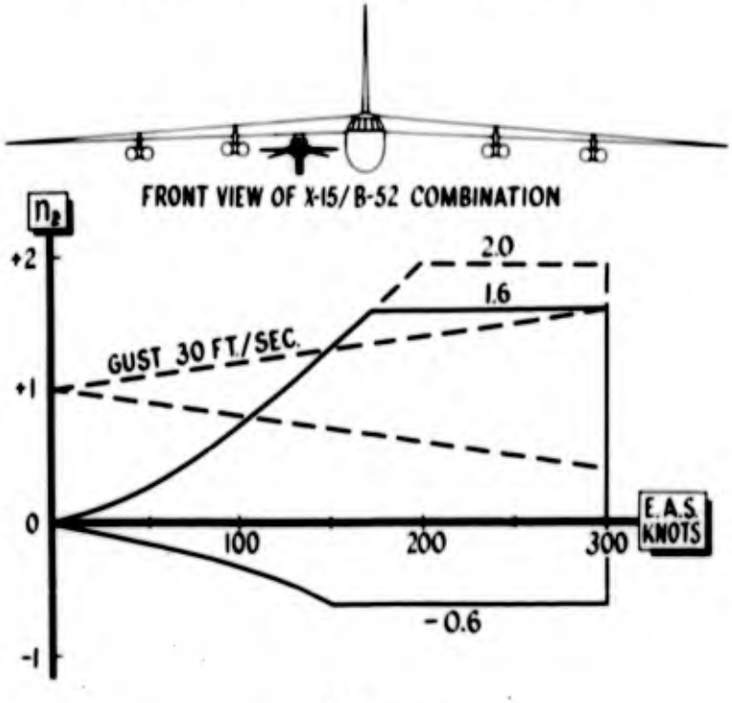

Figure 9

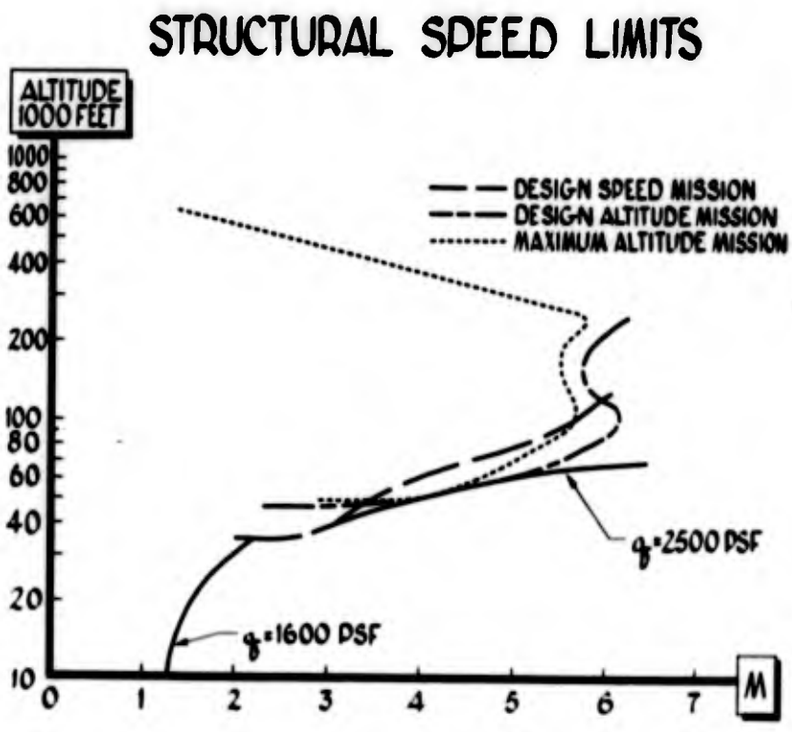
STRUCTURAL SPEED LIMITS
ALTITUDE 1000 FEET
1000
800
600
400
200
100
80
60
40
20
10
0
1
2
3
4
5
6
7
M
DESIGN SPEED MISSION
DESIGN ALTITUDE MISSION
MAXIMUM ALTITUDE MISSION
q=2500 PSF
q=1600 PSF

Figure 10

X-15 STRUCTURE AND STRUCTURAL DEVELOPMENT

By C. L. Davis

North American Aviation, Inc.

INTRODUCTION

The structure of the X-15 airplane is substantially the same as it was at the time of the X-15 conference in 1956. Pertinent structural details will be described in connection with each of the figures. Basically, the entire airplane structure is of monocoque and semimonocoque construction. The external skin is Inconel X and the internal structure is mostly titanium, with some Inconel X and aluminum. The structure is designed to carry thermal and load stresses without permanent set at limit load. Thermal stresses are disregarded in the calculation of failing strength. The validity of this philosophy is borne out by the tests to be discussed here.

FUSELAGE

The fuselage structure (fig. 1) is monocoque or semimonocoque, incorporating special frames and bulkheads at load distribution points. The outer skin is stabilized between the special frames and bulkheads by light J-section frames, and in some locations by longitudinal stiffeners.

The forward fuselage structure is semimonocoque and has double-wall construction in the cockpit and in some of the equipment bay areas. (See fig. 2.) The inner wall is an aluminum pressure seal and is loaded by pressure only. The forward fuselage is designed to withstand ground handling and landing conditions.

The center structure is monocoque. It contains the two main fuel tanks and incorporates the five wing-support frames. Details will be discussed in conjunction with tests covering this area. The structure is designed to withstand ground handling and normal flight conditions.

The aft structure (fig. 3) is semimonocoque and supports the empennage, main gear, and engine. It is designed to withstand engine thrust and unsymmetrical speed-brake conditions.

Center-Section Tank-Specimen Tests

Figure 4 shows a test specimen representing typical structure in the center section. In the airplane there are two tanks, each incorporating Inconel X semitorus end bulkheads, two aluminum semitorus intermediate bulkheads, and a cylindrical Inconel X tube running through the center of the tank. The specimen is effectively one-half of the forward tank and includes one Inconel X end bulkhead, one aluminum intermediate bulkhead, and the center tube.

A trapezoidal side fairing with flat outer sheet and a laterally corrugated inner sheet extends nearly the full length of both sides of the fuselage. The fairing houses fore-and-aft communication lines, such as the control system. The temperature is much lower inside the fairing than outside; consequently, the fuselage side skins inside the fairing are much cooler than the top and bottom skins. The fuselage skins in this area are vertically corrugated to relieve thermal stresses induced by temperature differentials. (See figs. 1 and 4.)

The specimen was subjected to a series of tests including bending, shear, and pressurization loads, with and without transient heating. These tests demonstrated that the fuselage could carry the design ultimate loads - in some cases with a considerable margin of safety.

An interesting result of the bending tests was that the transiently heated structure carried safely 95 percent of the failure load determined in a subsequent room-temperature test. It is concluded, therefore, that the effects of transient heating on the failing strength are small.

The side fairings were tested by loading them to ultimate design loads in compression and with simulated external pressure loads.

Torus-Tube Test

During the positive pressure tests of the specimen the torus tube failed as a result of external pressure at 73 percent of the design ultimate load. Additional tests were therefore performed on a separate torus-tube specimen. It was found that by adding more stiffening rings and refining the welding technique the strength was raised to 150 percent of ultimate without increasing the skin gage of the tube.

Torus Tests

Negative pressure tests (inward on the torus crown) were performed on the torus end and torus baffle installed in the fuselage specimen.

(See fig. 5.) The Inconel end torus withstood ultimate pressure without failure. The aluminum baffle torus failed at 71 percent of design ultimate. The baffle had no stiffening members at the time of the test. A specimen of the baffle was subsequently tested with various skin gages and various arrangements of radial stiffeners like those shown in figure 5. The results of these tests are plotted in figure 6, where pressure is plotted against shell thickness. The curve and circular tests points are for the unstiffened torus. The diamonds indicate test results for 30° and 15° spacing. The pressure for the final configuration (15° spacing) is 107 percent of design ultimate. The baffle would have weighed 10.9 pounds, or 62 percent, more if the skin gage had been increased instead of adding stiffeners.

Curved Panels

As a supporting investigation to the design of the fuselage shell, a series of compression tests were run on curved ring-stiffened panels. The results are shown in figure 7. Most of the panels tested were of 4130 steel but four 6061 aluminum panels were included, and after an optimum configuration had been determined with the aid of the test results, one panel representing the Inconel X final design was tested. The panel skin gage and ring frame spacing were varied among the panels. The important point shown in the graph is that closely spaced, light ring frames are very effective in raising the strength of the panels and, in this case, resulted in a much lighter structure than if the skin gage had been increased instead of adding more frames.

In addition to their higher buckling loads, the strength of the panels with closely spaced rings was much less erratic and seemed to be less sensitive to deviations in contour. After buckling, the panels would support about 85 percent of the failing load. With widely spaced rings, the strengths were much less consistent and the panels would support only about 66 percent of the failing load after buckling.

Test of Wing Support Frame

A specimen of a fuselage frame at the wing attachment (fig. 8) was tested under load and design temperature gradient. The temperature in the outer skin was 700° and the temperature in the inner flange of the frame was -25°. A crippling failure occurred near the wing attachment fitting. The frame was then repaired and the opposite side was tested at room temperature. Failure occurred at a load 3 percent higher than for the temperature test. Taking into account the reduction in material strength at high temperatures, this test showed negligible effects of thermal stresses on the failure of the specimen.

WING

The wing (fig. 9) is of multispar construction with multirib leading and trailing edges. The external skin is Inconel X and the substructure is titanium. Inboard, the front and rear spars have beaded flat webs and the front spar has occasional lightening holes. The 15 intermediate spars have corrugated webs. Outboard there are nine intermediate spars and all spars have flat webs.

The leading-edge nose contains a concentrated heat-sink mass of Inconel X. To reduce the thermal stresses resulting from the extremely high temperature gradients in the nose, the leading edge is divided into five spanwise segments.

Wing Structural Boxes

Two structural boxes representing the tip and inboard regions of the wing structure were tested in bending under design temperature gradients. Figure 10 shows cross-section sketches of the two boxes. The upper sketch represents the tip box; the lower sketch represents the inboard wing box. The graph shows the ultimate strength plotted against compression skin temperature. The failure strength of the tip box is shown by the triangle at 800° F and is compared with the theoretical curve which is calculated for no thermal stress. The agreement is satisfactory even though at this cover temperature of 800° elastic theory would predict a thermal stress in the cover amounting to 40 percent of the direct bending stress.

The box failed in wide flange buckling across the entire surface but did not collapse. The load supported by the box after failure was nearly the same as at failure. Incidentally, the skin of this box was buckled at limit load and temperature gradient, but the buckles caused no permanent set. The inboard box failed by local buckling and had a theoretical elastic thermal stress of 15 percent of the direct bending stress. The failure point is shown by the triangle on the lower curve. Again, the agreement with the simple theory is excellent, showing negligible effect of thermal stress on failure.

A test was performed at room temperature on a box which was constructed for other tests but which had the same compression panel parameters as the inboard box shown in figure 10. The result of that test is shown by the circle, which is also in good agreement with the theoretical curve.

Stagnation-Point Test

At the top of figure 11 is a sketch representing one of the five segments of the wing leading edge shown in figure 9. The ribs are titanium and A-286 or Inconel X fasteners are used for attachment. The Inconel X heat-sink mass is shown by the hatched area in figure 11.

The purpose of this test was to investigate the behavior of the leading-edge structure and attachments when subjected to high temperature gradients caused by the local stagnation point "hotspot." The stagnation-point mass was heated to 1,330°, giving a chordwise gradient of 830° per inch at the nose. After the test, the only damage to the specimen was a permanent set in the end fastener holes equal to $1\frac{1}{2}$ percent of their diameter. This is well within the acceptable permanent-set range for fasteners. The maximum spanwise bow in the specimen during the test was 0.03 inch. The specimen was cycled five times to the design temperature. No additional permanent set occurred in the holes and no other damage appeared.

After this test, an exploratory series of tests were run at increasing temperatures to determine the strength of the specimen under high thermal gradient. There was no additional damage to the specimen under the maximum temperatures producible by the laboratory heating equipment. The maximum temperature distribution attained during these tests was 2,100° at the nose, 1,800° on the skin, and 1,300° in the titanium nose rib. These temperatures exceed the generally accepted usable range of these materials. However, in this configuration, which is loaded almost entirely by thermal expansion, no damage was visible. This means that in actual flight the leading edge might not suffer from at least one exposure to these temperatures.

Leading-Edge Panel Test

Another test was run on the leading-edge structure and on one of the leading-edge skin panels to determine whether, under design load and temperature, there would be any aerodynamically significant deformations. The leading edge was loaded to its design loading and was heated to 1,100°. Deflection measurements were taken at the center of one panel and at the nose. The test results are shown in figure 12. In the upper graph, the vertical deflection of the panel center line relative to the front spar and nosepiece is plotted against length. In the lower graph, the deflection of the panel center relative to its supporting ribs is plotted against width. The panel developed a single-wave deformation under either heat or load alone, with a maximum deflection less than in the combined case shown here. A maximum

deflection of the nose relative to the front spar of 0.37 inch occurred during the test. These deflections were not considered to be serious.

A-Frame Test

A test performed to verify the strength of the wing-to-fuselage transition structure, or "A-frame structure" will be discussed next. (See figs. 1 and 13.) The wing-to-fuselage attachment consists of five ties at fuselage frames, the transition from the distributed wing surface loads and multispar shear loads being accomplished through a root rib, and the side tunnel structure. The side tunnel structure consists of the outside sheet and trapezoidal frames, five of which are tied to the fuselage. There are also intermediate frames which are not tied to a fuselage frame.

This specimen incorporates, as fore and aft boundaries, two of the fuselage-tie A-frames, an intermediate A-frame, a portion of the root rib, and enough of the inboard wing box to distribute the test loads properly. The specimen was loaded to ultimate design loads and temperatures. The temperature on the lower A-frame surface was 1,125° and the temperature on the adjacent lower wing surface was 975°. There was no residual permanent set after the test, even though deep buckles appeared in the A-frame intermediate panels on the application of temperature. The chordwise distribution of bending stress at section A of the wing box was measured by strain gages at room temperature and is shown in figure 13. The effect of the unsupported intermediate A-frame is quite apparent and the test results agree with analysis.

Front-Spar Test

The front spar is subjected to high temperature gradients through its depth and, consequently, high thermal loads are generated in the web and in the attaching fasteners to the spar caps. In order to investigate this condition, a full-scale full-span front spar specimen was cycle tested under design temperature gradients. The sketches in figures 14 and 15 show the spar and the flange temperatures. The temperatures were cycled 50 times from room temperature to the maximum values. The thermal stresses in the center of the web and the permanent deformations of the spar web and end-fastener holes were recorded during the cycling. The results of the test are shown on the graphs. Figure 14 shows the effects on spar deformation. The curve shows theoretical deflection and the four circles are test points. After the tests were completed, there was a permanent tip vertical deflection of 0.20 inch relative to the root. The spar had also crept spanwise 0.1 percent. A strain corresponding to a thermal tensile stress of 65,000 psi was indicated by a strain gage at the center of the web

during the last cycle. This stress level had decreased during the cycling. Later the cycle tests were repeated on a spar with web lightening holes, such as now exist in the airplane inboard spar. The indicated web stress was reduced by 30 percent. The four end spar fastener holes were checked for permanent set periodically during the tests. The results are plotted in figure 15. It can be seen that the permanent set first increased fairly rapidly and then leveled off, approaching a constant value at the end of the cycling. The maximum permanent set occurred in the inboard holes and amounted to 5 percent of the hole diameter. The residual permanent set remaining in the spar and attachment holes does not affect structural integrity. Theoretically, on an elastic basis, the level of thermal stress measured in the web should have failed the spar fasteners, but apparently the combination of plastic relief and friction relieved the fastener loads sufficiently to avoid any shear failure.

HORIZONTAL TAIL

The final series of tests to be described was for the determination of a configuration of horizontal-tail structure which would satisfy torsional-stiffness requirements for flutter.

Basically, the horizontal-tail structure consists of a main bending member (the main spar), two torque boxes formed by the skin and the three spars, ribs for torsional stability, a torque-collecting rib at the root, and a segmented leading edge. (See fig. 16.) The leading edge is divided into 16-inch spanwise segments to reduce thermal-expansion effects from stagnation-point temperatures. Each segment has a welded-in heat-sink mass of Inconel X in the nose. The main spar and root rib form a rather massive unit which offers a very large restraint to thermal expansion of the hot skins. The design chordwise temperature distribution is typical for the entire span, except for variations in the depth of the valleys over the heat sinks at the spars.

A series of test boxes were constructed with varying rib spacing, rib material, rib gage, and outer-skin gage, and then tested. (See fig. 17.) The governing test parameter was the torsional stiffness remaining after thermal skin buckling and application of high torque loads. The tests were conducted by applying the torque in increments up to 45,000 inch-pounds, and applying heat after each increment of loading had been applied. The data are plotted as the ratio of twist at room temperature to twist under thermal gradient plotted against torque at the various load levels. They thus indicate the percentage of torsional stiffness retained.

Four boxes were tested; they are numbered in chronological order of testing. Box 3 would give satisfactory stiffness but had thick skins. Consequently, a lighter configuration was sought. Box 4 had lighter skins, the improved stiffness over boxes 1 and 2 being attained by modifying rib spacing, material, and design. Box 4 has satisfactory stiffness and was chosen as the configuration for the airplane at the time of these tests.

The curves of figure 17 do not show the comparison of actual stiffness in the boxes, but the ratio of stiffness hot to stiffness cold. Box 4 was actually stiffer than box 2 over the whole torque range. However, subsequent changes in external temperatures and loads made necessary a redesign to heavier skin gages and modified rib material. There was no further testing, however, since the revised configuration obviously exceeded the stiffness requirements.

A bending test, under design temperatures, was performed on one of the boxes with a leading edge attached. The slotted leading edge relieved the thermal stresses as expected and the box failed at a stress in good agreement with calculations.

All loadings used in this series were in excess of the design limit.

CONCLUSIONS

In conclusion, the series of tests described here have proven that the X-15 structure not only has ample strength to withstand the loads for which it was designed, but also has reserve strength for increased loads and temperatures.

Key design effects demonstrated by the tests were:

1. A confirmation that light stiffeners are very effective for stiffening shell structures and usually result in lighter structure than would be provided by increasing skin thicknesses.

2. Thermal stresses have little effect on structural failing strength.

3. A small number of overheat cycles on a lightly loaded structure may not result in prohibitive damage.

4. Reduction in box-beam stiffness due to thermal buckling is large in some cases and may be critical if not accounted for in the design.

X-15

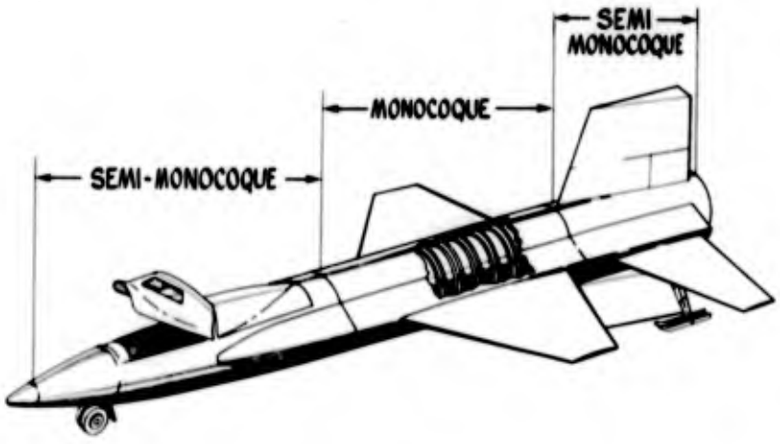

Figure 1

FUSELAGE SKIN

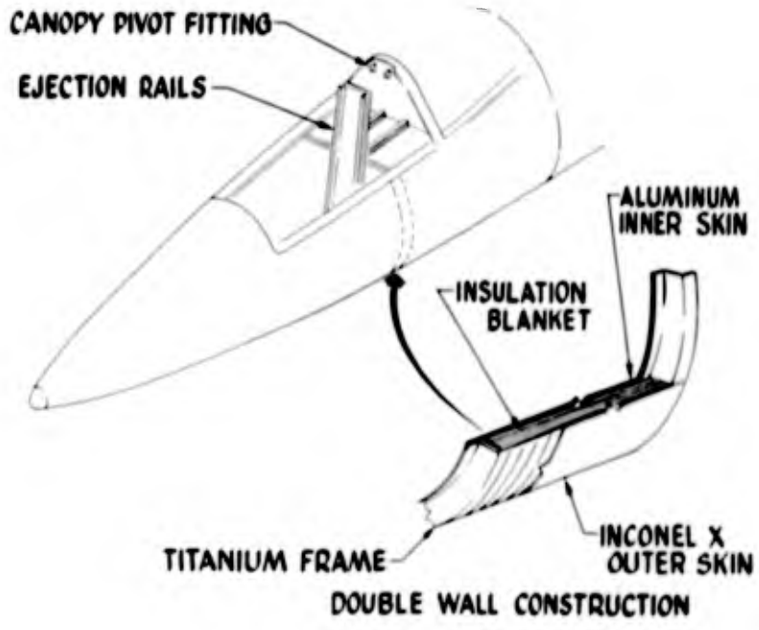

Figure 2

AFT FUSELAGE STRUCTURE

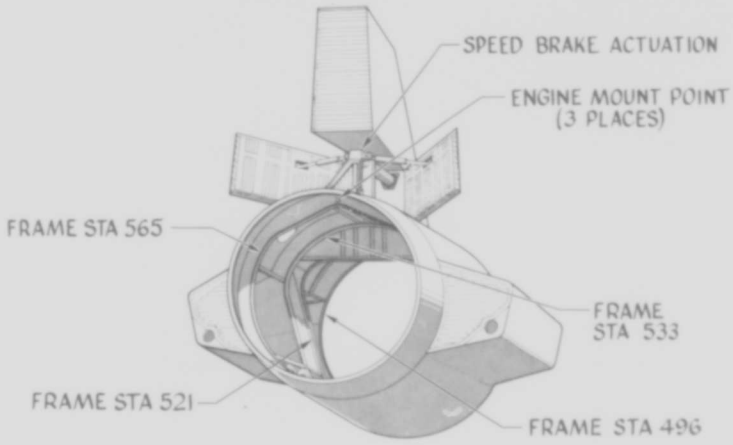

Figure 3

X-15 FUSELAGE TEST SPECIMEN

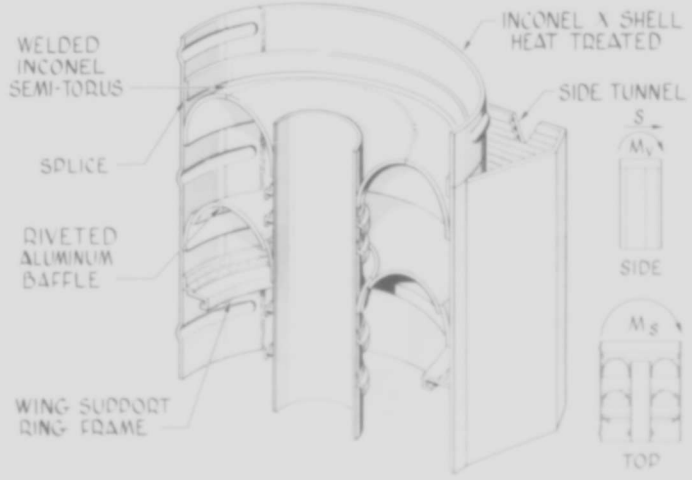

Figure 4

ALUMINUM TORUS

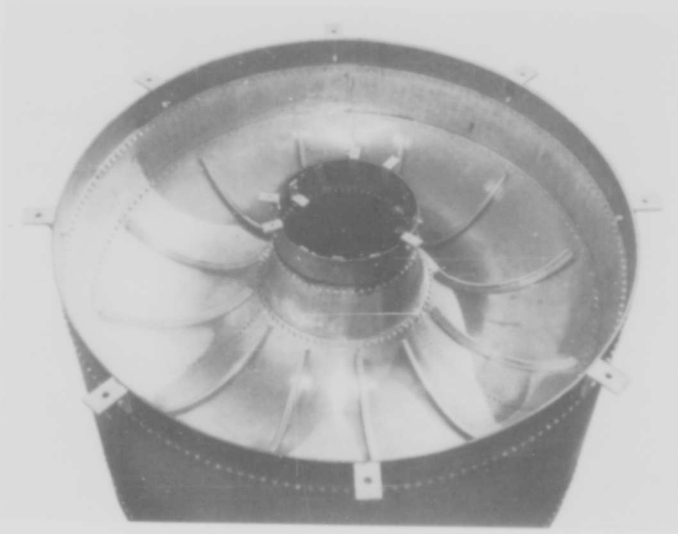

Figure 5

TORUS INSTABILITY TEST
STRENGTH VS GAGE

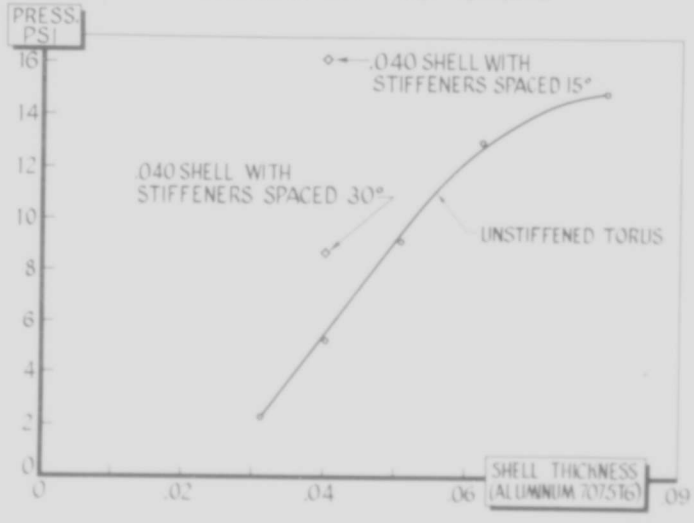

Figure 6

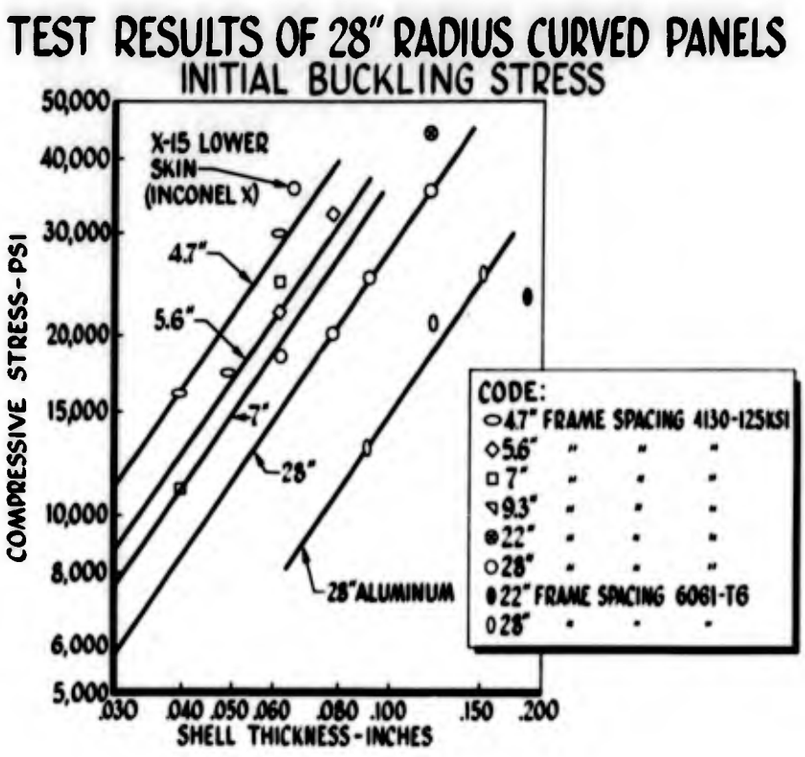

Figure 7

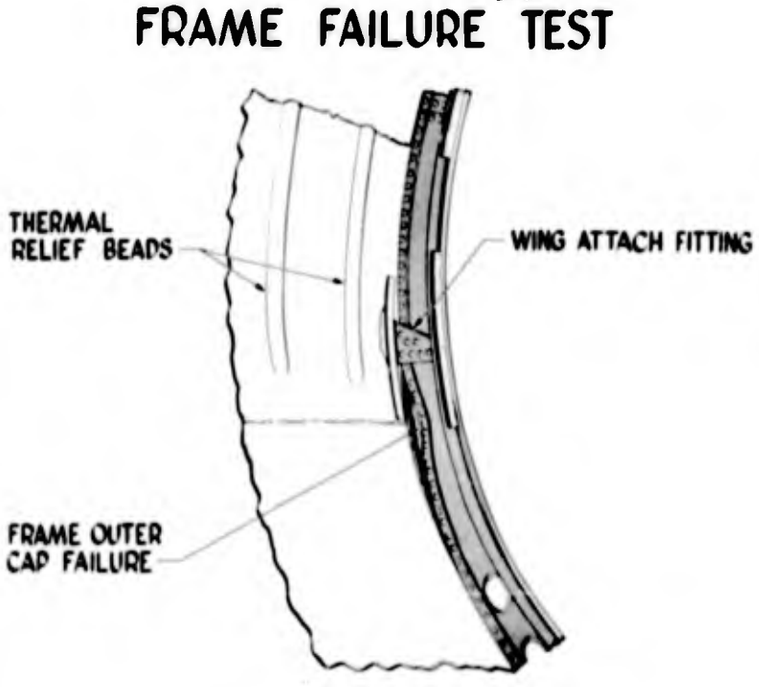

Figure 8

X-15 WING STRUCTURE

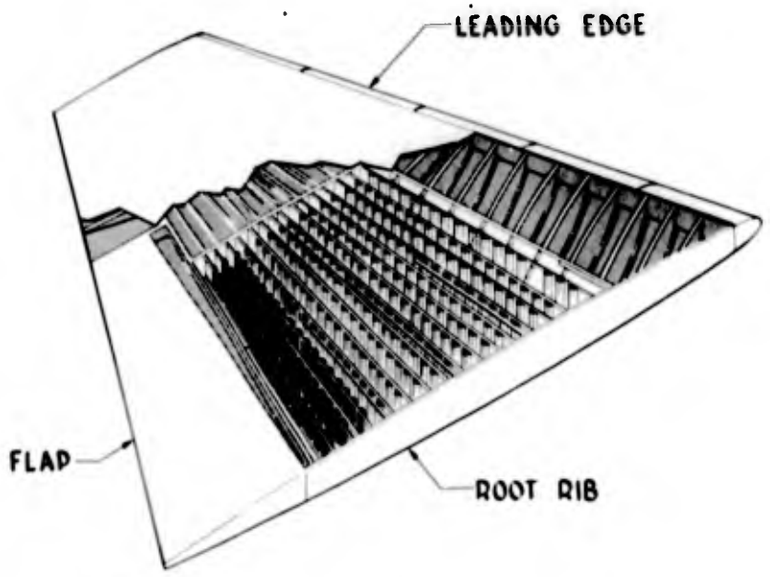

Figure 9

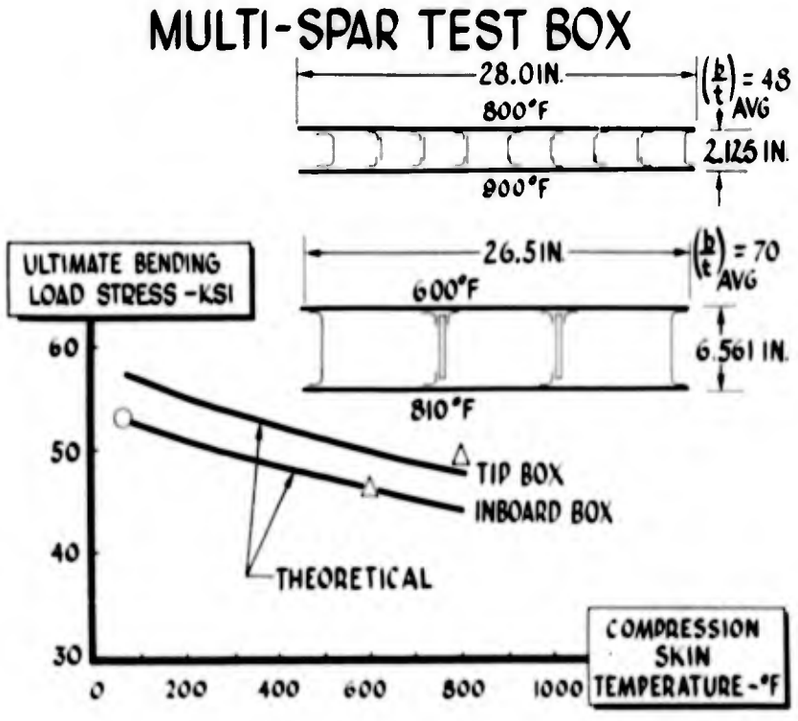

Figure 10

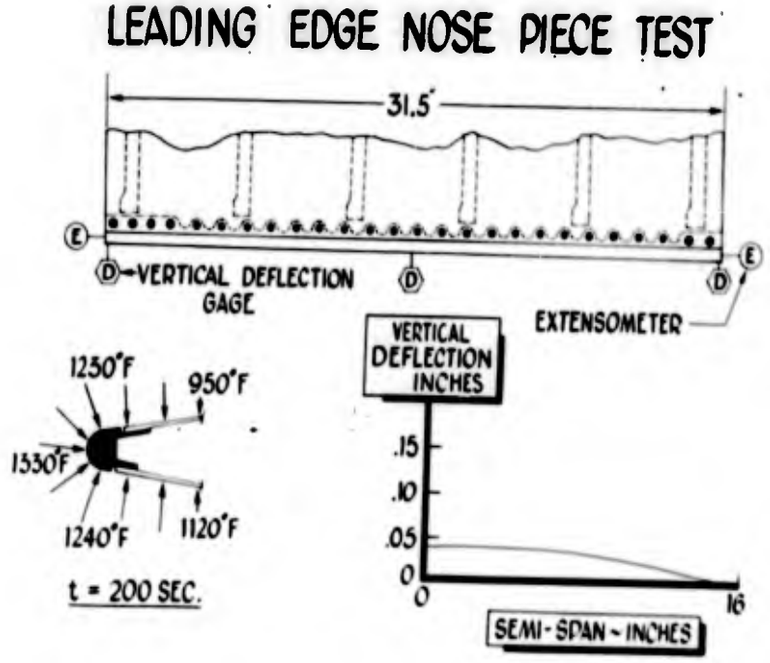

Figure 11

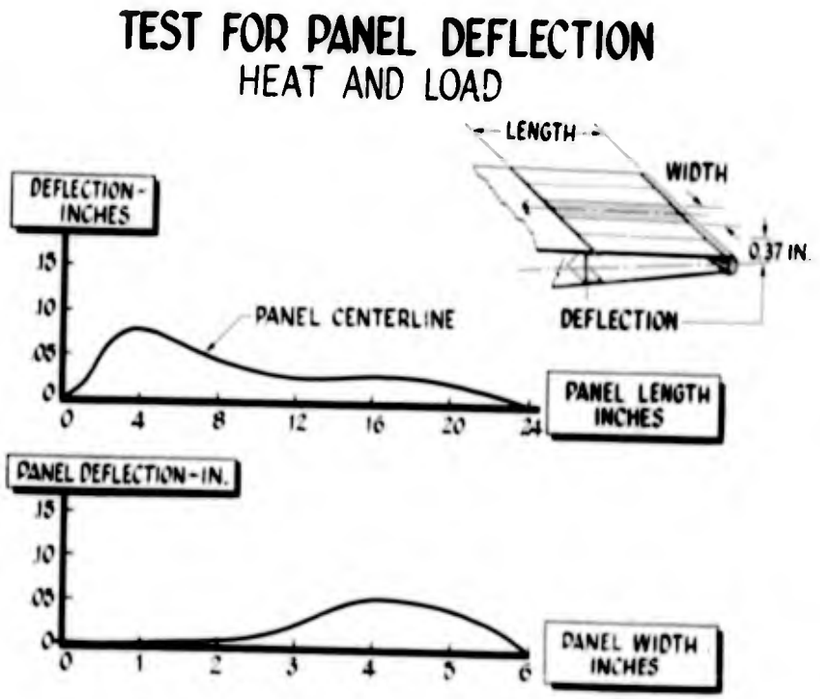

Figure 12

WING A-FRAME THERMAL TEST

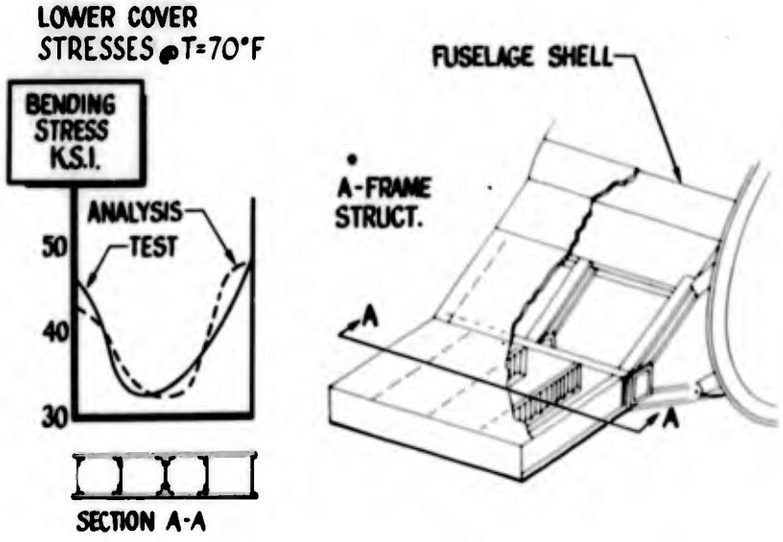

Figure 13

FRONT SPAR THERMAL DEFLECTION TEST

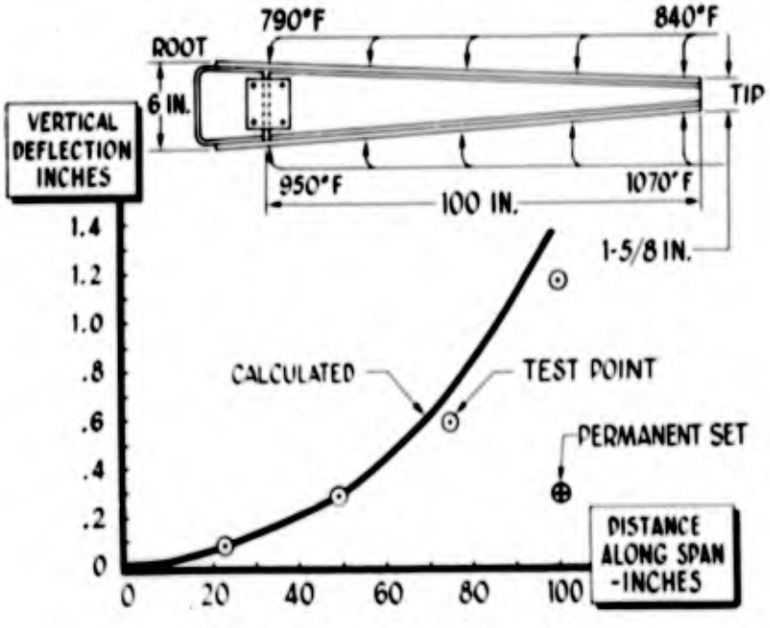

Figure 14

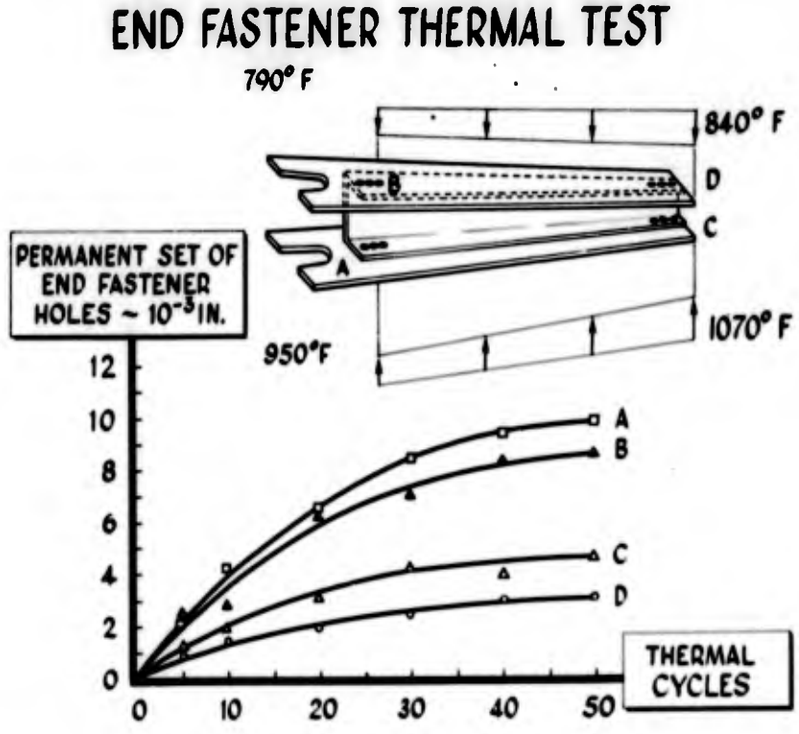

Figure 15

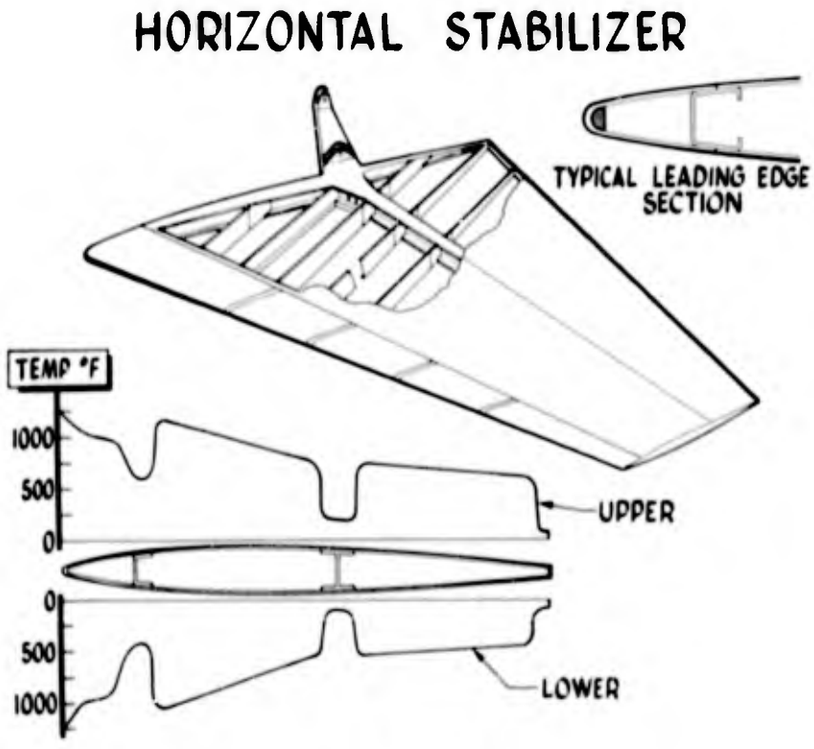

Figure 16

HORIZONTAL TAIL BOX TEST

$$\%\ \text{STIFFNESS RETAINED} = \frac{\text{TWIST AT ROOM TEMP}}{\text{TWIST UNDER THERMAL GRADIENT}}$$

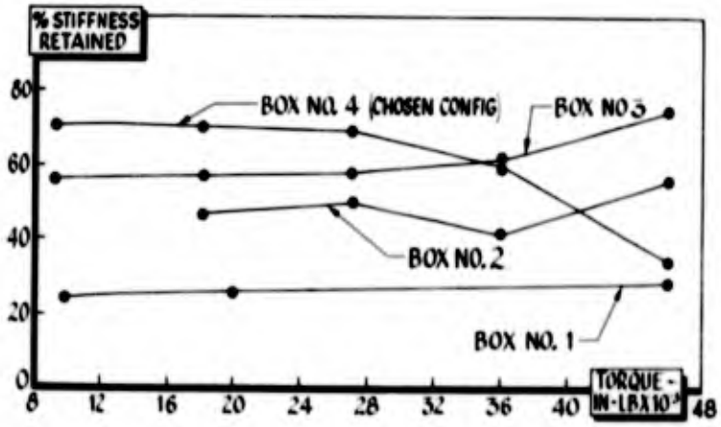

Figure 17

FLUTTER, NOISE, AND BUFFET PROBLEMS RELATED TO THE X-15

By Harry L. Runyan
NACA Langley Aeronautical Laboratory

and Harold R. Sweet
North American Aviation, Inc.

From an aeroelastic standpoint, the high Mach number capabilities of the X-15 and the associated aerodynamic heating presented two new problem areas. For instance, at the time of the initiation of the project no experimental flutter results were available above $M = 3$, and an adequate aerodynamic theory to use at these high Mach numbers had not been established. Thus, the X-15 has provided an impetus and focal point for research into these new areas, which of course is one of the purposes of such a project. With regard to aerodynamic heating, reduction in stiffness due to transient conditions has been relatively small. However, large reductions in stiffness were found due to permanent buckling of the skins which was induced by aerodynamic heating. Thus, the effects of aerodynamic heating could be incorporated into the aeroelastic problem simply as a reduction in structural stiffness, and small-scale models can be tested cold but with a reduced stiffness to simulate the hot condition. These reductions in stiffness were determined largely from laboratory tests on structural samples subjected to the load and the temperature-time history of the airplane recovery mission. For example, some of the reductions in stiffness were found to be as much as 60 percent.

In this paper, flutter, noise, and buffet problems will be considered. The flutter program will be examined first.

In figure 1 is shown a sketch of the X-15. The shaded areas are those components whose design was affected by flutter considerations. The remaining portion of the flutter section will be devoted to a discussion of various components.

The flutter test program is presented in table I. Dynamic models of the horizontal and vertical stabilizers have been tested in the Langley 8-inch hypersonic aeroelastic tunnel which utilizes helium as a test medium, in the 26-inch Langley transonic blowdown tunnel, in the Langley 9- by 18-inch supersonic flutter tunnel, and in the Langley 11-inch hypersonic tunnel. Full-scale tests of the tail surfaces were originally scheduled to be made on a ground-launched rocket to the maximum flight Mach number and also on a sled up to $M = 1$. These tests were deleted in favor of full-scale tests in the Langley 9- by 6-foot thermal structures tunnel at $M = 3$ and a

stagnation temperature of 660° F. A research model of the wing has been tested throughout the Mach number range of 0.5 to 7 in the facilities listed. An addition to the original test program consisted in the testing of the influence of the wing-mounted X-15 on the flutter of the B-52. These tests were accomplished in the University of Washington wind tunnel.

The main lifting surface has not posed a problem with regard to flutter. Its stiffness is dictated mainly from thermal considerations and has resulted in a very stiff wing. The only changes were to the landing flaps; a positive up-lock was provided in order to increase the stiffness of the flap actuating system and an inner corrugated skin was used to provide a higher torsional stiffness of the flap. The flutter tests of the research wing, which, however, did not provide complete dynamic similitude, indicated a very wide margin of safety, as did the theoretical results for the full-scale wing.

Now, examine the results of the flutter studies of the horizontal stabilizer. The horizontal tail, being of the all-movable type in which its right and left sides could be moved differentially, appeared from the outset to constitute a major aeroelastic problem and will require detailed investigation. Early in the flutter studies, it was decided to move the axis of rotation forward from the 35-percent mean aerodynamic chord to the 25-percent mean aerodynamic chord in order to increase the flutter speed. In addition, the hydraulic actuator size was increased in order to increase the system torsional stiffness, since the compressibility of the fluid in the actuators constituted a weak link in the stiffness of the pitching degree of freedom. In addition, as determined from the laboratory tests mentioned previously, thermal buckling of the panels lowered the torsional stiffness to an unacceptable point. A reduction in rib spacing decreased the buckle depth to a point where the resulting stiffness level was satisfactory. More recently, reevaluation of the recovery mission indicated larger chordwise temperature gradients than were originally anticipated (gradients such that permanent skin buckles would occur). At the altitudes at which this would occur, the loss in stiffness would be permissible, but the stiffness loss from the permanent buckles would not be tenable at lower altitudes. To prevent this permanent buckling of the skin from the chordwise temperature gradient, the skin gage was increased approximately 20 percent.

The results obtained for the flutter of the horizontal stabilizer are given in figure 2. A stiffness-altitude parameter $\frac{b\omega_\alpha}{a}\sqrt{\mu}$ is plotted against Mach number M. In this parameter, b is the stabilizer half-chord, ω_α is the torsional frequency, μ is a mass ratio

consisting of the ratio of the mass of the surface to the mass of a certain volume of air surrounding the surface, and a is the velocity of sound. The flutter or unsafe region is below the curves. In this figure, radial lines emanating from the origin represent constant-dynamic-pressure lines. The shaded area is the operating region of the X-15. The design q of 2,500 lb/sq ft is shown in figure 2. However, since the pilot must execute a pull-up at M = 2.75 to provide ground clearance, he will be operating at lower dynamic pressure than the 2,500 lb/sq ft given in this range. The bottom of the shaded area represents sea level. Now, examine the experimental results. These models were designed to simulate the loss in stiffness due to aerodynamic heating and were designed with a 40-percent reduction in torsional stiffness and a 60-percent reduction in bending stiffness. The open points represent no flutter and the solid points represent flutter. The series of open points in the range of M = 0.8 to 1.2 show no flutter up to the maximum q of the tunnel and show no intersection with the operating region. Flutter was obtained, however, from M = 1.3 to M = 7. It is interesting to note that there appears to be no pronounced transonic bump such as have been found in the past on other configurations. The open point with the cross at M = 3 was obtained from the full-scale tests of the tail in the Langley 9- by 6-foot thermal structures tunnel for a stagnation temperature of 660° F. Although no flutter was obtained, the test provided a good proof test since q was 3,400 lb/sq ft, well above the design value of 2,500 lb/sq ft. Now, examine the theoretical results. Two sets of calculations are shown; one using piston theory for the aerodynamic input for the high Mach numbers and one using the three-dimensional kernel function for subsonic Mach numbers. Excellent agreement with experiment has been found for the range of M = 2 to 7. The usual modal type of analysis was not used here but instead the piston theory was used to formulate the aerodynamic influence coefficients and these combined with the structural influence coefficients provided a procedure whereby the flutter speed was obtained directly by iteration as given in reference 1. The subsonic portion was obtained by the use of the usual modal approach except that the three-dimensional kernel function (ref. 2) was used for the aerodynamic input. That is, the plan form of the tail as well as the effects of compressible flow were taken into account up to M = 0.95. These results have been obtained at 0° angle of attack.

Some calculations using piston theory for the effect of angle of attack on flutter have indicated a possible enlargement of the flutter region. (See fig. 3.) Calculated results are given in figure 3 for $\alpha = 0^\circ$, 10°, and 20°. The effect of angle of attack is destabilization and becomes larger as the Mach number is increased. However, the section of each curve that is solid is believed to be within the limitation of piston theory. This limitation is fixed by the ratio of

the normal velocity of the airfoil to the local speed of sound; this ratio must be less than unity.

A research program was set up to investigate the ranges of validity of piston theory. In figure 4, the stiffness-altitude parameter $\frac{b\omega_\alpha}{a}\sqrt{\mu}$ is plotted against the ratio of bending frequency to torsion frequency $\frac{\omega_h}{\omega_\alpha}$. The model had an aspect ratio of 1, was rectangular and rigid, but was mounted on a flexible shaft. The airfoil sections were symmetrical double wedges with thickness ratios of 5, 10, and 15 percent. The experimental result of the 5-percent-thick wing is in remarkable agreement with theoretical predictions. The 10-percent experimental result is about 5 percent below that of the theoretical result, but the 15-percent-thick model is about 16 percent below the theoretical result. This curve points out the validity of using piston theory for the wing with smaller thickness ratio at zero angle of attack. However, for the 15-percent-thick wing the slope of the surface is such that limitation of piston theory is exceeded, that is, the ratio of the downwash to the speed of sound exceeds unity. In figure 3, sections of the curve for which w/a is less than 1 are shown solid. In figure 3 the results of an experiment on the horizontal tail are shown. The tail was set at 11° angle of attack and the tunnel density increased. The test was terminated at the circular point without flutter. Thus, it appears that the X-15 will be safe from flutter at the higher angles of attack. However, this effect of angle of attack does constitute a research area requiring additional theoretical and experimental work.

With regard to the vertical surface, no experimental flutter has been obtained in the transonic and supersonic range, even though in one case the stiffness of the spindle attachment was reduced to about 15 percent of the design stiffness. Calculations indicate a very large flutter margin. However, flutter was obtained at $M = 7$ but with a large margin of safety. This wedge configuration appears to be a rather stable airfoil section from a flutter standpoint. So far, no flutter has been found on the dive brakes, either classical or buzz. However, difficulty has been experienced in modeling the dive brakes. In attempting scaling to obtain the minimum expected frequency, the dive brakes could not take the static load in the open position, and the springs simply deformed until they hit the stop. Some new models are being built utilizing measured frequencies which permit a higher stiffness in the open position to further study the problem.

With regard to panel flutter, it does not appear that a problem exists. In using the criterion presented in reference 3, for the flutter of flat panels, all panels appear to be in a safe region

except one which is located at the forward end of the tunnel. However, this panel has a large amount of curvature which should raise the flutter speed a considerable amount above that of the flat panel. No panel flutter was observed on the full-scale test of the horizontal tail.

Up to this point, the X-15 has been considered. Originally, the X-15 was to be installed on the B-36. Later, however, it was decided to use the B-52 as the carrier airplane; and, of course, the question immediately is raised as to what will be the effect of this asymmetrically placed mass on the flutter of the B-52. Since Boeing had a flutter model of the B-52, it was decided to conduct tests of this combined configuration. These tests were conducted by Boeing and were made in the University of Washington wind tunnel. The X-15 model was rigid but was scaled for total inertias and mass. The pylon, however, was scaled to provide the proper frequencies. The results of these tests are shown in figure 5 in which altitude is plotted against Mach number. These tests were made at $M = 0.2$ and then extrapolated to the higher Mach number condition. The airplane flight plan is shown as well as the flutter boundary for two conditions. Both of these boundaries contain a 15-percent margin in velocity. First, the flutter boundary was determined for the airplane having its take-off weight throughout the flight, and there appeared to be an adequate margin of safety. The fuel consumption was then simulated for the various altitudes, and the second curve indicates these results. An even larger margin of safety is found. Three pylon stiffnesses were investigated in these tests, and no appreciable change in the flutter speed was found. Thus, it appears that the location of the X-15 on the B-52 does not create a flutter problem.

In addition to the problem of the influence of the X-15 on the B-52 flutter speed, there still remains the problem of the effect of noise from the two inboard engines of the B-52 on the X-15 especially during take-off, as well as the buffeting of the horizontal tail of the B-52, as induced by the presence of the X-15 ahead of the tail. With regard to noise, the noise field produced by the B-52, as well as a sketch of the location of the X-15, is shown in figure 6.

It is to be noted that the wing of the X-15 is located in a very severe noise environment of the order of 156 decibels, and the tail is very close to the 156-decibel curve. Typical structural components of the X-15 are now being tested in a discrete frequency noise facility. These tests have been conducted at a decibel rating of 158. Unfortunately, on the first test the thermocouples failed after 10 minutes and the specimen failed after 1 hour of testing. On a second series of tests, the thermocouple staple spacing was reduced to one-third of the original spacing, which has now been found to be

satisfactory. On a second specimen, failure occurred after 1/2 hour of testing, even though the skin thickness had been increased by 20 percent. Additional testing and detailed examination of the structure are planned in order to extend the service life of the airplane. However, if this problem continues to be important, there remains the possibility of attempting to reduce the sound field of the B-52. There are two obvious methods of doing this. First, reduce the engine power during take-off. It appears practical to obtain a 6-decibel drop by this method. Another procedure would be to add tailpipe extensions to the two inboard engines in order to remove the severe sound field of the B-52 from the X-15 structure.

Of course it must be remembered that the time duration of each take-off is measured in seconds rather than hours, so that the structure may be able to withstand the noise for these short periods.

No information as yet has been obtained of the influence of the X-15 rocket motor on the structure surrounding the engine. The near-noise-field measurements are in progress, and in these tests the engine is mounted in an aft fuselage. Thus, the effect of the noise field on the actual structure will be determined.

With regard to buffeting, some studies have been made of the influence of the X-15 on the B-52 horizontal tail. These tests were conducted by William J. Alford, Jr., and Robert T. Taylor, who have already reported on the force tests in a previous paper. No attempt was made to scale dynamically the horizontal stabilizer. However, a flexible right-hand stabilizer was installed on the B-52 model and instrumented with a strain gage at the root and one pressure cell was installed at approximately 60 percent span.

The root mean square of the bending moment was obtained for various configurations. Some of the results are plotted in figure 7 where C_L is plotted against Mach number. Flight buffet limit is shown for the full-scale B-52. The results of the model test are shown for $M = 0.4$, 0.75, and 0.820. From the model test at $M = 0.4$, it is actually possible to establish the buffet boundary, and the comparison with the full-scale airplane is excellent. The other two curves indicate the limit of the model tests, and no appreciable buffet was found at either of these places. The flight envelope is shown here and appears to be in a buffet-free region. Therefore, based on these model tests, at least, it can be concluded that there should be no buffet problem.

In conclusion, the flutter program has been discussed in detail, and with the modifications that have been made on the airplane, it appears that the airplane will be safe from flutter. Noise, on the

other hand, could still remain a service problem, but methods of moving the noise environment from the tail do appear practical if it becomes necessary. Buffet tests of the influence of the X-15 on the B-52 tail indicate that there should be no problem.

REFERENCES

1. Rodden, W. P.: A Matrix Approach to Flutter Calculations. Rep. No. NA-56-1070, North American Aviation, Inc., May 1, 1956.

2. Watkins, Charles E., Runyan, Harry C., and Woolston, Donald S.: On the Kernel Function of the Integral Equation Relating the Lift and Downwash Distributions of Oscillating Finite Wings in Subsonic Flow. NACA Rep. 1234, 1955. (Supersedes NACA TN 3131.)

3. Sylvester, Maurice A.: Experimental Studies of Flutter of Buckled Rectangular Panels at Mach Numbers From 1.2 to 3.0 Including Effects of Pressure Differential and of Panel Width-Length Ratio. NACA RM L55I30, 1955.

TABLE I.- FLUTTER TEST PROGRAM

Configuration	M	Scale	Test facility
Horizontal and vertical stabilizers	7	1/12	Langley: 8-inch hypersonic aeroelastic tunnel
	0.85 to 1.3	1/12	26-inch transonic blowdown tunnel
	1.3 to 4.0	1/12	9- by 18-inch supersonic flutter tunnel
	3	Full	9- by 6-foot thermal structures tunnel
	7	1/12	11-inch hypersonic tunnel
Wing	0.5 to 1.2	1/15	Langley: 2- by 2-foot transonic flutter tunnel
	1.2 to 2.0	1/15	9- by 18-inch supersonic flutter tunnel
	5	1/15	9-inch gas dynamics tunnel
	7	1/20	8-inch hypersonic aeroelastic tunnel
X-15/B-52	0.2	1/20	University of Washington wind tunnel

COMPONENTS AFFECTED BY FLUTTER

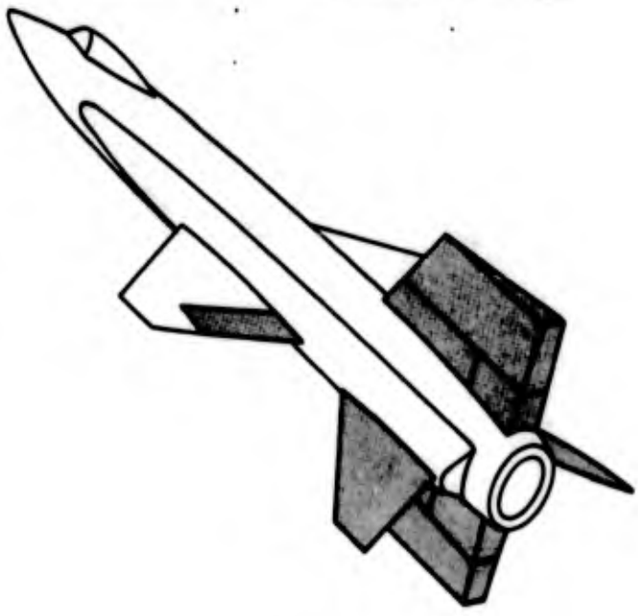

Figure 1

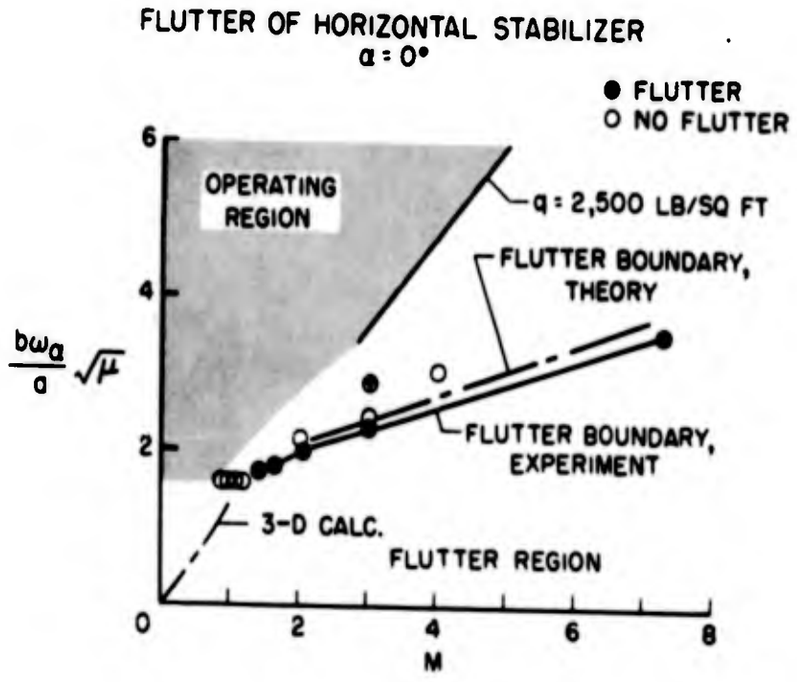

Figure 2

EFFECT OF ANGLE OF ATTACK ON FLUTTER
OF HORIZONTAL STABILIZER

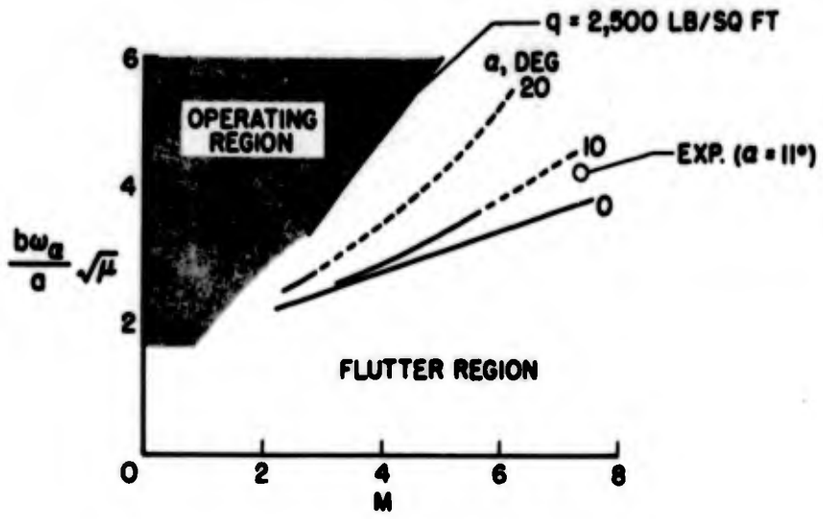

Figure 3

FLUTTER OF A DOUBLE WEDGE
RECTANGULAR; A=I; M=7

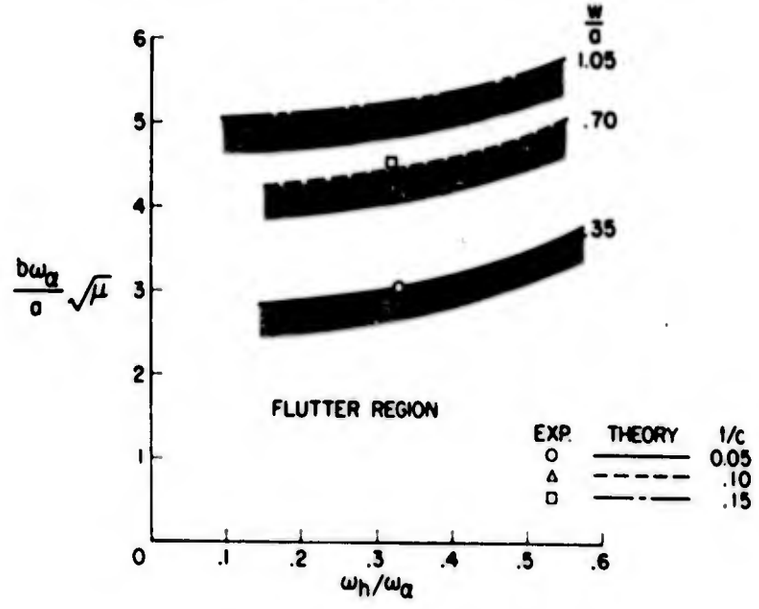

Figure 4

FLUTTER OF X-15/B-52

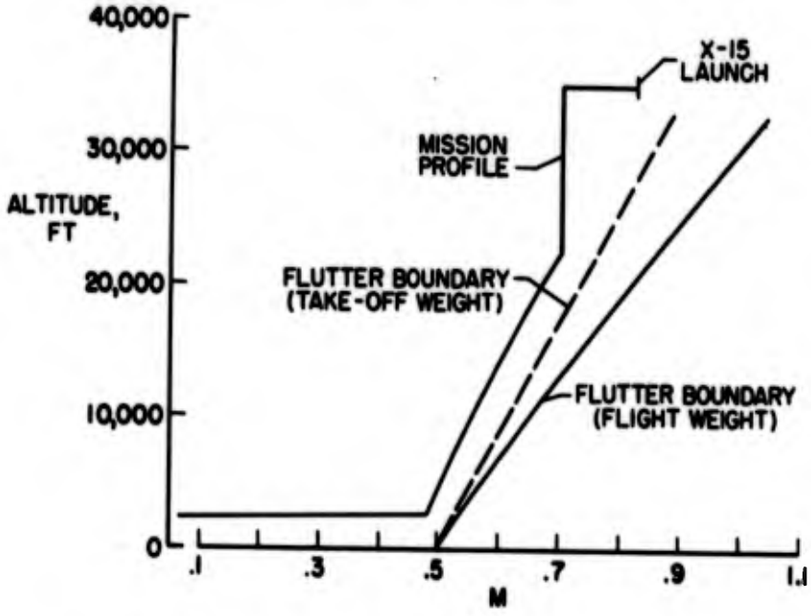

Figure 5

SOUND LEVEL DURING TAKE-OFF

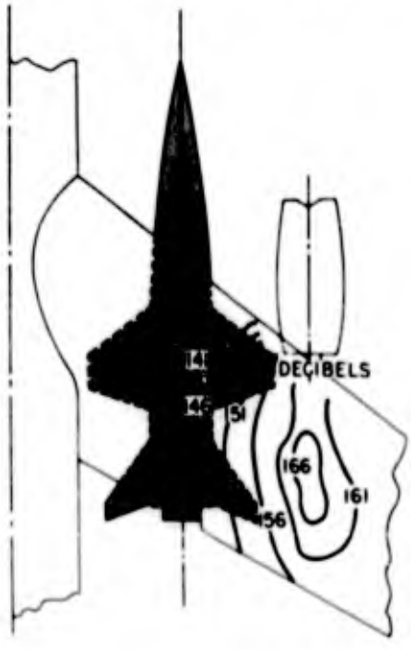

Figure 6

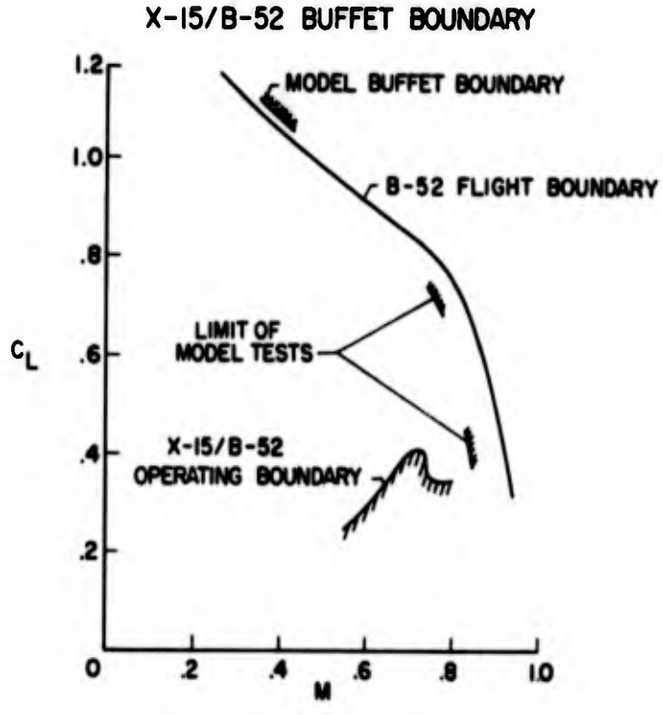
X-15/B-52 BUFFET BOUNDARY
MODEL BUFFET BOUNDARY
B-52 FLIGHT BOUNDARY
LIMIT OF MODEL TESTS
X-15/B-52 OPERATING BOUNDARY
C_L
1.2
1.0
.8
.6
.4
.2
0
.2
.4
.6
.8
1.0
M

Figure 7

X-15 FORMING AND FABRICATION METHODS

By I. J. Wilson

North American Aviation, Inc.

INTRODUCTION

The X-15 research airplane is a high-speed, high-altitude, rocket-propelled vehicle. These performance parameters have dictated a design with component configurations and material requirements which differ from those previously encountered in the more conventional type of aircraft. The nickel-base and titanium alloys that comprise the bulk of the X-15 structure have presented a challenge in the areas of forming, machining, and fabrication. In general, conventional methods have been employed with necessary modifications to accommodate the configurations of the airplane components and the limitations of the materials. In many instances an involved and exhaustive development program was required to establish the method and technique required to make a part successfully. In some instances, success was met only by compromising the design to accommodate the best effort of manufacturing.

Figure 1 is a cutaway view of the X-15 showing the various structural components to be discussed. The skin and the fuel tanks, which comprise the bulk of the fuselage, are of Inconel and Inconel X. The internal structure, frames, bulkheads, and other components are principally of titanium.

TITANIUM-ALLOY PROBLEMS

The titanium alloys, particularly 5Al-2.5Sn, have presented the most problems from a material-properties standpoint. Poor surface, notch sensitivity, low ductility, and inconsistency of properties are some of its characteristics. These items compound the difficulties encountered in a basically not-too-formable material. This is a characteristic of both the rolled and extruded form.

Titanium Surface Condition

Surface condition is probably the most important factor governing the formability of titanium. A poor surface is characterized by oxygen

contamination, inclusions, and grind marks. These defects may be removed by machining, polishing, or Chem-Milling.

Titanium extrusions are procured with sufficient material added to the basic shape to allow for machining of all surfaces prior to use, as illustrated in figure 2. Approximately 1/16-inch of material is required per surface for cleanup. A surface roughness of 125 microinches is satisfactory in all areas except where forming will occur; for example, in bends, joggles, etc. Here the maximum roughness should not exceed 63 microinches.

Formability of titanium sheet and plate may be significantly improved by resurfacing. This resurfacing may be accomplished by belt slab grinding and polishing or Chem-Milling. A limited test of 3/8-inch-thick material indicated that the minimum bend radius was reduced from 6 to 4 times the material thickness by using polished instead of unpolished material. The inability to determine, without destructive tests, the depth of oxygen penetration in a given area makes it difficult to determine whether complete cleanup has been effected.

If cleanup is to be insured, there should be a sufficient amount of excess material to allow for machining prior to polishing.

Forming Titanium Extrusions

The limited amount of stretch and shrink which may be introduced into a titanium extrusion during stretch wrapping presented a problem in forming the side-fairing frames. Figure 3 shows such a frame in the assembly jig. This frame is composed of four parts: the two fuselage caps and the two fairing caps. The extrusion is 5Al-2.5Sn. It will be noted that the inside flanges in the areas of the small bend radii have been relieved. This was necessary to prevent compression failure. Compression may be reduced by increasing the pull on the machine; thus the bend axis is shifted closer to the inboard edge. This, however, would result in a tension failure of the outboard flange. The relieved area was later filled by welding in a gusset.

Stress-Relieving Titanium

A formed titanium part is prone to crack until the residual stresses resulting from forming have been removed. This delayed cracking may occur within a few minutes or weeks later. Stress relief immediately after forming is a necessary safeguard, even though the

part may, subsequently, be fully annealed. This relief is required on all but the most slightly formed parts, such as skins.

FORMING PRESSURE VESSELS

Forming of pressure vessels has presented a number of problems. There are seven different pressure-vessel configurations used on the X-15. Where compatibility with the contained fluid permitted, titanium was the first choice from weight considerations. The hemispherical ends for the 14-inch cylindrical tank were formed on a 26-inch Cincinnati Hydroform with little difficulty. The 16-inch hemispheres for the helium tank were also attempted on the hydroform but this forming method was not successful. The optimum blank size was greater than the maximum machine capacity of 26 inches. Using a smaller than optimum blank required excessive hold-down pressure, which resulted in minute surface cracks. Figure 4 shows the hydroform setup for the 16-inch hemispheres. It may be seen that the flange is practically nonexistant; thus, too small a blank size is indicated. Normally, the flange would be about $1\frac{1}{2}$ inches wide. The flange is necessary for hold-down pressure, which controls metal flow during forming. All drawn titanium was staged by using one die with interstage annealing.

At the time fabrication was started on the 16-inch and 23-inch hemispheres, the only alternate to drawing was spinning. The titanium hemispheres were spun in stages with the use of heat. The blanks were preheated, the spinning chuck was internally heated, and additional heat was applied by torches to raise the temperature to approximately 1,600° F. This produced an oxygen-contaminated surface which had to be removed. The spun parts were thicker than required and, in some cases, were not true hemispheres. Sizing was accomplished by machining, which also removed the contaminated surface. Machining was also required to match the two hemispheres prior to welding.

The 32-inch hemispheres of AM 350 corrosion-resistant steel were formed on a 7,000-ton hydraulic press using a deep-drawing process. Figure 5 shows the first stage of a hemisphere being removed from the die. This figure also shows the draw rings and pressure pins.

Excessive thinning occurred until the optimum pressure on the draw ring was established. Some difficulty was encountered due to uneven force of the pressure pins which resulted in nonuniformity of the draw around the periphery of the hemisphere. This difficulty resulted from small variations in pin lengths. These same parts were also drawn from Inconel X with little difficulty.

The hydrogen peroxide elliptical aluminum tank was formed in two halves on the hydroform to the maximum depth capacity of the machine and finished by spinning.

FORMING PROBLEMS WITH NICKEL ALLOYS

Nickel alloys used in the X-15 are Inconel and heat-treatable Inconel X. Both alloys, in the fully annealed condition, display good ductility and can be readily formed. However, because of the work-hardening characteristics of these materials, severely formed parts must be formed in stages with interstage annealing.

Forming of Torus Bulkheads

One of the first major forming problems concerned with X-15 fabrication was spinning the Inconel propulsion-tank bulkheads. The tank (fig. 6) comprises a large part of the fuselage. The tank is composed of an outer cylindrical shell and an inner cylinder. These are joined by torus bulkheads, one of which may be seen at the end of the tank. These bulkheads are formed in two segments with the split located midway between the inner and outer cylinders. Figure 7 shows the inner-cylinder assembly with the inner-torus segment welded into place. Similarly, the outer-torus segments are welded to the outer cylinder, and the two assemblies are then joined. The bulkheads are spun from preformed shapes consisting of welded cones. Figure 8 illustrates the preform and the final configuration of both the inner and outer segments. Early attempts were made to spin the inner segment from a flat sheet using heat. This method was unsuccessful and was not pursued further.

It was recognized from the beginning that spinning would have to be accomplished in stages and that a full anneal would be required after each stage. Figure 9 illustrates the various stages required for each segment from the initial preform to the last stage prior to final spinning.

The first spin blocks used for staging were made from hardwood; cast iron was used for the final sizing. The lathe used is shown in figure 10. Roller pressure is applied hydraulically. Because of the force developed, the wood blocks proved to be inadequate in that they deflected under the force of the roller. This over-deflection increased the rate of work hardening of the Inconel and resulted in fractures. The wood was then replaced by cast iron which eliminated fractures in parent metal.

Another problem which arose was weld cracking. The cones were machine-welded and radiographically inspected. Each weld was considered perfect prior to spinning. However, during spinning, multiple transverse cracks occurred in the welds. This problem started an extensive program to determine the cause of failure. The weld structure was analyzed both by North American Aviation, Inc., and the International Nickel Company and was found to be satisfactory. Different types of welding wire were tried, and the speed, feed, and pressure of the spinning lathe were varied, but the welds continued to crack. It became apparent that a complete recrystalization of the weld structure was required to obtain ductility equal to or better than the parent material. It was found that this requirement could be met by these steps in preparing the weld (fig. 11). The original weld had sufficient buildup to be ground flat a given distance above the parent material. This was then planished by peening and rolling flush with the parent material and finally is fully annealed. The amount of weld reduction during planishing is predetermined to introduce the required amount of work to recrystalize the weld when annealed. In most cases, this process produced a weld softer than the parent material, and no further problems were encountered with weld fractures.

Once a part was completely formed, thinning was evaluated. It was found that the Inconel had been "ironed out" between the iron spin block and the steel roller and was below the minimum thickness in some areas. This spinning is illustrated by figure 12. There were three approaches to solving this problem: increasing the material thickness with a resulting weight penalty, machining off the excess material, or reducing the amount of thinning. Obviously the latter was the most desirable, but also the most difficult. Reducing the amount of thinning was accomplished by substituting a hardwood tool for the steel roller on all but the final stage. The elasticity of the wood allowed the force to be distributed over a sufficiently large area. The only thinning encountered was that which resulted from stretching the metal to the required configuration.

Forming the Ogive Forward-Fuselage Section

Forming the ogive section of the forward fuselage presented some problems. Figure 13 illustrates the forming method employed. Being the outside skin, the material is Inconel X. The usual method of making a part of this type is to form the four segments and weld them together. However, in view of the size and the mold-line-tolerance requirements, sizing of such an assembly by any method other than bulge-forming would be difficult. Hence, it was decided that the most expedient production method would be to weld a cone and bulge-form the cone to the final configuration in one operation. The initial cone is made of 4 pieces

welded together. It is then placed in the bulge-form die; gas pressure is applied, and the part to the configuration is forced to the die. The only difficulty occurred in forming one part. One of the Inconel X sheets that was welded into the cone had a tensile yield strength about 28,000 psi greater than the other three sheets. During forming, this piece resisted stretching, so that the welds were distorted and wrinkles created. Reasonably uniform thickness and tensile properties are required for a good bulge-formed part.

Forming Beaded Side Panels

Some difficulty was encountered in forming the large beaded side panels. The fuselage section, which contains these beaded panels, is shown in figure 14. These panels would normally be produced by the drop hammer press. Due to size, however, the panels were made on a hydraulic press using matched drop-hammer-type dies. In forming the beads, the material is stretched so that stresses are induced. These stresses result in a "sway back" effect when the panel is removed from the die. This distortion perhaps would not have occurred if the part could have been formed by a hammer action. The rapid forming and the use of rubber would have resulted in localized stretching of the beads without stressing the adjacent area.

As a result of the deformation, resizing was required. This resizing was accomplished by stretching the panel over the male die using a Sheridan-Gray 750-ton stretch press. The minor wrinkling which occurred was subsequently removed by hand working.

CHEM-MILLING

An important technique to control weight is metal removal by a chemical etching process called Chem-Milling. This process allows for forming of a uniform section. Sculpturing of the formed part is not only economical but often is the only solution. Chem-Milling is often preceded by machining to eliminate variations in thickness within a sheet. Chem-Milling removes material at a constant rate; hence, thickness variations are not eliminated. This process has been used extensively on the X-15 for both the nickel and titanium alloys. Figure 14 also shows the Chem-Milled areas of the beaded side panels.

MACHINING

The principal difficulty in machining Inconel and titanium results from the toughness of the materials. There is a rapid breakdown of the tool cutting edge, which necessitates frequent and costly tool replacement. Also, cutting feeds and speeds are very slow. As a comparison, it takes approximately 15 times longer to machine Inconel X than aluminum. The average feed for Inconel X is 2 inches per minute with a speed of 50 surface feet per minute. The surfaces as machined average 125 microinches roughness, and hand finishing is generally required to meet requirements. Sheet flatness required for surface machining is a function of the thickness. The sheet must be held flat on a vacuum chuck. On thick sheets, this requirement introduces difficulty and a considerable amount of time and effort are required to straighten the sheets prior to machining.

A surface roughness of about 16 microinches can be achieved by belt slab grinding. Each pass removes about 0.0002 inch of material. Due to the small amount of material removal, belt slab grinding is used only as a final surfacing operation, with the bulk of the material removed by machining. Belt slab grinding has been an important method in controlling weight by reducing thickness tolerances and by providing material to the required thickness when standard gages are unsatisfactory or unavailable.

Figure 15 shows a wing skin being trimmed in the Keller machine. The top panel is the pattern, the lower the work. The entire surface of this skin has been machined on a skin mill using a special low-speed head. The periphery of the skin has a tapered land that varies from 0.100 inch at the inboard edge to 0.080 inch at the tip; the center section is tapered from 0.080 inch at the inboard edge to 0.040 inch at the tip.

FASTENERS

The majority of the mechanical fasteners used in the X-15 are of an A-286 corrosion-resistant steel. These include rivets, nuts, and bolts. Some Hi-Shear rivets, in which 17-4PH corrosion-resistant steel shanks with Monel collars were used, and Inconel X bolts with A-286 nuts are also used.

Corrosion-resistant steel nuts and bolts created a seizure problem after exposure at 1,200° F. Use of a high-temperature thread lubricant (DuPage) on assembly made breakaway possible.

Most of the screws used have heads of reduced diameter to allow for countersinking of thinner sheets than would be possible with standard screws. All flush-head screws have the Torq-Set recess to improve breakaway.

Steel blind A-286 rivets were used. An annealed stem was required for thin sheets so that the upsetting effect would not enlarge the hole and force the sheets apart. Where sheet thickness allowed, a hard stem was used for strength.

CONCLUSIONS

In conclusion, it may be said, that through the combined efforts and cooperation of a large number of people, not only within North American, but also by the many suppliers, difficult and sometimes seemingly impossible forming and fabrication problems have been solved. Knowledge has been gained in fabricating such specialized items as pressure vessels and in working with Inconel, Inconel X, and the titanium alloys. Also, manufacturing processes and techniques have been developed which will prove invaluable in the future.

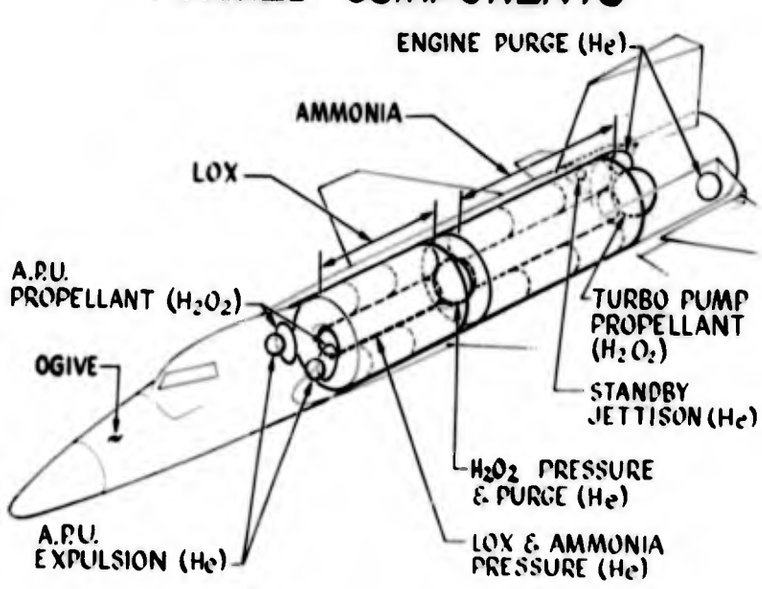

Figure 1

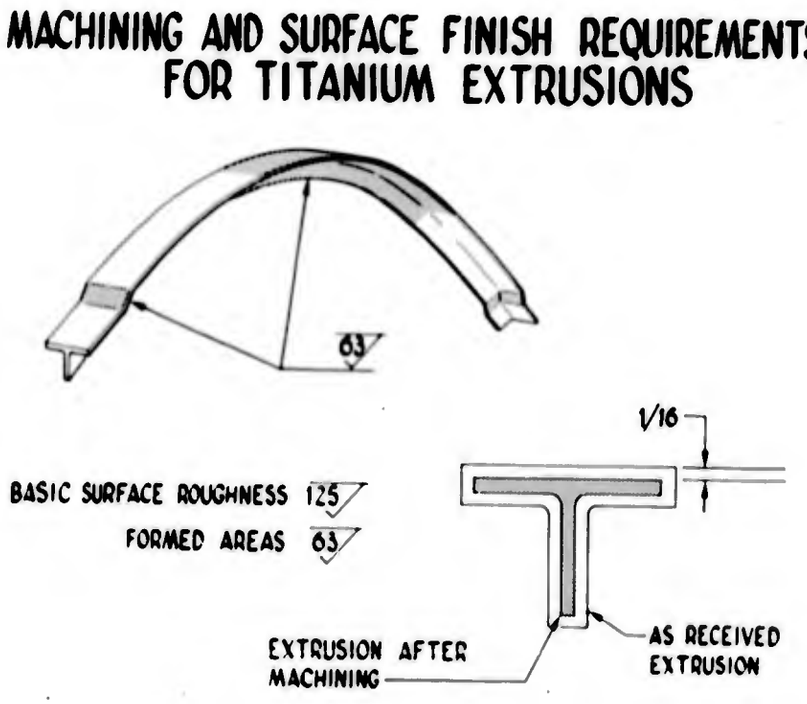

Figure 2.

BULKHEAD CAP TITANIUM EXTRUSION

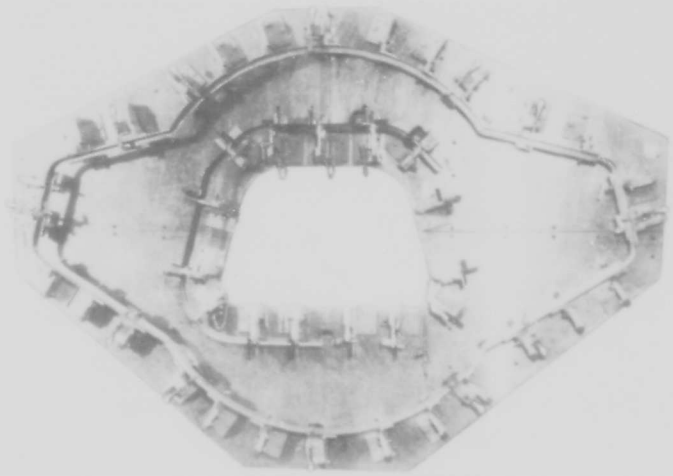

Figure 3

DEEP DRAW PRESSURE VESSEL
7000 TON PRESS

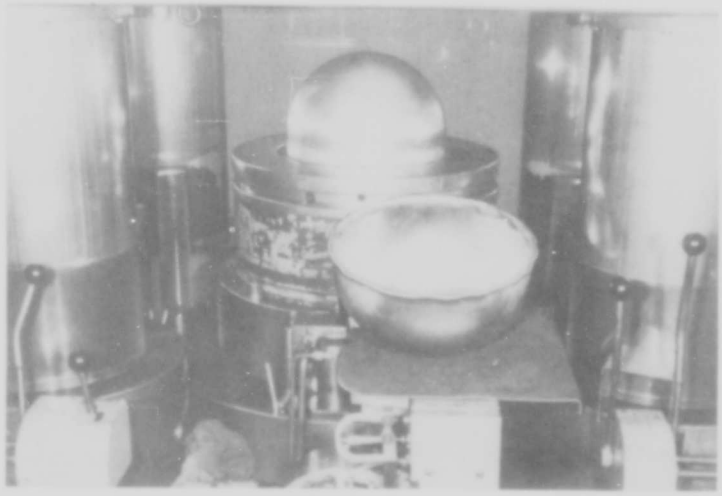

Figure 4

HYDRO FORMING PRESSURE VESSEL

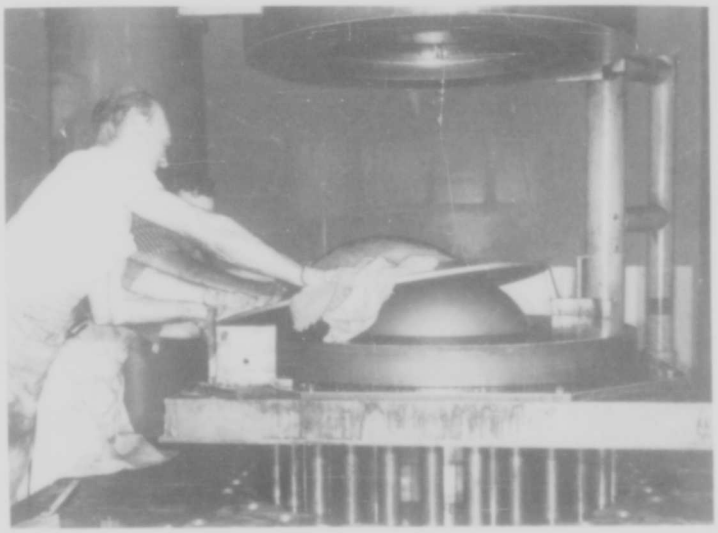

Figure 5

PROPELLANT TANKS

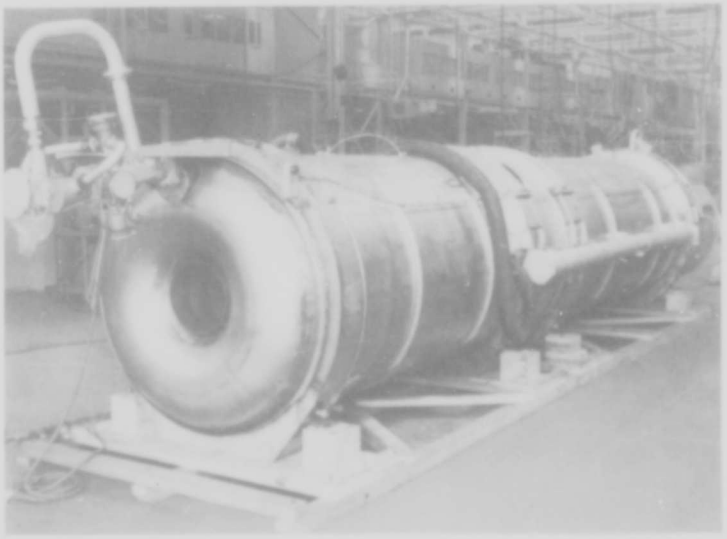

Figure 6

TANK INNER SHELL ASSEMBLY

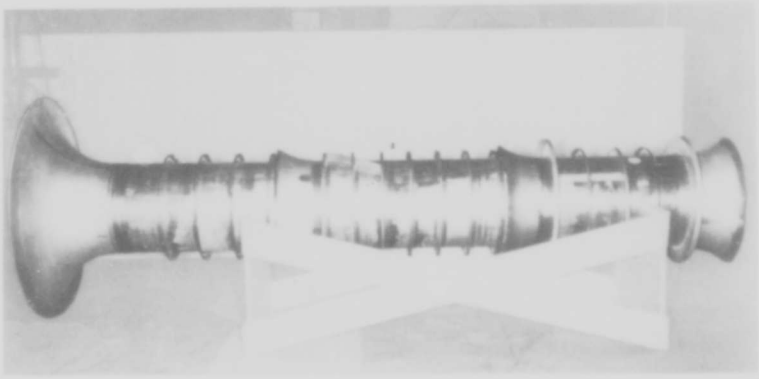

Figure 7

INNER AND OUTER TORUS BULKHEAD
BEFORE AND AFTER SPINNING

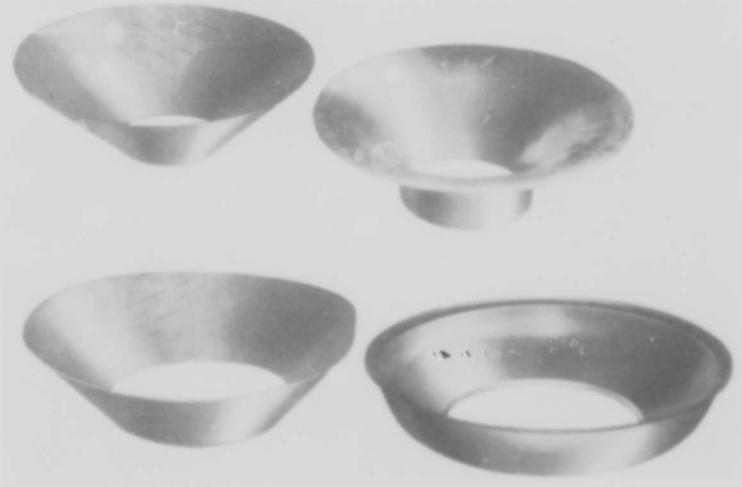

Figure 8

STAGES OF SPINNING INCONEL TORUS BULKHEADS
SPIN BLOCKS

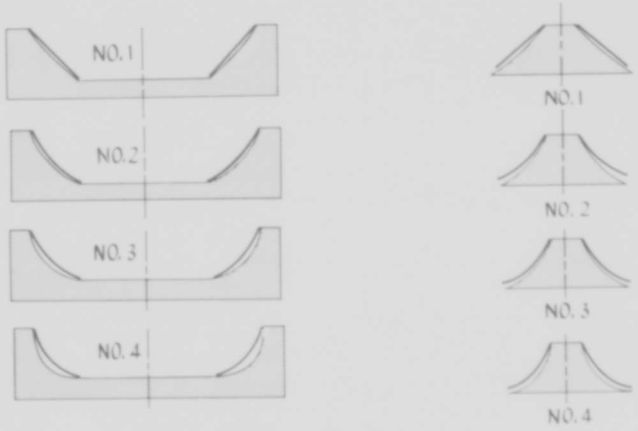

Figure 9

SPINNING INNER RING TORUS BULKHEAD

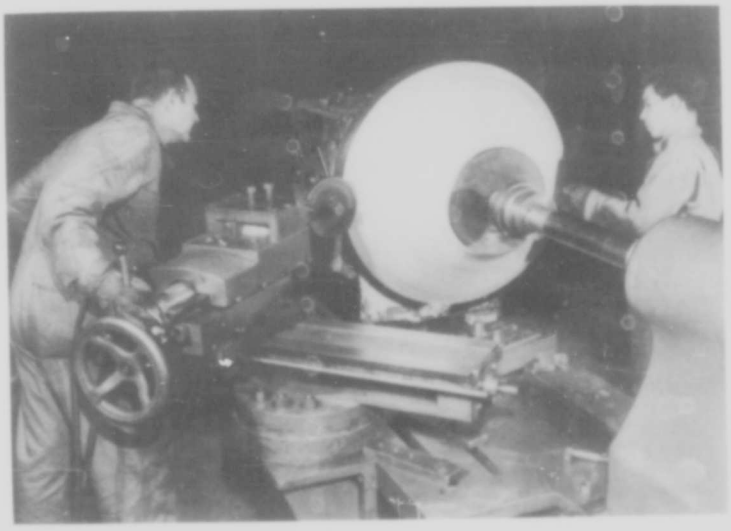

Figure 10

STEPS IN PREPARING INCONEL WELDS FOR SPINNING

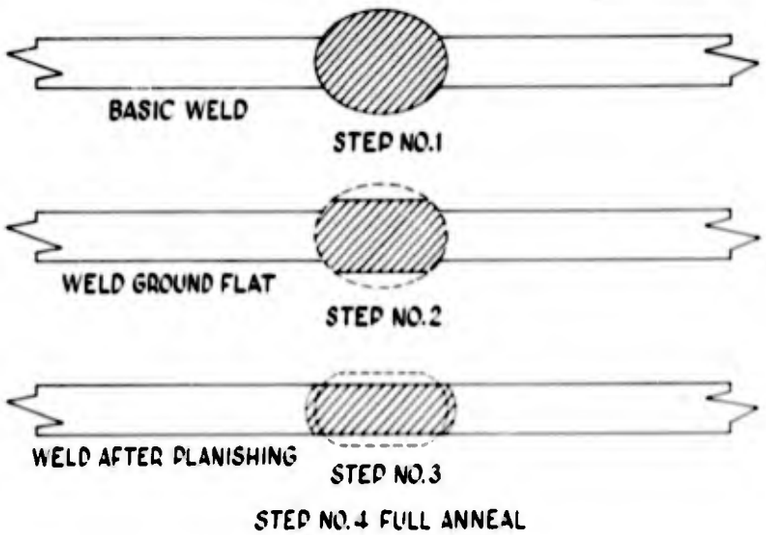

Figure 11

SPINNING INCONEL

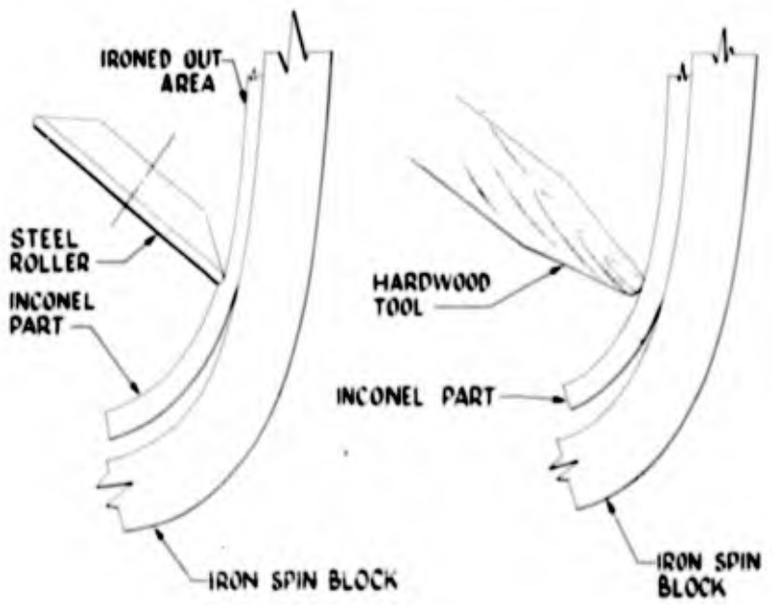

Figure 12

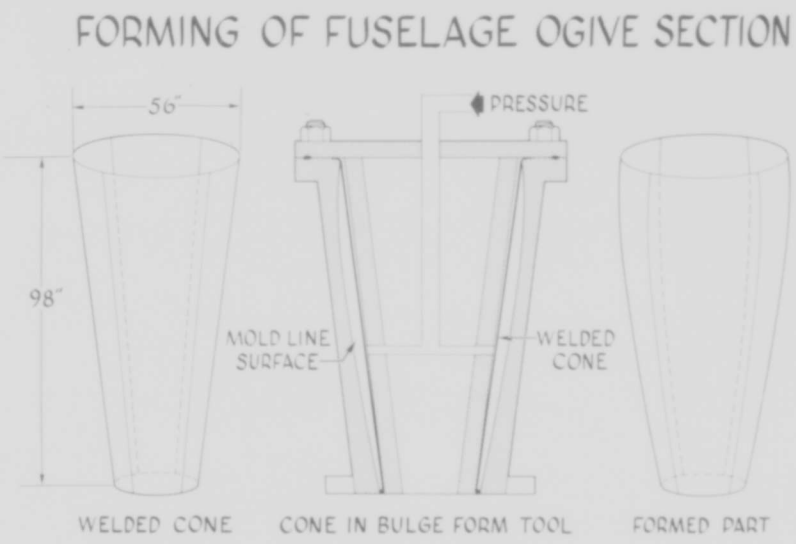

Figure 13

Figure 14

WING SKIN MACHINING

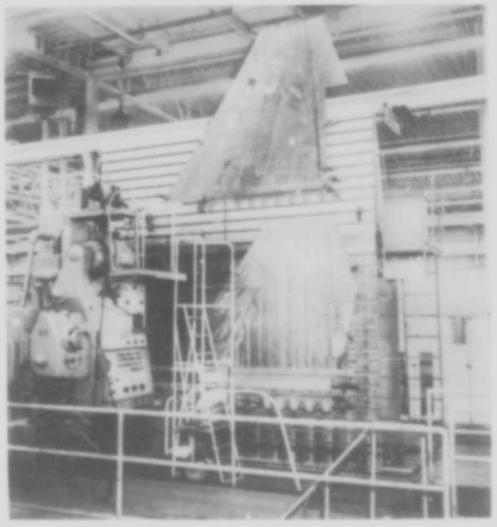

Figure 15

X-15 MATERIAL AND PROCESS DEVELOPMENT

By F. R. Kostoch

North American Aviation, Inc.

INTRODUCTION

The structural arrangement and the selection of materials for the X-15 have been described in previous papers. Instead of reviewing the materials and their application throughout the vehicle, a number of specific items are presented in this paper. These do not follow any particular sequence, but represent highlights and interesting developments in the material and process applications on the X-15.

At the X-15 conference in 1956, two problems were discussed: the use of Inconel X and seal developments. This paper presents several examples of the work done on Inconel X. Forming problems are discussed in the paper by I. J. Wilson. The seal problems have been successfully solved by detail designs and do not pose any significant developmental problem today.

STRUCTURAL MATERIAL SELECTION

Material Selection Based on Operating Temperatures

The dual role of the main fuselage tanks, that of carrying structural loads as well as fuel, produced a dual temperature problem. Not only must the high temperature of operation be considered, but the very low temperature for liquid-oxygen containment must also be handled. Most steel and common heavy structural alloys gain strength but lose ductility when operated at low temperatures; however, Inconel X appears insensitive, as shown in figure 1.

Martensitic alloys, such as heat-treated 4130 low alloy and AM 350 precipitation-hardening corrosion-resistant steels, follow predictable curves showing severe ductility loss as the temperature decreases below -100° F. The titanium alloy containing 5% aluminum and 2½% tin shows a favorable trend (which would also be true in the case of aluminum) but the titanium alloy would not have the requisite strength at 1,200° F; hence Inconel X was selected for the major tank material.

Material Selection Based on Temperature Differentials

Significant thermal gradients exist in several areas on the X-15. Those for the wing internal structure are shown in figure 2. To overcome the problem of thermal gradients, both design ingenuity and material selection were employed. It is desirable to employ a material having a low modulus of elasticity so that the gradients (which may be as large as 900 Fahrenheit degrees) will not produce unduly high stresses. The idealized graph in figure 3 illustrates the magnitudes of tensile thermal stresses in webs made of materials with different moduli: 15,000,000 psi for titanium alloy and 28,000,000 psi for the iron- or nickel-base material. In the case of the wing, the outside skin operating at 1,200° F expands, and this strain is transmitted to the cooler substructure. Because of the lower modulus of titanium, the induced stress is much lower than would be the case if an iron- or nickel-base alloy were used.

WELDING

In the effort to achieve high-order structural efficiency and to provide good integral tank design, both fusion and resistance welding have been used as primary assembly procedures. The methods used and the problems encountered in welding are illustrated by the propellant tanks and the horizontal-stabilizer beam, which are made of Inconel X, and the propellant pressurization vessel, which is made of titanium alloy containing 5% aluminum and $2\frac{1}{2}$% tin.

The X-15 is the first air vehicle to use Inconel X sheet and plate extensively, and while Inconel X is considered a weldable alloy, there was little or no detailed experience available on welding for airframe structures.

Resistance Welding of Inconel X

Resistance welding has been employed for both structural and leakproof welds. (See fig. 4.) As might be expected, it was necessary to develop weld machine settings in the typical fashion used for stainless and aluminum grades. Several different reactions were found which markedly influenced the welding sequences.

It was determined that high pressures are required to contain the nugget, but these high pressures, if continuous, would cause indenta-

tion. Consequently, an overlapping spotweld* sequence was developed, with a lower pressure being used during the welding portion of the cycle and a higher one during the forging and solidification portion. These pressures are, respectively, about 2 times and 3 times those used on annealed 18-8 stainless steels. Good fit-up of detail parts is essential so that the welding and forging pressures may be used for these purposes and not to achieve matching of the parts.

All weldments are made in the annealed condition and the biggest single problem has been the control of the effect of work hardening due to forming. The problems resulting from varying hardnesses of material during resistance welding are common to most alloys, but are extremely critical with Inconel X. Because of the high pressures and long weld times, settings are very critical, and obtaining coupons with the proper degree of work hardening for selecting the settings is a laborious and difficult control problem. Further, the spread in hardness over the whole area of forming is a serious consideration. It has been found that a spread of ±5 Rockwell B is about all that can be tolerated. If the spread is wider than this, the detail must be annealed before welding.

All welds are stress relieved after welding at 1,625° F and before heat treatment. Inconel X has a low ductility in the range from 1,250° to 1,500° F, and unless the welds are stress relieved, "locked-in" welding stresses can cause cracking during the heat-treating cycle.

Two other processing features to be noted are the short welding-tip life due to the high pressures required and the cleaning problem of providing a uniform oxide surface. The latter is analogous to the problem with aluminum but the surface is not as critical.

Fusion Welding of Inconel X

Fusion welding of Inconel X can be done by using many of the standard techniques used for stainless steels. Response is similar in such things as the chilling effects required of tooling fixtures and the rates of contraction on cooling. However, in most cases, the total weld shrinkage is greater.

Welding of heat-treated material is not recommended as a regular procedure. Such welding can be done, but a high degree of skill is needed and a very careful analysis of welding sequence must be made and rigid process control must be exercised.

To circumvent the welding of heat-treated Inconel X, as in cases where weldments are employed for final assembly procedures (closeouts), intermediate sections of Inconel are used. These sections are added before heat treatment, and since the Inconel is not affected by the heat treatment the closeout weld can be made with normal procedures.

Two applications of this design method are shown in figure 4. The hemispherical torus bulkhead on the left of the figure is made of two sections of Inconel with a closeout weld joining them. To the right, a door is shown which is made by welding a section into a cutout in the Inconel X skin. After heat treatment another, smaller cutout is made and an Inconel door with a plumbing outlet is welded into the cutout hole.

Figure 5 is representative of the type of tooling required for welding of large components of airframes. The welding head shown is making a circumferential fusion weld.

Another example of complicated welding which, when properly tooled and sequenced, can be done successfully is shown in figure 6. This horizontal-stabilizer beam required much checking and test welding to arrive at the proper size for detail parts and for tooling dimensions. This piece is an all-welded assembly made up of 17 details ranging in gage from 0.032 to 0.325 inch. The overall length of the longest section is 84 inches. The part is heat treated after welding, and with proper fixturing a very satisfactory part is produced. With proper controls and tooling, Inconel X is not a difficult material to fusion weld in the annealed condition.

Fusion Welding of Titanium

One of the more difficult welding tasks on the X-15 is the fabrication of the helium pressurization bottle shown in position in figure 7. This bottle is made from titanium alloy containing 5% aluminum and 2½% tin. Titanium is severely embrittled by oxygen and nitrogen during fusion welding unless extreme precautions are taken to exclude air from the weld area. Such exclusion of air is most difficult even in the laboratory. In the shop, the problem is further complicated by the wide variety of sizes and shapes to be welded.

An example of this problem is the machine welding of the cylinder which, with domed ends, makes the vessel assembly. The cylinder is 86 inches long and 14 inches in diameter, with 3/8-inch walls. Two longitudinal welds are required to join the formed half-shells.

Welding is performed by the inert-gas-shielded tungsten-arc process, and a conventional welding fixture (fig. 7) is used to position the parts for welding and to maintain dimensions. Even when a trailer shield was used on the welding torch, samples welded with this unmodified equipment were discolored and laboratory tests indicated weld embrittlement. It was evident that air was coming in contact with the hot weld area due to inadequate protection from Venturi effects, drafts, and leaking pneumatic equipment during the full welding cycle.

The following modifications of conventional welding equipment were made and have successfully eliminated embrittlement of the longitudinal welds due to air contamination:

(1) Enclosing the entire bottom of the welding fixture by means of a plastic bag (fig. 8). This bag is purged with inert gas, and is capable of being partially evacuated to facilitate purging (fig. 8).

(2) Enclosing the entire top of the welding fixture by means of a sliding aluminum cover (fig. 9). This enclosure is purged with inert gas.

(3) Attachment of a trailer shield to the welding torch.

(4) Use of an oxygen-detecting device for determining the effectiveness of elimination of air from the enclosures.

(5) Use of argon for pressurization of pneumatic hold-down fingers.

The use of such modifications affords a positive means of consistently providing the required degree of weld shielding to avoid weld embrittlement by air contamination. Similar modifications of conventional welding equipment have been successfully used on a number of weld joints in X-15 components.

HEAT TREATING ON INCONEL X

As was mentioned earlier, all fusion welding is designed to be done before heat treatment. Consequently, some elaborate fixtures are needed for control of contour during the heat-treating cycle. Figures 10 and 11 show the fixture for heat treating a wing skin. This skin is made by welding together three tapered sheet details prior to heat treatment. The weight of the fixture is 4,300 pounds whereas the skin weighs 180 pounds. This comparison illustrates the complexity of manufacture which can be encountered.

BRAZING OF HELIUM-GAS LINES

The fuel system uses helium gas for pressurizing the system. Helium gas is somewhat difficult to contain, and problems with standard line fittings were envisioned. To insure a reliable leak-free system, a method for joining tubing with brazed-in-place fittings was developed.

The tooling for use on the X-15 is shown in figure 12. A temperature-controlling power unit coupled to a clamshell resistance heating tool is used. The tool permits brazing in place during assembly, and with proper process control, joints having predictable and adequate strength can be made. Figures 13 and 14 show the failure modes for both static and pressure testing. These failures are exactly what is anticipated when satisfactory brazing is accomplished on such a design.

LUBRICANT TESTING AND SELECTION

Typically, the X-15 employs both antifriction and journal bearings. The designers, by location and heat-sink provisions, have kept bearing operating temperatures below 600° F. Therefore the major problem was to find suitable lubricants, the materials for bearings not being a problem at this temperature. Through test work, satisfactory lubricants have been selected. For the antifriction bearings 10 greases were tested, and for plain bearings 25 greases were tested.

Extensive tests of lubricants and bearings by North American Aviation, Inc., have indicated that the only good method for obtaining comparative data on lubricant capabilities is by testing the lubricants in bearings. Shown in figure 15 are two journal shafts used for tests of two greases which were recommended on the basis of simulated tests. The severe galling of the piece on the left after a few (350) cycles compared with the "no-failure" 20,000-cycle piece on the right illustrates a result which is frequently attained when a representative rather than a simulated test is run.

The effect of high-altitude operation, such as boiling-off of the lubricant, has been investigated for antifriction bearings. In figure 16 are plotted the torque changes on an antifriction bearing caused by changes in temperature and simulated altitude. The initial drop in torque is typical because the lubricant softens with increasing temperature. After this initial softening, a relatively constant torque prevails even after the temperature is reduced to 70° F and held for an

appreciable time. The altitude (low pressure) had no apparent effect. Similar tests on plain bearings are in progress.

Concern has been expressed about the operation of bearings at high altitudes, particularly in connection with loss of lubricant effectiveness at low ambient pressures. The possibility of the lubricants "boiling off" has also been expressed. A demonstration test was made in the high-altitude chamber at Litton Industries, employing a sliding block on an inclined plane. At simulated high altitudes the block would not slide down the steeply inclined plane. This apparently corroborated the fear that bearings might not operate satisfactorily at high altitudes. Tests of antifriction bearings by North American did not show the same phenomenon and the plain bearings are not expected to show it either. The reason for the difference between results with the sliding block and with lubricated bearings arises from the preparation given the test specimens. The sliding block and the plate were degreased, vapor-honed, and degassed by long exposure to the high-altitude environment; hence the surfaces were very clean. High friction coefficients are common between clean surfaces. Lubricated bearings exhibit the opposite condition because the surface is intentionally soiled by covering it with a lubricant.

CONCLUDING REMARKS

A variety of examples of material application and process development on the X-15 have been presented. They are illustrative of the kind of problems which have been encountered and solved during the course of design and fabrication of the vehicle.

Some problems which have arisen are not yet completely solved. There are currently two major problems which are under intensive study: (1) the manufacture of satisfactory pressure bottles from titanium alloy containing 5% aluminum and 2½% tin and from AM 350 precipitation-hardening stainless steel and (2) the welding of Inconel X in the heat-treated condition to simplify initial manufacturing assembly and to minimize repair procedures.

COMPARATIVE NOTCH STRENGTHS

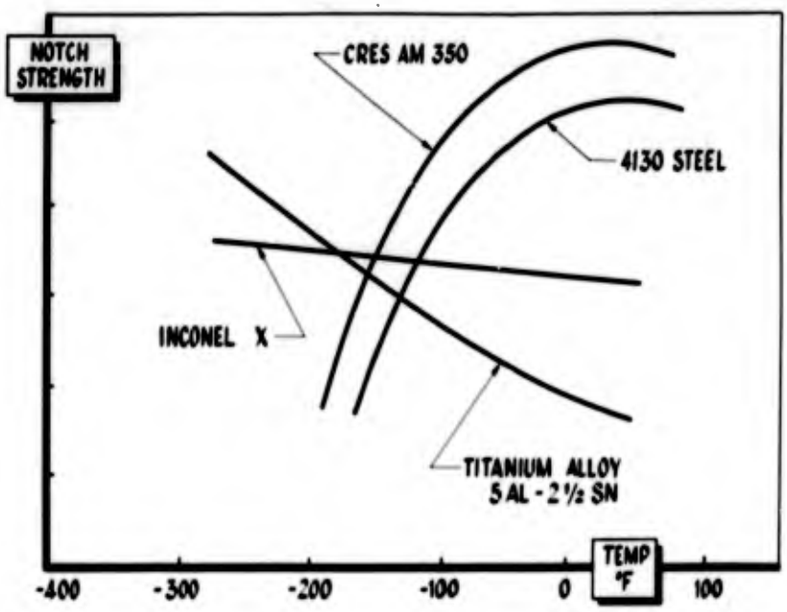

Figure 1

WING TEMPERATURE GRADIENTS

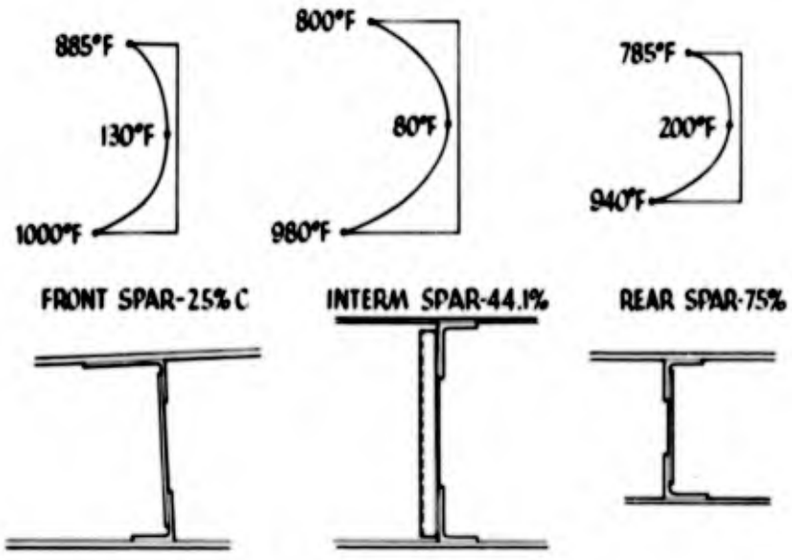

Figure 2

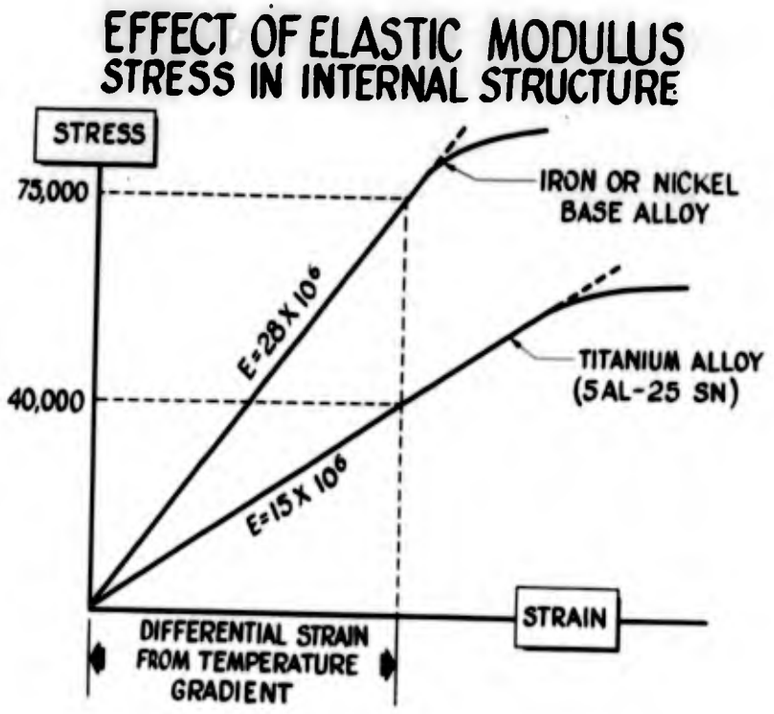

Figure 3

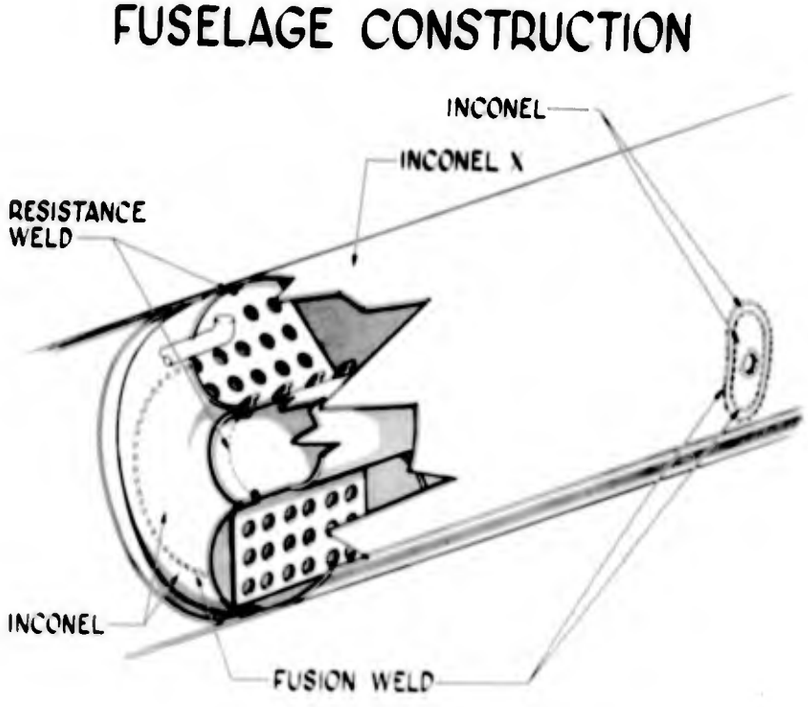

Figure 4

FUSELAGE TANK WELD FIXTURE

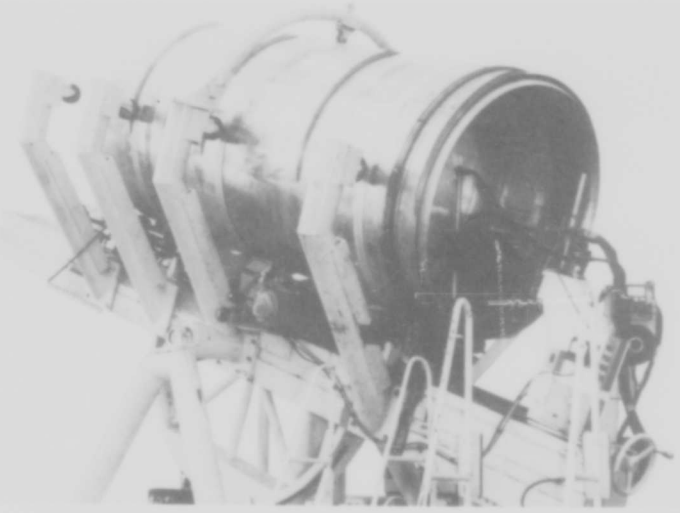

Figure 5

STABILIZER SUPPORT BEAM

Figure 6

MACHINE WELDING FIXTURE

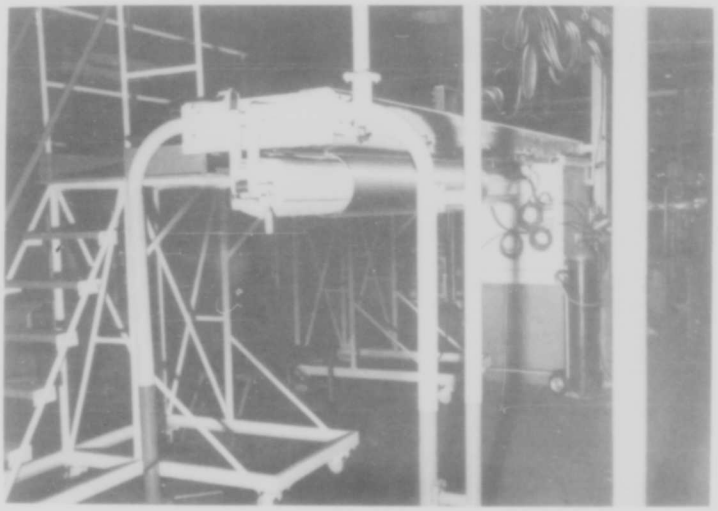

Figure 7

WELD FIXTURE WITH GAS SHIELD

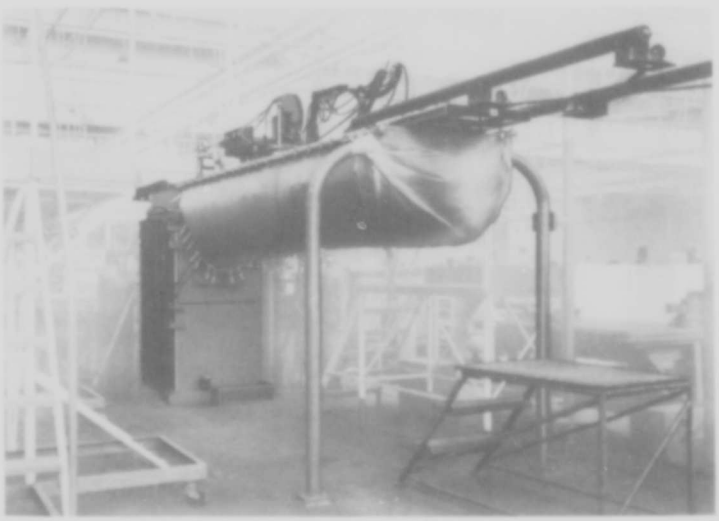

Figure 8

WELD HEAD & CONTROL UNITS

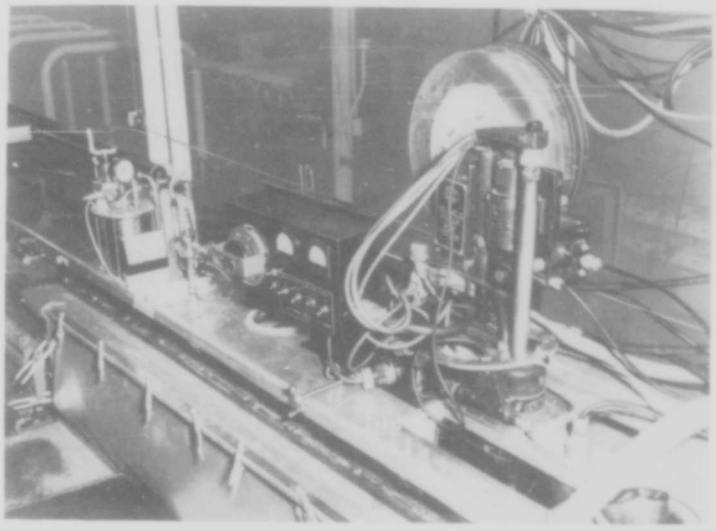

Figure 9

WING SKIN HEAT TREAT FIXTURE

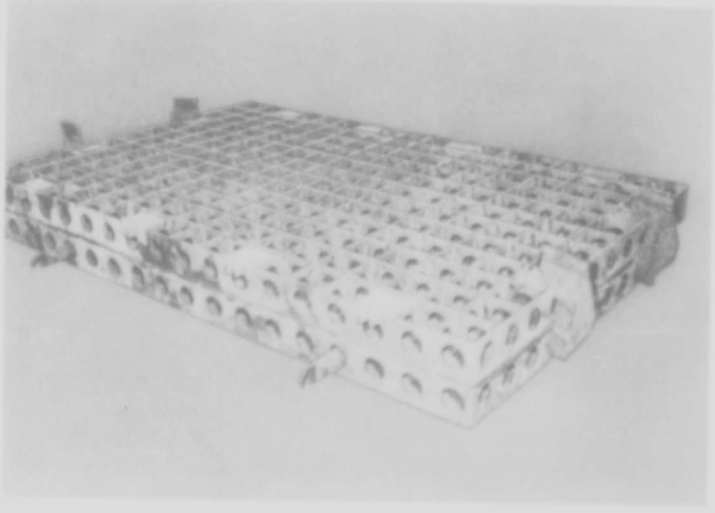

Figure 10

WING SKIN IN HEAT TREAT FIXTURE

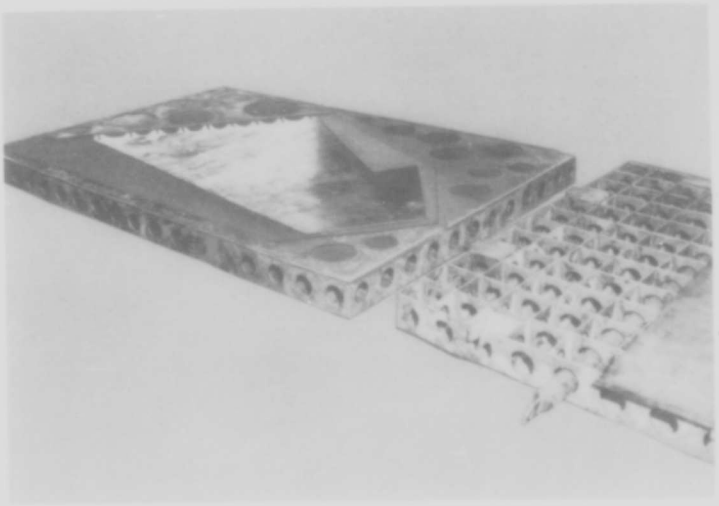

Figure 11

BRAZING OF LINE FITTINGS

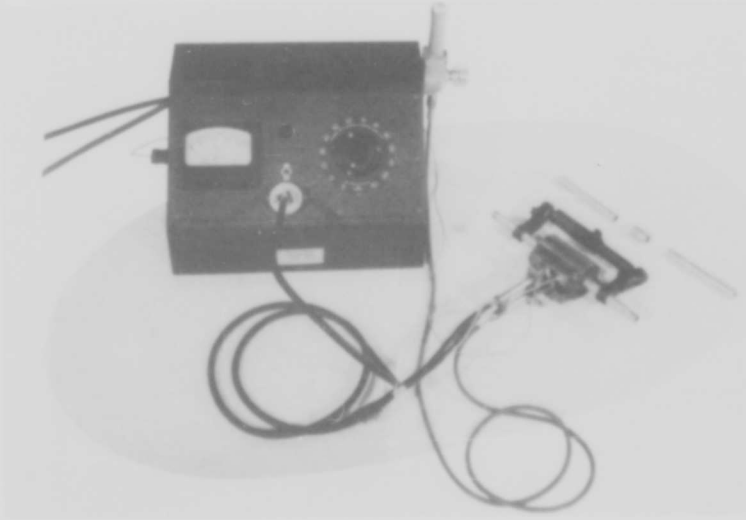

Figure 12

BRAZED TUBE ASSEMBLIES
FAILED BY HYDROSTATIC BURSTING

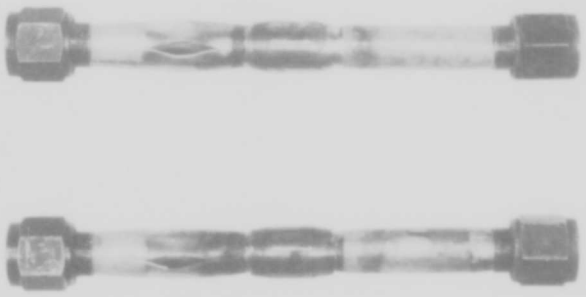

Figure 13

BRAZED TUBE ASSEMBLIES
FAILED IN TENSION

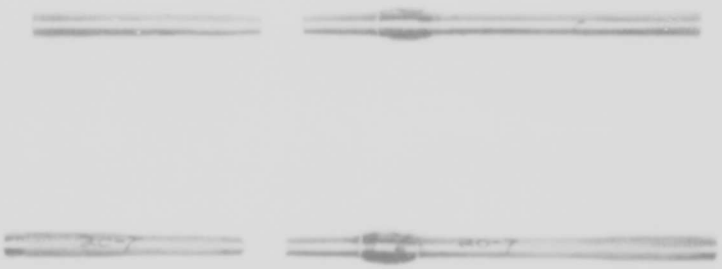

Figure 14

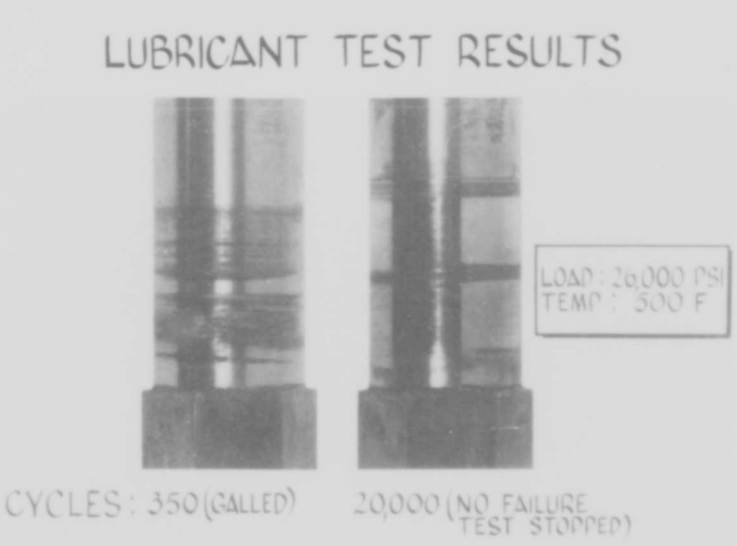

Figure 15

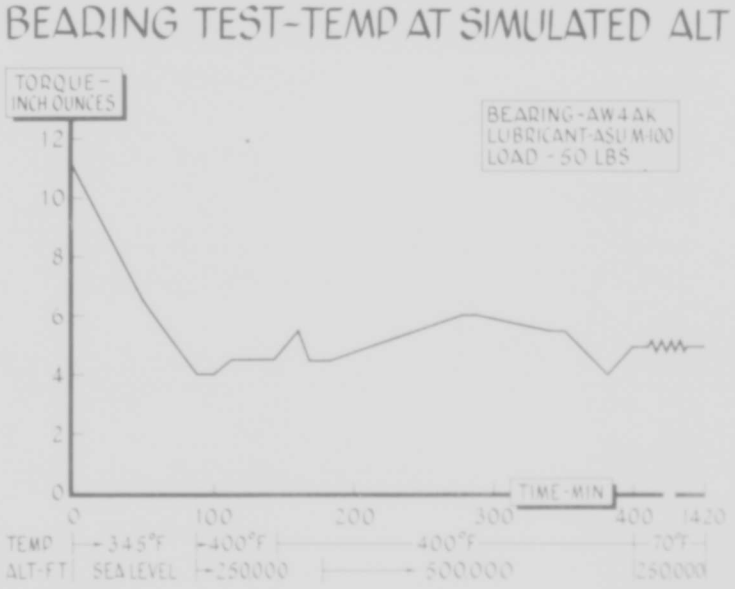

Figure 16

THE XLR99-RM-1 ENGINE FOR THE X-15 AIRPLANE

By Robert W. Seaman

Reaction Motors Division
Thiokol Chemical Corporation

The basic functional requirements of the XLR99-RM-1 rocket engine for the X-15 aircraft are:

(1) Pilot-controlled power output from 15,000 lb thrust to 50,000 lb thrust at sea level, giving approximately 58,500 lb thrust maximum at 100,000 feet

(2) Restarting capabilities while airborne by use of pilot controls only

(3) Operations over a broad range of environmental conditions and tolerance of an even broader range while not operational

a. Temperature -40° F to approximately 200° F when firing
b. Temperature -40° F to approximately 500° F when nonfiring
c. Attitude, all positions
d. Altitude essentially unlimited

(4) Piloted aircraft safety

(5) Duty cycle approximately 1 hour of accumulated firing time and 100 starting cycles over a period of 1 year

The overall dimensions of the engine are approximately 72 inches in length and 43 inches in diameter. The engine consists of two basic sections, the thrust-chamber—turbopump assembly and a hydrogen-peroxide valving assembly. (See fig. 1.) The North American airframe engine mount is placed in the engine assembly during construction of the engine. The engine is installed in the aircraft as a single assembly with the hydrogen-peroxide valving assembly attached to the aircraft firewall. An installation bracket is then removed between the main engine section and the hydrogen-peroxide valving assembly allowing for relative motion between the main engine section and the firewall. A flame shield is provided at the exhaust of the chamber to effect closure with the aircraft in order to prevent backwash of jet flame into the engine compartment. Installation connections necessary are:

(1) Engine-mounting attachment at the North American Aviation, Inc. mount

(2) Mounting of hydrogen-peroxide valving assembly

(3) Flame-shield closure attachment

(4) Supply lines for liquid oxygen, liquid ammonia, hydrogen peroxide, and control gas

(5) 24-volt direct-current and 115-volt 400-cycle alternating-current power-supply lines.

All drain lines and overboard vents are passed through the flame shield and require no installation connections.

Prime elements in the assembly are, of course, the thrust-chamber assembly, turbopump assembly, gas generator for turbine drive, igniter assembly, thrust-chamber propellant valving assembly, and hydrogen-peroxide valving assembly.

The basic engine-system schematic showing the adjustments made since the conference of 1956 is shown in figure 2. The electrical system, purge-gas system, and pump lubricating-oil system are not shown. The sequence of operations is as follows: The electrical system is energized and engine "arm" is actuated, starting: (1) lubrication pump and system, and (2) hydraulic pump and system. Engine prime is commenced for cooldown of the oxidizer and fuel system through the pumps and to the propellant valves of both the thrust chamber and igniter. (The dashed lines between units indicate mechanical linkages.) The turbine gas-generator preheat cycle is also performed by prime function. The turbopump is started. Reference is made to figure 3 for illustration. All combustion sections are purged with helium for approximately 2 seconds; the first-stage igniter section fires, then the second-stage igniter section, and finally the main chamber. Shutdown is accomplished by shutoff of the main-chamber, second-stage-igniter, and first-stage-igniter propellant valves with gas purge entering downstream of the valves automatically when propellant pressures fall below the minimum thrust-operation point. The pump hydrogen peroxide shutoff valve is closed at the same time. The second-stage igniter continues to burn for approximately 1 second (following the shutoff of the main chamber) on propellants purged into the igniter from the line cavities between the upstream and downstream igniter valves. The first-stage igniter also runs during this period from the same source. The igniters burn or evaporate the propellants purged into the main chamber from the main-chamber injector section. Gas purge automatically commences on the igniter areas with the runout of propellants in those items.

Adjustments which have been made to the engine-system sequencing and configuration since the 1956 conference concern the elimination of the igniter-system accumulators, revision of the starting cycle, addition of an engine-idle condition, and elimination of the first-stage-igniter start-tank system.

The igniter-system accumulators have been eliminated by the substitution of a line volume between an upstream and a downstream second-stage propellant-valving system to perform this accumulator function on a blowdown cycle during engine shutdown. (See fig. 2.)

The elimination of the igniter start-tank system has been accomplished as a result of the determination that the turbopump system can actually maintain pumping operation under prime-flow conditions; therefore, the turbopump is utilized to supply the propellants for the first-stage igniter during the start cycle. Elimination of the start tanks results in the following three advantages: (1) Simplification of system, with increased reliability since the change removes 10 valving components, 2 tanks, and 26 feet of lines and connections, (2) elimination of the need for preflight and postflight servicing of the two start tanks, and (3) removal of approximately 20 pounds of dry weight and 6 pounds of wet weight.

The revision of the engine starting cycle and the addition of the engine-idle condition, which are closely related, results in:

(1) Starting the turbopump prior to the first-stage igniter instead of after to provide igniter propellant supply and operating the pump at the minimum thrust-level condition

(2) Firing of the first-stage igniter at the minimum thrust-level condition (a stable feed system no longer requiring transfer from the tanks to pump supply)

(3) Firing of the second-stage igniter at minimum thrust-level conditions (a single-level start as opposed to the prior system in which the second stage fired as the pump was starting and accelerating to the pilot demand thrust level)

(4) Firing of the main chamber at minimum thrust-level condition (again a single-level start requirement as opposed to the prior system in which the main chamber started when the second-stage-igniter chamber pressure exceeded minimum thrust level while both the turbopump and the igniter were in a transient state)

(5) Automatic unblocking of the governor system when the main chamber reaches minimum thrust, allowing thrust to increase to the throttle setting requirement

Operations (1), (2), and (3) represent the idling condition. This is with the turbopump operating at the minimum thrust condition, the first-stage and second-stage igniters operating at the minimum thrust condition, and the main chamber not firing. A minimum idling capability of 10 seconds is required, and a 30-second capability is desired. To

date, testing both on engines and on the "breadboarded" engine system (which is utilized in thrust-chamber evaluation) has demonstrated that at least the minimum time of 10 seconds can be provided.

The advantage of the start cycle adjustment is that it provides a stable platform for the start of the second-stage igniter and the main chamber, as opposed to the prior system which started both these items while the engine system was in a transient-rise state (ignition source as well as the item to be ignited). The provision of the engine-idle condition increases significantly the reliability of successful operation after release of the X-15 from the mother aircraft, since 90 component functions out of the 106 required component functions have been accomplished prior to release, leaving 16 to be accomplished following the release of the aircraft. Also, it has been the experience with prior aircraft that the ignition system is the most likely unit to cause the aborting of a successful flight. With the engine-idle configuration it is, therefore, possible to determine that the ignition system and the turbopump are operating satisfactorily before committing the aircraft to a flight.

Figure 4 depicts the variation of several major parameters for the engine, plotted against time, for a typical operation. In this sequence the engine pump is started and brought up to idling condition. The first- and second-stage igniters are started and brought up to the engine idling condition. At this point in this test, the engine is operating to the prescribed engine-idle requirement. After a short idling period, the main thrust chamber is fired with thrust rising to the minimum thrust value. At this point the governor is slowly advanced to higher thrust level. After a slight stabilization period the engine is throttled to an intermediate thrust range, which is followed by a fairly sharp increase in thrust, and finally by a second increase in thrust. After a stabilization period at this last thrust value, there is a sharp reduction to an intermediate thrust value, followed by a gradual thrust reduction and then shutdown, with main chamber and pump operation shut off first. The first- and second-stage igniters are then operating on blowdown cycle with the second-stage phasing out prior to the first stage thereby accomplishing the igniter purging operation on the thrust chamber.

(A motion-picture film was shown at the conference to demonstrate operation of the engine-igniter system and also operation of the complete engine assembly. The igniter sequence particularly demonstrated the shutdown sequence of the igniter system showing the blowdown cycle and gas purge. The sequence on an engine in operation showed the firing test from which the data in figure 4 were taken. Particular features noted were the engine-idle condition, the thrust control and variation, and the shutoff sequence including purge of the main chamber by the igniter.)

Figure 5 is a bar graph indicating the total accumulated testing time for various subsystems of the engine and for the complete engine which had been accumulated as of July 11, 1958. Covered in this graph is the total time accumulated on the engine assemblies and the "breadboard" engine (which is the thrust-chamber-development test installation), total time in the engine-idle condition, and total turbopump system time. As shown, engine and breadboard engine time is approximately 140 minutes, idle time approximately 15 minutes, and pump time slightly over 400 minutes. In addition to the items indicated, slightly over 1,000 minutes of time have been accumulated on the two-stage igniter section and approximately 1,400 minutes have been accumulated on the gas generator for the turbopump system.

Figures 6 and 7 depict preliminary data obtained on the vibration spectrum of the engine. Vibration conditions are shown during full-engine operation with the main chamber firing. These data illustrate the spectrum both along the thrust axis and normal to the thrust axis at the station of the engine to airplane mount connection.

During main-chamber operation, peaks of approximately 6g are realized in the plane along the thrust axis and peaks of approximately 5g are realized normal to the thrust axis (figs. 6 and 7). These data were obtained at an operational level of about 35,000 lb thrust. Additional vibration work is scheduled for the immediate future.

Figure 8 is a depiction of the sound level against distance and position obtained from preliminary sound measurements. As indicated, levels of 135 decibels are expected at approximately 50 feet forward of the engine assembly in line with the thrust axis and extending outward to approximately 250 to 300 feet at an angle of about 45° from the exit of the thrust chamber, with a reduction of noise level along the thrust axis in the aft direction to approximately 135 decibels at 100 feet. All the data used for this determination were obtained with the engine operating in the region of 45,000 to 50,000 pounds of thrust. Further data on noise level are being developed at shorter distances in the area affecting the B-52 mother aircraft.

In conclusion, developmental problems on the XLR99-RM-1 engine concerning life of the thrust-chamber-injector section have necessitated the use of the XLR11 engine for initial flight tests of the X-15. However, gains made recently have shown that this problem has been resolved and work is proceeding at a stepped-up pace toward successful conclusion of the engine development.

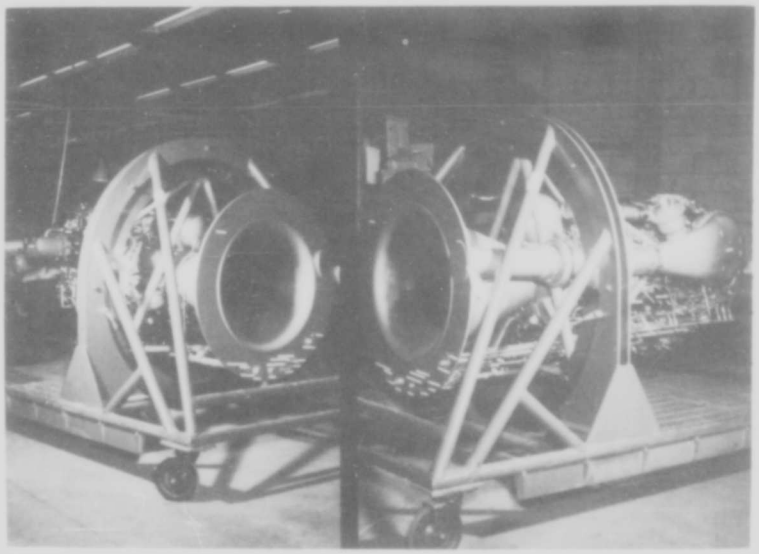

Figure 1

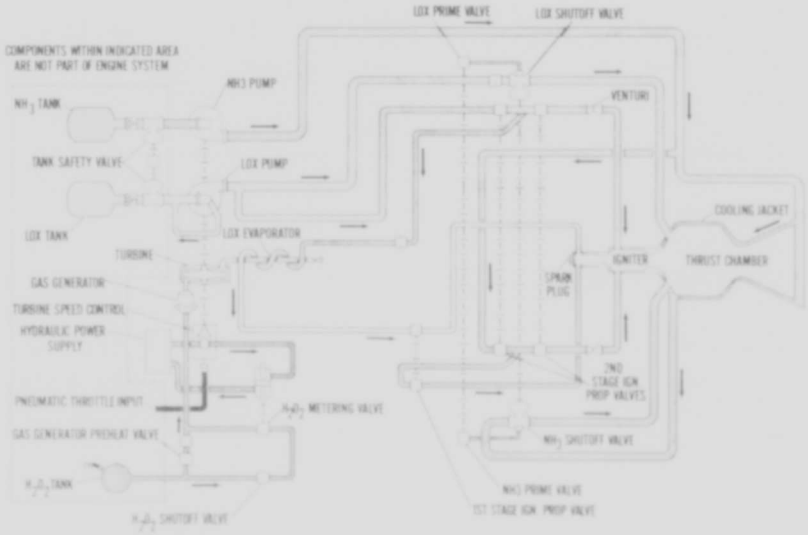

BASIC ENGINE SYSTEM

Figure 2

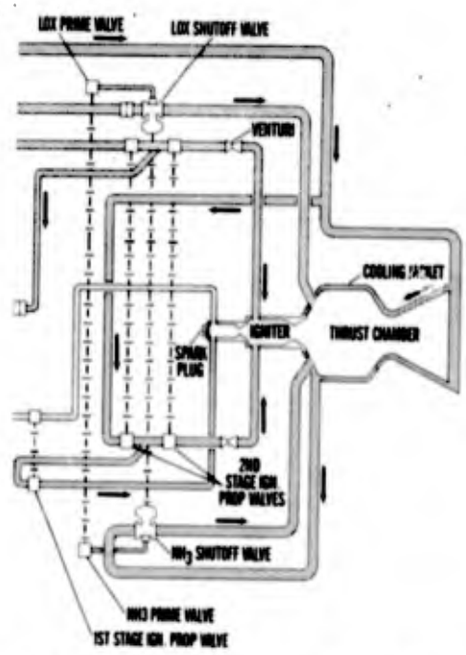

ENGINE COMBUSTION AND PROPELLANT VALVING SUBSYSTEM

Figure 3

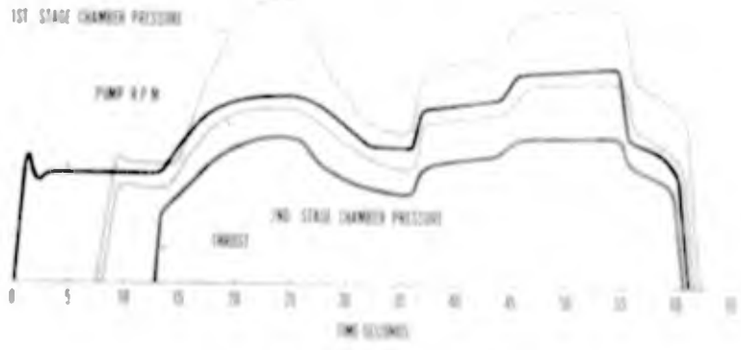

TYPICAL HOT RUN XLR 99-RM-1 ENGINE

Figure 4

ACCUMULATED TIMES ON THE XLR 99-RM-1 ENGINE AND COMPONENTS

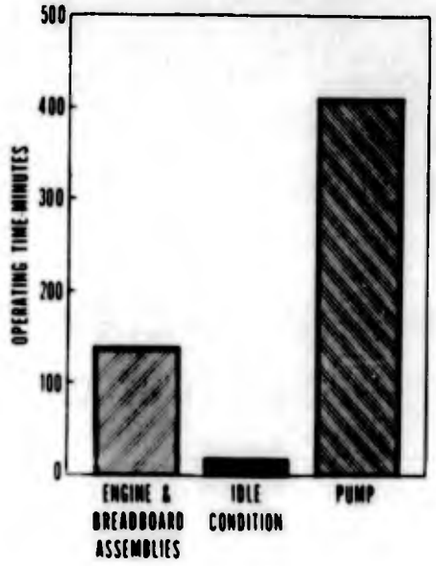

Figure 5

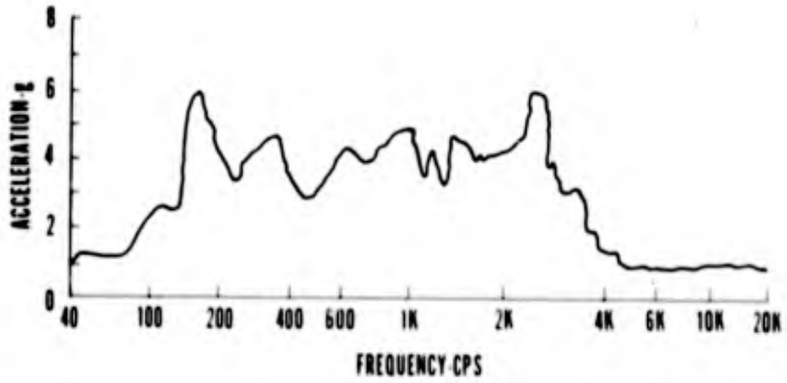

VIBRATIONS INDUCED BY XLR 99-RM-1 ENGINE ALONG THRUST AXIS

Figure 6

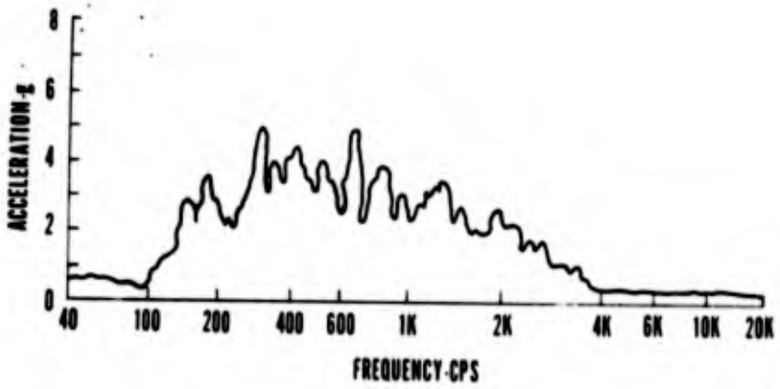

VIBRATIONS INDUCED BY XLR 99-RM-1 ENGINE NORMAL TO THRUST AXIS

Figure 7

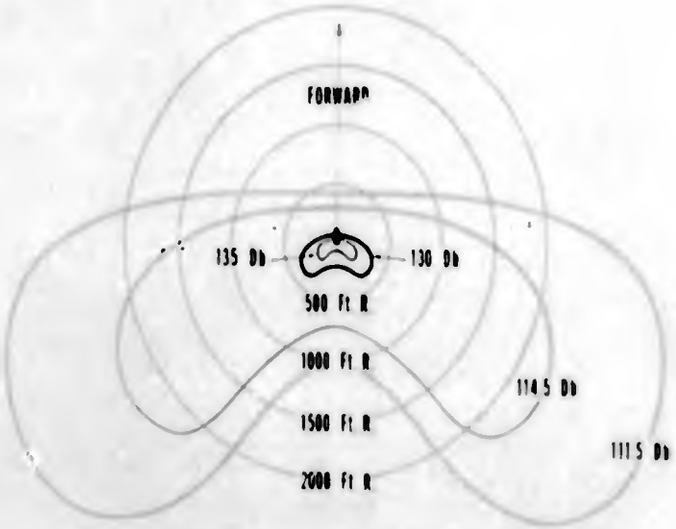

LINES OF CONSTANT SOUND INTENSITY SURROUNDING THE XLR 99-RM-1 ENGINE DURING FIRING

Figure 8

X-15 PROPELLANT SYSTEM DESCRIPTION

By J. W. Gibb

North American Aviation, Inc.

The present X-15 propellant system is basically of the same configuration as that described in the conference in 1956. The important design changes are that the carrier airplane has been changed from a B-36 to a B-52 and the internal plumbing between the compartments in the liquid oxygen (LOX) and ammonia tanks has been revised. Also, additional helium tanks have been incorporated into the pressurization system because the requirement for engine purge gas was increased.

The total propellant flow to the X-15 engine is in excess of 12,000 lb/min, or almost 20 times the fuel flow of a jet airplane engine. Transfer pumps for such high flow rates are not very practical, so the X-15 uses a pressure feed system for each of its propellants. Also, pressure is required to suppress LOX boiling. Each fuel container thus becomes a pressure vessel, and since, from a weight and safety standpoint, the pressure within the container must be a minimum, the plumbing was designed to keep the system pressure drops low. This means large line diameters and carefully designed tube inlets, outlets, and bends.

Figure 1 shows the major elements of the total propulsion system within the airplane profile. This picture is approximately to scale and demonstrates how much of the internal volume of the airplane is devoted to propellants. The liquid-oxygen tank of approximately 1,000-gallon capacity and the liquid-ammonia tank of approximately 1,400-gallon capacity are arranged to straddle the airplane center of gravity. A 75-gallon hydrogen-peroxide tank is located behind the ammonia tank. This peroxide, which is in addition to and separate from that used in the auxiliary power units, is decomposed into high-temperature gas and used to drive a turbine-propelled pump to boost the LOX and ammonia to engine manifold pressure.

Helium gas for tank pressurization and liquid expulsion, for engine purging, and for operation of pneumatically controlled valves is stored at 3,600 lb/sq in. in vessels located throughout the area of the propulsion system. For liquid expulsion from the LOX and ammonia tanks, a cylindrical vessel with a capacity of about 7 cubic feet is maintained at -300° F within the core tube of the LOX tank. For peroxide expulsion, engine purging, and pneumatic control three spherical vessels maintained at about -30° F contain an additional 6.5 cubic feet of gas.

Figure 2 is a simplified schematic diagram of the propellant feed and transfer systems, including the portion associated with the carrier

airplane. This carried-flight "top-off" system for the X-15 LOX tank has two tanks within the fuselage of the B-52 carrier airplane. These tanks are initially filled simultaneously with the X-15 LOX tank. The "climb" tank of about 1,000-gallon capacity is used during climb and the initial phase of cruise-out. During this time, the "cruise" tank of about 500-gallon capacity is free-vented to the atmosphere, and its LOX temperature is thus reduced. About 30 minutes prior to launch, the system is switched over to this cruise tank in order that the final top-off cycles may be accomplished with the colder, denser LOX.

The X-15 LOX tank contains a level-sensing device used for controlling valves in the B-52 to maintain the liquid level in the X-15 between limits low enough to minimize liquid loss by boiling and splashing but high enough to keep the X-15 always ready for launching without being out of balance.

Filling of the ammonia and hydrogen-peroxide tanks is accomplished on the ground with no subsequent top-off provisions. The ammonia tank is filled through a quick-disconnect fitting. Prior to filling, the ammonia is refrigerated to about -35° F; after filling, to prevent evaporation losses, the tank is sealed by closing its vent valve.

The peroxide tank is also filled through a quick-disconnect fitting. After filling, until pressurization, this tank is free-vented to prevent self-pressurization from slowly decomposing peroxide.

The helium systems are filled on the ground with gas preconditioned to the correct temperature. In addition, during filling, liquid nitrogen is forced in around the low-temperature pressure vessel in order to reduce its temperature more rapidly. Again, there are no top-off provisions. A leak-proof system is mandatory.

Figure 3 shows the liquid-oxygen and ammonia systems separately from the total system shown in figure 2. Each of the main propellant tanks is divided into three compartments, the expulsion sequence of the LOX tank compartments being forward, center, and aft, while that of the ammonia tank compartments is aft, center, and then forward. This forces the propellant center of gravity to converge on the airplane center of gravity and permits satisfactory balance during liquid expulsion at any flight attitude. Expulsion of liquid oxygen is accomplished by closing the tank vent valve and pressurizing the tank with helium gas to approximately 48 lb/sq in., the pressure required to prevent engine-pump cavitation. When the LOX feed or jettison valve is opened, the compartments empty in turn. The check valves prevent sudden shifts of liquid and thus of center of gravity. The feed and jettison systems are one and the same to a point just forward of the valves where the systems branch. Jettisoned liquids are discharged at the aft end of the fuselage. Pneumatically actuated "fail closed" valves are provided in each propellant line

at the firewall in order to isolate the engine compartment. Except for the reversed compartment sequence, ammonia expulsion is similar to LOX expulsion.

Figure 4 shows the hydrogen peroxide, pneumatic, and engine-purge systems; also the propellant emergency jettison provisions. The ability to jettison the propellants completely and in proper proportion to maintain airplane balance is of prime importance. To accomplish this, even with certain pneumatic failures, the tank vent valves are designed to fail closed and the pressurization valves to fail open. This means that even with a loss of pneumatic control gas, the main tanks will automatically pressurize. The jettison valves fail closed, to prevent inadvertent liquid spillage, but a separate control-gas system is provided. The main and emergency systems feed through linked selector valves controlled by a direct mechanical system from the cockpit, and then to shuttle valves which automatically select the higher gas pressure; either system can open the valves. To correct airplane balance in the event of unequal jettison rates, solenoid valves, individually controlled by the pilot, permit the closure of the jettison valves in any one or more of the systems.

Hydrogen peroxide is expelled from its tank by closing the vent valve and simultaneously admitting 600 lb/sq in. helium to the tank. Peroxide is forced into a swinging inlet tube which automatically seeks the bottom of the tank regardless of airplane attitude. The jettison system starts at the lower center line of the tank, and in this case is separate from the feed system.

Figure 5 is an overall view of the Santa Susana test facility of North American Aviation, Inc., and shows a liquid-oxygen expulsion test in progress. Preliminary testing had previously been performed with water in order to prove the systems and the components. The tank on the tower was used for water storage. Initial testing was necessarily done with many "off the shelf" components. Testing is continuing with these substitutes replaced with prototypes of actual flight components. Three of these propellant system tankage check-out stands have been built. Two are currently in operation at Reaction Motors, used in association with the engine development program. The third stand is undergoing tests at Santa Susana and will, in the near future, be used at Edwards Air Force Base for engine runs and additional system testing.

The fan at the lower left in figure 5 was used to keep oxygen vapor away from the test house. To the right is a helium-gas supply trailer, and immediately above it is the tank attitude stand.

Figure 6 shows an ammonia tank in the attitude stand. This stand was adaptable to either oxygen or ammonia tanks and was capable of rotating the tank to any attitude from 30° nose-down to 90° nose-up.

These attitude tests demonstrated the ability of the system to empty the tanks to well below specification requirements. The windows in the tanks were used to observe fill and feed-out characteristics. Water testing, followed by actual propellant testing, proved the capability of delivering propellants to the engine at acceptable rates and pressures.

It is expected that the tankage check-out stands will be in profitable use long after the X-15 airplanes are making powered flights. Figure 7 is a view of the engine test site at Edwards Air Force Base. Engine run-ups, check-outs, and thrust measurements and alinements, in addition to future engine development, can be performed in the check-out stands, freeing the airplanes for flight use and thus greatly accelerating the X-15 program.

PROPULSION SYSTEM ARRANGEMENT

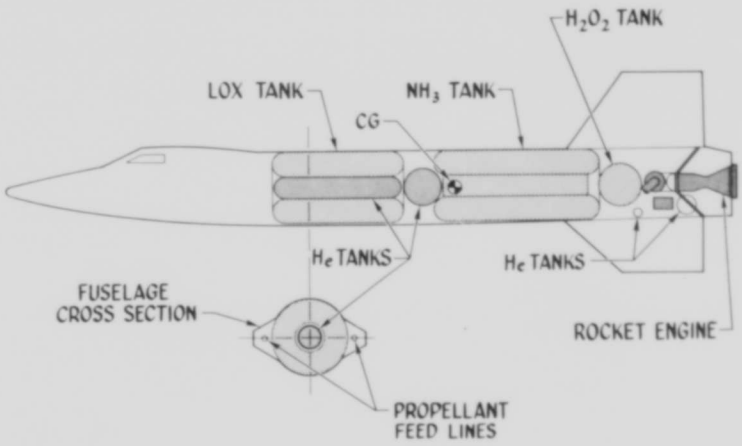

Figure 1

PROPELLANT SYSTEMS

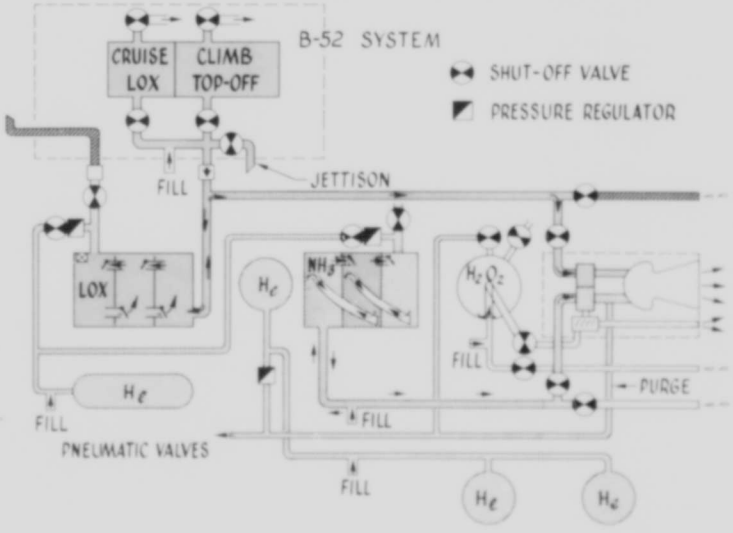

Figure 2

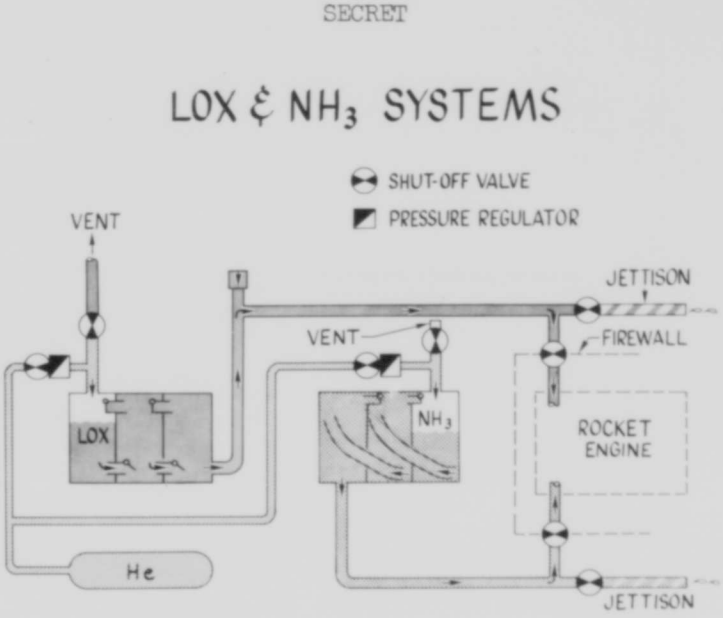

Figure 3

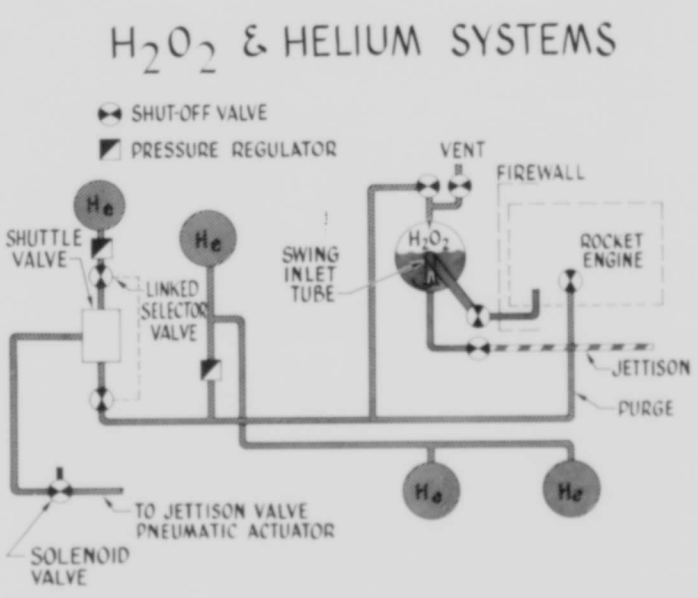

Figure 4

LOX EXPULSION TEST

Figure 5

ATTITUDE STAND

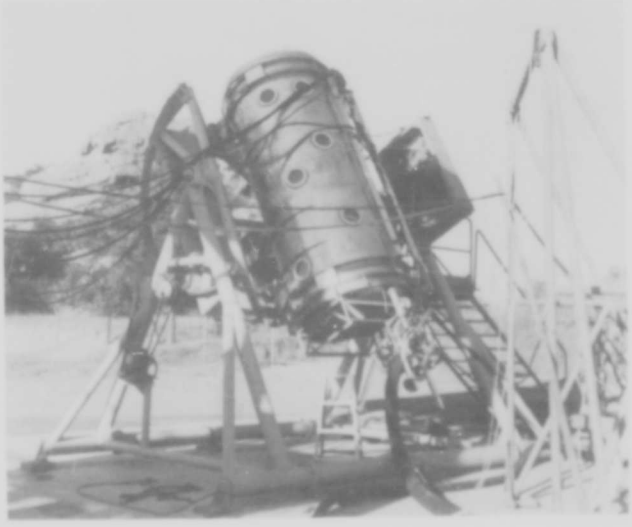

Figure 6

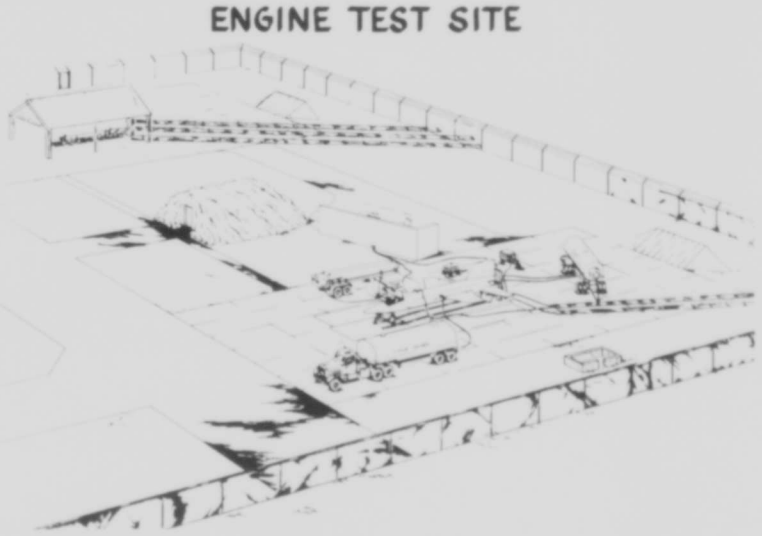

Figure 7

X-15 HYDRAULIC-SYSTEM DEVELOPMENT

By R. J. Culleton

North American Aviation, Inc.

INTRODUCTION

The X-15 hydraulic system consists of two completely separate, airless, modified Type III, 3,000-psi systems operating in parallel. Only the flight control surfaces are driven hydraulically, as there is no utility system. The operating temperature range of the equipment, lines, and fittings is from -65° F to 400° F. The main problems encountered in the design of this system are due to the extreme temperature and vibration conditions. These problems made it necessary to find a new hydraulic fluid, new seals, new materials, better methods of fabrication, installation, and contamination control, and tighter "quality" controls.

Applicable specifications in existence were found to be inadequate in many ways and could only be used as guides. Suppliers of purchased equipment were made aware of these requirements by a completely new set of specifications. Test data, obtained in research programs, was made available to them as required.

HYDRAULIC INSTALLATION

Figure 1 shows the relative location of the major hydraulic system components and the dual, parallel operating circuitry including the vertical and horizontal stabilizer actuators, directional mode and pitch-roll servos, speed-brake and flap actuators, console-stick master controls, and the NACA flow-direction sensor actuators. These actuating cylinders are driven by power furnished from the APU-driven hydraulic pumps, which receive the flow from completely airless reservoirs and deliver it through the side-fairing area to the system relief valves and back to the reservoirs.

In order to prevent the elastomer seals from freezing during LOX tank servicing, various methods were considered and tested. Elimination of integral heating devices for the line temperature control resulted in considerable weight saving and simplified the overall hydraulic installation. A thermocouple will be attached to the system

return line and connected to a self-balancing potentiometer at the two-system hydraulic ground-test stand for indicating airplane temperature. When temperature drops below -20° F, the test stand will be started. The system relief valve is remotely located from the hydraulic two-system test-stand connections and, with the test-stand pressure set just above the relief-valve level, fluid will be pumped through the entire power system and reservoir. This operation will raise the temperature of the fluid and, when it reaches 0° F, the test stand will be shut off. This operation will be repeated as often as required to maintain the desired system temperature. Having the system relief valve remotely located helps during flight by removing heat from the pumps and reservoirs and distributing it to cooler parts of the system; thus heat lag to the actuators is reduced.

TEMPERATURE PROFILE

In order to establish temperature requirements for the hydraulic equipment, an analysis, based on the high-altitude maximum-speed mission which appeared to cause the most severe heat problem, was made. It was calculated that if the temperature of the hydraulic fluid was maintained at approximately -20° F at take-off time (fig. 2), it would rise to 0° F during captive flight, reach 50° F during the five minute warmup period, and 300° F to 400° F during the last eight minutes of free flight. In addition there would be an estimated 22 minutes of soak after landing. For 15 flights of this type, the total time that the system would be at or near 400° F would be about 7.5 hours. All the hydraulic equipment has been designed on the basis of these data, together with low temperature (-65° F) and proper transient-condition considerations. Considerably more hours of usage are available at lower temperatures as determined by testing.

HYDRAULIC FLUIDS

Many fluids were considered and those most likely to meet the X-15 requirements were tested, and the comparisons indicated in figure 3 are referenced to the normal MIL-O-5606 hydraulic oil. The allowable temperature is plotted and the evaluation is based on the minimum recommended temperature of 400° F. It must be understood that each of these fluids (MIL-O-5606, Oronite 8515 and 8200, G.E. F-50, and Monsanto's OS-45-1) may be used at temperatures slightly above the values shown, but with a definite change in properties with a given time exposure. Viscosity at 400° F was considered very critical in that this

property, if too low, would reduce the volumetric efficiency of the pump and also would allow for excessive leakage in our valves, so that increased pump output would be required, and this in turn would cause system fluid temperatures to be elevated. Adiabatic bulk modulus is extremely important in establishing and maintaining consistent rate of response and elimination of flutter on all control surfaces. Lubricity was considered a very important factor in that the operation of the hydraulic pump, especially at 400° F, is the prime part of the life of the hydraulic system. From consideration of the physical properties shown, which are the most critical, but also including density, thermal stability, foaming characteristics and compatibility with sealing materials in the evaluation, Oronite 8515 was chosen as the best fluid available to satisfy the X-15 requirements. Although Oronite 8200 appears on the charts to be comparable, it was eliminated because the most desirable elastomer (NEOPRENE WRT) was developed for use with Oronite 8515.

The handling and usage problems of Oronite 8515 appear to be many; however, the dynamic simulator has been in use since January with excellent results. Process specifications have been released to control the fluid properties and to establish firm controls for handling and usage. All suppliers of components have been advised as to the proper procedures by our equipment specifications. A new series of procedures governing testing with this fluid has also been established.

SEAL DEVELOPMENT

Testing at elevated temperatures first showed VITON A to be a most desirable elastomer. However, as the testing entered the cold-temperature range, NEOPRENE WRT appeared to have a definite advantage. VITON A became quite hard and brittle at temperatures below -20° F. NEOPRENE WRT remained somewhat flexible even at -65° F and sealed where VITON A failed.

Both compounds were tested with a variety of antiextrusion backup devices. The Duroid single turn, heavy cross section, scarf cut backup shown on the left in figure 4 was recommended and at initial testing appeared to have merit. A typical failure is as shown after 13,000 cycles at 400° F in a piston application. The backup has extruded considerably and, in changing shape has damaged the seal by cutting pieces out of it and deforming it permanently. Failures like this would result in excessive leakage and could mean complete loss of system pressure.

Additional development finally produced a combination which, as shown in figure 4, has twice the life expectancy of the Duroid under the same operating conditions. This assembly has gone 26,000 cycles at 400° F. The bi-material backup in this final configuration is composed of a heat-treated, graphite-impregnated Teflon split ring of heavy cross section with a Zytel insert at the extrusion corner because of its greater rigidity at 400° F. The NEOPRENE WRT seal shows hot flow but retained its sealing ability well beyond the number of cycles at 400° F to be encountered in the life expectancy of the X-15. Approximately 25 hours of "O" ring life are available at this temperature, even under the most severe usage conditions. NEOPRENE WRT was developed for use with Oronite 8515 and, among its features, displays a definite swelling condition in this fluid which improves its sealing characteristics considerably.

TUBE AND FITTING VIBRATION TESTS

In order to reduce the total system weight and to qualify a hydraulic-fitting assembly in which pressure, temperature, and vibration are considered, a laboratory test program was initiated.

A test setup as shown in figure 5 was used in selecting the best combination of fittings, tubing, and sleeves for the hydraulic installation. Four line assemblies at a time and their fittings were mounted so that all but one end was inside the oven at 400° F as shown by the phantom outline. These assemblies were vibration and impulse tested to the duty cycle and life expectancy of the X-15 airplane. This testing, under actual environmental conditions, has proven the MS type of flareless fittings to be quite satisfactory for use on this airplane. The AN type of flared connections through usage and previous tests, have been found to have many disadvantages, among them the loosening and subsequent leakage when subjected to high-frequency vibration. Use of aluminum-alloy tubing, fittings and "B" nuts with electroless nickel-plated carbon steel sleeves has been verified and will be used, with few exceptions, on all hydraulic system return, suction, vent and drain lines. For system pressure lines, corrosion resistant steel tubing, aluminum alloy fittings and "B" nuts with electroless nickel-plated carbon-steel sleeves are quite satisfactory. This final choice of materials has resulted in a considerable weight saving over the originally considered corrosion-resistant steel lines, fittings, and "B" nuts. Titanium fittings were considered in the light of weight saving, but were abandoned due to extreme galling characteristics which caused a number of faulty installations even under very favorable laboratory conditions.

RESERVOIR

Due to the necessity of keeping Oronite 8515 fluid free of moisture, the reservoir (fig. 6) was designed to keep the expansion chamber separate from the fluid by means of a moving piston. Dry nitrogen flows across the top of the piston from the purge port to the vent port during all flight conditions and is trapped in the system while on the ground by means of a small relief valve attached to the vent outlet. Pressurization of the reservoir is by a "bootstrap" method in which 3,000-psi system pressure acts on a small area in the center of the piston. This creates approximately 90-psi pressurization on the system and supercharges the pumps. The fluid-level indicator is actuated directly by the moving piston. The return port is at an angle which causes the returning warm fluid to flow up and around the chamber so that it is mixed with the cooler reservoir fluid instead of flowing directly to the suction port. The relief valve is operated by contact with the top during system filling and bleeding and also provides safety blowoff features.

HEAT REJECTION AND HORSEPOWER

The peak flow requirements as established by the rates of deflection of the various control surfaces is 16 gal/min. The average duty cycle, however, indicates a flow requirement of only 1.5 gal/min for 90 to 95 percent of the operating time (fig. 7).

The system temperature is increased to its peak by the continuous heat rejection from the pump, coupled with poor heat dissipation due to the higher ambient temperatures caused by skin friction. The pump output varies with the system flow demands. Since this installation is a 3,000-psi system, the desired full flow output horsepower of the variable-volume-type pump is at 2,900-psi minimum. It will be noted that the heat rejection of the standard 3913 type variable-volume pump with its 16 gal/min rotating group is approximately 135 Btu per minute with an equivalent loss in horsepower.

PUMP SELECTION

The new E-14101-A pump consists of a small fixed-displacement-type pump operating for most of the APU driven flight time at a flow output of 1.5 gal/min to cover system leakage requirements, geared to and in the same housing with a special 3913 type variable-volume pump, which

can destroke itself depending on flow demands to a no-flow condition during the same flight time. This reduction in the horsepower required shows a much lower heat input of approximately 90 Btu per minute and a corresponding horsepower loss to the system. The slight increase in required horsepower over the small remaining time is negligible in the effort to reduce the overall system temperature.

This new unit has been nicknamed the PIGGY-BACK pump and also incorporates a special relief valve that does not operate under normal pressure and temperature conditions but protects the main system at conditions below -20° F and protects the fixed displacement part of the pump if operated inadvertantly on a test stand without an additional relief valve.

This combined unit provides flows in excess of the required 16 gal/min at 2,900 psi. In comparing the PIGGY-BACK unit with the 3913 or the 3911 conventional type pump (fig. 8) a reduced rotational speed is possible and this reduced speed results in a considerably longer life at 400° F. There is also a definite weight saving, because less APU fuel is required with the more efficient unit and because no heat exchanger is needed to lower the temperature to the range of the standard type units.

CONCLUDING REMARKS

Despite the exacting requirements and conditions of the X-15, including much higher temperature, high horsepower, and extreme vibration and duty cycles, the hydraulic flight control systems compare favorably, weightwise, with preceding models. Although some items, such as the pumps, are heavier, the total system, excluding actuators, weighs approximately 195 pounds as compared with 196 pounds for the F-100C airplane and 295 pounds for the F-107A airplane. Use of the new PIGGY-BACK pump, with its low flow during most of the operating time, also permitted a reduction in fluid capacity of the hydraulic reservoirs and the total systems, even though the volume of some of the actuators is quite large. This effected a considerable saving in fluid weight.

Complete ground-support equipment is available and this equipment, as well as the airplane systems, contains means for complete 5- to 15-micron filtration under controlled temperature conditions.

By use of advanced engineering techniques and extensive laboratory testing, it has been possible to provide a sound, lightweight hydraulic system for this advanced, high-performance airplane.

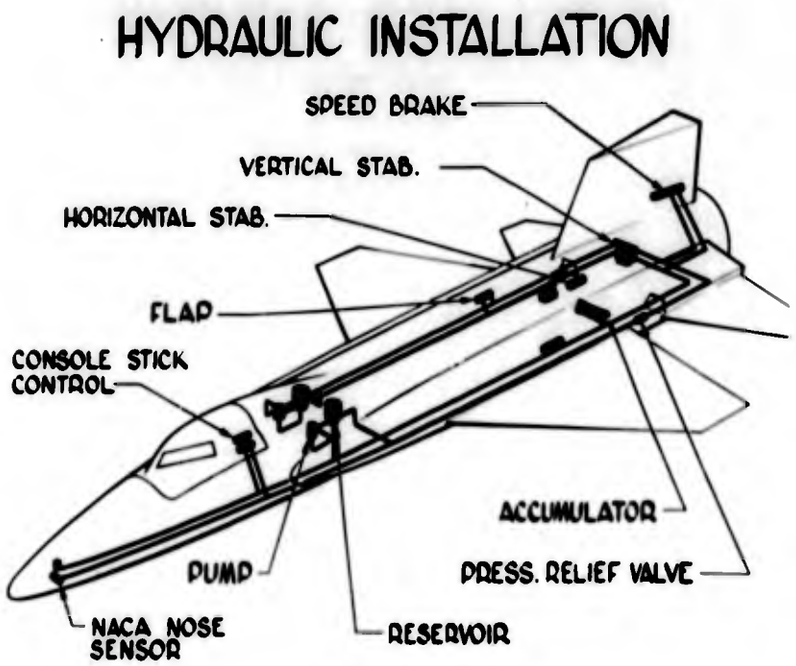

Figure 1

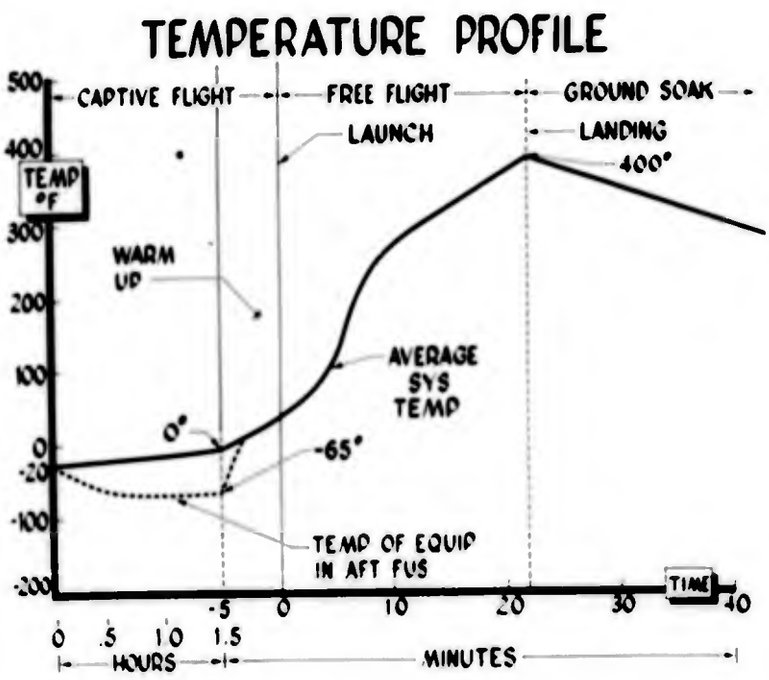

Figure 2

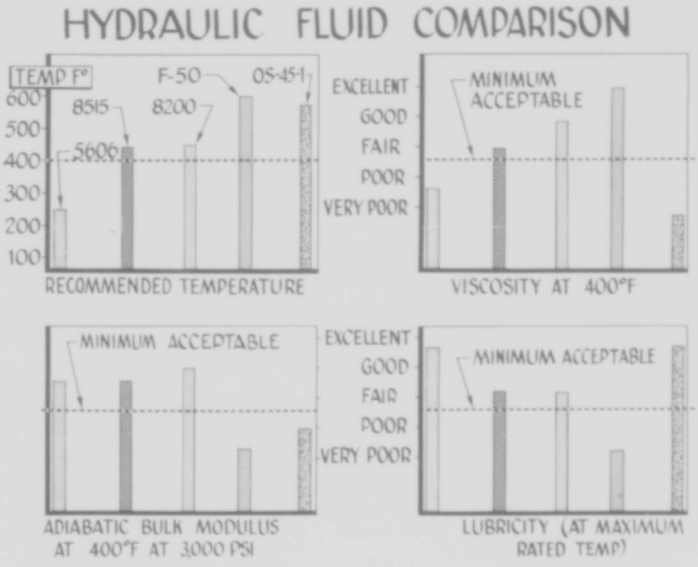

Figure 3

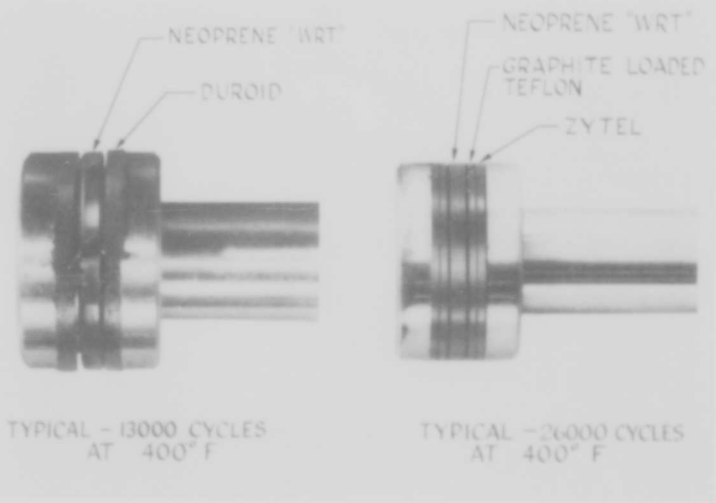

Figure 4

TUBE AND FITTING VIBRATION

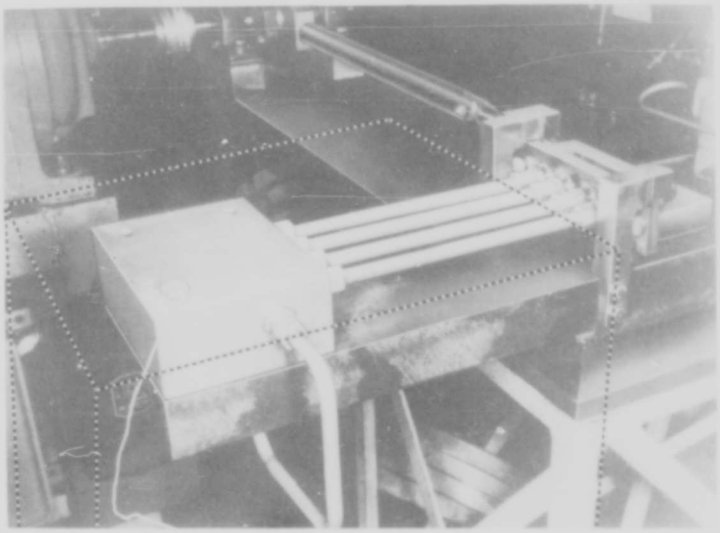

Figure 5

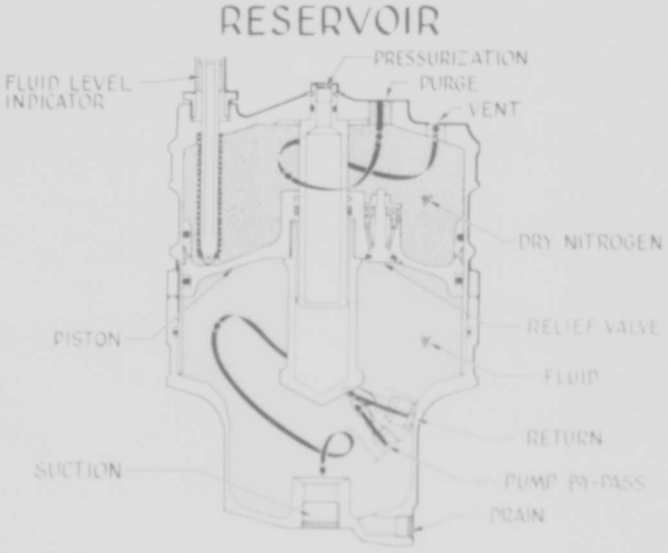

Figure 6

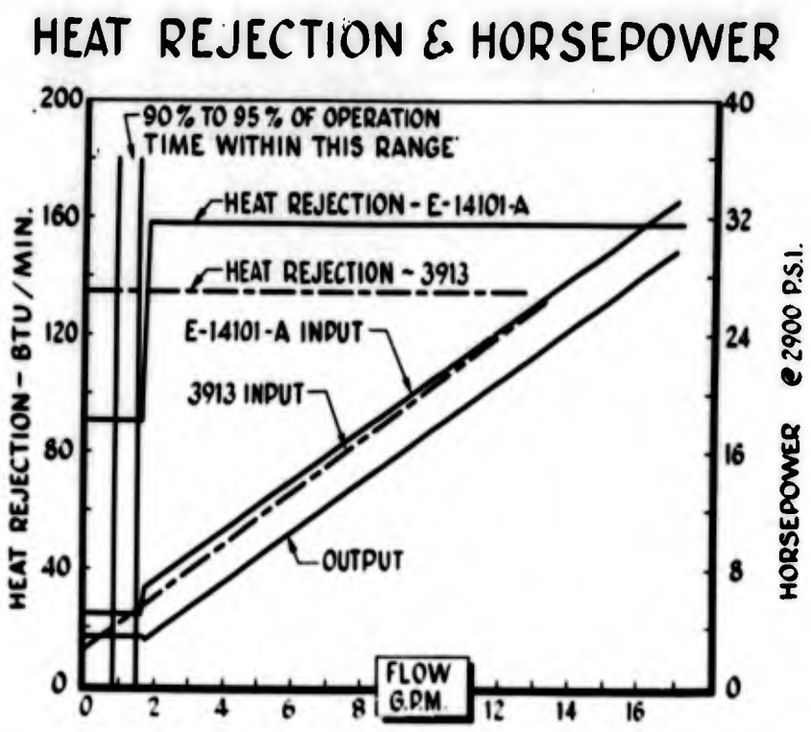

Figure 7

PUMP SELECTION

PUMP: E-14101-A (PIGGY-BACK PUMP)

REQUIREMENT: UP TO 16 G.P.M. AT 3000 P.S.I.

ITEM / PUMP	E-14101-A	3913	3911
SPEED, RPM	3925	4200	7000
LIFE, HOURS (AT 400°F)	100	45	30
WEIGHT PER SHIP, LB			
PUMP (2)	54	43	36
EXTRA H_2O_2 FOR APU	0	31	29
EXTRA WEIGHT CAUSED BY HIGH TEMPERATURES	0	48	48
PUMP SYSTEM TOTAL WEIGHT	54	122	113

Figure 8

X-15 AUXILIARY POWER UNITS AND REACTION CONTROLS

By Bruce O. Wagner

North American Aviation, Inc.

INTRODUCTION

Electrical and hydraulic power within the X-15 airplane is developed by a monopropellant auxiliary power unit, which is identified in the figures as APU. In addition, airplane attitude control at extreme altitude is by monopropellant rockets identified as ACR. Two duplicate installations are used to provide reliability beyond single-system capabilities to assure continuous availability of aerodynamic flight controls and space-attitude controls.

Figure 1 shows the duty cycle for these power units for a typical flight mission. It depicts the requirement for power generation by a single system which is in turn also a measure of propellant consumption. The propellant tanks will be pressurized for operation about 5 minutes before research airplane launch, and a predrop functional check of attitude rockets consumes 1/3 gallon of propellant. The auxiliary power units would also be started 5 minutes prior to launch. Electrical power and aerodynamic surface control, the only hydraulic power demand, follows an approximate pattern as shown. Total power peaks of 38 horsepower and a low continuous demand of 10 horsepower are developed. The flight path is shown by the altitude scale in relation to the power output. During approximately 6 minutes at extreme altitude, control rockets may consume an additional 2 gallons of propellant.

SYSTEM ARRANGEMENT

During the 1956 conference on progress of the X-15 airplane, a system of attitude control rockets was presented briefly. The auxiliary system for electrical and hydraulic power generation was not covered at that time. Since that date, relocation of installed equipment to facilitate airplane balance has caused these two systems to be integrated into one area of the airplane. The final combination system is shown in figure 2. Major components are the gas and propellant storage tanks, the supply-system valving, the auxiliary-power units, and metering valves and attitude rockets.

REACTION CONTROLS

The attitude-control rockets receive 90-percent hydrogen peroxide propellant from the 550 lb/sq in. gage helium pressurized tank. This propellant is metered by valves which are manually operated through a control-stick type of lever mounted in the left console of the cockpit.

Maximum propellant flows of 0.06 gallon per second for pitch or yaw and 0.02 gallon per second for roll pass through pressure opening valves at the inlet of the rocket motor catalyst unit. These valves maintain the propellant supply lines fully charged to assure rapid response to control action. A singular item of special interest in the control rockets as developed by Bell Aircraft Company is the "ring slot - pintle" type of nozzle for rocket units which fit into the thin wing section. This design shown in the upper corner of figure 2 made possible a unit having conventional performance despite the short right-angle nozzle which was a design necessity. Rated performance is a specific impulse of 160 seconds at an altitude of 200,000 feet with a chamber pressure of 295 lb/sq in. gage at 40 pounds of thrust. Other items involving principal effort in the control-rocket development were:

(1) Detail construction of the catalyst pack to provide 97-percent decomposition efficiency at a pressure loss of 60 lb/sq in. within the limited space available and also to eliminate propellant bypass flow along the chamber wall.

(2) Overall rocket construction arranged to accomplish a low unit weight of $2\frac{1}{2}$ pounds for roll units and 3 pounds for pitch-yaw units.

(3) Attainment of proper distribution of pressure loss through the unit to eliminate "chugging" or erratic operation.

One questionable design area still remaining is the rocket's quick-starting characteristics after cold soaking during the 2 to 3 hours that it is carried in flight prior to research airplane launch. Tests to determine heating effects from introduction of the predrop propellant quantity of 1/3 pound per rocket failed to demonstrate the capability of better than a 4-second start at high altitude within 4 to 8 minutes after the preheat. A 12-watt electrical heating element was then installed on inaccessible wing propellant lines to assure that electrical heating could be provided if needed to prevent propellant supply temperatures to the control rockets below 60° F. During the final phase of attitude rocket development, a propellant additive, dioctyl sodium sulfosuccinate, was examined briefly as a means of accomplishing cold environment starts. Brief tests by the Bell Aircraft Company have indicated 0.2-second starts by this means. North American Aviation, Inc. is

now exploring this possibility further with added consideration for application also to the main engine turbopump and auxiliary power units.

AUXILIARY POWER UNITS

Figure 3 is a photograph of the auxiliary power unit which is being obtained from the General Electric Company. This unit is shown with the driven accessories attached. Propellant enters at a gear-case fitting and passes through a heat-exchange pass to provide cooling of the gear-case lubricant; thence it passes through the metering valve and into the catalyst chamber. The products of decomposition are ejected through five nozzle units into a single-stage impulse turbine, which exhausts into a short fitting at the surface of the airplane compartment.

Turbine torque at the constant controlled speed of 51,200 rpm is transferred to the 4 KVA alternating-current generator running at 12,000 rpm and to the 16 gal/min hydraulic pump running at 3,925 rpm. The gear case contains 175 cc of MIL-L-7808 oil. Attitude-free lubrication is accomplished by small centrifugal and Archimedes screw-type pumping elements incorporated into the various rotating drive shafts. Since the high-altitude, high-temperature operating environment taxes lubricant cooling possibilities, 0.2 pound per minute of gaseous nitrogen is drawn from the cockpit conditioning system and circulated through the gear case between the main turbine bearing and the hot turbine wheel. The nitrogen inlet temperature is approximately -200° F.

The demountable electrical control box, shown in position in figure 3, receives a signal proportional to speed from a 40-watt tachometer generator built on the turbine shaft. In figure 4 (the APU operational diagram), a tuned circuit frequency sensor compares this signal with a fixed 400-cycle reference. The amplified signal proportional to frequency error is then used to position the torque-motor-driven propellant-metering valve. A separate frequency-sensitive overspeed circuit will signal closure of the system propellant shut-off valve in the event of turbine overspeed beyond 54,800 rpm.

Principal points of interest in the auxiliary-power-unit development transition would be the following. The decomposition unit, although not attaining targeted low-temperature starting characteristics, has accomplished design performance and 8 hours of rated life at typical duty-requirements conditions. This rated life had been regarded as a questionable possibility at the initiation of the project. Specific fuel consumption demonstrated by the prototype unit was improved 20 percent by further refinement of the turbine housing and nozzle box, the nozzles being increased from 4 to 5, with a 15 percent reduction in their total

area. Turbine-wheel overspeed safety design evolved from a radial blade parting used in the original design to a wipe-off design with periodic blades as weak members. This design was proof-tested with failures occurring within the speed range of 59,000 to 64,000 rpm, and the blades are contained within the exhaust duct. Considerable development effort also went into the controller and metering valve designs. Figure 5 describes three elements that are better than the equipment specification requires, insofar as speed or generator frequency control is concerned, as follows:

(1) Upon instantaneous addition of a 15 horsepower load increment, the drop in frequency was 2 cps, whereas 20 cps are allowed.

(2) The shift in steady-state frequency after load increase was 1/2 cps, whereas 4 cps are allowed.

(3) Short-time steady-state variation was 0.1 cps, whereas 0.5 cps is allowed.

Advantage has been taken of these characteristics in the elimination of inverters originally intended for stable platform and instrumentation power in the X-15 airplane.

PROPELLANT SUPPLY SYSTEM

Figure 6 is a simplified schematic diagram of the auxiliary power unit and attitude rocket-propellant feed system. If a typical operational sequence is followed, helium gas from a 3,600 lb/sq in. gage storage bottle is regulated to 550 lb/sq in. gage pressure. The helium shut-off valve enters this gas pressure into the 13-gallon propellant tank, and a bladder within the tank assures positive gas-free feed during the indeterminant zero g phases of the flight mission. A central perforated metal core tube stops the bladder collapse at 80 percent expulsion and the gas pressure takes a bypass into the inside of the bladder. A pressure differential exists across the bladder under this condition and is used to signal the pilot of 10 minutes available time under normal g flight attitudes prior to landing. The top connection on the tank joins the auxiliary power unit shut-off valve and a valve providing either shut-off isolation of the attitude rockets or jettison of all propellant. The attitude-control-meter valves, pressure-opening valves, and rockets are shown as described earlier. System servicing is accomplished through filler and vent receptacles, as shown. Pressure-relief safety provisions are installed in both the gas and liquid section, and a temperature probe in the bottom of the tank will signal propellant overheat at any temperature above 160° F.

Propellant-system components are being obtained from various suppliers. Their principal development problems have been as expected; that is, compatibility of materials with hydrogen peroxide, and sealing and gas passage erosion with helium. The helium bottle manufactured by North American Aviation, Inc. is of 4130 steel. A specially compounded Kel-F elastomer propellant-tank bladder is furnished by the Firestone Rubber Company.

SYSTEM TESTING

An assembled test system including all of the previously described units is shown on figures 7 and 8. This test installation has been in operation at North American Aviation, Inc. since May of this year in demonstration of the operational compatibility of all elements. The simulated fuselage compartment and the remote rocket locations are seen in figure 7. Figure 8 shows the propellant feed system in the simulated compartment, and the auxiliary power unit seen previously in figure 3 is mounted on the hidden side. All components have been development and evaluation tested by the individual suppliers. The principal item, the auxiliary power unit, has completed a 150-hour endurance test comprising 300 typical mission duty cycles as presented in figure 1.

TYPICAL MISSION POWER REQUIREMENT

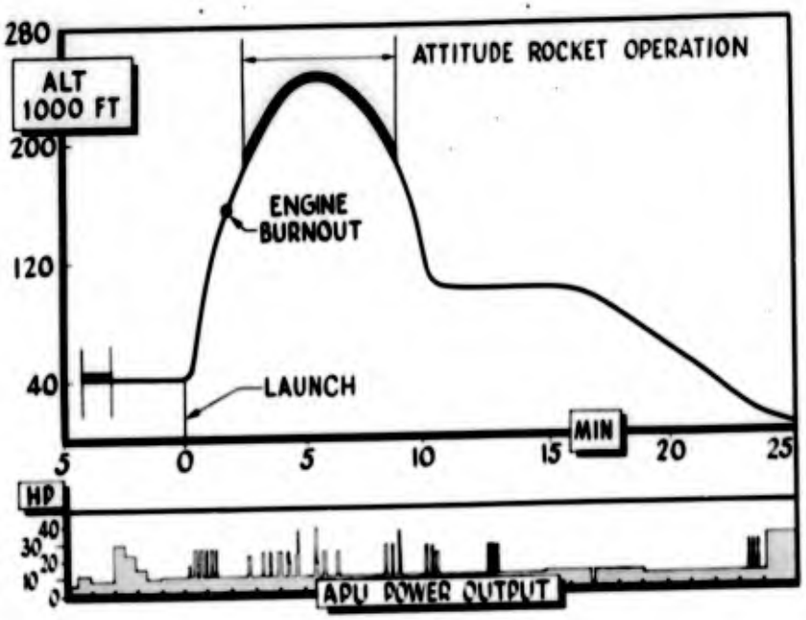

Figure 1

GENERAL ARRANGEMENT APU-ACR

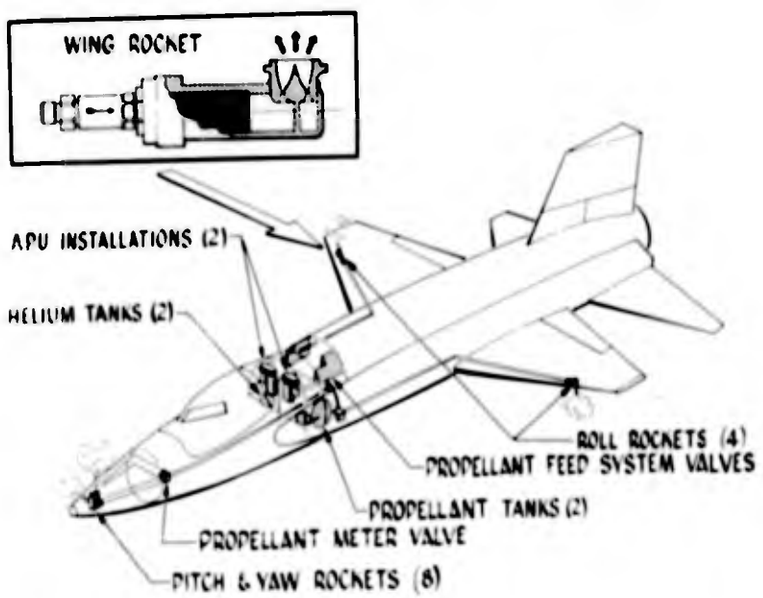

Figure 2

APU

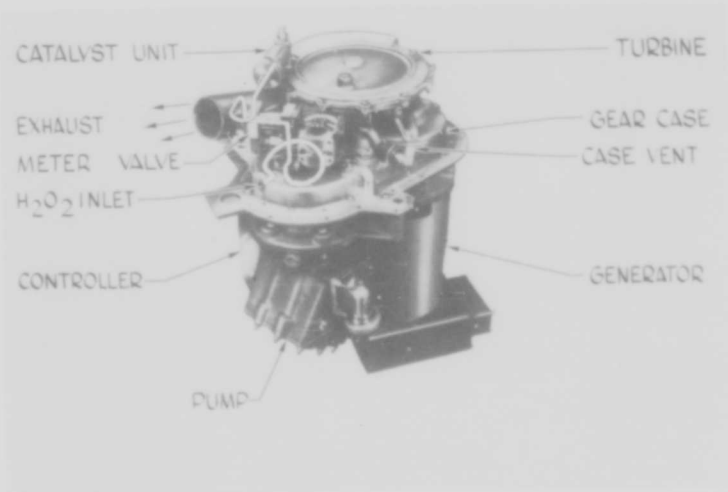

Figure 3

APU DIAGRAM OF OPERATION

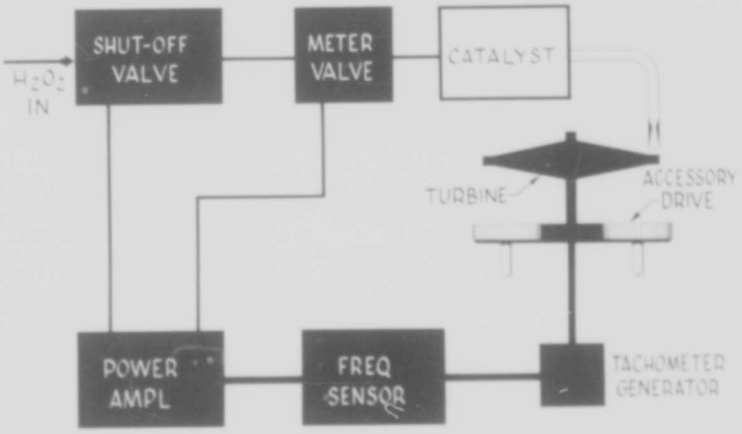

Figure 4

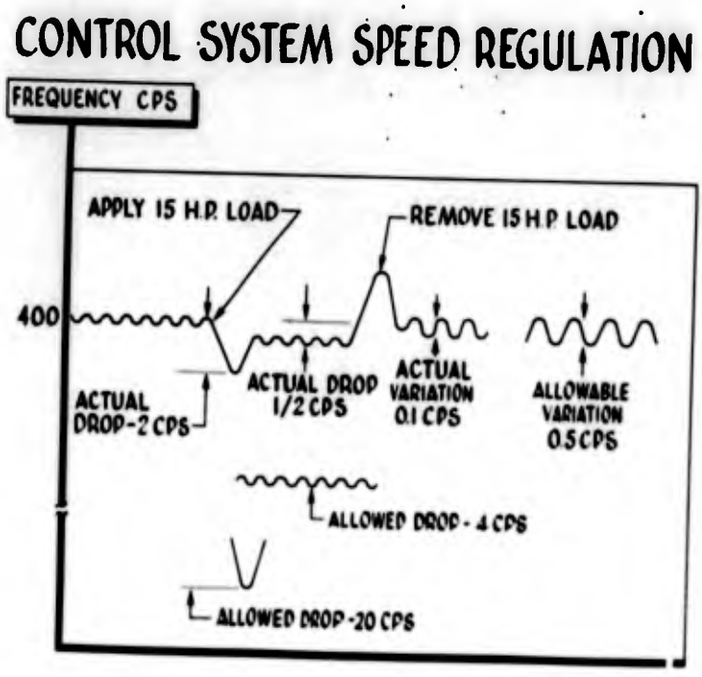

Figure 5

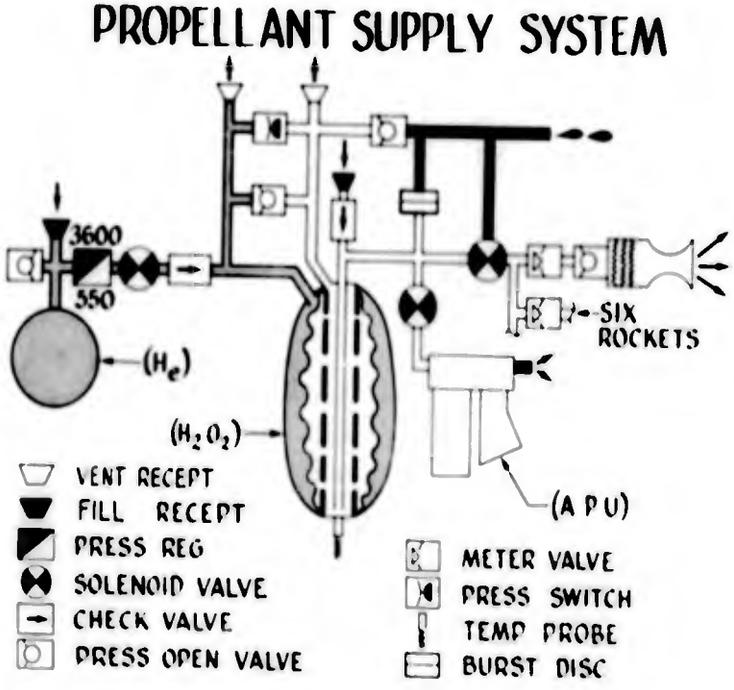

Figure 6

APU - ACR TEST STAND

Figure 7

APU - ACR TEST STAND

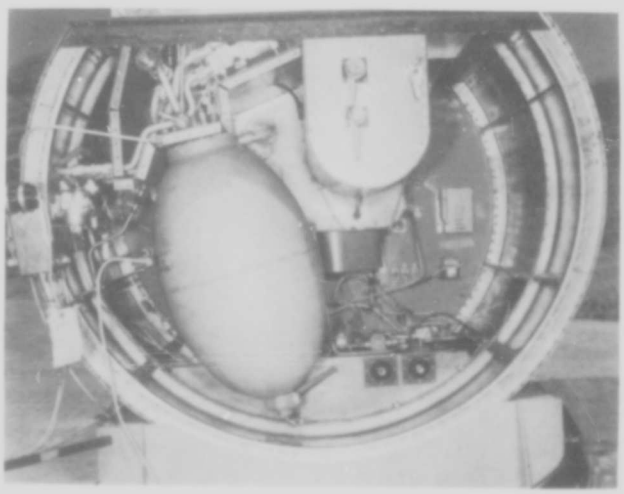

Figure 8

LANDING-GEAR DESIGN AND DEVELOPMENT TESTING FOR THE X-15 AIRPLANE

By L. L. Rhodes

North American Aviation, Inc.

INTRODUCTION

The X-15 airplane performance and operational requirements define a landing-gear system that will be subjected to high temperatures and high landing speeds and that will expend a minimum of airplane space and weight. This presentation is concerned primarily with the landing-gear-configuration design concept, the reporting of several unique design features that were incorporated, and description of the developmental testing of the subject system.

DESCRIPTION OF LANDING GEAR

The X-15 landing-gear configuration, illustrated in figure 1, is basically a tricycle arrangement composed of a conventional dual-wheeled nose gear and two main gears equipped with steel skids. The tricycle gear was selected for its inherent directional-stability characteristics and airplane roll stability on the ground, which thereby eliminated outriggers or wing-tip bumpers that might be required with a single skid installation.

Design requirements for the landing gear included:

(1) Landing touchdown speeds: 164 to 200 knots

(2) Airplane attitude: 6° angle of attack

(3) Sinking velocity: 9 feet/second

It will be noted that the main gear is located extremely far aft on the fuselage. This feature is quite unconventional but provides several valuable advantages for this airplane as follows:

(a) Elimination of a tail bumper

(b) Improved directional stability during the landing run

(c) Improved aerodynamic characteristics during flight

(d) Reduction in size and weight of the skids and main gear

(e) Improved back-up structure for the gear attachment

It was determined that these advantages far outweighed the associated disadvantages of (1) increased nose-gear loads, and (2) increased pilot accelerations. It was possible to move the gear from its usual location adjacent to the center of gravity because the X-15 has no requirements for taking off from the ground; thus, the usual "nose lift-off" problem was eliminated.

The cantilevered strut legs and drag braces pivot in trunnion fittings in the fuselage, and the struts are linked to high pressure air-oil-type shock absorbers, which are installed within the fuselage for protection from exposure to high temperatures. The skid may appropriately be termed a "ski" as it is universally mounted to the strut leg. The skid is pin-jointed in two planes to allow pitch and roll motion but is restrained from yawing, and thus provides the necessary parallel alinement of the two skids. The drag brace attaches directly to the skid, at a point ahead of the main pivot joint, in such a manner as to lift the nose of the skid to improve planing action.

No hydraulic power is needed for operation of the landing gear. All gears are retracted manually on the ground and extend aft by action of the air stream and gravity.

The nose gear is stowed in the fully compressed position. As the strut has a stroke of eighteen inches, this feature accomplishes a considerable space saving in the airplane. The strut is held in the "shrunk" position by a "boot-strap" lock arrangement which is automatically released as the gear extends.

Co-rotating dual wheels are installed for prevention of shimmy, without the additional weight of a hydraulic shimmy damper and torque links. The co-rotating wheel arrangement also results in less castering torque resistance than a hydraulic damper. This fact is an important consideration in the design because excessive castering friction and damping can cause directional instability to the extent of ground looping the airplane.

TEST PROGRAMS

Three major test programs were conducted on the landing-gear system. These consisted of (1) a dynamic-model test of stability

during the landing run, (2) nose-wheel shimmy tests using the actual airplane nose gear, and (3) full-scale skid tests at the lake bed landing site.

Dynamic Model Stability Tests

The model tests were made to investigate the stability of the twin skid main gear and dual co-rotating nose-wheel configuration. The 1/10-size model (fig. 2) did not simulate aerodynamic characteristics but was scaled for size, weight, and mass moments of inertia for yaw and roll. Scale-size metal skids were fabricated so they could be mounted either rearward or forward near the center of gravity. The scaled nose gear was equipped with dual co-rotating rubber-tired wheels, was 360° free castering, and was fitted with an adjustable caliper-type friction clutch on the spindle. The model was catapulted along a concrete runway by means of a 100-foot length of 5/8-inch-diameter shock cord. High-speed movie cameras were operated from overhead towers to record yawing oscillations during each run. A typical run consisted of launching the model in a 10° to 30° yaw angle. After several convergent oscillations the model ran straight for a distance of 250 to 350 feet (equivalent to airplane runout of approximately 6,000 feet). A number of parameters were varied in order to investigate their influence on directional stability. Of these, spindle friction in the nose gear was the most critical, and a maximum allowable torque value equivalent to 130 foot-pounds in the airplane was established. (The actual friction torque in the airplane is expected to be below 50 foot-pounds.) As spindle friction was increased beyond the allowable limit, by means of the adjustable clutch, the model would become unstable, with the yaw oscillations becoming divergent to the point of ground looping. The aft skid configuration proved to be considerably more stable than that with the skids mounted forward. As a direct result of the model tests the nose-gear caster length was increased from 2 inches to 3 inches in order to improve lateral stability.

Full-Scale Nose-Gear Shimmy Tests

The Langley landing-loads-track facilities were used for evaluation tests of the shimmy characteristics of the dual co-rotating nose gear. The complete nose gear was mounted on the track carriage illustrated in figures 3 and 4 and was catapulted at speeds up to 125 mph. Blocks were bolted to the concrete runway (fig. 5) in such a position as to be run over by only one wheel, and in this manner a shimmy oscillation was induced. Tests were made to explore the velocity range from 20 mph to 125 mph in increments of approximately 20 mph. Later tests were made to investigate the effects of wet pavement, sand on runway, uneven tire pressures, one flat tire, and unbalanced wheels.

Throughout the tests the co-rotating wheel arrangement proved extremely stable with no tendency toward shimmy. It was, therefore, concluded that neither shimmy damper nor torque links will be required on the airplane; thus a weight saving of approximately 25 pounds was realized.

Full-Scale Lake-Bed Skid Tests

The landing-gear-skid tests were conducted at Rogers Dry Lake in April 1958. For these tests the complete main gear was mounted on a two-wheel trailer vehicle and towed behind a truck at speeds up to 70 mph. (See figs. 6, 7, and 8.) After the truck and trailer reached full speed, an electric switch was utilized to actuate bomb-release-type solenoid locks and to drop the 6,000-pound load on the skid landing gear. The gear was instrumented to record vertical and drag loads and shock-strut position in order to plot load-stroke curves and to measure coefficients of friction between the skids and the lake surface. High-speed cameras mounted on the truck and trailer recorded motion of the gear and skids. Test runs included straight-line landings on the smooth lake surface, "fishtail" runs through rutted and bumpy areas near the edge of the lake, and one landing on a concrete runway. Results of all tests were very satisfactory. Skid wear on the lake runs was light, and this result proved the skids to be adequate for the minimum design requirement of one landing. From measurements of skid wear, it is estimated that three or more landings can be made on each pair of skids. Wear during the run on concrete proved very severe as expected. Friction coefficients on the lake proved to be within the values used for design (0.35 at high velocities increasing to 0.8 at point of stopping). There was no evidence of any detrimental skid shimmy nor tendency for the skids to roll over, even in very severe side skids. The skids appeared to plane satisfactorily in soft areas and through ruts and bumps. Tracks on the level lake surface appeared to be 1/32 inch or less in depth.

CONCLUDING REMARKS

In conclusion, the objectives of the design were to obtain satisfactory stability characteristics and landing capabilities for the airplane. The purposes of the test programs were to prove the design before first flight. The tests are now essentially complete and it is concluded that these objectives were accomplished successfully.

X-15 LANDING GEAR

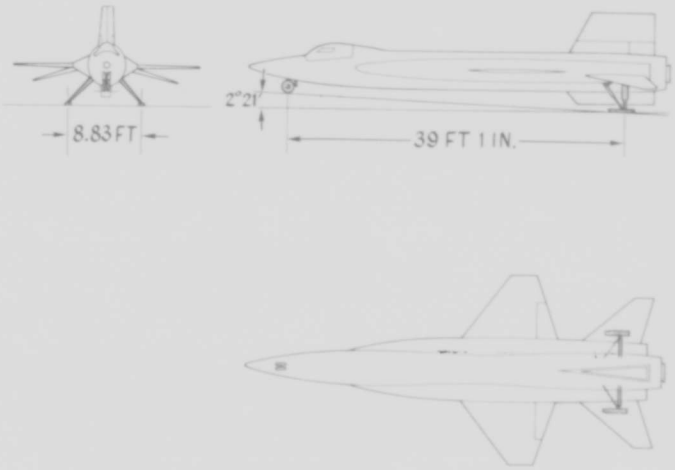

Figure 1

X-15 LANDING GEAR DYNAMIC MODEL

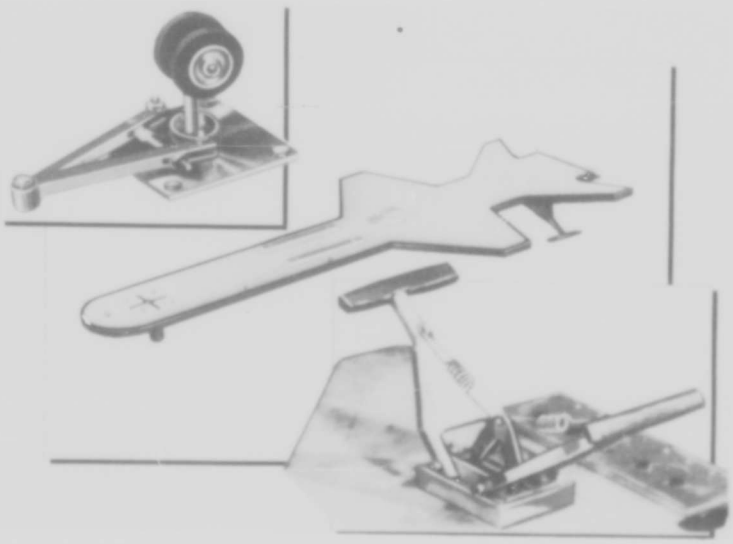

Figure 2

LANGLEY LANDING LOADS TEST VEHICLE

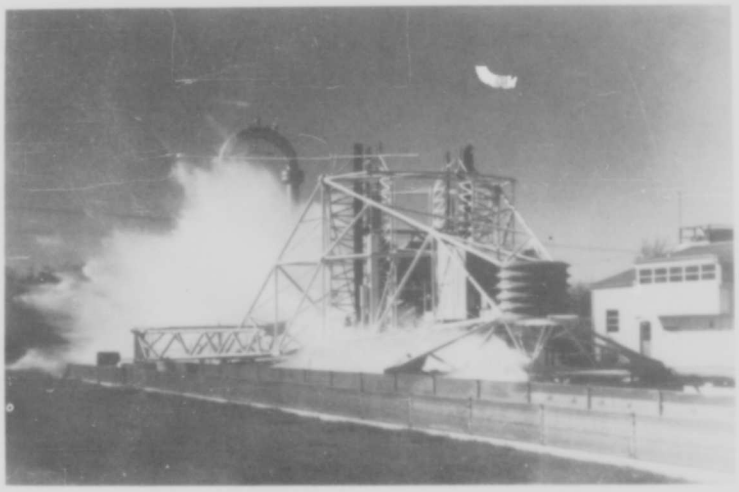

Figure 3

X-15 NOSE GEAR

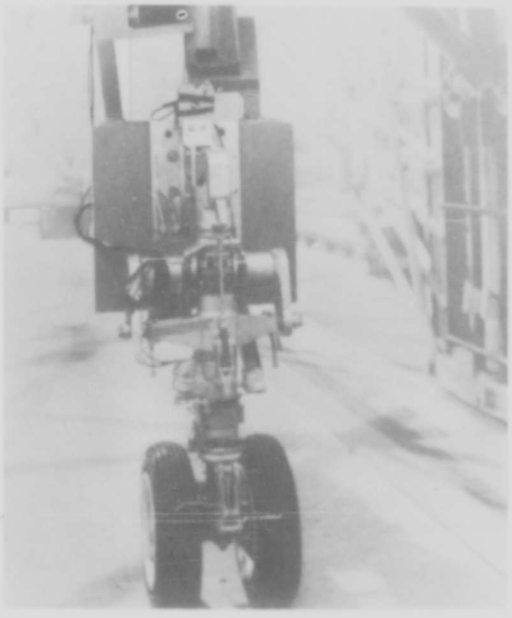

Figure 4

X-15 NOSE GEAR SHIMMY INDUCING BLOCKS

Figure 5

LANDING GEAR TEST TRUCK AND TRAILER

Figure 6

LANDING GEAR TEST TRAILER

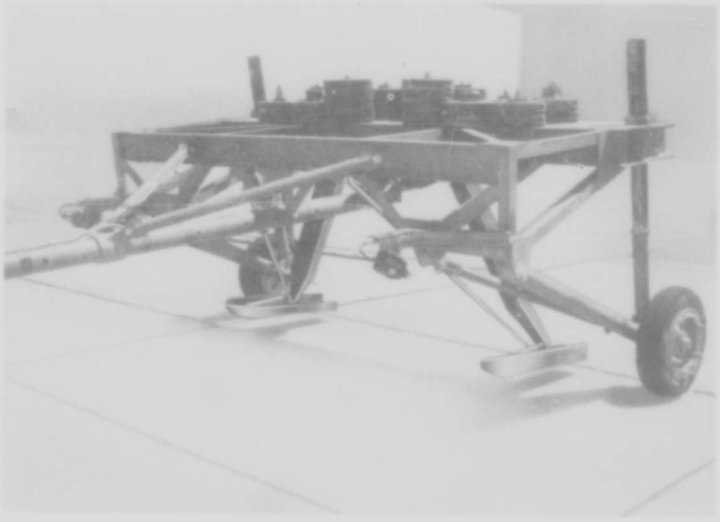

Figure 7

LANDING GEAR SKID AFTER TESTS

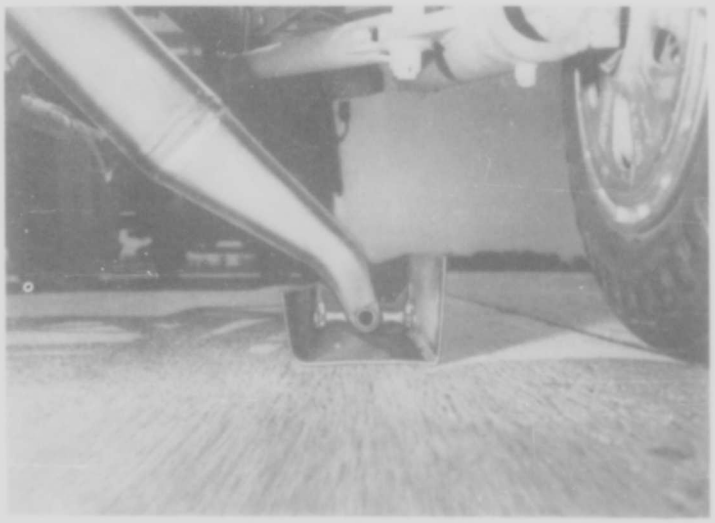

Figure 8

X-15 CONDITIONING AND PRESSURIZATION SYSTEM

By C. P. Bouman

North American Aviation, Inc.

INTRODUCTION

The cooling system for the X-15 airplane incorporates insulation as partial protection against high-temperature effects plus liquid and gaseous nitrogen to control specifically environmental and equipment temperatures. Electronic-equipment cooling represents the largest single cooling load; however, other items to be considered are the cooling requirements for the generators, auxiliary power units, pressure-suit ventilation, aerodynamic-heating effects, sensor-head cooling, and windshield antifogging.

The design concept of a sealed cabin is complicated by the problems of emergency escape, which requires a cockpit design permitting rapid egress from the airplane. The possibility of a totally sealed cabin was ruled out because of structural deformation due to high temperature differentials and inflatable canopy-to-cockpit seals, which at best are leak sensitive. Therefore, the system must also be capable of providing a sufficient amount of makeup gas to maintain cockpit pressure.

DISCUSSION

Initially, various types of cooling systems were investigated in order to arrive at an optimum system. A review of these systems, considering design advancements made over the past thirty months, still indicates that an expendable, stored, cooling system is the most efficient for short-duration missions. Figure 1 presents a simplified schematic diagram showing the system as currently used. The storage capacity of the system is 150 pounds of liquid nitrogen which represents a total cooling capacity of 27,000 Btu at the operational temperature level. The coolant is divided among components and equipment, as follows:

A.C. generator	14 pounds
APU gear box	11 pounds

Pressure-suit ventilation	6 pounds
Sensor head	20 pounds
Hydraulic-reservoir purging	3 pounds
Liquid-nitrogen reserve	12 pounds
Evaporation loss	13 pounds for six-hour standby
Electronic equipment cooling system (fig. 2)	71 pounds

The storage and feed system basically consists of a liquid-nitrogen storage tank, a high-pressure helium tank, and related pressure regulators, relief valves, fill valves, controls, and ducting (fig. 1). The liquid-nitrogen tank is a heliarc-welded, double-walled, stainless-steel vessel with the space between the inner and outer wall evacuated to a high vacuum. The outside of the inner container and the inside of the outer container are plated and polished to a high finish to reduce radiant heat transfer. It is calculated that liquid evaporation loss will be less than 20 percent of the total liquid volume of 88 liters for a 24-hour period. A plastic bladder suspended within the tank is inflated with stored helium gas to expel forcefully the liquid during negative or zero g conditions.

The system pressure is controlled by a two-stage regulator which reduces helium pressure from 4,400 lb/sq in. to 65 lb/sq in. High and low pressure-relief valves in both the helium and the nitrogen system prevent overpressurizing of either system.

Cooling gas flow rates for the A.C. generators are controlled by flow-limiting orifices located in the supply lines leading to these units. Laboratory testing of the generator cooling system indicated that at the approximate time the cooling requirements became critical, the gas supply line would cool down to the saturation temperature of the liquid, thereby discharging liquid into the generator cooling system, providing additional cooling.

Based on calculations and data from the A.C. generator cooling tests, flow control orifices were also provided in the APU gear box cooling circuit. It is expected that some changes in orifice sizes may be required during actual aircraft operation as complete environmental conditions to which the airplane will be subjected cannot be duplicated in the laboratory.

The hot gas exhausted from the generators is ducted forward and discharged across the inner windshield glass for antifogging purposes. Nitrogen gas is also discharged between the inner and outer glass panels to purge the area of moisture.

Ventilating gas for the pilot's pressure garment is supplied through a manually operated valve which will provide gas flows up to

10 cu ft/min. An electric heater and two thermoswitches mounted in the supply system allow the pilot to select a suit gas-supply temperature between 50° F and 90° F. A finned-tube heat exchanger with a liquid-flow-limiting orifice assists in changing the liquid to gas prior to entry into the heater section. Approximately 350 watts of power are needed to heat the gas to 90° F at the maximum required flow rates at 35,000 feet.

At this point, it might be well to emphasize that the cockpit ambient temperature is limited by the instruments and equipment rather than by pilot capabilities. The pilot, having the ability of controlling his own pressure-garment ventilation flows can withstand ambient temperatures well in excess of the 130° F limits imposed by the electronic equipment; in fact, the average cooling-gas flow rates for pressure-suit ventilation are less than 1.0 percent of the total cooling gas flow rates for the equipment.

A ram air system is used for cooling electronic equipment from take-off to launch in order to conserve the liquid-nitrogen supply. The ram air system may also be used for emergency cooling and cockpit purging at altitudes below 35,000 feet.

Figure 2 shows the method used for providing cooling gas to various items of electronic equipment that require forced cooling. The complete assembly consists of two temperature-control systems, each with a high-capacity blower, liquid-nitrogen injector, thermostat, and mixing chamber. Each system feeds into a common plenum, from which the cooled gas is ducted to the equipment. As the temperature of the recirculated gas forced through the mixing chamber by the blowers raises or lowers, the thermostat, by pneumatic action, varies the flow of liquid nitrogen from the injectors to maintain mixed gas flow temperatures into the plenum of -40° F. A shutoff valve in each system prevents liquid-nitrogen flow when the blowers are in the off position. The plenum is provided with flapper valves which prevent reverse flow into either the ram air ducting or the mixing chambers, depending upon which system is used. The blowers are two-stage, electrically driven, axial-flow units with an output of 232 cu ft/min with a pressure rise of 8 inches of water at 35,000 feet. A high-slip motor is used to decrease fan speed from 21,000 rpm at altitude to 11,000 rpm at sea level with the power varying from 0.6 horsepower to 1.2 horsepower, respectively.

Control of the complete system is fully automatic, once it is placed in operation. The pilot need only open the system shutoff valve, monitor the vent-suit gas flow and temperature for personal comfort, and switch on the two blowers to put the system in operation. Pressure sealants currently available are limited to a maximum

temperature of 500° F. This limitation necessitated the use of a double-walled structure in all pressurized areas with adequate insulation to assure a lag in inside-wall temperatures to a reasonable limit.

The curves in figure 3 show the effectiveness of the insulation selected for use in the X-15 airplane. Note that with a maximum outside-wall temperature of 1,000° F, the inner cockpit wall remained well below 185° F. The insulation blanket is constructed of one high-density layer of Q-felt, and two low-density layers of fiber glass separated by aluminum radiation foils of 0.001-inch thickness. The blanket which is 2 inches thick and weighs 0.25 lb/sq ft effectively reduces peak aerodynamic heat input to 6,700 Btu/hr within the entire pressurized area. Although the X-15 heat loads are of short duration, the blanket also shows good insulation qualities for extended operation at high temperatures.

At present, most of the components used in the conditioning and pressurization system have been laboratory tested with satisfactory results. Figure 4 shows an expulsion test being conducted on the liquid-nitrogen tank under static conditions.

Complete-system functional tests are planned with heat load, cooling requirements, and environmental conditions simulating as closely as possible the actual airplane operating conditions. These tests are scheduled to start before September 1958.

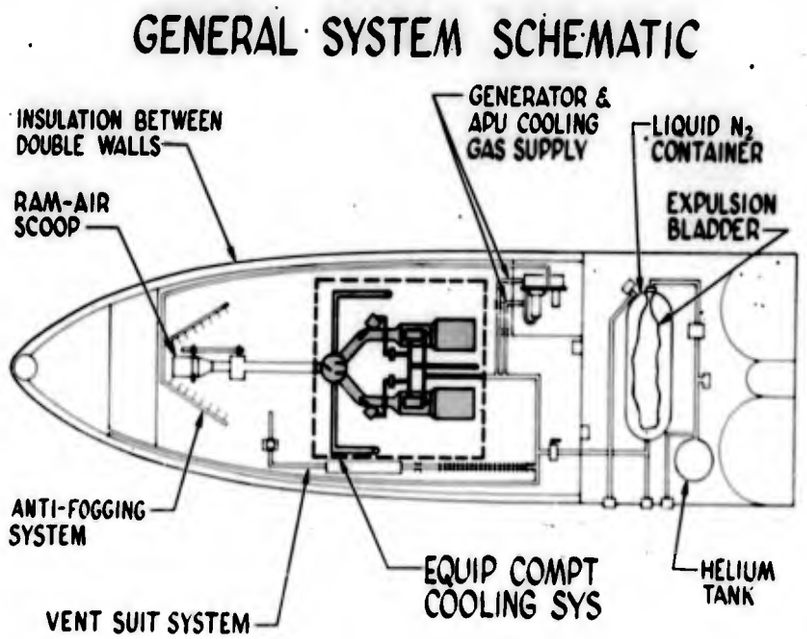

Figure 1

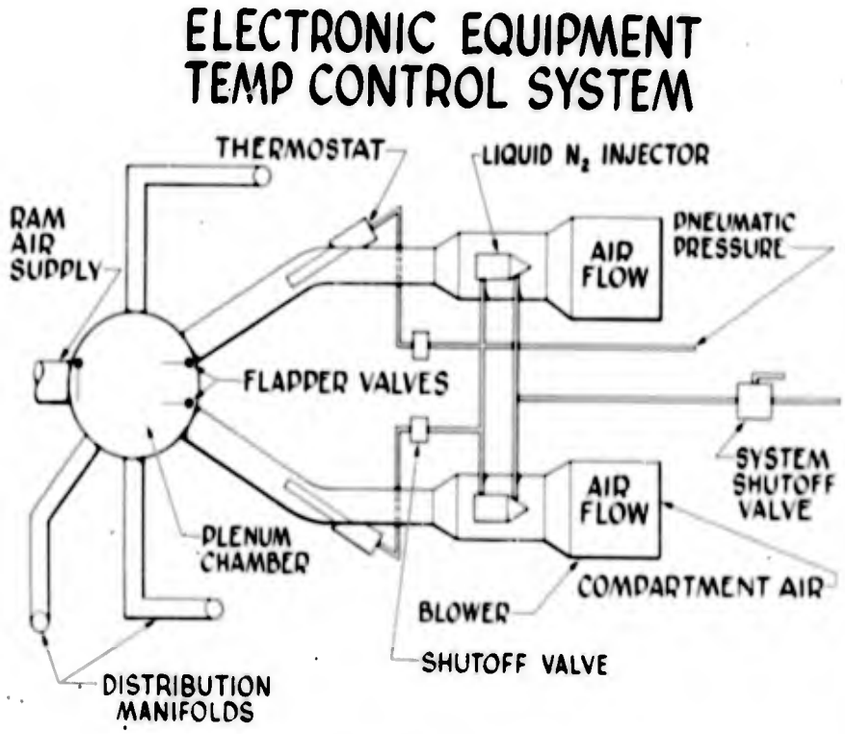

Figure 2

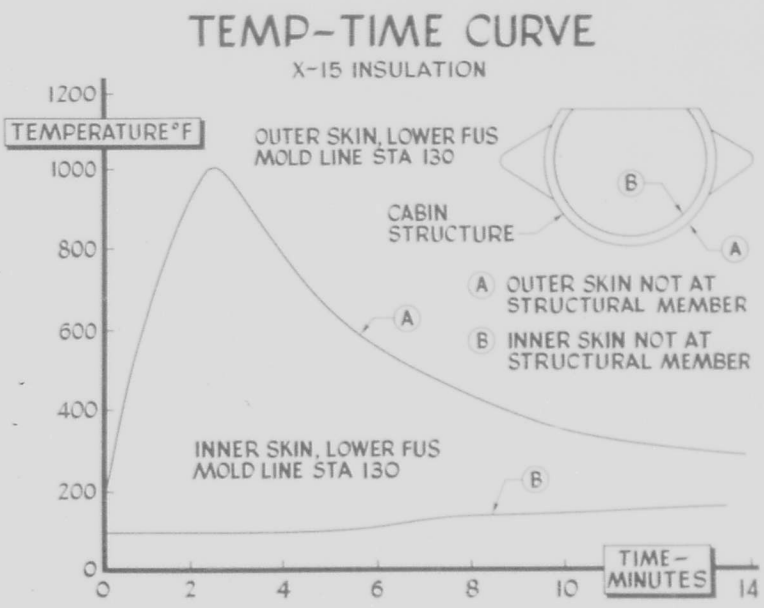

Figure 3

Figure 4

X-15 RESEARCH OBJECTIVES

By De E. Beeler

NACA High-Speed Flight Station

INTRODUCTION

Various speakers at the X-15 conference in 1956 and during the present conference either by inference or by conclusions reached have stated that a flight validation is now required before a real and complete assessment of their particular problems can be made. If, instead of discussing the flight-research objectives of the X-15 in these various areas, it could be announced that a successful flight of a mission as typified in figure 1 had been accomplished, it is believed that all would agree that the mere knowledge of this accomplishment would be a major contribution toward understanding the problems that confront the design of hypersonic aircraft and manned satellite vehicles. In fact, completion of this type of mission would be a successful demonstration by the pilot of the exit flight from the atmosphere, control of the airplane outside of the atmosphere where little or no aerodynamic damping exists in the environment of weightlessness, and entry back into the atmosphere involving conditions of aerodynamic heating, high dynamic pressure, and loads. It is considered that the successful accomplishment of this type of mission would be of significant value much in the same way as was the first X-1 sonic flight. The basic flight-research program and instrumentation have therefore been directed toward obtaining a better understanding of the problem areas of these regions.

SYMBOLS

A_x	longitudinal acceleration
A_z	normal acceleration
C_L	lift coefficient
$C_{L_{max}}$	maximum lift coefficient
$C_{D_{min}}$	minimum drag coefficient
C_{m_α}	rate of change of pitching-moment coefficient with angle of attack

C_{n_β}	rate of change of yawing-moment coefficient with angle of sideslip
c_p	specific heat at constant pressure
H	pressure altitude
H_i	altitude at which constant α is initiated
h	heat-transfer coefficient
M	Mach number
M_o	initial exit Mach number
q	dynamic pressure
q_{max}	maximum dynamic pressure
R	Reynolds number
V	velocity
α	angle of attack
ρ	density
θ_o	initial climb angle for exit

DISCUSSION

The specific problems of research interest for the X-15 are as follows:

(1) Aerodynamic and structural heating

(2) Control at low dynamic pressure

(3) Simulation

(4) Exit and entry.

Papers of both conferences on the X-15 have pointed out very clearly the difficulty of predicting the heating environment of

hypersonic vehicles, even after rather extensive wind-tunnel tests have been conducted on the specific X-15 configuration. There is urgently needed, for actual flight conditions, the determination of transition Reynolds numbers and heat transfer in the laminar and the turbulent boundary layer, not only for the X-15 application but also for studies of more advanced design proposals. Also, the actual measurement of temperatures of the structural components as they are exposed to the aerodynamic-heating environment is greatly needed. These items are the first order of business in the X-15 flight program.

The control requirements at low dynamic pressure and some account of operational experience with the control-simulation studies have been reported in previous papers at both X-15 conferences. Flight experience is now needed to determine the control levels required and an assessment of the blending of the aerodynamic and reaction controls. In this regard, it was reported by several pilots that the reaction controls were used to advantage not only near zero dynamic pressure but also at dynamic pressures greater than 300 lb/sq ft.

It will be necessary in conducting research flights to perform many exit and entry missions of varying degrees of severity. In these regions much effort has been expended in simulator studies, and several papers concerned with simulation have been given. It has also been reported at this conference that the probability of successfully accomplishing these missions is low unless the pilot is adequately trained on suitable static and dynamic simulators. The extensive background of basic aerodynamic data and experience on ground simulators has been applied to analog studies now under way to provide this pilot guidance. These studies will, of course, be refined as required by inclusion of measured flight data and flight experience.

The value of and need for adequate ground simulation will be expected to increase as more advanced vehicles are proposed. The X-15 simulator and flight work will provide the basis for the validation now needed for present simulation methods and will serve as a guide for future studies of this type.

Figures 2 and 3 give an idea of the conditions that have to be considered for flight planning, particularly when end-point flight conditions may be approaching critical areas.

In figure 2 is shown the exit flight mission where altitude is plotted against time. For an initial flight condition of Mach number 2.0 and a climb angle of 4.3°, the peak altitude would be about 250,000 feet. A constant deviation of 2° would result in an altitude different by 100,000 feet.

In figure 3 is shown the entry mission, where the maximum dynamic pressure q_{max} that would be experienced in the mission is plotted as a function of an angle of attack held constant in recoveries from 250,000 feet. The solid lines are shown for the altitude at which the constant angle of attack has been initiated. For instance, an intended angle of attack of 10° held from 200,000 feet would be expected to result in a dynamic pressure of 1,600 lb/sq ft; however, if an actual angle of attack of 8° were achieved, a dynamic pressure of 2,500 lb/sq ft would result - or for an intended angle of attack of 10° held accurately but not initiated until an altitude of 120,000 feet is reached, a dynamic pressure greater than 2,500 lb/sq ft would be experienced. All these deviations may be within the realm of possibility when the actual flight conditions involve instrument malfunctions, instrument errors, thrust variations, and, of course, the occurrence of unexpected flight circumstances. The assessment of the real problems and the development of piloting techniques and presentation would be the flight objectives in this area.

Next to be discussed is the capability that is available with the X-15 in conducting these types of flight investigations. Figure 4 shows a performance capability of the airplane in terms of altitude and Mach number. The performance boundary on the far right is that for the engine (XLR99) designed for the X-15 and shows a Mach number capability of slightly less than 7 and an altitude greater than 200,000 feet. Other reports at this conference have shown probable maximum altitudes of approximately 700,000 feet. Also shown in figure 4 for reference are dynamic-pressure lines of 10 lb/sq ft and 1,500 lb/sq ft. In order to initiate the flight program on schedule, an interim power plant consisting of two LR11 engines that were designed for the X-1 airplane will be installed. The performance boundary for this engine installation is derived from the latest wind-tunnel lift and drag data for the final X-15 configuration, in-flight thrust measurements of the X-1 airplane and from many trajectories studied to realize the required research missions. It may seem that a performance capability slightly greater than Mach number 4 between 50,000 and 80,000 feet is possible. Typical missions are shown by the dashed lines, where a minimum-drag trajectory to burnout at 80,000 feet is accomplished, followed by a change from minimum drag to either maximum lift for trim or to zero lift.

The possibility of achieving higher performance of the X-15 with the interim engine by increasing the chamber pressure from 250 to 300 lb/sq in. and by the use of high-energy fuels has been considered by the NACA High-Speed Flight Station. The ground tests for qualifying the engine for flight have been completed, and the first flight of the modified engine in the X-1 airplane should be flown next month. The performance calculations for the X-15 with the modified engine is

indicated with a lighter solid line and indicates that a Mach number of 5 is possible.

It should be pointed out that the interim engine will provide a logical approach for the first flight tests of the X-15. The LR11 engines can provide eight equal thrust increments up to a maximum total thrust of about 16,000 pounds in their present form and up to about 28,000 pounds when modified.

Figure 5 shows the performance capability in terms of time. The solid lines in the upper part of this figure show the time available for testing at a weightless flight condition (vertical acceleration $A_z = 0$). The data are plotted against a level of longitudinal acceleration from 0 to 0.024g. Approximately 100 seconds of operation at longitudinal accelerations of 0.024g or less are available with the interim engines as compared with about 140 seconds with the final engine. At longitudinal accelerations of 0.004g or less, the final engine can provide a period of operation of about 120 seconds, whereas the interim engines can provide a period of only about 60 seconds.

The dashed lines indicate the amount of time available with the X-15 for testing in a q range from 0 to 60 lb/sq ft. Approximately 90 seconds are available for both powerplant installations at $q = 10$ lb/sq ft. It should be pointed out, at this point, that the XLR99 engine has been arbitrarily limited to its design specified altitude of 250,000 feet for the purpose of calculating these times. Higher altitudes will allow greater times at these flight conditions. The times given for $A_z = 0$ and low dynamic pressure are generally for the same types of trajectories; therefore, control at low dynamic pressure can be investigated in the weightless flight condition.

The lower part of figure 5 indicates the amount of time available at various Mach numbers for an altitude of approximately 80,000 feet. With the interim LR11 engines, for instance, about $2\frac{1}{2}$ minutes are available at a Mach number of 3. With the XLR99 engine, about $2\frac{1}{2}$ minutes are available at a Mach number of about 5. For a Mach number of 3, more than twice the amount of time is available with the final engine. Preliminary calculations have indicated that accurate heat-transfer information can be obtained to a Mach number of 3.8 with the interim engine.

Figure 6 shows the capabilities of the X-15 in investigating the Reynolds number pertinent to heat transfer and aerodynamic measurements, where Stanton number is plotted against the Reynolds number based on airplane length. Included in this figure are two curves which show the variation of expected Stanton number with Reynolds number for Mach

numbers of 4 and 7. It will be possible with both propulsion versions of the airplane to investigate a Reynolds number from less than 1 million to greater than 100 million. It will be possible also to correlate and compare these data with the heat-transfer and aerodynamic information from the heat-transfer model tested at the Langley Laboratory and at the Arnold Engineering Development Center at Reynolds numbers up to about 12 million. Probably more important is the fact that the flight information will make it possible to extend the data up to much higher Reynolds numbers associated with the lower altitudes and higher dynamic pressures where reentry conditions exist. For instance, reentry conditions in this area for the interim engine and the final engine are indicated in figure 6 as points at a Reynolds number of about 120 million.

In the process of determining Stanton number, the transition Reynolds number, as well as heat-transfer coefficients associated with the areas of laminar and turbulent boundary layers, can be determined.

Figure 7 shows the stability and control boundaries for the airplane, where angle of attack is plotted against Mach number. The solid lines indicate the trim limit of the longitudinal control. In the lower left-hand corner is shown an area of longitudinal instability. Several present high-performance airplanes have similar areas, and this instability region has not been found detrimental to normal flight operation of these aircraft. The upper left-hand corner indicates an area of directional instability. At supersonic speeds, this area is protected by the control limit. At subsonic Mach numbers (for instance, at landing-approach speeds), the pilot will not normally fly in this region because of buffetting and high rates of sink associated with the high angles of attack. For the first X-15 flights this region will be avoided. The area may possibly be of interest later in the program, when rotation to high climb angles immediately after launch at low speed may be required to achieve extremely high altitudes and long periods of flight at low dynamic pressure. The upper right-hand portion of this figure shows an area of directional divergence where the high positive directional stability is more than offset by the unstable dihedral effect as reported in the paper by Penland and Fetterman. Increasing difficulty of control in this area during simulator studies was experienced, even with dampers operating. It may be seen from this figure, on the basis of the knowledge at the present time, that an appreciable range of angle of attack and Mach number is available for conducting research investigations.

Figure 8 shows a sketch of the airplane and indicates the areas in which research instrumentation has been installed. Pressure and temperature instrumentation has been provided in the darker areas and only pressure instrumentation in the lighter areas. Temperature instrumentation has been included primarily to determine the heat-transfer coefficients from the skin temperatures and to determine the actual structural

temperatures at approximately 600 selected locations. It is desirable to relate the flight heat-transfer coefficients to the local flow conditions in order to obtain temperature data for general-research use. Provisions have been made at approximately 140 locations to measure pressures for determining the local flow conditions. The airplane, of course, includes the usual handling-qualities instrumentation that measures the pilot input, control positions, and airplane response. Provisions for strain gages at the locations shown were made to measure structural and aerodynamic loads of the individual panels. The entire instrumentation of the airplane, weighing approximately 1,300 pounds, has been so provided that during the time when information is being obtained for the specific problem areas mentioned earlier, data will at the same time be recorded for use in analyzing subjects such as aerodynamic loads, handling qualities, aerodynamic noise, performance, and many of the operational problems.

Up to this point, discussion has been confined to areas of immediate research interest and areas directed toward a better understanding of the fundamental problems concerning heating, flight control outside of the atmosphere, and problems of reentry and exit. There are other important research areas of interest in this speed range for which the X-15 can make additional contributions, as follows:

(1) Flight control systems

(2) Research on structural components

(3) Structural cooling

(4) Celestial photographic missions.

The X-15 would be a valuable vehicle in which to investigate and concentrate on various flight control systems toward optimumizing and simplifying the systems for use in more advanced vehicles. The areas of concern here are the problems of exit, entry, and landing.

It is not always possible to select the most promising high-temperature structures from the many attractive specimens that are being developed in laboratory research because of questions pertaining to well-known aerodynamic and structural factors concerning full-scale and flight environment. The investigation of promising full-scale high-temperature structural components (such as replaced ventral fins of the X-15), instrumented in the same manner as described previously, would be proposed.

The X-15 project is well suited to conducting a structural cooling investigation where actual flight conditions in terms of boundary-layer conditions and temperature are present. Investigations would be

directed toward providing supplementary results to wind-tunnel proposals and assessing the operational problems involved.

With the capability of the X-15 of obtaining manned flight above 100,000 feet, the use of the celestial camera mounted in the airplane would permit photographs of space areas. In this method, the limitation on the resolution as a result of turbulence of the earth's atmosphere could be circumvented.

CONCLUDING REMARKS

An effort has been made to present the areas of research interest for the most important and urgent problems at the present time. Indications have been given of other types of data that will be obtained, as well as possible additional research uses of the X-15. In the course of conducting the flight research for the X-15, it is obvious that the emphasis will change from one area to another and problems of new and different significance will result. Those problems that are found to be real will be better understood as a result of the flight investigations and those problems that have been imagined will assuredly be replaced with the unexpected or overlooked problems.

RESEARCH OBJECTIVE REGIONS

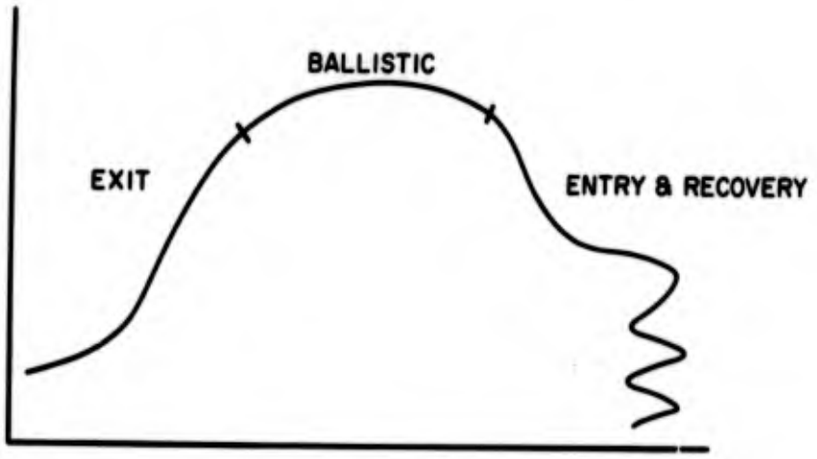

Figure 1

EFFECT OF EXIT ANGLE OF ATTACK ON PEAK ALTITUDE

$M_0 = 2.0$ $\theta_0 = 43°$

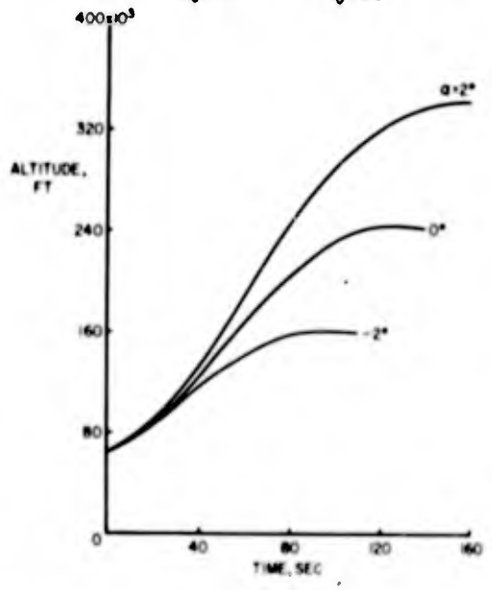

Figure 2

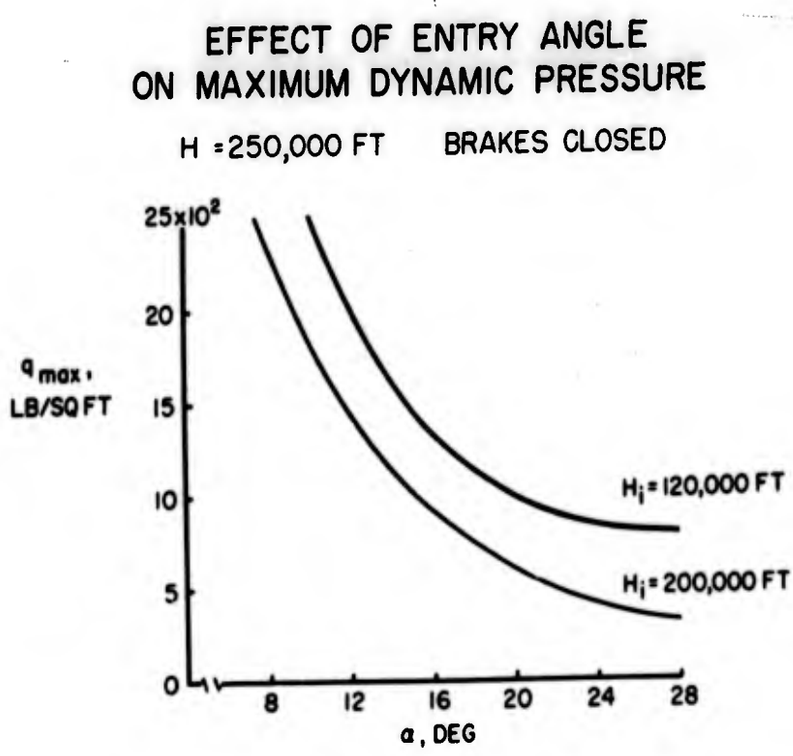

Figure 3

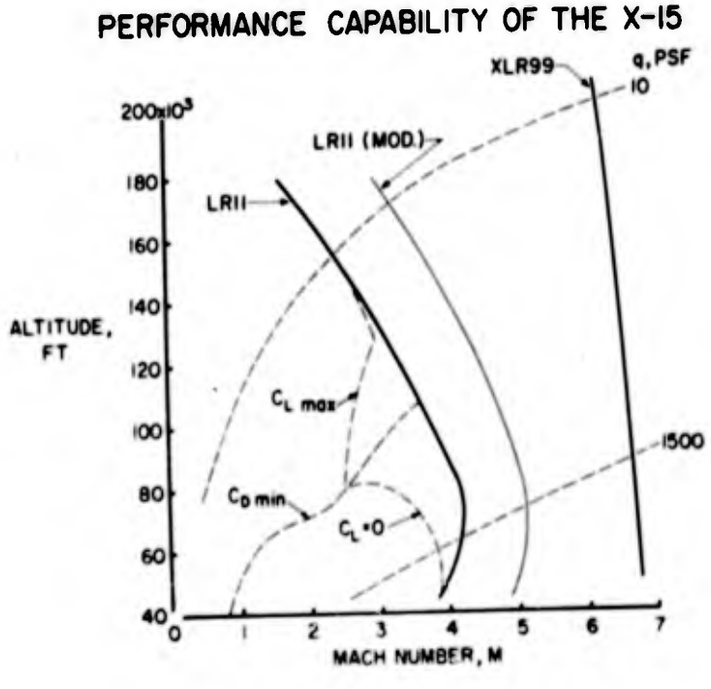

Figure 4

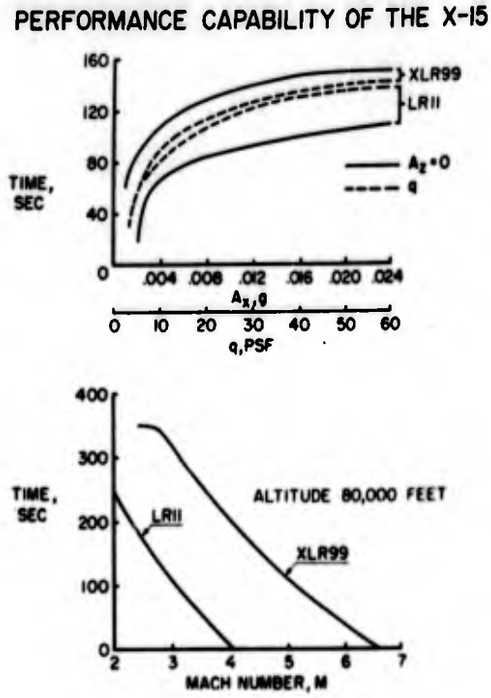

Figure 5

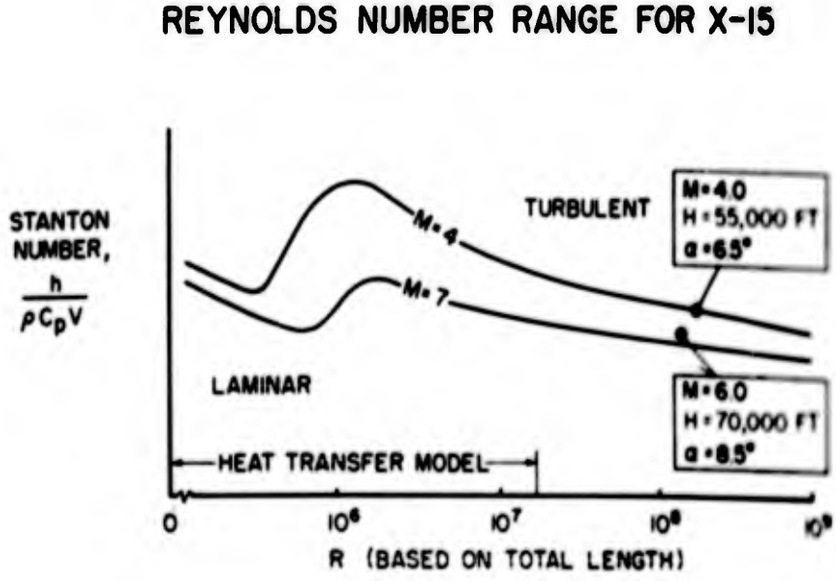

Figure 6

X-15 STABILITY AND CONTROL BOUNDARIES

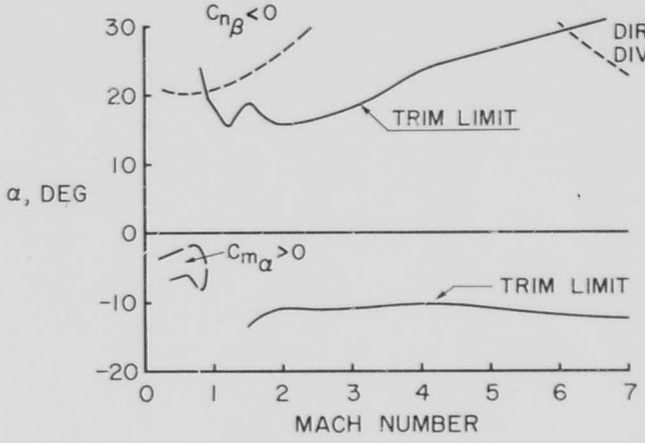

Figure 7

RESEARCH INSTRUMENTATION

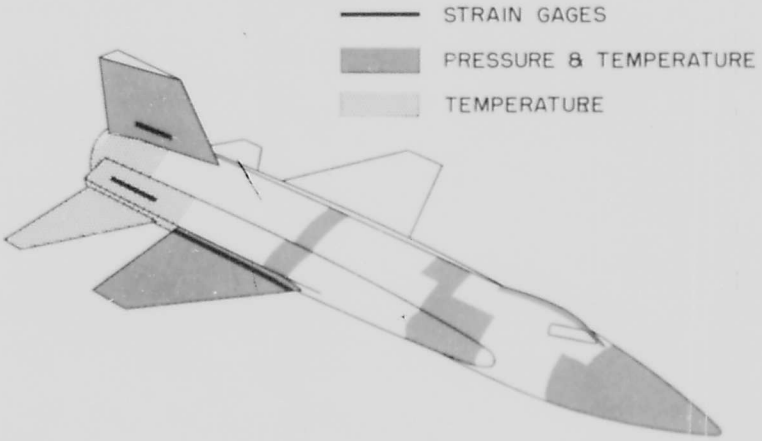

Figure 8

NACA - Langley Field, Va.

UNCLASSIFIED